CHAPTER-5

RESULTS AND DISCUSSIONS

5.1 Qualitative Analysis of Groundwater

The examination of water quality is a highly effective approach for the assessment and evaluation of the presence of contaminants in a specific region, enabling the determination of their quantity. Water is widely acknowledged as an essential resource for supporting life on earth. Consequently, it is essential to regularly assess the quality of water (Adimalla, 2018; Li et al. 2018a). The groundwater samples collected during the pre-monsoon and post-monsoon seasons of 2022 were utilised in the study to explore the effects of water pollution in the region under study. Geostatistical tools are regarded as one of the most effective options for the collected data sets from different locations around the mining area to represent the changes between various physicochemical parameters during both the pre and post monsoon seasons.

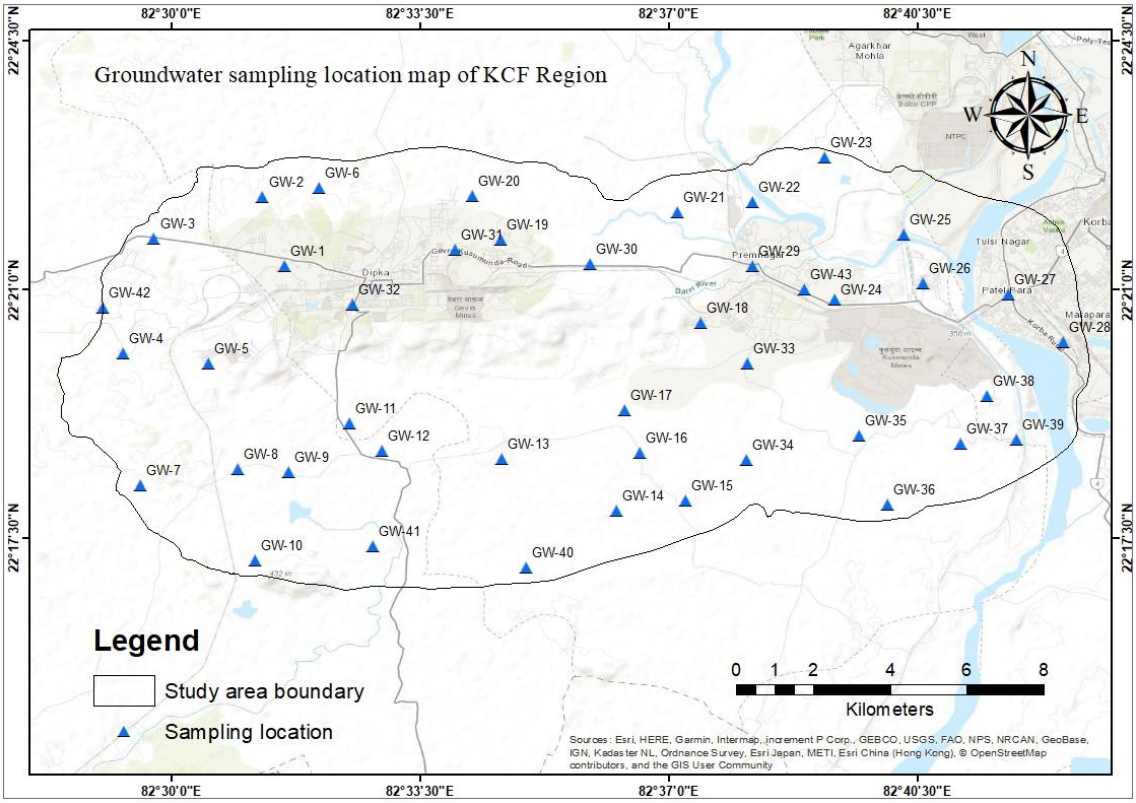

Fig.5.1 Sampling locations map for groundwater in KCF region

This is particularly relevant as groundwater serves as a significant water source, fulfilling not only drinking water demands but also meeting the needs of agriculture and industry. The groundwater chemistry of the study region is having complex contamination. A total of 86 groundwater samples from various water sources (bore well =56, hand pump =20, dug well =10) were collected from the pre monsoon and post monsoon season in the year 2022 (Fig.5.1 and Table.5.1). The samples were subsequently subjected to analysis of thirteen major physicochemical parameters, including pH, EC, TDS, Total Hardness, Calcium, Magnesium, Sodium, Potassium, Bicarbonate, Fluoride, Chloride, Nitrate, and Sulphate. The groundwater samples obtained were subjected to analysis in order to determine their suitability for both drinking and irrigation applications. The sterilized polypropylene bottles were washed twice with distilled water having 400 ml capacity and used to collect the water samples. Prior to the analysis of physicochemical properties, all water samples underwent filtration using a 0.22 µm Nylon syringe filter.

Three parameters were examined simultaneously just after sampling, including pH, TDS, and EC using calibrated ISO-TECH multiparameter system as given in Table.4.1. Ion-Chromatography (IC) was used to measure the cations (Ca^{2+}, Mg^{2+}, Na^{+}, and K^{+}) and anions (F^{-}, Cl^{-}, NO_3^{-}, SO_4^{2-}, and HCO_3^{-}) for each groundwater sample that were collected during the pre and post monsoon seasons in Central Instrument Facility (CIF) IIT (BHU). The summarized result of all physicochemical parameters is given in Appendix A.1 to Appendix A.6 respectively. The concentrations of physicochemical parameters in the pre-monsoon season are high as compared to the post-monsoon season are only influenced by high evaporation rates, reduced water volume, increased agricultural and industrial activity, and stagnation of water. The rapid development of mining and thermal power plants in the study region has resulted in the degradation of water quality and other resources. The stated purpose was achieved by conducting a comparison between the data obtained during both the pre and post monsoon seasons, and the drinking water quality standards recommended by the WHO (2011).

Table.5.1 Sampling locations details of groundwater samples

Sample code	Sampling locations	Latitude	Longitude
GW-1	Jhabar hand pump water	22.35551	82.5265
GW-2	Batari Dugwell water	22.3716	82.52132
GW-3	Tiverta hand pump water	22.36196	82.49582
GW-4	Ratija borewell water	22.33492	82.48852
GW-5	Chainpur bore well water	22.33275	82.50858
GW-6	Binjhari bore well water	22.37373	82.53445
GW-7	Andikachhar bore well water	22.30412	82.49255
GW-8	Renki bore well water	22.30783	82.51542
GW-9	Suwabhondi borewell water	22.30712	82.5273
GW-10	Suberpara handpunp water	22.28639	82.51951
GW-11	Malgaon borewell water	22.31865	82.54161
GW-12	Haldibazar borewell water	22.31222	82.54929
GW-13	Raliya bore well water	22.31038	82.57747
GW-14	Mahowadih borewell water	22.29811	82.60419
GW-15	Keshla hand pump water	22.30063	82.6205
GW-16	Bhilaibazar borewell water	22.3117	82.60981
GW-17	Bethora dug well water	22.32171	82.60628
GW-18	Mangaon borewell water	22.34216	82.62397
GW-19	Durena borewell water	22.36174	82.57711
GW-20	Durena dugwell water	22.37203	82.57059
GW-21	Rohina borewell water	22.36817	82.6185
GW-22	Bhairotal borewell water	22.37061	82.63626
GW-23	Balkikhar dugwell water	22.3810	82.6530
GW-24	Barpali borewell water	22.34756	82.65545
GW-25	Hasdev power plant bore water	22.36282	82.67161
GW-26	Durpa handpump water	22.35141	82.6763
GW-27	Patel Nagar borewell water	22.34877	82.69613
GW-28	Sitamadi borewell water	22.33772	82.70906
GW-29	Kuchaina mod borewell water	22.35557	82.63618
GW-30	Awadh Nagar road borewell water	22.35602	82.59811
GW-31	Vijay Nagar handpump water	22.35921	82.56636
GW-32	Dhara chauk Dipka borewell water	22.34635	82.5424
GW-33	Gevra basti handpump water	22.33272	82.63503
GW-34	Salora handpump water	22.31004	82.63481
GW-35	Rishdi borewell water	22.31581	82.66115
GW-36	Ghanadabri borewell water	22.29963	82.66788
GW-37	Padhania borewell water	22.31383	82.68492
GW-38	Chandra nagar handpump water	22.32497	82.69116
GW-39	Sonpuri borewell water	22.31471	82.69799
GW-40	Mudhali handpump water	22.28482	82.58316
GW-41	Bamhanikona borewell water	22.2899	82.54711
GW-42	Ratija ka para dugwell	22.34577	82.48384
GW-43	Vikash Nagar borewell water	22.34992	82.64822

5.1.1 Physicochemical parameter characteristics and spatial contour distribution mapping

The use of geostatistical analysis is employed together with the ArcGIS 10.8 software to calculate different physicochemical parameters and the water quality index within the study area, providing a study of their spatial distribution. The measured physicochemical parameter values for both seasons are presented in Table.5.2 and Table.5.3, respectively, along with the standard recommended values established by the WHO (2011).

Table.5.2 Statistical summary of physicochemical parameters of groundwater in pre-monsoon season compared with WHO (2011) standards.

S No.	Parameters	Minimum	Maximum	Std dev	Median	WHO (2011)
1.	pH	6.05	7.78	0.32	6.74	6.5-8.5
2.	EC	58.00	1880.00	349.14	331.00	1400
3.	TDS	39.00	1266.00	233.58	222.00	500
4.	Calcium (Ca^{2+})	20.46	92.37	17.55	34.37	75
5.	Magnesium (Mg^{2+})	2.41	74.03	13.53	11.66	50
6.	Sodium (Na^{+})	2.07	76.95	18.60	27.37	50
7.	Potassium (K^{+})	0.15	17.02	4.25	2.31	15
8.	Fluoride (F^{-})	0.00	1.10	0.28	0.37	1.5
9.	Chloride (Cl^{-})	1.79	194.80	44.76	38.16	250
10.	Nitrate (NO_3^{-})	0.33	123.61	28.43	15.06	45
11.	Sulphate (SO_4^{2-})	0.42	162.08	33.00	17.51	150
12.	Bicarbonate (HNO_3^{-})	22.00	311.00	61.43	93.00	200
13.	Total Hardness	14.54	501.18	101.88	147.56	500

Table.5.3 Statistical summary of physicochemical parameters of groundwater in post-monsoon season compared with WHO (2011) standards.

S No.	Parameters	Minimum	Maximum	Std dev	Median	WHO (2011)
1.	pH	5.32	8.11	0.58	6.43	6.5-8.5
2.	EC	81.00	1736.00	309.37	301.00	1400
3.	TDS	54.00	1156.00	203.29	189.00	500
4.	Calcium (Ca^{2+})	7.35	79.26	17.46	21.26	75
5.	Magnesium (Mg^{2+})	3.55	81.01	16.84	11.20	50
6.	Sodium (Na^{+})	2.49	80.51	17.73	25.66	50
7.	Potassium (K^{+})	1.02	14.17	3.13	2.14	15
8.	Fluoride (F^{-})	0.00	1.10	0.25	0.35	1.5
9.	Chloride (Cl^{-})	2.11	234.44	43.38	41.26	250
10.	Nitrate (NO_3^{-})	0.22	171.11	34.88	19.20	45
11.	Sulphate (SO_4^{2-})	0.19	274.00	53.89	20.84	150
12.	Bicarbonate (HNO_3^{-})	34.00	298.00	55.73	79.00	200
13.	Total Hardness	51.14	452.85	90.58	111.78	500

All parameters are expressed in mg/l except pH, EC (µS/cm)

5.1.1.1 pH

The measurement of the pH level in groundwater serves as a significant indicator to determine its inherent acidity or alkalinity. The negative logarithm of hydrogen ion concentration expressed in power to demonstrate hydrogen ion concentration can be used to quantify pH as a measure of hydrogen ion activity in a solution (Bates 1973). The pH of the water sample is < 7, indicating its acidic nature. However, a pH > 7 signifies a basic solution. At a temperature of 25 ℃, a pH = 7 denotes a neutral water solution. Moreover, pH typically does not affect directly to the people's health (WHO, 2008). The pH of a solution can experiences changes due to the interaction between organic substances and minerals. The ideal pH range for drinking water is between 6.5 to 8.5 WHO (2011).

The pH level in groundwater was significantly below the allowable range as suggested by WHO (2011) at all selected locations during both seasons respectively. The observed pH values varied from 6.05 to 7.78, with an average of 6.76 during the pre monsoon, and varies from 5.32 to 8.11, with an average of 6.43 during the post monsoon season, indicating that the groundwater from both seasons is slightly acidic to alkaline in nature. The spatial distribution map of pH values for both seasons is shown in Fig.5.2 and Fig.5.3, respectively.

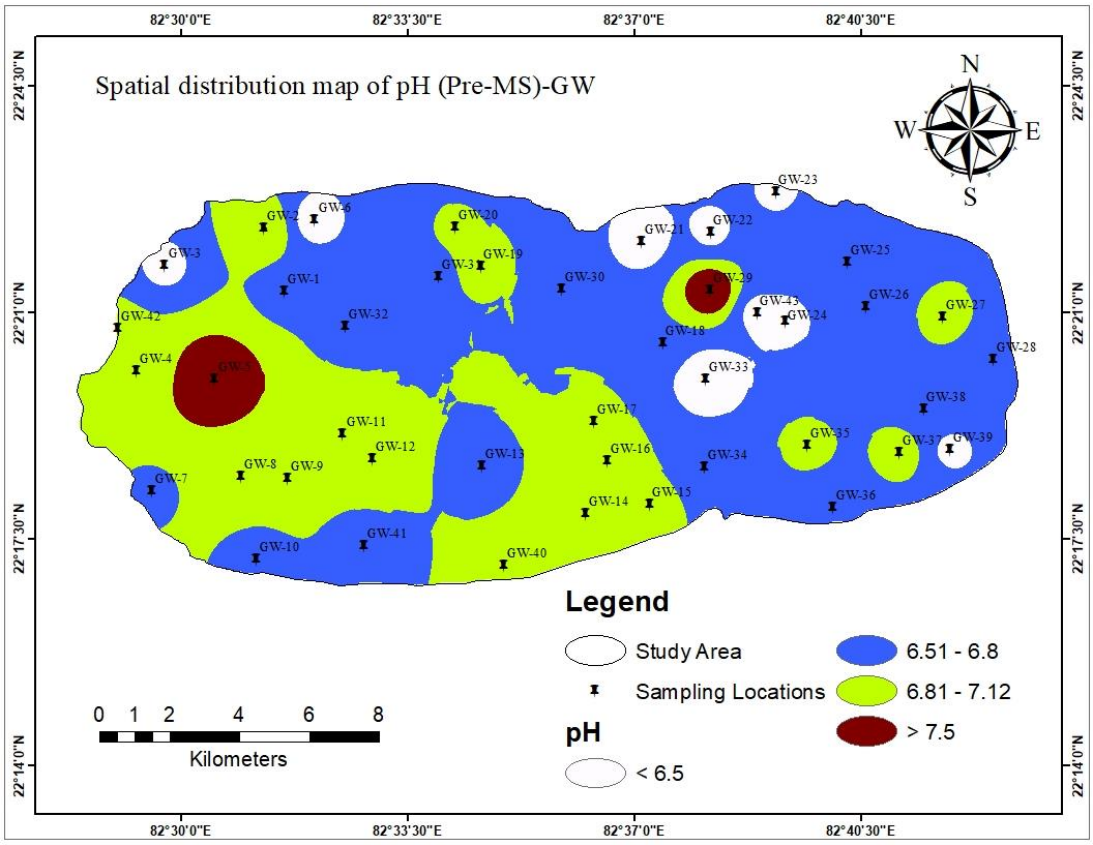

Fig.5.2 Spatial map of pH during pre-monsoon season in study region

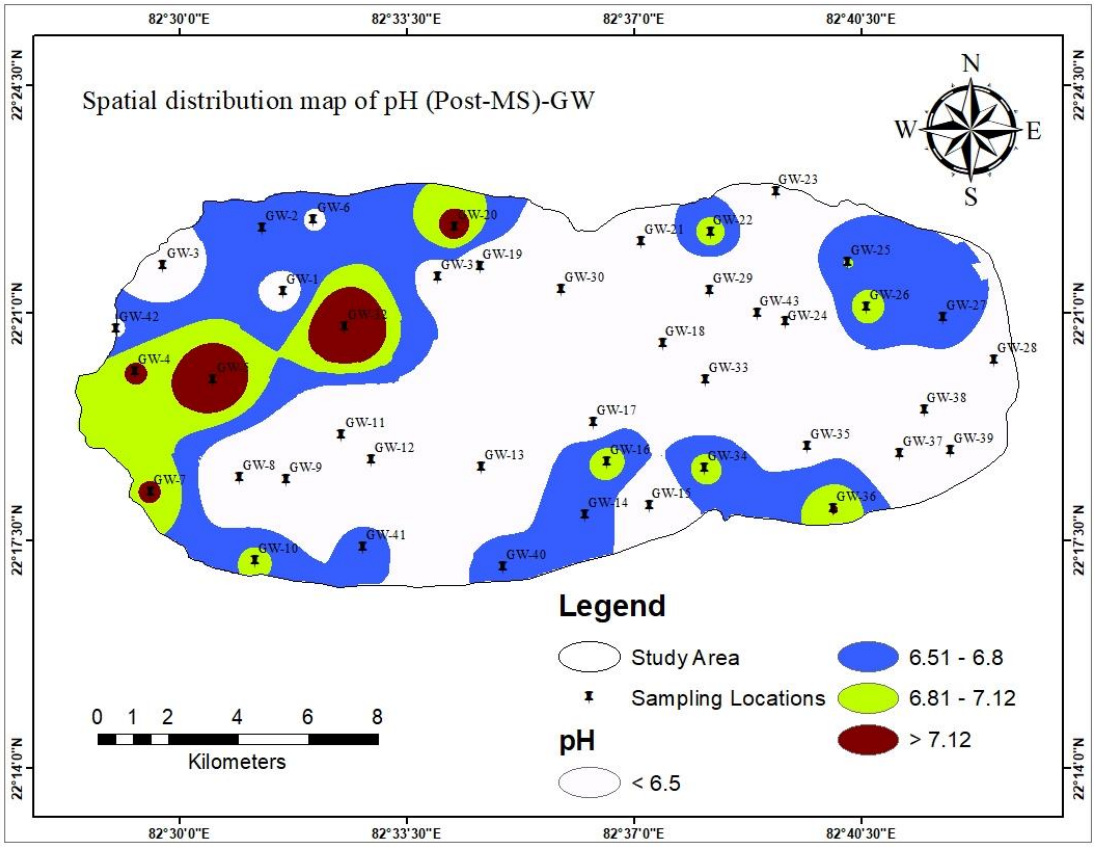

Fig.5.3 Spatial map of pH during post-monsoon season in study region

5.1.1.2 Electrical Conductivity

Electrical conductivity (EC) is an essential variable for assessing the ionic concentrations in a water body. Moreover, an increase in EC concentration can lead to increased levels of salinity and total dissolved concentration (Pande et al., 2018). Water is capable of carrying electric current due to the existence of various cations and anions. EC is a frequently used means of assessing the presence of TDS in water. This approach facilitates the determination of EC by using the direct relationship between EC and TDS concentrations. Consequently, as the TDS content increases, the EC value also increases, and conversely, a decrease in TDS leads to a decrease in EC (Rusydi 2018).

The observed EC values ranged from 58 to 1880 µS/cm, with an average of 331 µS/cm during the pre monsoon and from 81 to 1736 µS/cm, with an average of 301 µS/cm during the post monsoon season. This result is indicating that 1880 µS/cm in pre and 1736 µS/cm in post monsoon season at only site (GW-16) exceeded the WHO (2011) standard limits. Large fluctuations in EC values are primarily attributed to geochemical processes occurring in the area. The high EC value indicates the presence of sedimentary rocks and their dissolution in the examined locations. The remaining samples fall significantly below of the allowable limits as recommended values by the WHO (2011). The spatial map of EC values for both seasons is shown in Fig.5.4 and Fig.5.5, respectively.

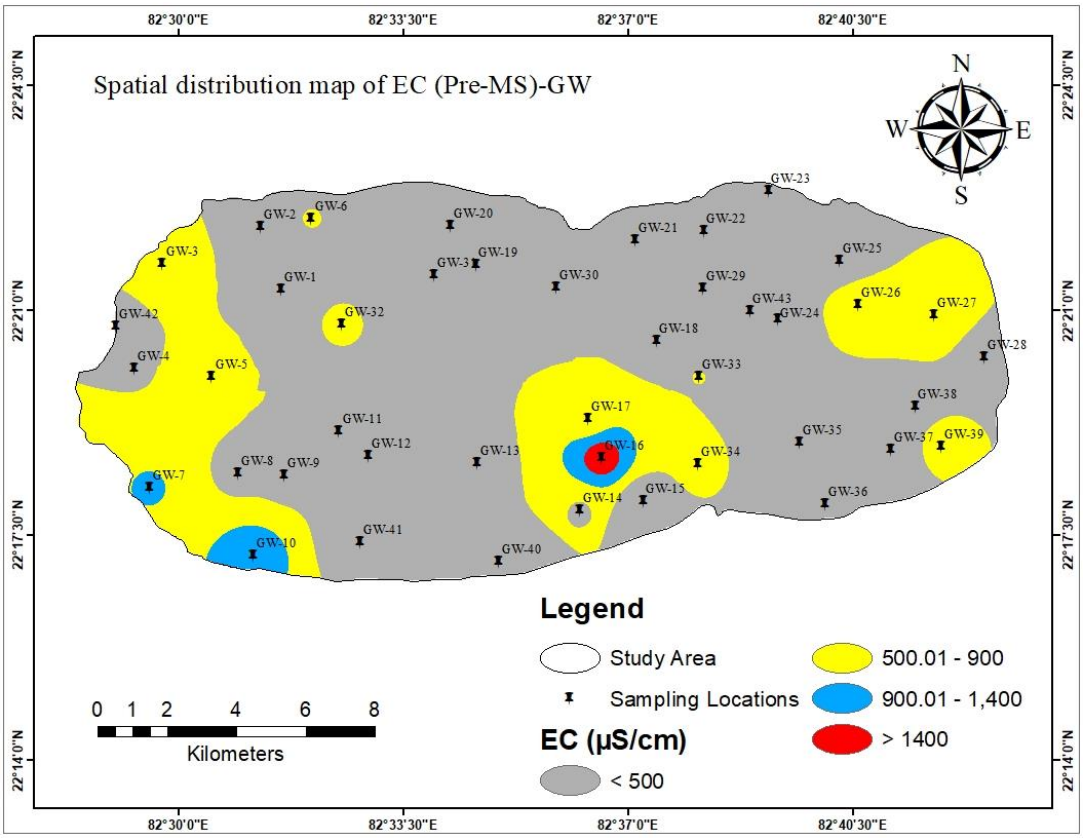

Fig.5.4 Spatial map of EC during pre-monsoon season in study region

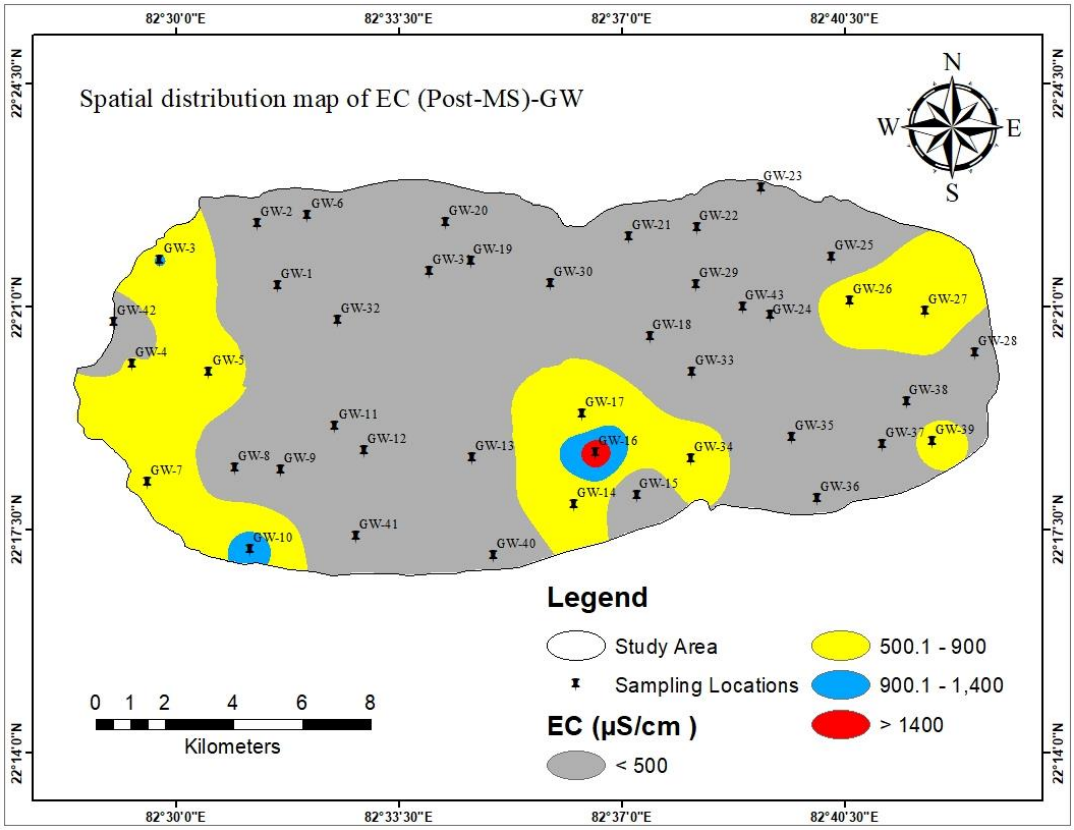

Fig.5.5 Spatial map of EC during post-monsoon season in study region

5.1.1.3 Total Dissolved Solid

The measurements of TDS concentration in water samples are an essential factor in evaluating water quality since it directly influences its suitability for both drinking and agricultural use (APHA 1999). The water has a distinct TDS concentration, mostly consisting of inorganic minerals such as Ca^{2+}, Mg^{2+}, K^{+}, Na^{+}, HNO_3^{-}, Cl^{-}, and SO_4^{2-}, among others. The TDS levels less than 600 mg/L are typically regarded as beneficial for human health and those larger than 1000 mg/L as unpleasant WHO (2011). The proportion of TDS in water samples keeps changing due to changes in mineral solubility carried on by different geological regions WHO (2008). The high levels of TDS in water can result in diseases including arthritis, kidney and gallstone stones, joint stiffness, and more.

The TDS concentration ranged from 39 to 1266 mg/L, with an average of 222 mg/L during the pre monsoon and from 54 to 1156 mg/L, with an average of 189 mg/L during the post monsoon season. These results indicate that six samples (GW-3, 7, 10, 16, 26) from pre monsoon and five samples (GW-7, 10, 16, 26, 27) from post monsoon season were exceeded the WHO (2011) guideline limits. A few areas may have high TDS concentrations due to the surrounding sedimentary rocks, which have a comparatively high concentration of bicarbonate, sulphates, chlorides, and sodium, among other elements, present in the mining zone (Murkute 2014). The remaining samples indicated that their concentrations were well below the permitted limit of 500 mg/L as established by WHO (2011). Since the groundwater in the area is freshwater and a majority of the samples except GW-16 have TDS less than 1000 mg/L, they can be used for drinking and irrigation purposes. The spatial map of TDS for both seasons is shown in Fig.5.6 and Fig.5.7, respectively.

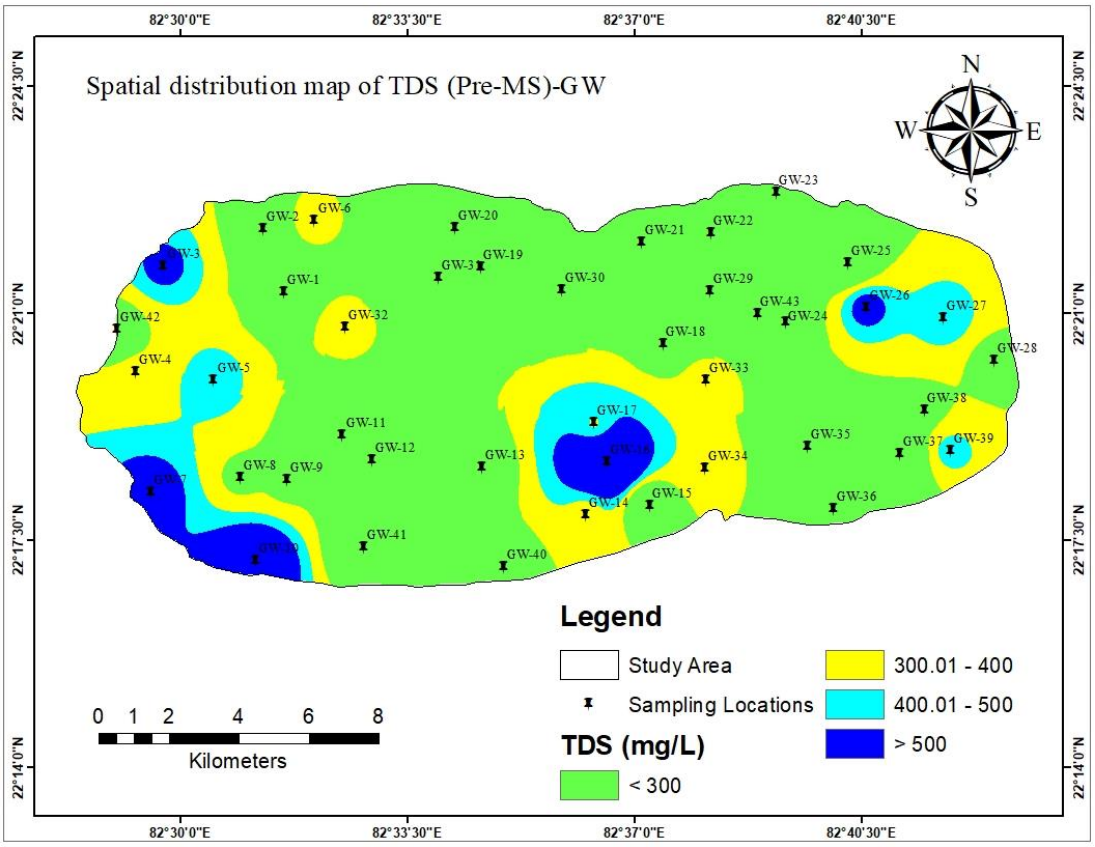

Fig.5.6 Spatial map of TDS during pre-monsoon season in study region

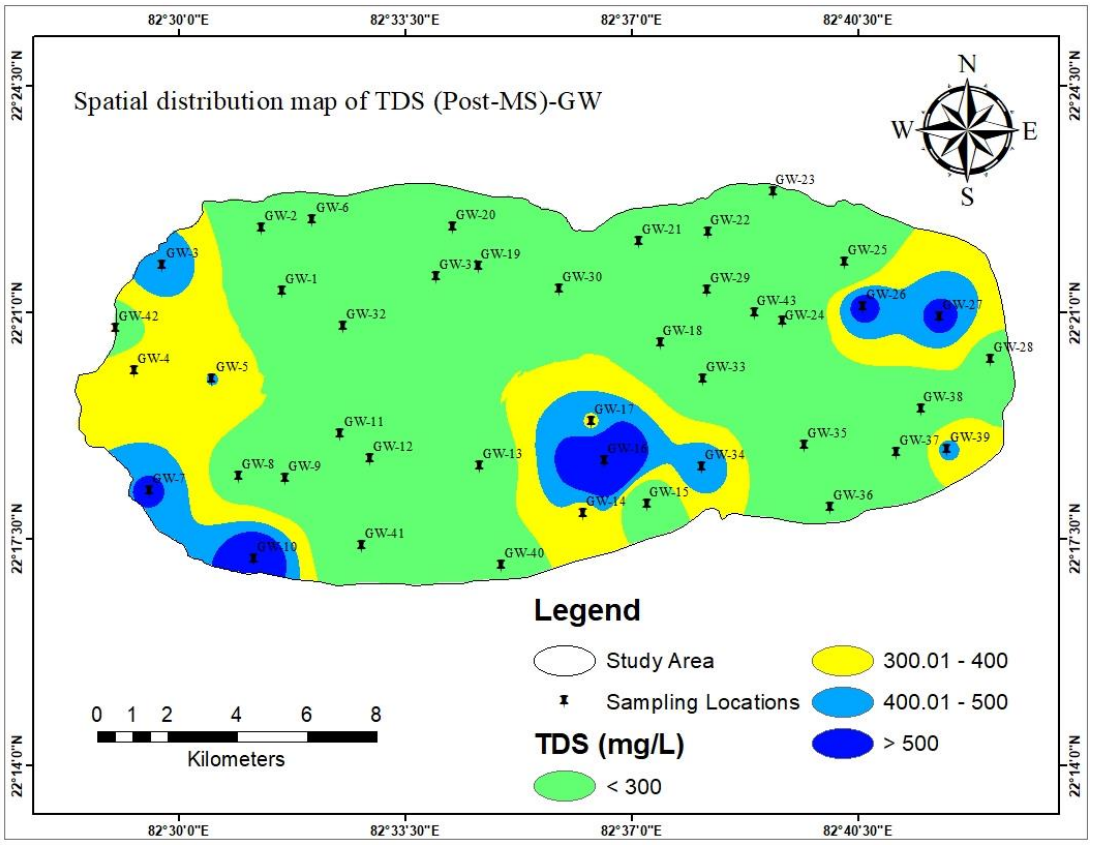

Fig.5.7 Spatial map of EC during post-monsoon season in study region

5.1.1.4 Calcium

The classification of water suitability frequently depends on the calcium and magnesium levels, which are the predominant alkaline earth elements found in the aquifer. The normal functioning of our skeletal system, nervous system, muscles, and blood clotting all strongly depend on concentration of Calcium. A deficiency in calcium during early stages of life can lead to the development of rickets and osteoporosis. The calcium carbonate content of the water is increasing due to the process of limestone and dolomite weathering. In water, the calc-silicate minerals amphibole and pyroxene, in addition to plagioclase, are responsible for the production of calcium ions in larger quantities (Hem, 1989).

In the pre monsoon season, the measured Calcium concentration ranged from 20.46 to 92.37 mg/L, with an average of 34.37 mg/L, while it ranged from 7.35 to 79.26 mg/L, with an average of 21.26 mg/L during post monsoon season. However, it has been observed that the concentration of calcium in the study region is slightly lower during the post-monsoon season. These findings demonstrate that GW-10 and GW-26 in the pre monsoon and GW-26 in the post monsoon season exceeded the WHO (2011) guideline limits. This can be attributed to the fluvial flux occurring in the presence of an alluvial environment. While the rest of the groundwater samples were well below the suggested allowable limit of 75 mg/L and can be used for drinking and other purposes. The spatial map of Calcium values for both seasons is shown in Fig.5.8 and Fig.5.9, respectively.

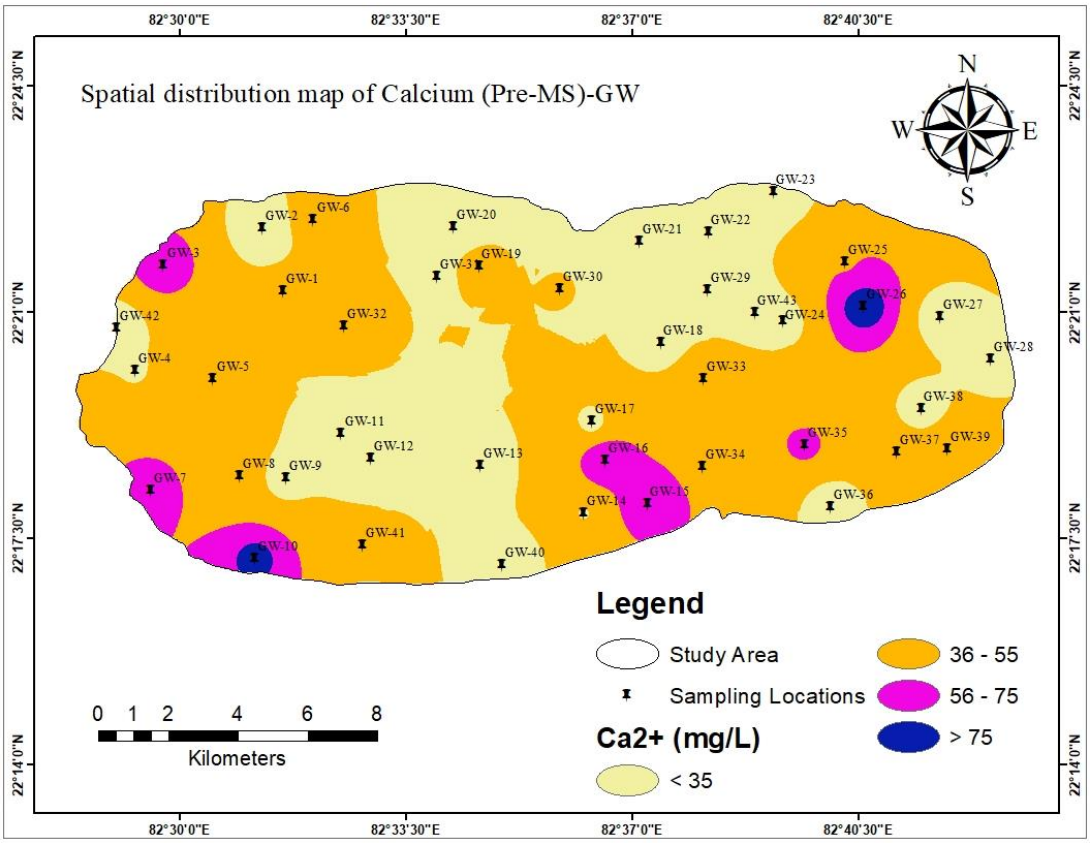

Fig.5.8 Spatial map of Calcium during pre-monsoon season in study region

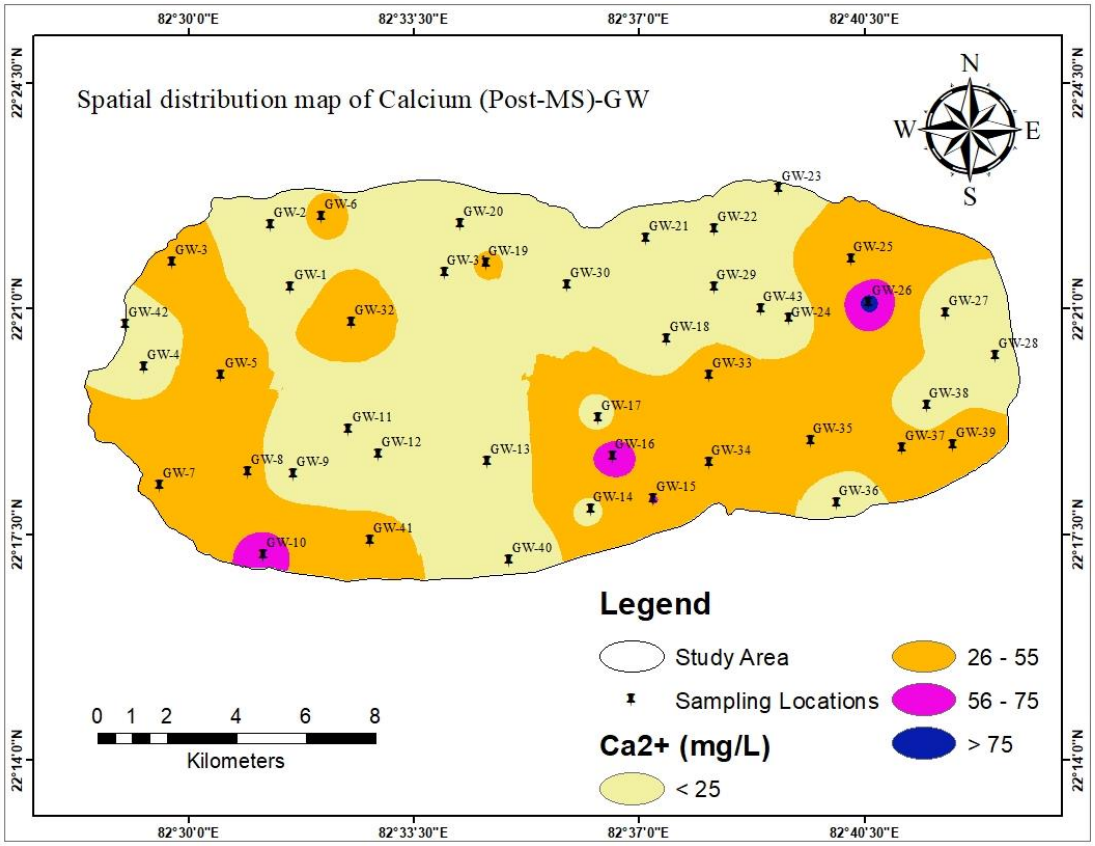

Fig.5.9 Spatial map of Calcium during post-monsoon season in study region

5.1.1.5 Magnesium

The magnesium ion concentration is important in assessing water quality. The water becomes hard due to the presence of calcium and magnesium ions into it. It is found in groundwater as a result of the leaching of anhydrite, gypsum, dolomites, and limestone etc. Magnesium is found in considerable quantities in natural water systems, originating from many sources such as the Ferromagnesian minerals olivine, biotite, diopside, augite, and hornblende. The many salts that include magnesium can have significant negative effects on human health, including cathartic and diuretic alterations as well as a laxative effect (CPCB 2008). It has a substantial impact on the amount of water hardness. The local geology exhibits sedimentary rock formations, specifically dolomite, which significantly impact the water quality for both domestic and industrial applications (Tiwari et al. 2016).

The magnesium values varied from 2.41 to 74.03 mg/L, with an average of 11.66 mg/L, in the pre monsoon whereas it varied from 3.55 to 81.01 mg/L, with an average of 11.20 mg/L, in the post monsoon season respectively. These results show that one sample (GW-10) in the pre monsoon and two samples (GW-10 and GW-36) in the post monsoon season exceeded the WHO (2011) guideline limits. The excess of magnesium ions is due to high-Mg^{2+} calcite, dolomite, and magnesite present in sedimentary deposits in the region. In contrast, the remaining samples from both seasons were well below the suggested allowable limit of 50 mg/L WHO (2011) and can be used for drinking and other purposes. The spatial map of Mg^{2+} values for both seasons are shown in Fig.5.10 and Fig.5.11, respectively.

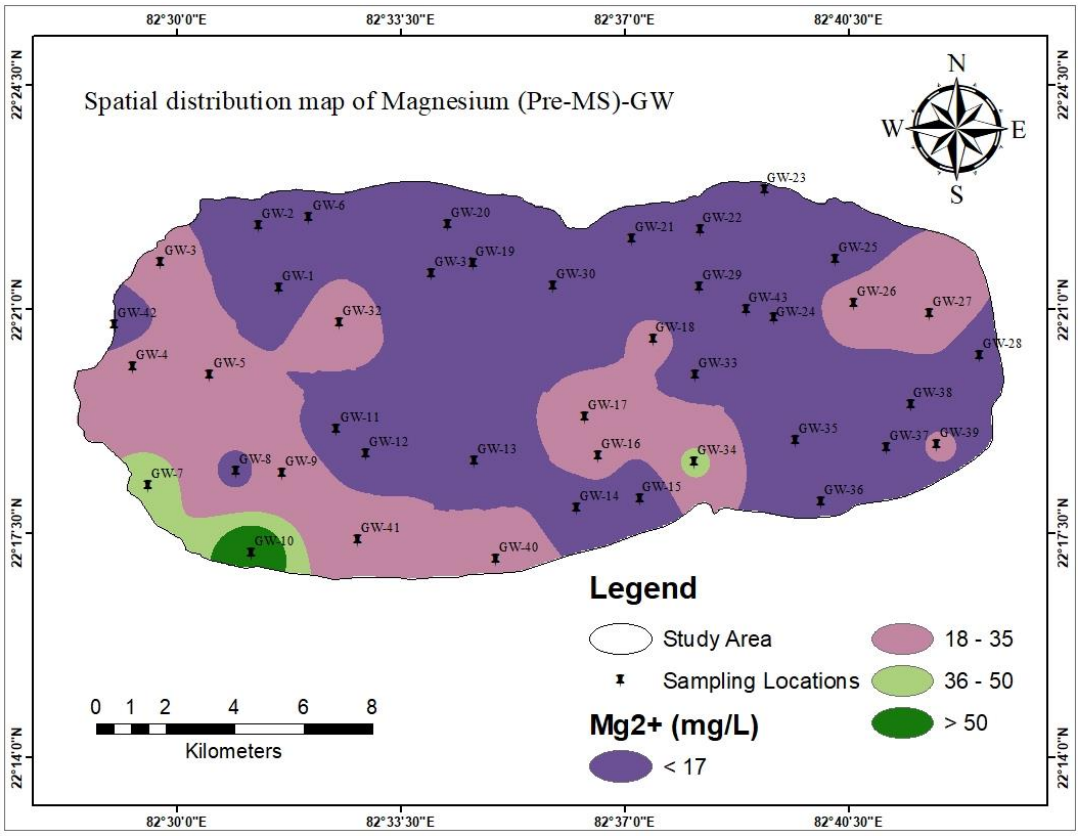

Fig.5.10 Spatial map of Magnesium during pre-monsoon season in study region

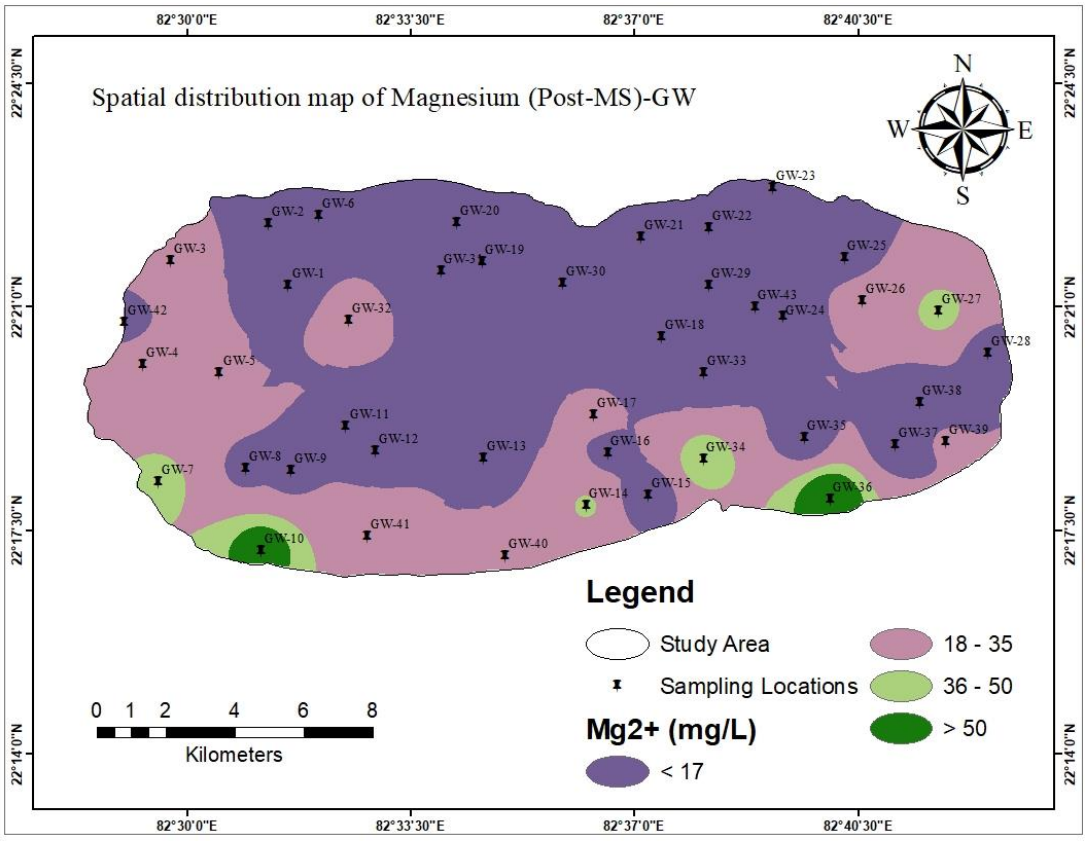

Fig.5.11 Spatial map of Magnesium during post-monsoon season in study region

5.1.1.6 Sodium

Sodium is well recognised as an essential nutrient. The salt concentration of the watercourse is important in determining groundwater quality for irrigation purposes since it increases with the soil hardness and permeability (Tijani 1994). The excess sodium consumption by humans can lead to hypertension, kidney failure, and nervous system problems. However, a deficiency of sodium in water results in a number of symptoms, including fatigue, lethargy, reduced appetite, and dehydration (Selinus et al. 2005). Therefore, the high salt containing water should not be used for irrigation or household purposes.

The sodium concentration ranged from 2.07 to 76.95 mg/L, with an average of 27.37 mg/L, in pre monsoon while it ranged from 2.49 to 80.51 mg/L, with an average of 25.66 mg/L in post monsoon season respectively. According to these data, four samples (GW-3, 5, 10, and 27) in the pre monsoon and four samples (GW-5, 10, 26, and 27) in the post monsoon season exceeded guideline limits of WHO (2011). The increase in sodium concentrations in groundwater is due to the presence of sediments from weathering, erosion, and agricultural drainage in the catchment basin. The remaining groundwater samples from both seasons were significantly lower than the recommended allowed limit of 50 mg/L WHO (2011). The spatial map of Na^+ ion for both seasons is shown in Fig.5.12 and Fig.5.13, respectively.

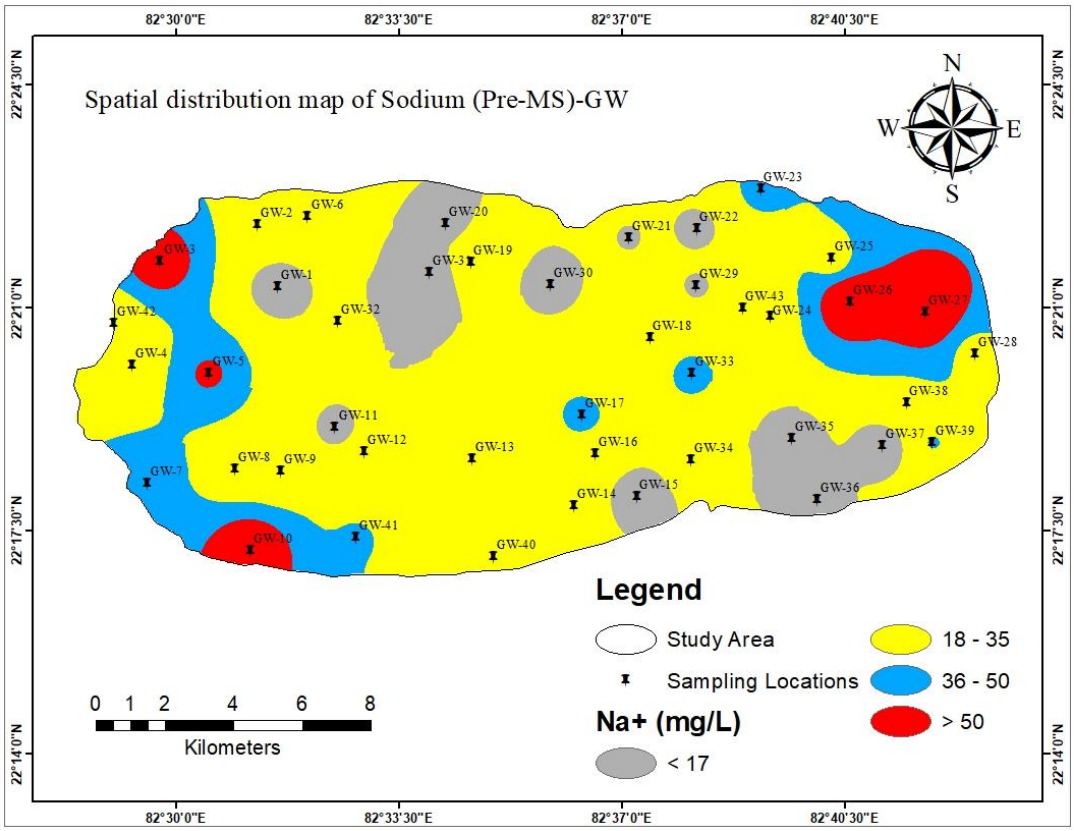

Fig.5.12 Spatial map of Sodium during pre-monsoon season in study region

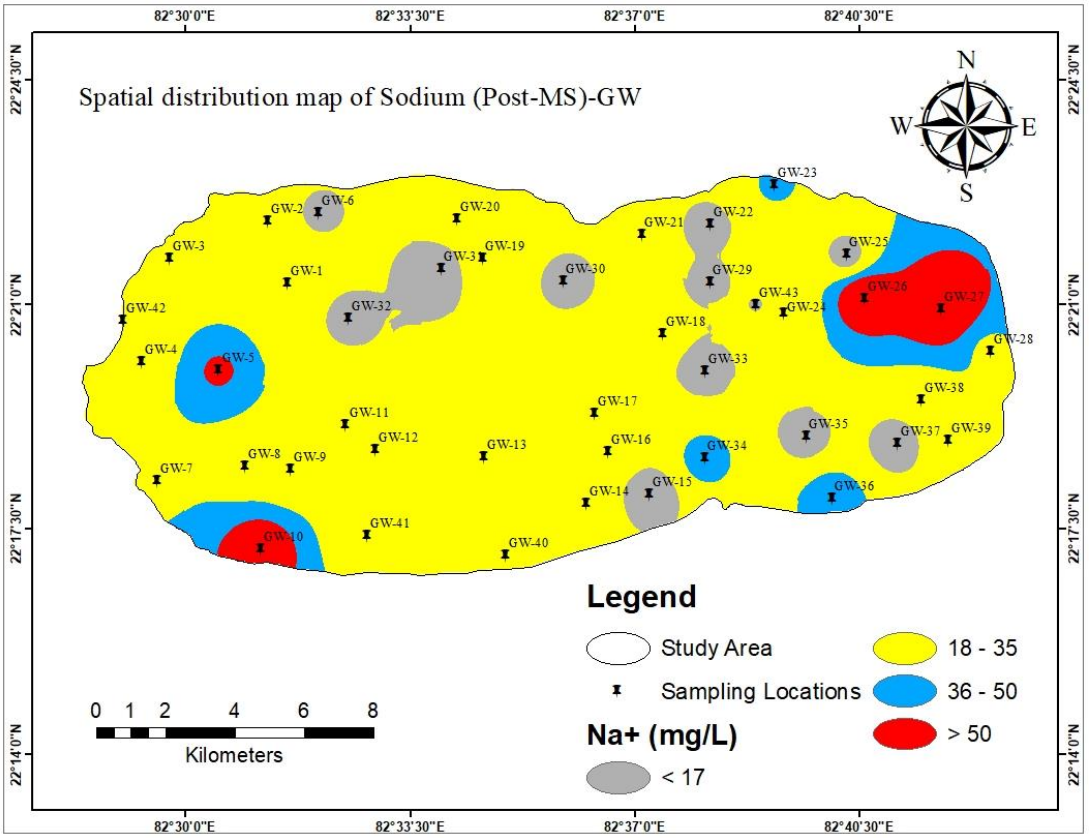

Fig.5.13 Spatial map of Sodium during post-monsoon season in study region

5.1.1.7 Potassium

The higher level of potassium ions in water can be attributed mostly to the weathering of surrounding rocks, while the weathering of potash silicate minerals is the main contributing factor to the higher potassium content in groundwater (Murkute, 2014). According to the guidelines provided by the WHO (2011), it is recommended that the concentration of potassium ions in water should not exceed 15 mg/L.

The measured potassium concentration varied from 0.15 to 17.02 mg/L, with an average of 2.31 mg/L, during the pre monsoon whereas it varied from 1.02 to 14.17 mg/L, with an average of 2.14 mg/L during post monsoon season. These results indicate that, only two samples (GW-15 and GW-24) in the pre monsoon exceeded the WHO (2011) guideline limit. The elevated potassium concentrations are either owing to the addition of industrial influents or to the weathering of rocks in the vicinity. whereas, all samples in the post monsoon season were well below the permissible limits. The remaining samples from pre-monsoon seasons were significantly below the WHO (2011) recommended limit of 15 mg/L and may be safe for drinking and other uses. There was a significant reduction in the potassium concentration in the pre-monsoon than post-monsoon seasons within the study area. The spatial map of potassium ion for both seasons is shown in Fig.5.14 and Fig.5.15, respectively.

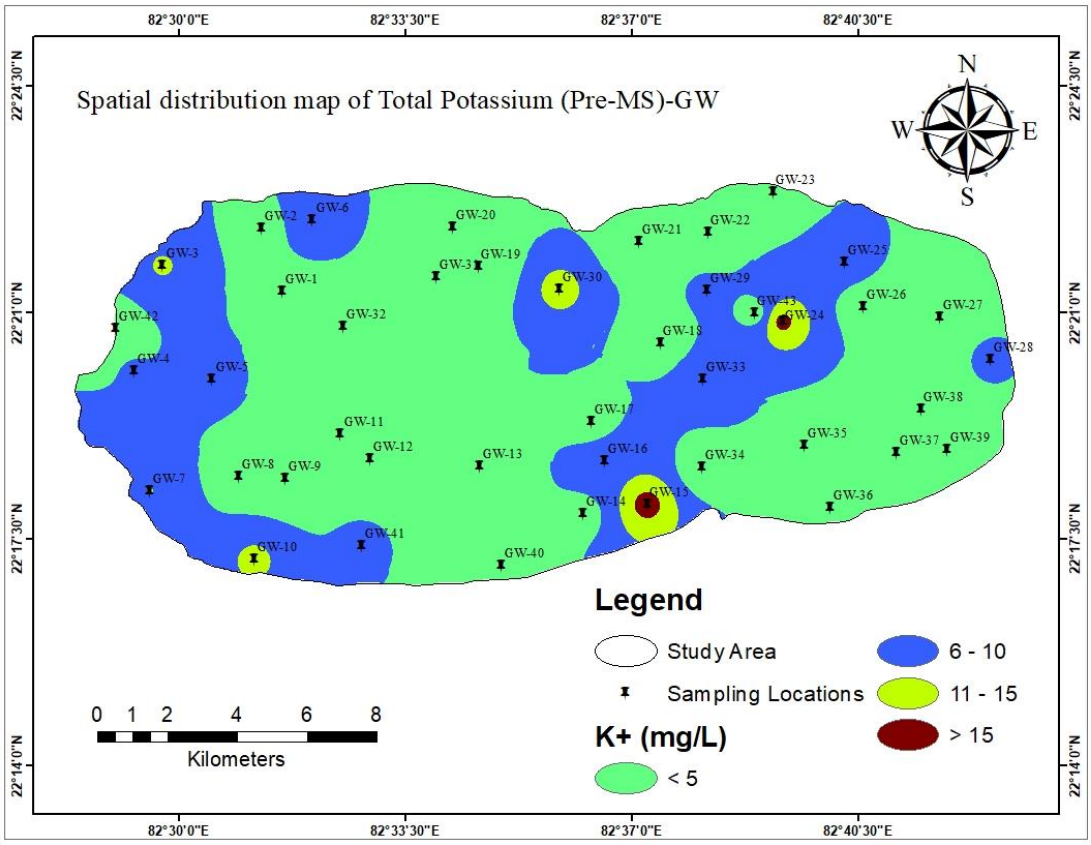

Fig.5.14 Spatial map of Potassium during pre-monsoon season in study region

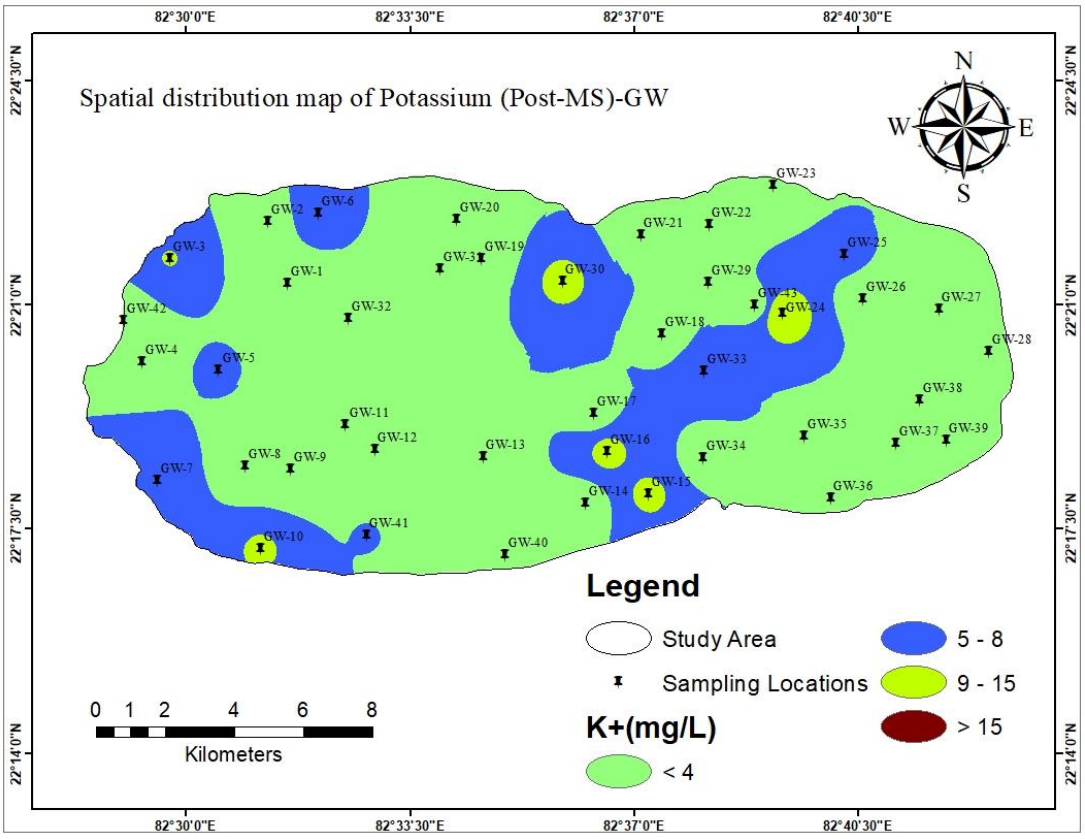

Fig.5.15 Spatial map of Potassium during post-monsoon season in study region

5.1.1.8 Fluoride

Fluoride, the most commonly encountered form of fluorine, is a naturally occurring water contaminants. Fluoride, which is commonly found in groundwater, is normally dissolved by geological processes (Kumar et al. 2010). The groundwater with fluoride concentrations < 0.5 mg/l has the potential to contribute to the development of dental cavities and weak bones. whereas concentrations > 1.5 mg/l can lead to many adverse effects such as physiological disorders, skeletal and dental fluorosis, hormonal imbalance, and kidney failure (BIS, 2012). Hence, it can be concluded that the consumption of fluoride in groundwater within the range of 0.5 to 1.5 mg/l is considered to be safe for human consumption. However, industrial wastewater discharges into adjacent water bodies that increase fluoride concentrations are part of the anthropogenic inclusion of fluoride concentrations (Kumar et al. 2019).

The concentration of fluoride ion ranged from 0.0 to 1.10 mg/L in the pre monsoon with the mean value of 0.37 mg/L, while 0.0 to 1.10 mg/L in the post-monsoon season, the mean value of 0.35 mg/L. The fluoride concentration in the groundwater was much lower than the recommended limit of 1.5 mg/L at almost all locations tested, both pre monsoon and post-monsoon season. This indicates that the groundwater is safe for human consumption with respect to fluoride content. The spatial map of fluoride ion for both seasons is shown in Fig.5.16 and Fig.5.17, respectively.

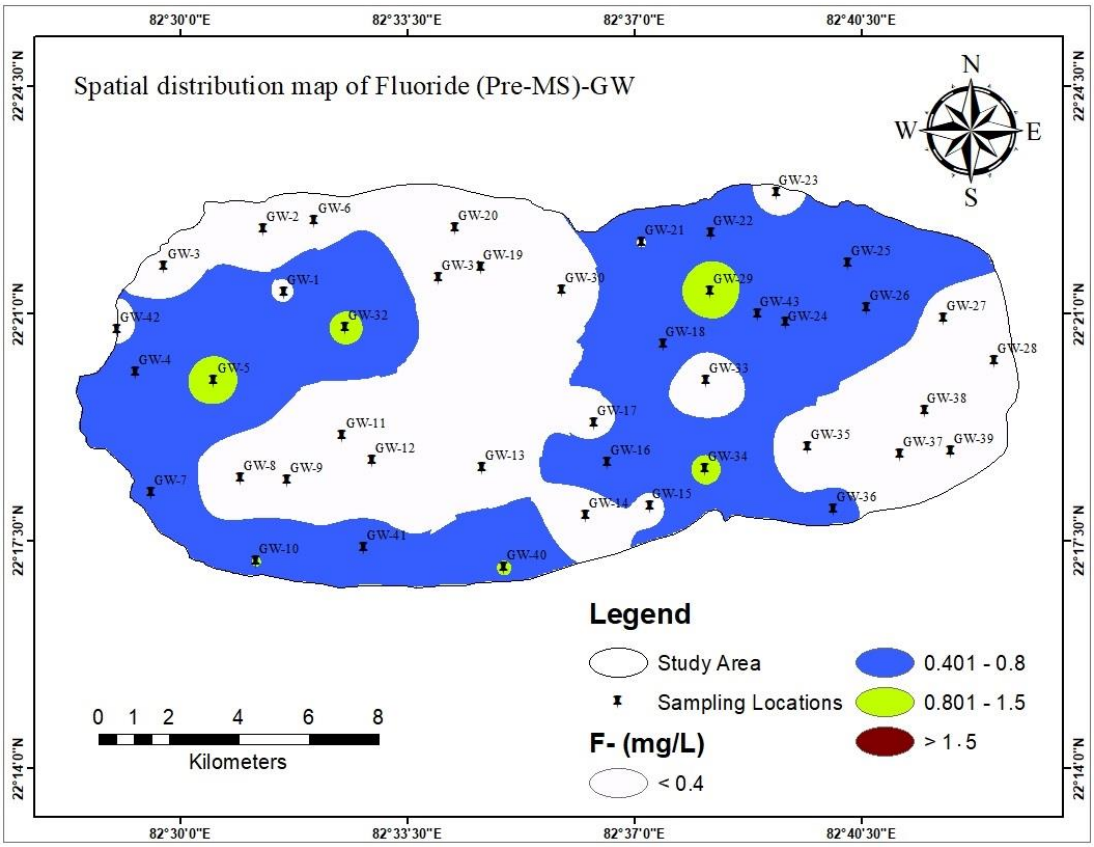

Fig.5.16 Spatial map of Fluoride during pre-monsoon season in study region

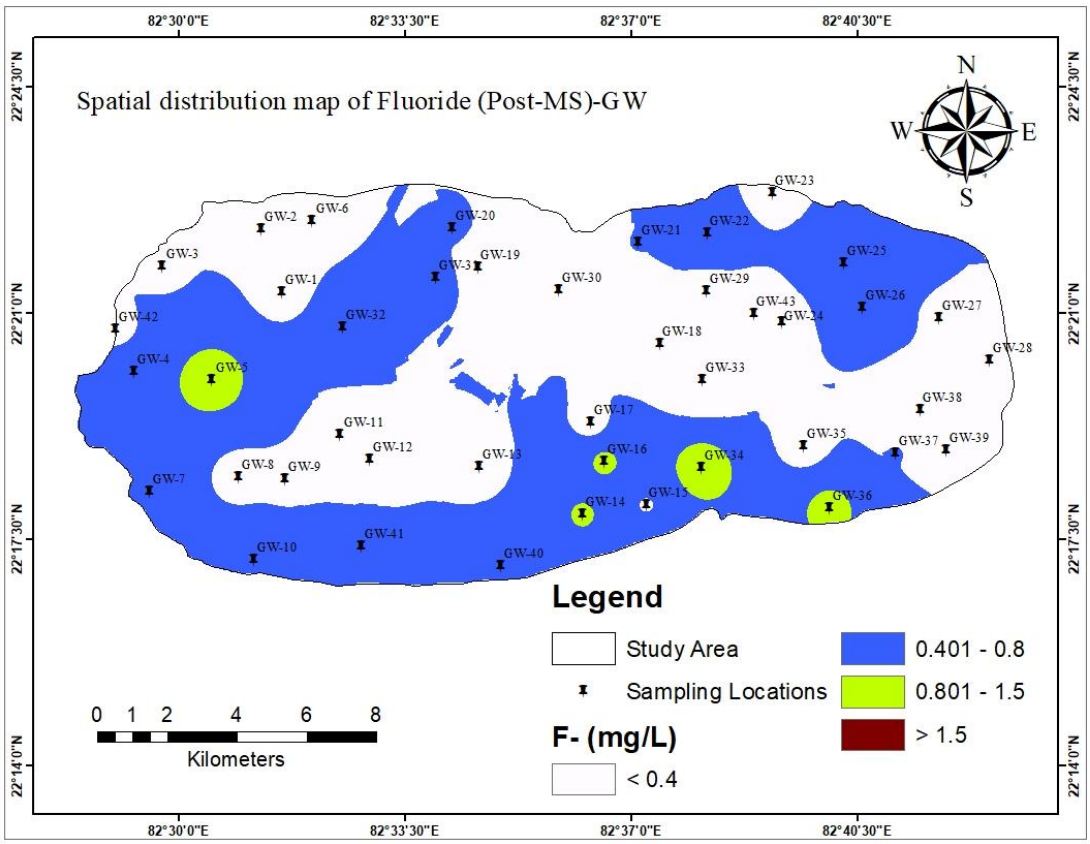

Fig.5.17 Spatial map of Fluoride during post-monsoon season in study region

5.1.1.9 Chloride

The process of weathering leads to the dissolution of chloride ions from various rock formations, resulting in their incorporation into both soil and water. Since chloride imparts a salty flavour to water and has laxative issues at higher amounts. It is widely employed as a gauge of water pollution. Moreover, it is mostly generated from municipal effluents, industrial waste, and garbage from homes (Adimalla, 2019; Narsimha and Sudarshan, 2013). The recommended concentration of chloride in drinking water is typically 200 mg/L, although it may be permissible to have concentrations as high as 600 mg/L in order to meet international standards (WHO, 2008). The higher chloride concentration may provide potential risks for individuals with existing heart and kidney issues. Additionally, it gives rise to issues related to taste perception, indigestion, and corrosion (CPCB, 2008).

The measured concentration of chloride values ranged from 1.79 to 194.80 mg/L, with its mean value of 38.16 mg/L, in the pre monsoon whereas varies from 2.11 to 234.44 mg/L, with its mean value of 41.26 mg/L, in the post monsoon season respectively. The chloride content was quite high in post monsoon than pre monsoon season which is due to rise in temperature in study region. The chloride concentration during both seasons was found to be significantly lower than the recommended standard of 250 mg/L set by the WHO (2011). This indicates that the water can be considered safe for use. The spatial map of chloride ion for both seasons are shown in Fig.5.18 and Fig.5.19, respectively.

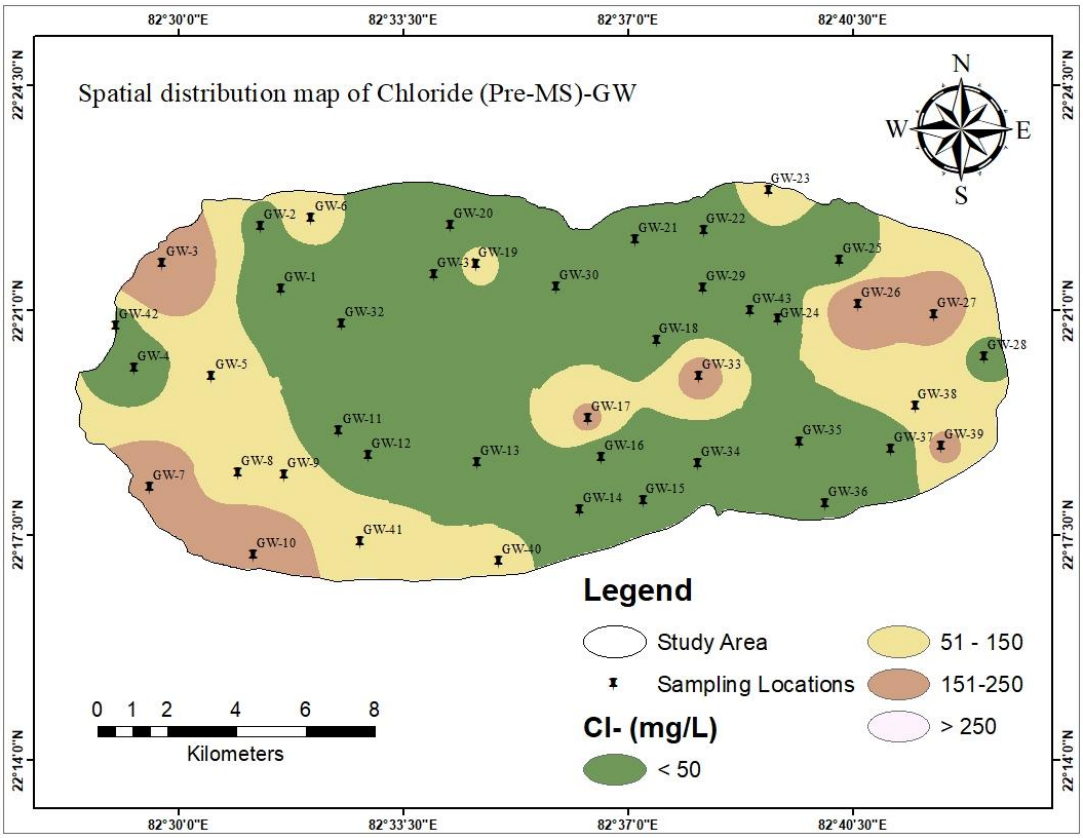

Fig.5.18 Spatial map of Chloride during pre-monsoon season in study region

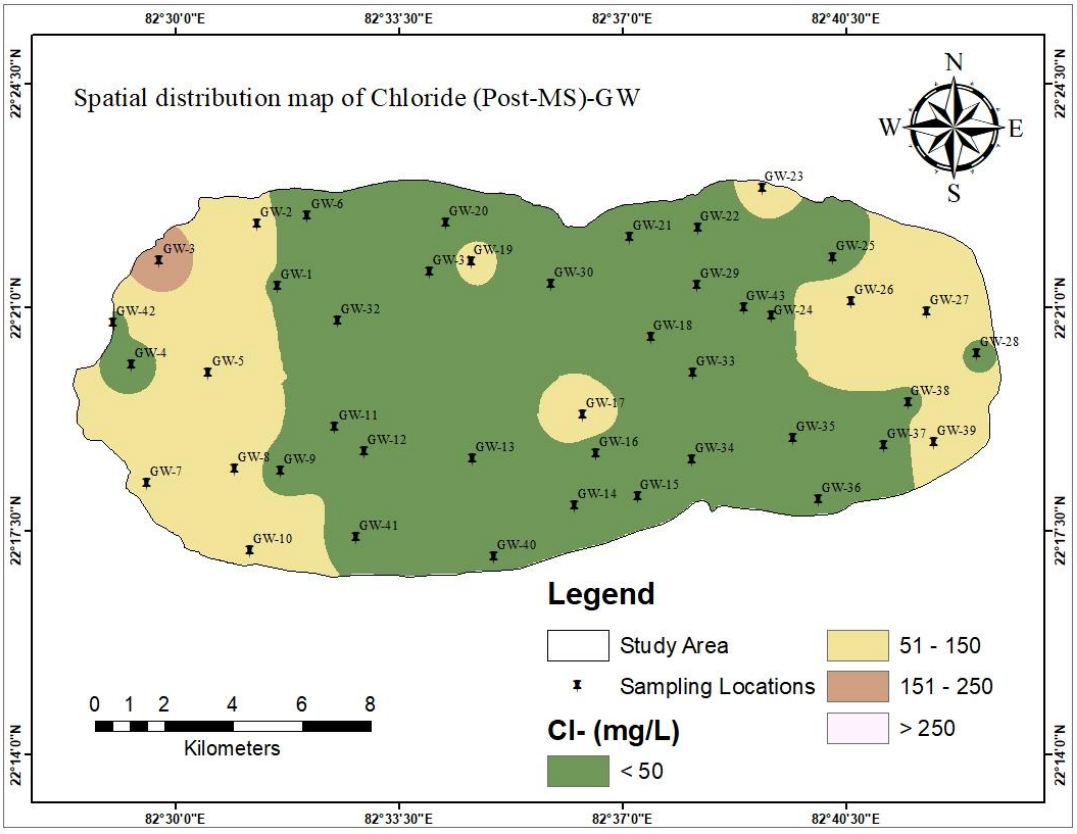

Fig.5.19 Spatial map of Chloride during post-monsoon season in study region

5.1.1.10 Nitrate

Nitrate is a prevalent pollutant in water sources found in agricultural regions across the world (Adimalla and Li, 2018; Adimalla et al. 2018c). Since nitrogenous elements are not commonly found in geological landscapes. The primary anthropogenic origins of nitrate in groundwater encompass the use of nitrate fertilisers, the deposition of animal waste, the discharge of domestic effluents, the release of human excreta, and the leakage from septic tanks (Maila et al. 2004). The primary sources of nitrate in aquatic environments are land runoff and industrial discharge. The rise in nitrate concentration is critical because it causes a number of chronic diseases, including new-born methemoglobinemia (blue baby syndrome), cardiovascular problems, gastric cancer, including harmful impacts on the central nervous system (CPCP 2008; Raju et al. 2009).

The nitrate concentration ranged from 0.33 to 123.61 mg/L, with its mean value of 15.06 mg/L, in pre monsoon while it ranged from 0.22 mg/L to 171.11 mg/L, with its mean value of 19.20 mg/L in the post monsoon season. These results indicate that eleven samples during the pre monsoon and nine samples collected during the post monsoon season both exceeding the standard limit WHO (2011). The primary source of nitrate concentration in aquatic environments is terrestrial runoff, which includes runoff from agriculture and industries. Nitrates are highly soluble in soil and are easily transported from the land through natural drainage systems (Nazneen et al. 2019). The other groundwater samples from both seasons, were well below the suggested allowable limit of 45 mg/L WHO (2011). The observed data indicates a substantial decrease in nitrate concentration within the study area from the pre monsoon to the post monsoon season. The spatial map shows that the east, north western, and southwestern parts of the study region had higher concentrations of nitrate in both seasons as shown in Fig.5.20 and Fig.5.21, respectively.

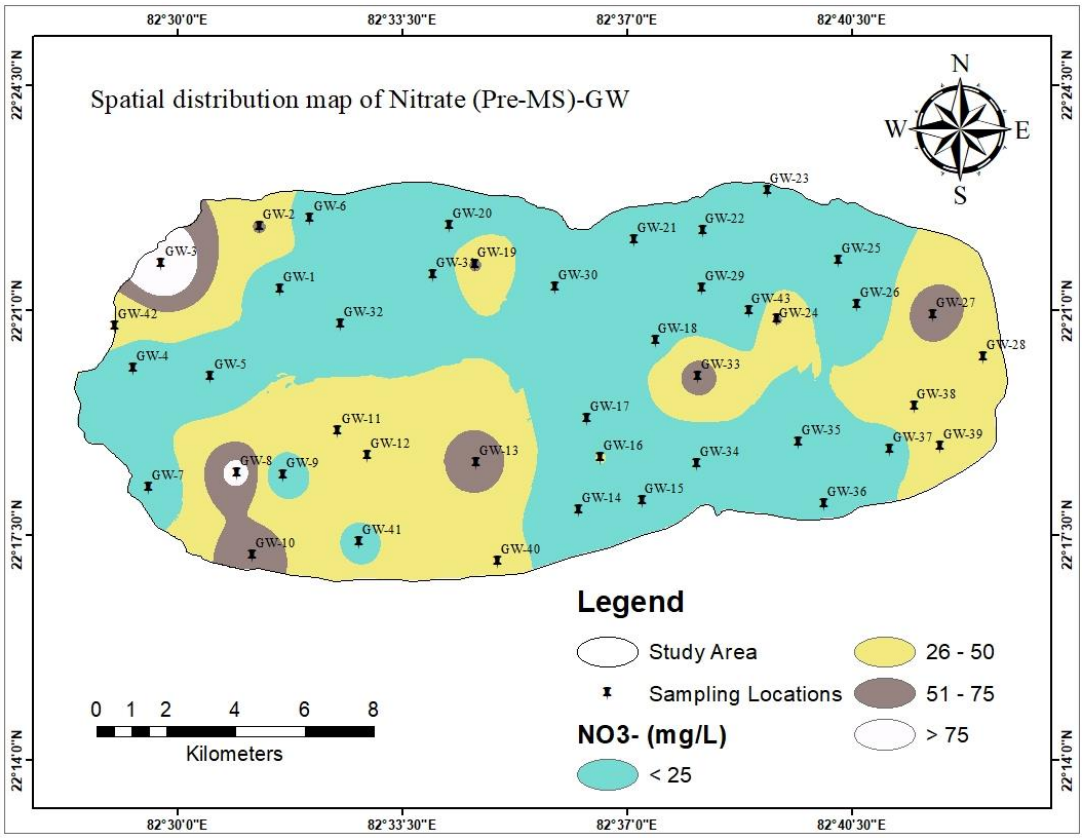

Fig.5.20 Spatial map of Nitrate during pre-monsoon season in study region

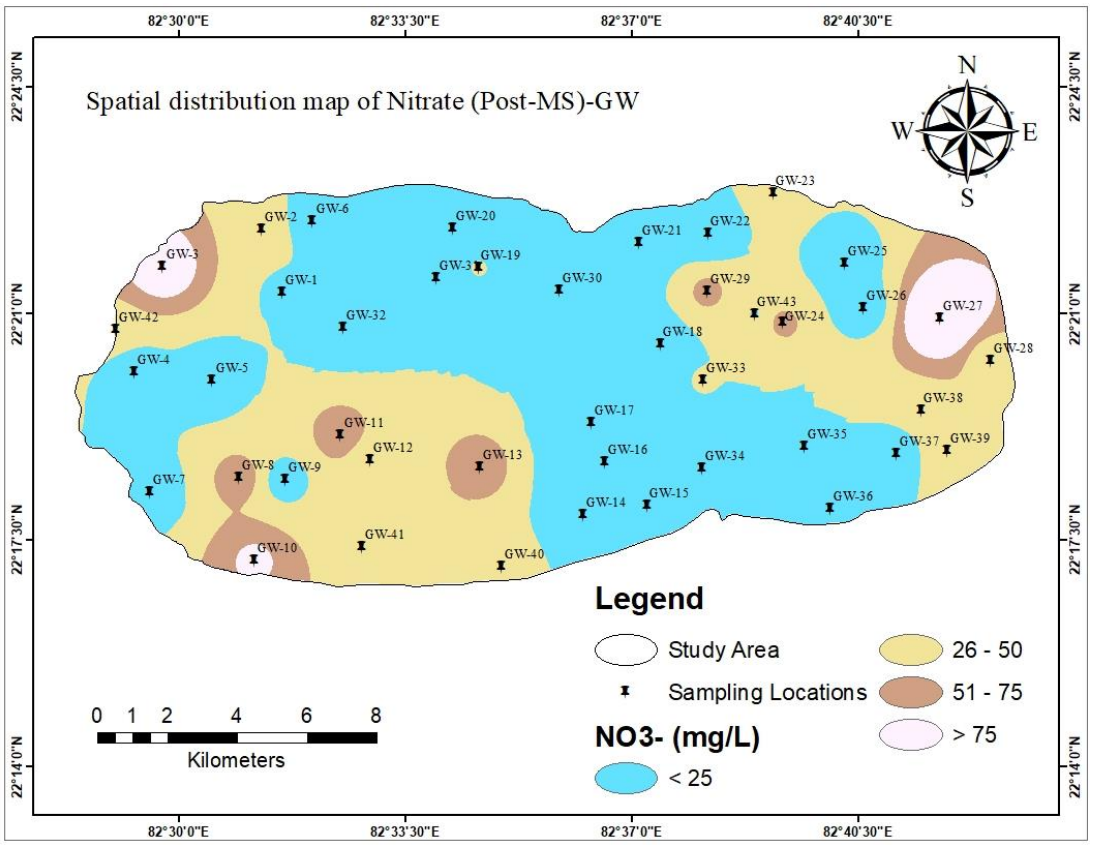

Fig.5.21 Spatial map of Nitrate during post-monsoon season in study region

5.1.1.11 Sulphate

The presence of sulphate concentrations in mining regions is often associated to the oxidation of minerals containing sulphides such as pyrite, anhydrite, arsenopyrite, and gypsum. This phenomenon is considered to be the primary factor contributing to the occurrence of acid mine drainage (Han et al. 2013; Singh et al. 2011). The process of oxidising sulphide in the aquifer materials, along with the leaching of terrestrial sulphate ions, contributed to the higher concentrations of sulphates found in both the aquifer materials and groundwater samples. Higher levels of sulphate concentrations in drinking water have the potential to induce lung disease in individuals.

The sulphate content varied from 0.42 to 162.08 mg/L, with an average of 17.51 mg/L, in pre monsoon and from 0.19 to 274.0 mg/L, with an average of 20.84 mg/L in post monsoon season. It is indicating that only one sample (GW-10) collected during the pre monsoon and three samples (GW-16, 32, and 36) collected during the post monsoon season exceeding the recommended permissible limit of 150 mg/L as per suggested by WHO (2011). Sulphate concentrations exceeded desired limits in a few locations, primarily associated with mining industry and thermal power plants. The runoff from these industries, containing sulphide-rich coal, flows directly into groundwater, thereby causing a high concentration of sulphate in them (Kumar et al. 2019). The spatial map of sulphate concentration reveals that the edge of the south-west in the pre monsoon season and one location of the south side in the post monsoon season had higher sulphate concentrations as shown in Fig.5.22 and Fig.5.23, respectively.

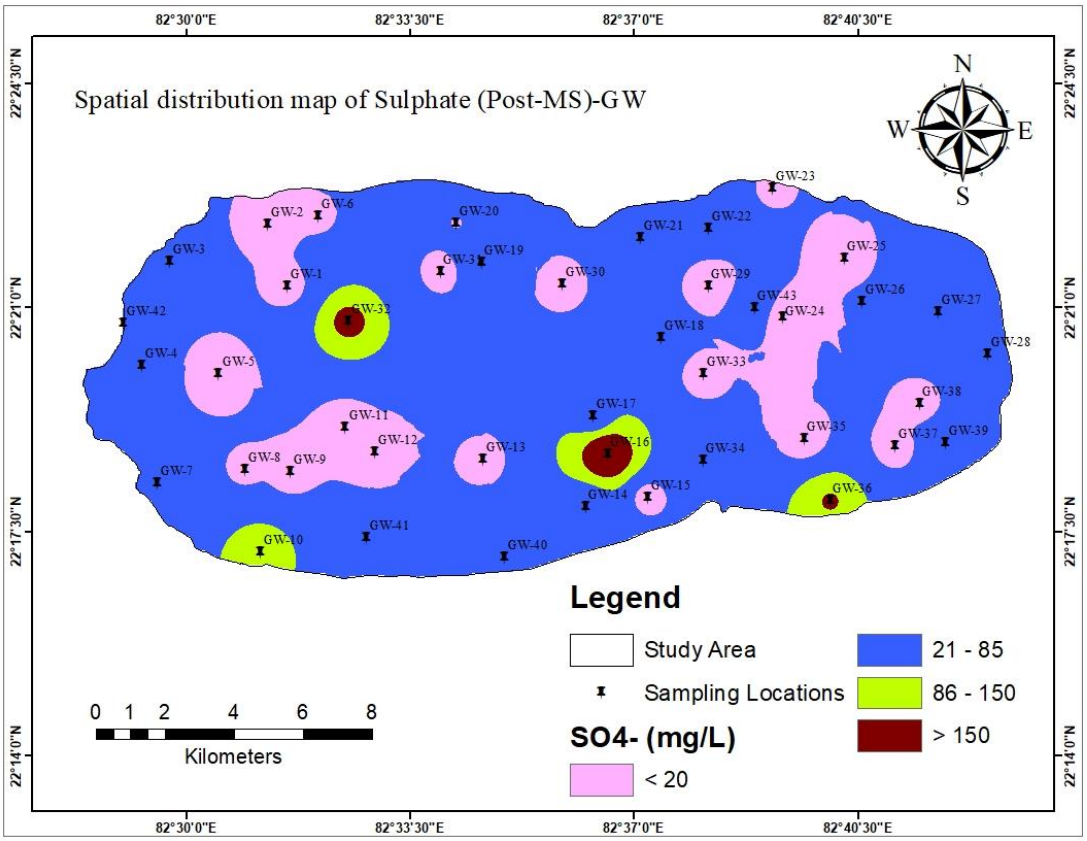

Fig.5.22 Spatial map of Sulphate during pre-monsoon season in study region

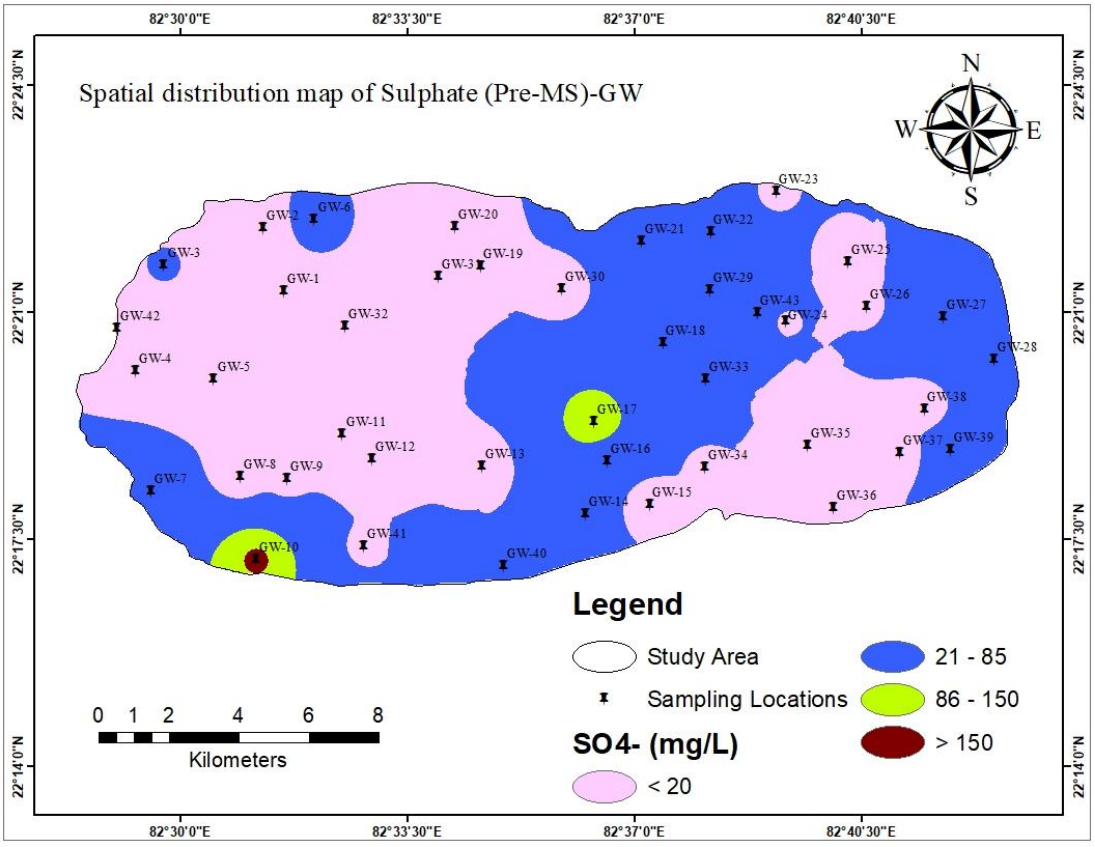

Fig.5.23 Spatial map of Sulphate during post-monsoon season in study region

5.1.1.12 Bicarbonate

The term bicarbonate refers to water's capacity to neutralise hydrogen ions. The amount of bicarbonate in freshwater controls its alkalinity. The concentration of Electrical Conductivity is strongly affected by bicarbonate as well (Tiwari et al. 2016). The elevated bicarbonate concentration in groundwater is caused by carbonate weathering and carbonic acid dissolution (Alaya et al. 2014). The potential risks associated with bicarbonate are often discussed in relation to residual sodium carbonate (RSA), a notable attribute that significantly influences the suitability of water for agricultural use (Adhikary et al. 2011). The high presence of bicarbonate in agricultural soil and its subsequent impact on plants have been observed to have physical and chemical effects, resulting in reduced yields of crops.

The measured bicarbonate concentration ranged from 22 mg/L to 311 mg/L with its mean value of 93 mg/L in the pre monsoon and varies from 34 mg/L to 298 mg/L with its mean value of 79 mg/L in the post monsoon season respectively. It has been observed that only two samples (GW-10 and GW-16) collected from both pre monsoon and post monsoon season exceeded the recommended permissible limit of 200 mg/L as per WHO (2011). Consequently, the primary source of excess HCO_3^- is the soil zone CO_2, parent material weathering, and carbonate mineral dissolution (Appelo and Postma 1993). These minerals are frequently found in coal seams as cleat filling and as a cementing matrix in sandstones of surrounding layers. The spatial map of the HCO_3^- demonstrates that the edge of the south-west and one spot on the south side, had higher HCO_3^- concentrations of during both the pre and post monsoon seasons as shown in Fig.5.24 and Fig.5.25, respectively.

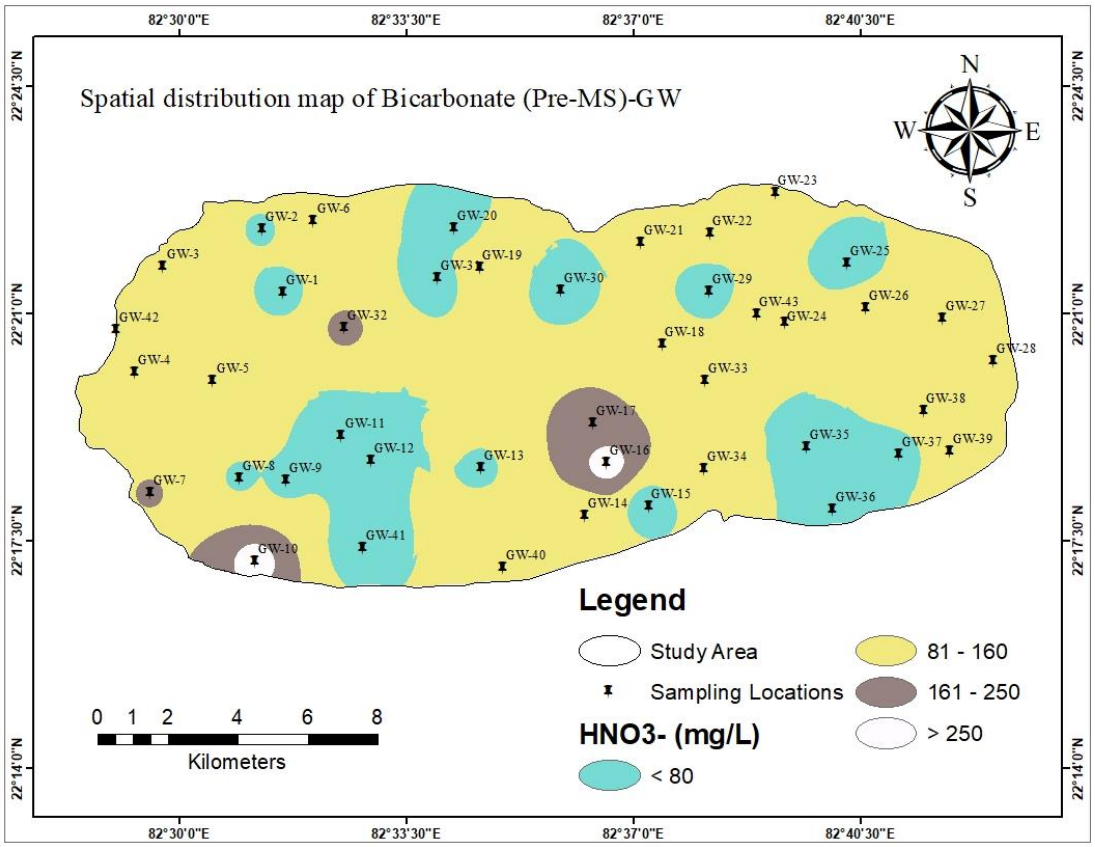

Fig.5.24 Spatial map of Bicarbonate during pre-monsoon season in study region

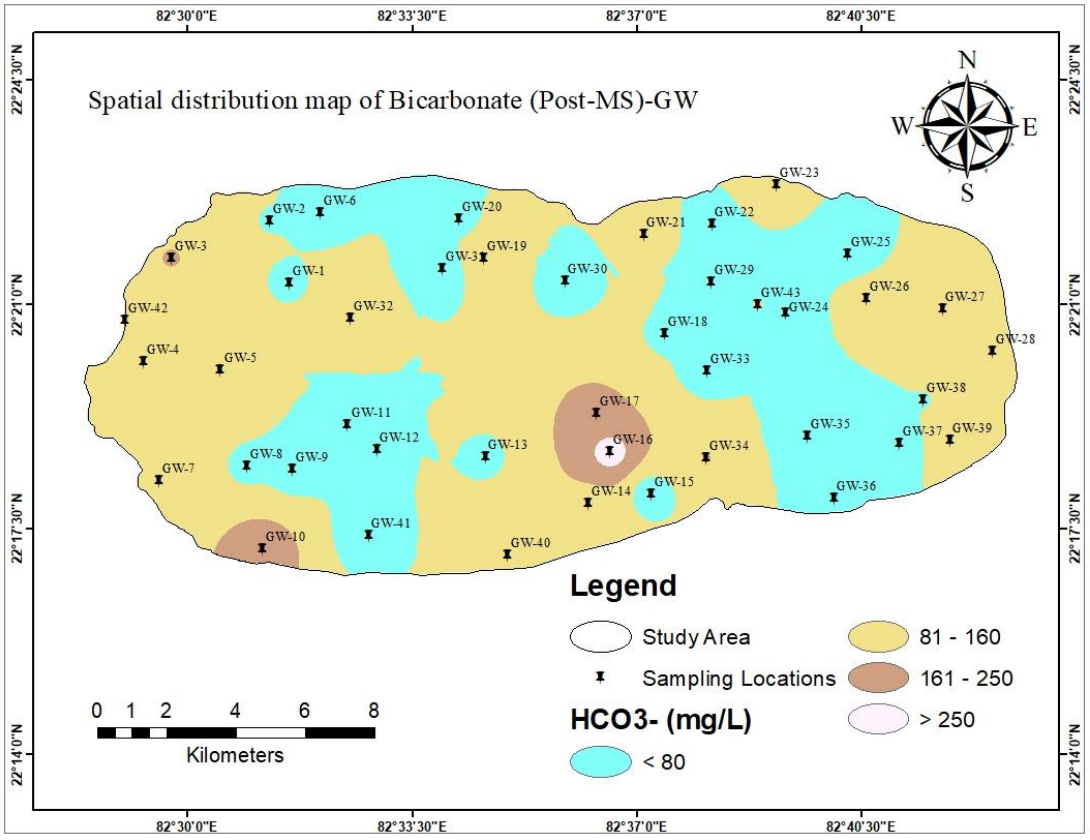

Fig.5.25 Spatial map of Bicarbonate during post-monsoon season in study region

5.1.1.13 Total Hardness

Hardness is defined as the capacity of water to produce a lather being combined with soap. Calcium (Ca^{2+}) and Magnesium (Mg^{2+}) are the two primary minerals that contribute to the hardness of water. The equivalent to the $CaCO_3^{2-}$ concentration is being used to express water hardness. Hardness in water is often caused by a variety of dissolved polyvalent metallic ions, most prominently magnesium and calcium (WHO 2011; Adimalla and Venkatayogi, 2018). In addition, Sawyer and McCarty (1967) classified water hardness into four categories: soft (< 75 mg/L), moderately soft (76–150 mg/L), hard (151–300 mg/L), and extremely hard (> 300 mg/L). It is completely safe for human ingestion despite the fact that it causes an increase in water temperature.

Total Hardness concentrations ranged from 14.54 to 501.18 mg/L, with its mean value of 147.56 mg/L in the pre monsoon while these values ranged of 51.14 to 452.85 mg/L, with its mean value of 111.78 mg/L in post monsoon season respectively. These results demonstrate that one sample (GW-10) exceeded the permissible limit in the pre monsoon whereas all samples were well within the permissible limits of 500 mg/L as per WHO (2011). Most of the samples exhibits Moderately to hard water except GW-10 in the study region. This result suggests that the hardness of water could be due to the leaching of minerals from the surrounding rocks through weathering processes. Additionally, the discharge of effluents from mining and thermal power plants located near the study area may also contribute to the observed water hardness. The spatial map shows that the corner of the south-west had higher concentrations of Total Hardness in the pre monsoon seasons. The spatial map of Total Hardness for both seasons are shown in Fig.5.26 and Fig.5.27, respectively.

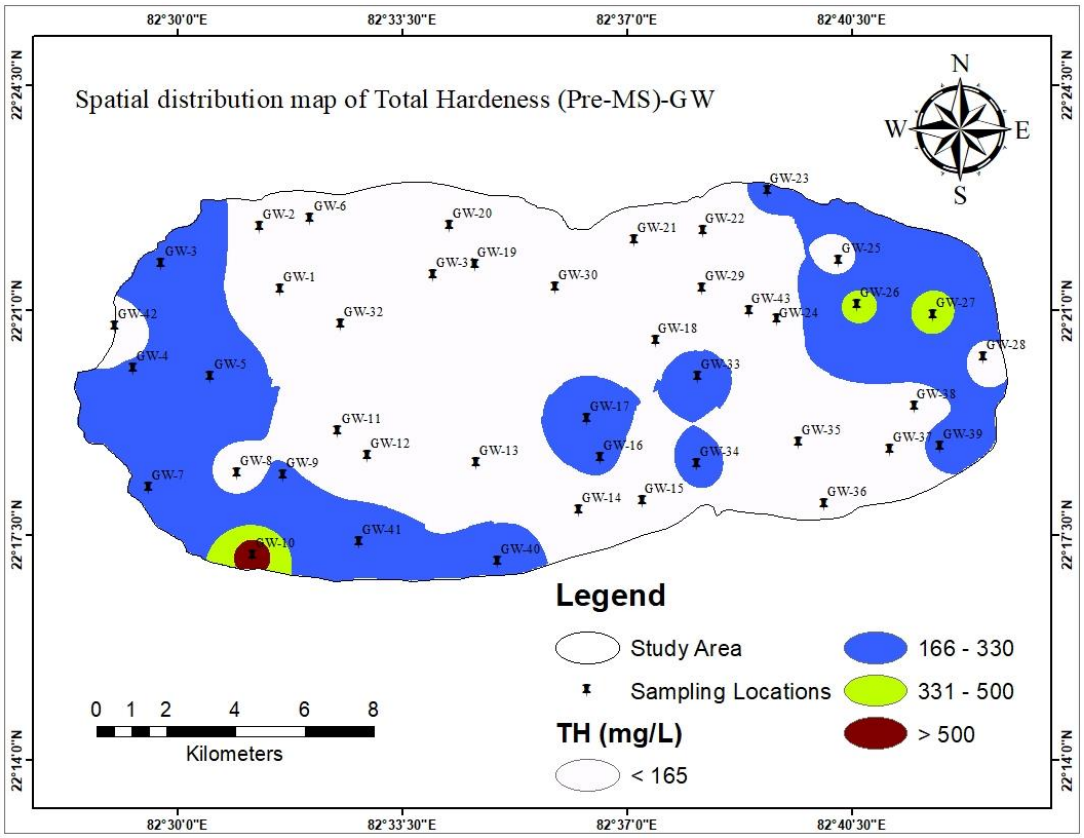

Fig.5.26 Spatial map of Total Hardness during pre-monsoon season in study region

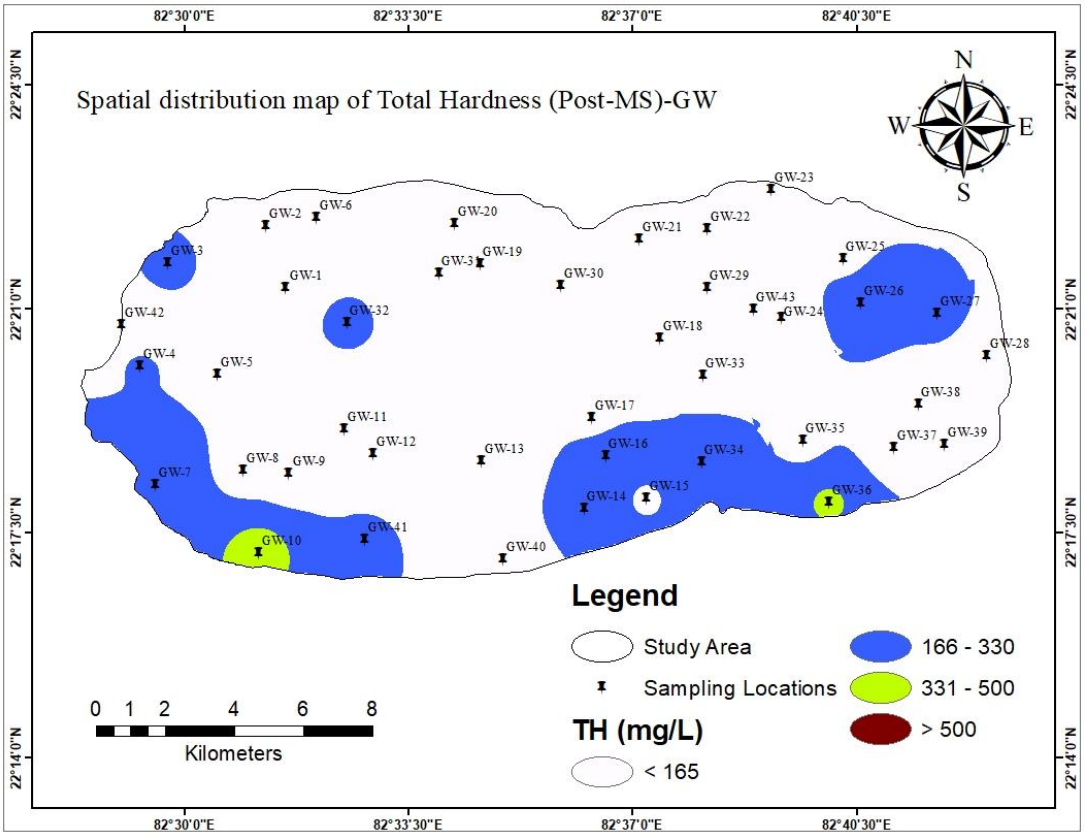

Fig.5.27 Spatial map of Total Hardness during post-monsoon season in study region

5.1.2 Major Ion Chemistry

It appears that major ions, which can have either a positive charge (cations) or a negative charge (anions), are the most common type of dissolved ions in the water. A statistical analysis of the major ions of groundwater samples has been accomplished for the collected samples, which is represented hereunder. The calcium (Ca^{2+}) and sodium (Na^{+}) are two most dominant cation while only HCO_3^- ion is the most dominant anion during both seasons respectively.

5.1.2.1 Cation Chemistry

In terms of cations, calcium (Ca^{2+}) and sodium (Na^{+}) were the most abundant, accounting for 45% and 43% of all cations in the pre and post monsoon seasons. The sodium (Na^{+}) and calcium (Ca^{2+}) ions were the second most abundant cations, accounting for 36% and 35% of total cations in the pre and post monsoon seasons. Only magnesium (Mg^{2+}) ion was a less dominant cation, accounting 16% and 19% of all cations in the pre monsoon and post monsoon seasons. The potassium (K^{+}) ion was least dominant cation, accounting for 3% and 3% of the total cation in the pre monsoon and post monsoon seasons respectively.

The order of most abundant of major cations were $Ca^{2+} > Na^{+} > Mg^{2+} > K^{+}$ in the pre-monsoon season and $Na^{+} > Ca^{2+} > Mg^{2+} > K^{+}$ in the post monsoon season respectively. In an aquifer system, K^{+} levels are typically lower than those of Na^{+}, Ca^{2+}, and Mg^{2+}. The percentage contribution of individual cations in groundwater samples during both seasons were shown in Fig.5.28 and Fig.5.29 respectively.

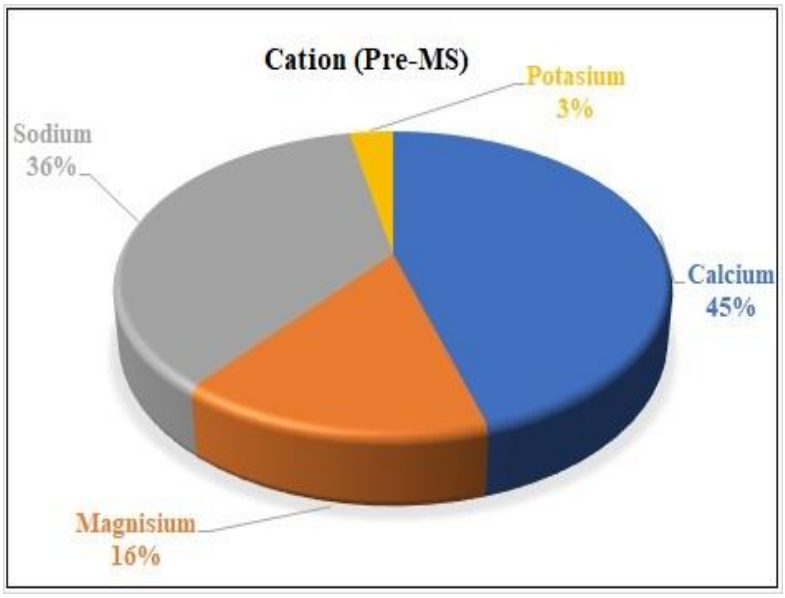

Fig.5.28 Percentage contribution of major cations in pre monsoon season

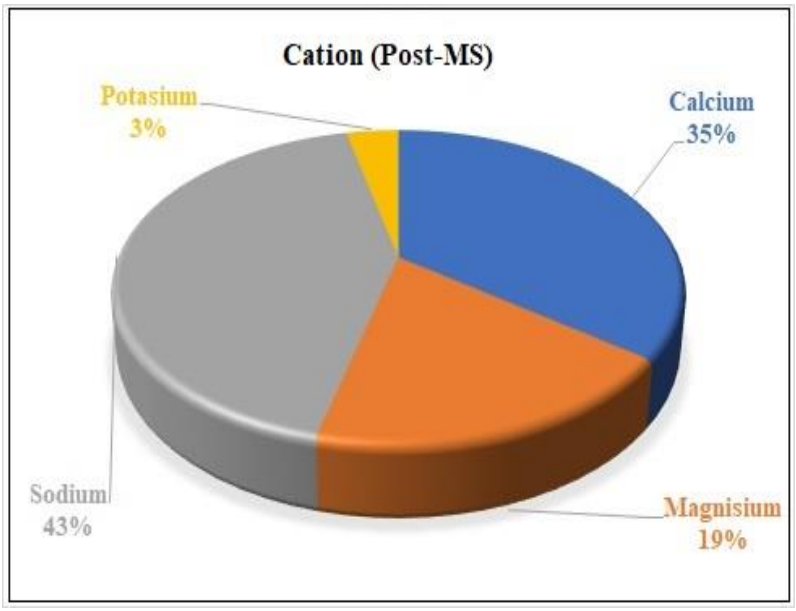

Fig.5.29 Percentage contribution of major cations in post monsoon season

5.1.2.2 Anion Chemistry

The bicarbonate (HCO_3^-) was the most abundant anion, accounting for 57% in pre monsoon and 49% in post monsoon season of all anions. The chlorine (Cl^-) was the second most abundant anion, accounting for 23% in pre monsoon and 26% in post monsoon season of total anions. The Sulphate (SO_4^{2-}), on the other hand, was a less dominant anion, accounting for 11% in pre monsoon and 13% in post monsoon season of all anion. Whereas, the nitrate (NO_3^-) was the least dominant anion, accounting for just 9% in pre

monsoon and 12% in post monsoon season of the total anion. Meanwhile, fluoride (F^-) ions seem to be the single anions to pass in both seasons with 0% contribution.

The order of mean abundance of major anions was $HCO_3^- > Cl^- > SO_4^{2-} > NO_3^- > F^-$ in both pre and post monsoon season respectively. The percentage contribution of individual anions of groundwater samples in pre and post monsoon season were shown in Fig.5.30 and Fig.5.31 respectively.

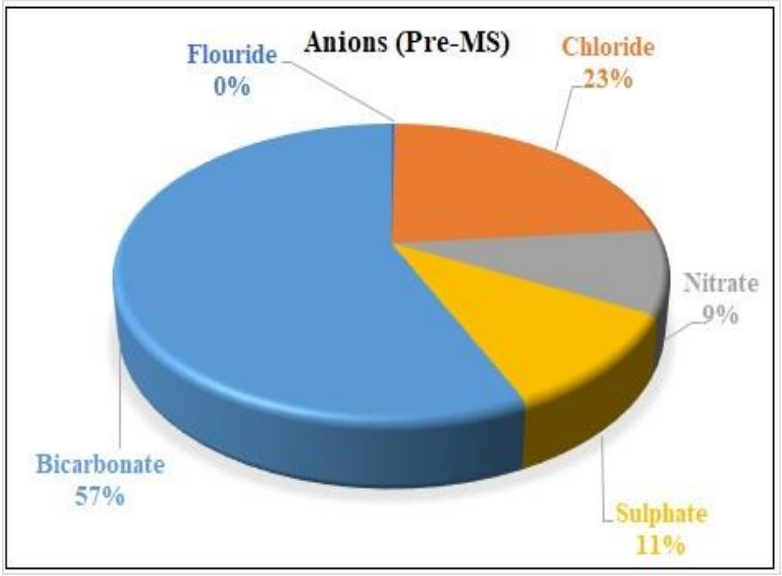

Fig.5.30 Percentage contribution of major anions in pre monsoon season

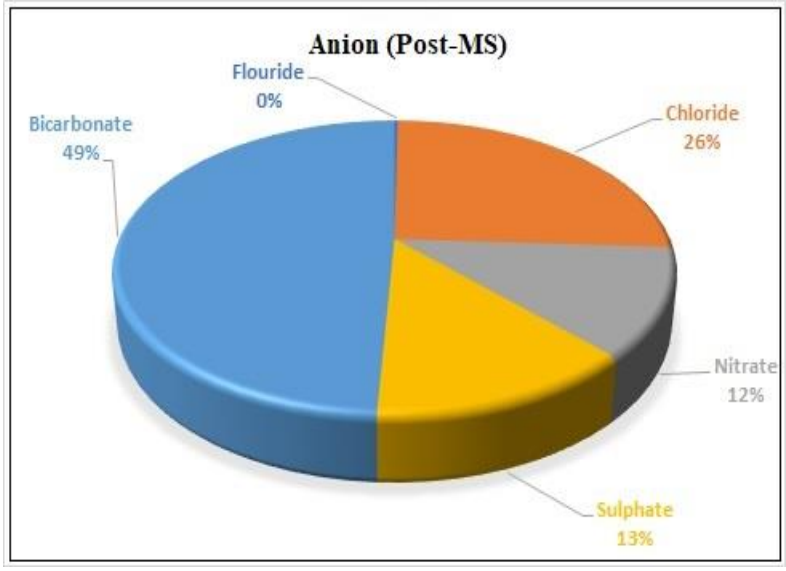

Fig.5.31 Percentage contribution of major anions in post monsoon season

5.1.3 CCME Water Quality Index (WQI) of groundwater samples

The CCME WQI approach was being used to calculate the water quality of groundwater samples for the study area. The Canadian Council of Ministers of the Environment's (CCME) Water Quality Index (WQI) is an efficient method for simplifying complex data regarding water quality and making it simpler to convey this information to a broad audience. The index generates a value from 0 represent lowest water quality to 100 represent excellent water quality. Moreover, these scores are classified into five distinct categories to make presentation simpler (Marine, 1999) as given in Table 5.4.

Table.5.4 CCME WQI category with its specifications

Ranking	CCME WQI	Water quality characteristics
Excellent	95-100	Water quality passes all standards for usage as a drinking water source.
Good	80-94	Water quality rarely or narrowly violates standards for usage as a drinking water source.
Fair	65-79	Water quality occasionally violates criteria for usage as a source of drinking water, possibly by a significant margin.
Marginal	45-64	Water quality frequently exceeds criteria for usage as a source of drinking water by a wide margin.
Poor	0-44	Water quality does not meet any of the standards for usage as a drinking water source.

The CCME WQI, method is being used to assess the water quality for a range of potential applications, including agricultural, the preservation of aquatic life, and production of purified water for drinking (Khan et al. 2003, 2004; Lumb et al. 2006). The higher concentrations major ion in groundwater have instant effect on their quality were found to be the cause of the lower value of the CCME WQI. The significance of calcium and magnesium concentration in water is evidence of water hardness in the water samples.

The CCME WQI values along with status of groundwater quality is given in Table.5.7 for the pre and Table.5.8 for post monsoon seasons respectively.

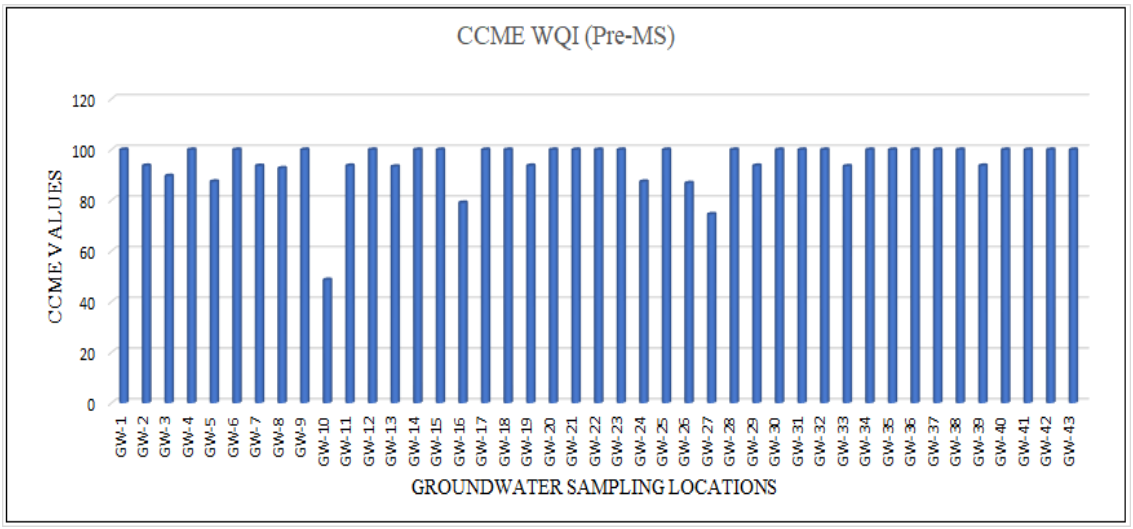

Fig.5. 32 Graphical representation of CCME WQI during pre-monsoon season

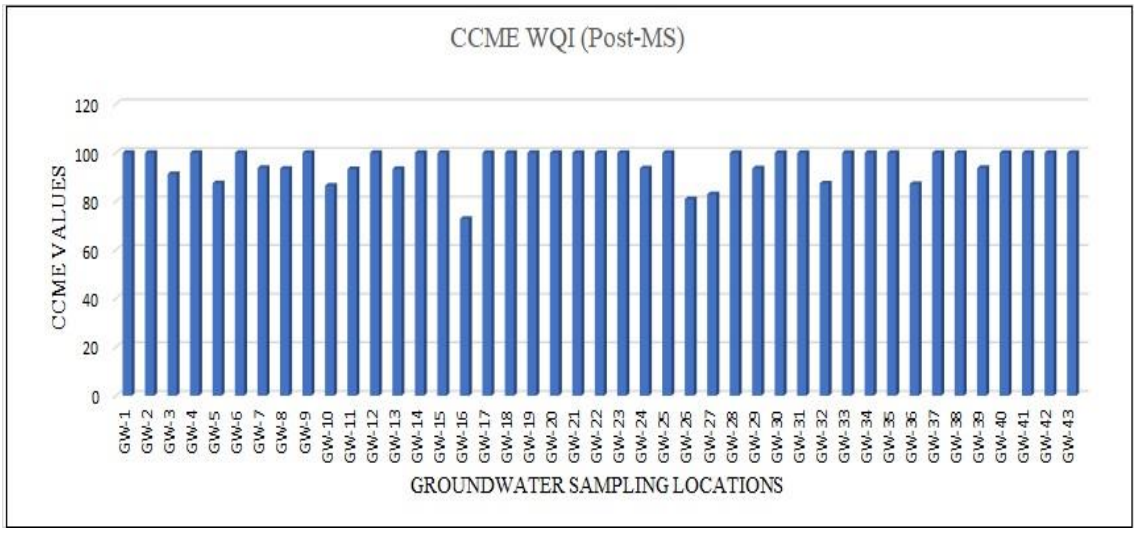

Fig.5. 33 Graphical representation of CCME WQI during post monsoon season

The CCME WQI of groundwater samples ranged from 48.63 to 100, indicating that 27 (62.79%) groundwater samples were categorised as excellent, 13 (30.23%) samples as good, 2 (4.65%) samples as fair, and rest 1 (2.3%) sample as marginal during the pre-monsoon season. No samples were assigned to the poor class of CCME WQI. Only two sample (GW-16 and GW-27) were found in the fair category, while only one sample (GW-10) was detected in the marginal category and rest 40 (93.02%) samples belong to

excellent to good category of water quality in the pre monsoon season. The spatial map of CCME WQI demonstrates that the east and south western sides of the area had lower CCME WQI values, whereas north, south, and south eastern area had higher CCME WQI values. This finding indicates that the groundwater of the area is safe for drinking and other uses in the pre monsoon season. The Bar chart and spatial map of CCME WQI of the area in pre monsoon season has been shown in Fig.5.32 and Fig.5.34 respectively.

The CCME WQI of groundwater samples ranged from 72.79 to 100 during the post-monsoon season. It indicates that 28 (65.12%) groundwater samples were excellent, 14 (32.56%) samples were good, and rest 1 (2.33%) samples were fair. However, 1 (GW-16) sample was found to be in fair category while the other 42 (97.67%) samples were found to be in the excellent to good category of water quality in the post monsoon season. Water quality exhibits significant variability due to a range of factors such as spatial, temporal, and random in nature. Addressing these variations is crucial for an accurate assessment of water resources such as geological differences**,** hydrological, LULC changes, seasonal changes, sampling errors, microbial activity, weather fluctuations. The spatial map of the CCME WQI shows that the water samples of north, west, and south-east part of the area are safe for drinking and other uses during the post monsoon season.

The quality of water is observed to enhance during the post monsoon season in comparison to the pre monsoon season. The enhancement can be attributed to a variety of physicochemical characteristics, which have a notable impact on defining water quality. These enhancement in the water quality could be attributed to the dilution effects caused by high rainfall in the area (Singh et al., 2017). The Bar chart and spatial map of CCME WQI in post monsoon season has been shown in Fig.5.33 and Fig.5.35 respectively. The pie chart of CCME WQI for pre and post monsoon season were shown in Fig.5.36 and Fig.5.37 respectively.

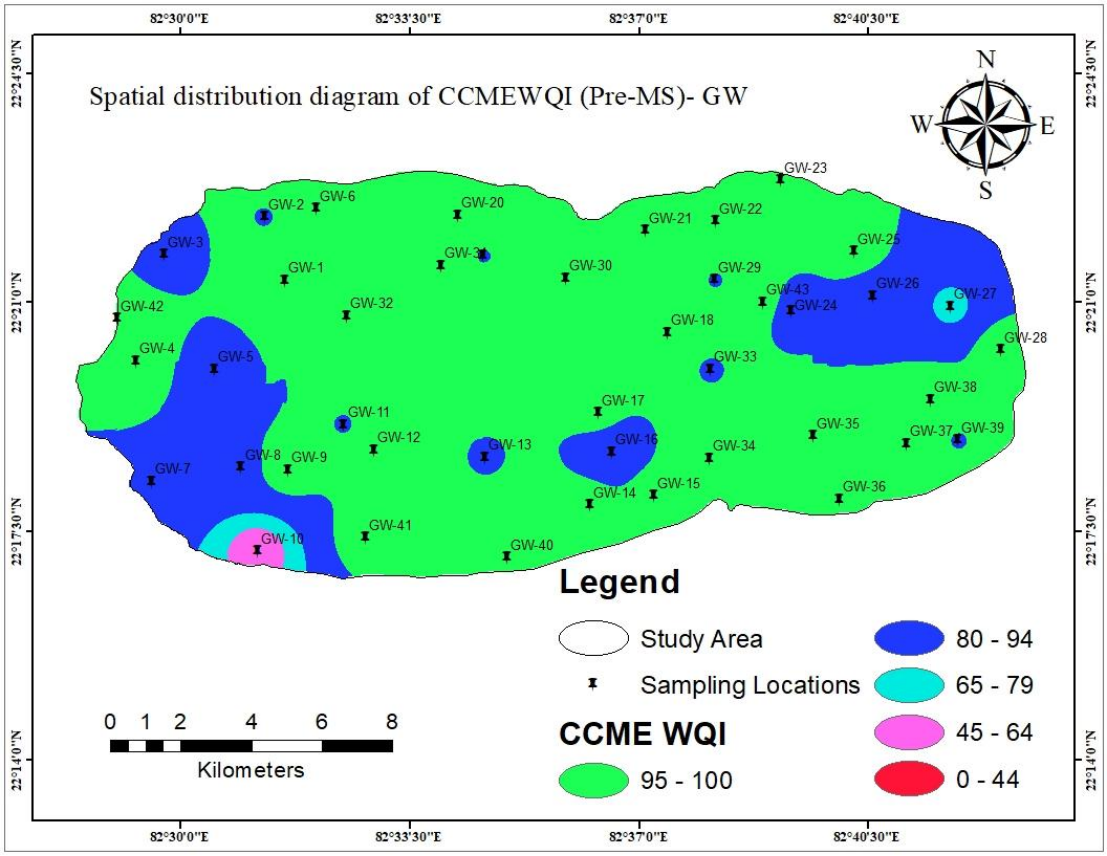

Fig.5.34 Spatial map of CCME WQI during pre-monsoon season in study region

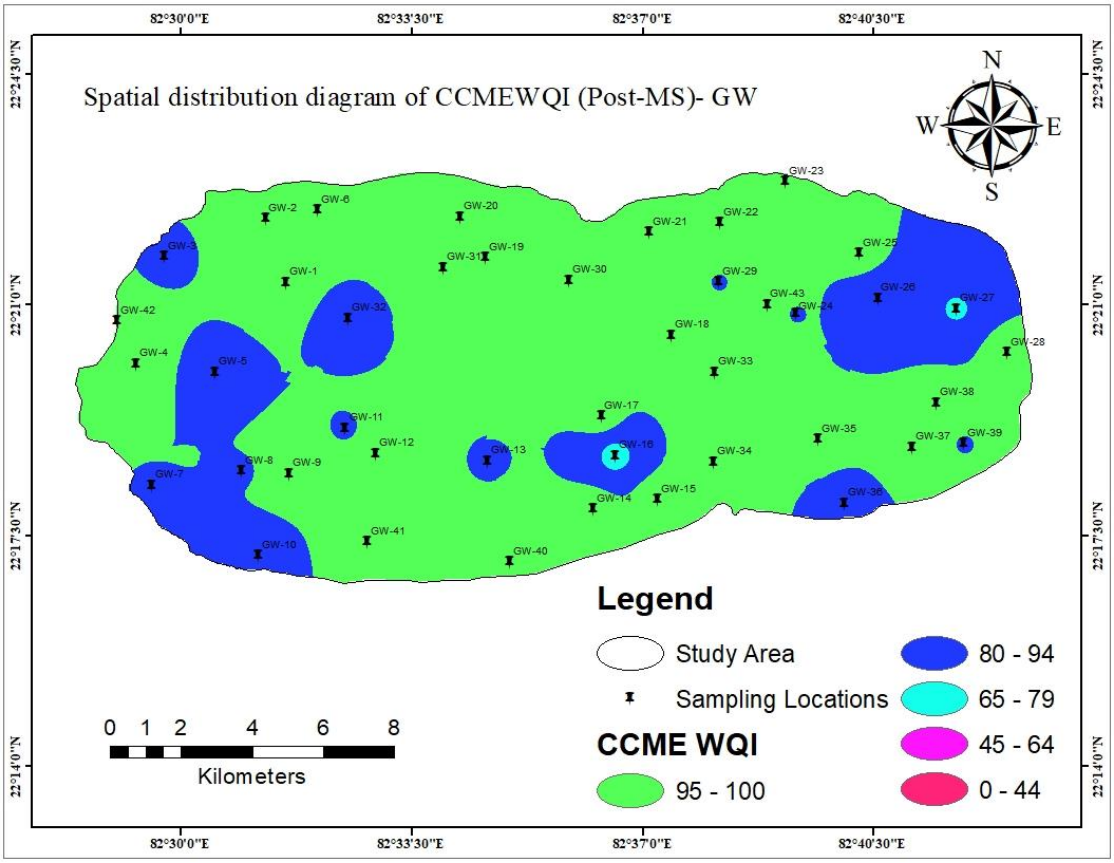

Fig.5.35 Spatial map of CCME WQI during post monsoon season in study region

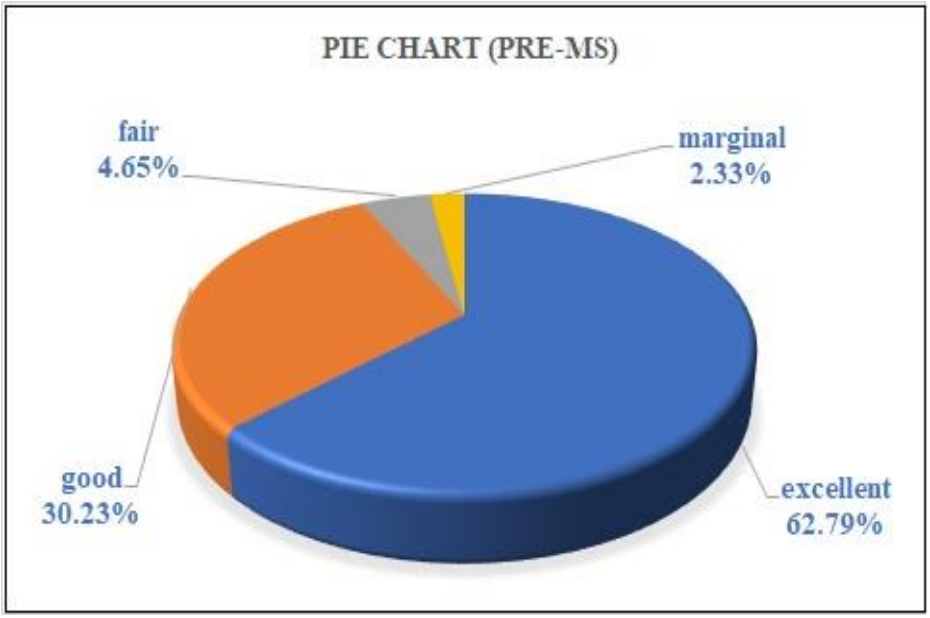

Fig.5.36 Pie chart showing CCME WQI category in pre monsoon season

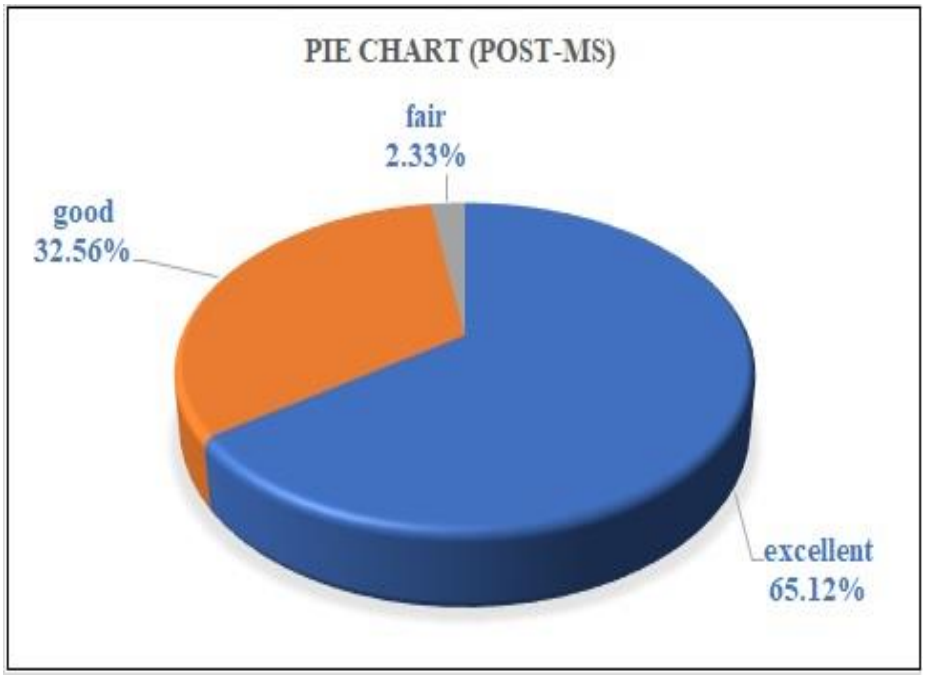

Fig.5.37 Pie chart showing CCME WQI category in post monsoon season

5.1.4 Statistical Analysis of groundwater Samples

Correlation matrix analysis technique is applied to assess the degree of linear relationship and the proximity between two independent variables. By doing an analysis of correlation matrices, it is possible to ascertain the degree of closeness between two variables (Singh et al. 2012; Dheeraj et al. 2020). Multivariate statistics is a significant technique for comprehensively evaluating large datasets, as it not only facilitates the identification of significant patterns but also serves as a powerful tool for interpreting complex data matrices within a certain domain. Therefore, as a result, multivariate analysis is an essential technique for identifying the similar as well as dissimilar features used in the evaluation of the water samples. Hence, this study has been applied multivariate techniques such as correlation analysis and Box whisker plot.

5.1.4.1 Statistical correlation

The Pearson correlation coefficient matrix represents the measure of variance for each parameter used in groundwater analysis and their relationship as well (Liu et al, 2003). The correlation coefficient ranges from -1 to +1, where a value of -1 indicates a significant negative relationship, a value of +1 indicates a strong positive correlation between two variables, and a value of 0 indicates no association between the two variables. This technique depicts the statistical association between two or more independent variables, which makes it easier to identify the processes that are responsible for the existing water chemistry. Additionally, for the research field, the correlation analysis facilitates in measure the extent of connection between the two parameters and in providing a general concept of their relationship (Peat et al 2009). The correlation coefficient matrix for the two seasons was evaluated, considering the temporal changes throughout the pre and post monsoon seasons.

The correlation coefficients (r) between 13 parameters were calculated during pre monsoon and post monsoon season and their existed correlation are tabulated as given in Table.5.5 and Table.5.6 respectively. It was found that out of 91 correlation coefficients, 13 were negative and 78 were positive in pre monsoon season. The measured positive correlations between parameters made it evident that the parameters were related to one another and might have come from the same origins within the study area (Mohamed et al. 2003). Therefore, a strong positive correlation were observed between parameters such as EC and TDS (r = 0.999), EC and HCO_3^- (r = 0.898), TDS and HCO_3^- (r = 0.866), TH and Mg^{2+} (r = 0.821), TH and Na^+ (r = 0.968), TH and Cl^- (r = 0.861), Na^+ and Cl^- (r = 0.872) in pre monsoon season, whereas a strong negative correlation observed between pH and Cl^- (r = -0.206), F^- and NO_3^- (r = -0.398), pH and NO_3^- (r = -0.179) respectively.

Similarly, it was observed that out of 91 correlation coefficients 6 were negative and 85 were positive during the post-monsoon season. The strong positive correlations were identified between parameters such as EC and TDS (r = 0.997), EC and HCO_3^- (r = 0.908), TDS and HCO_3^- (r = 0.910), TH and Mg^{2+} (r = 0.885), whereas a negative correlation identified between pH and K^+ (r = -0.178), pH and NO_3^- (r = -0.307), F^- and NO_3^- (r = -0.334) during the post monsoon season respectively.

Table.5.5 Correlation coefficient matrix of groundwater in pre-monsoon season

	pH	EC	TDS	TH	Ca^{+}	Mg^{2+}	Na^{+}	K^{+}	F^{-}	Cl^{-}	NO_3^{-}	SO_4^{2+}	HCO_3^{-}
pH	1.000												
EC	-0.013	1.000											
TDS	-0.003	0.999	1.000										
TH	-0.050	0.709	0.703	1.000									
Ca^{2+}	-0.121	0.605	0.603	0.498	1.000								
Mg^{2+}	-0.029	0.676	0.666	0.821	0.510	1.000							
Na^{+}	-0.053	0.645	0.641	0.968	0.438	0.652	1.000						
K^{+}	-0.108	0.241	0.240	0.157	0.429	0.127	0.152	1.000					
F^{-}	0.247	0.324	0.322	0.265	0.243	0.469	0.145	0.167	1.000				
Cl^{-}	-0.206	0.572	0.563	0.861	0.482	0.620	0.872	0.184	-0.041	1.000			
NO_3^{-}	-0.179	0.236	0.227	0.367	0.067	0.130	0.431	0.091	-0.398	0.586	1.000		
SO_4^{2+}	-0.122	0.487	0.478	0.567	0.175	0.612	0.485	0.071	0.213	0.468	0.117	1.000	
HCO_3^{-}	-0.078	0.898	0.896	0.641	0.455	0.666	0.559	0.127	0.344	0.513	0.163	0.619	1.000

Table.5.6 Correlation coefficient matrix of groundwater in post-monsoon season

	pH	EC	TDS	TH	Ca^{+}	Mg^{2+}	Na^{+}	K^{+}	F^{-}	Cl^{-}	NO_3^{-}	SO_4^{2+}	HCO_3^{-}
pH	1.000												
EC	0.396	1.000											
TDS	0.408	0.997	1.000										
TH	0.533	0.627	0.629	1.000									
Ca^{2+}	0.294	0.587	0.590	0.670	1.000								
Mg^{2+}	0.511	0.450	0.450	0.885	0.247	1.000							
Na^{+}	0.339	0.598	0.606	0.621	0.249	0.655	1.000						
K^{+}	-0.178	0.269	0.256	0.211	0.410	0.018	-0.031	1.000					
F^{-}	0.740	0.459	0.471	0.672	0.395	0.629	0.395	0.044	1.000				
Cl^{-}	0.017	0.577	0.535	0.447	0.323	0.381	0.646	0.175	0.024	1.000			
NO_3^{-}	-0.307	0.201	0.171	0.022	-0.168	0.134	0.378	0.102	-0.334	0.571	1.000		
SO_4^{2+}	0.473	0.665	0.674	0.541	0.360	0.480	0.270	0.196	0.423	0.104	-0.018	1.000	
HCO_3^{-}	0.388	0.908	0.910	0.569	0.490	0.435	0.512	0.203	0.419	0.482	0.108	0.685	1.000

5.1.4.2 Box and Whisker Plot Analysis for groundwater samples

The box plot known as box and whiskers plot is a tool for quick summarising and interpreting tabular data. It can be useful for showing trends even in very large data sets since they smooth out numerical details while preserving essential information about the distribution. A variety of statistical methods known as the exploratory data analysis, such as box plot was used to clearly identify trends in data sets that might otherwise go unnoticed (Williamson et al. 1989). A box plot is a graphical representation that depicts a unimodel distribution (Rossiter, 2007). The box plot technique is used to identify statistically significant variations across multiple physicochemical characteristics by examining the medians related to these parameters. This statistical technique has been employed to assess water quality by considering the quartile distribution of various water quality metrics. Moreover, it is used to display physicochemical parameter concentrations, includes means, maximums, and minimums.

The comparison study of several physicochemical parameters is shown respective for pre and post monsoon season datasets, as shown in Fig.5.38 (i) to (vi). According to the statistical data, the pH level exhibits slightly more alkaline during the post-monsoon season compared to the pre-monsoon season. Meanwhile, EC, TDS, and Total Hardness levels in pre monsoon were significantly higher than post monsoon season as shown in Fig.5.38 (i) & (ii). The concentration of anions such as F^-, Cl^-, NO_3^-, SO_4^{2-}, and HCO_3^- were higher in the pre-monsoon season than the post-monsoon season as shown in Fig.5.38 (iii) & (iv). The concentrations of cations, specifically Ca^{2+} and K^+ exhibited higher levels during the pre-monsoon season compared to the post-monsoon season. However, the concentrations of Mg^{2+} and Na^+ were notably lower during the pre-monsoon season as shown in Fig.5.38 (v) & (vi) respectively.

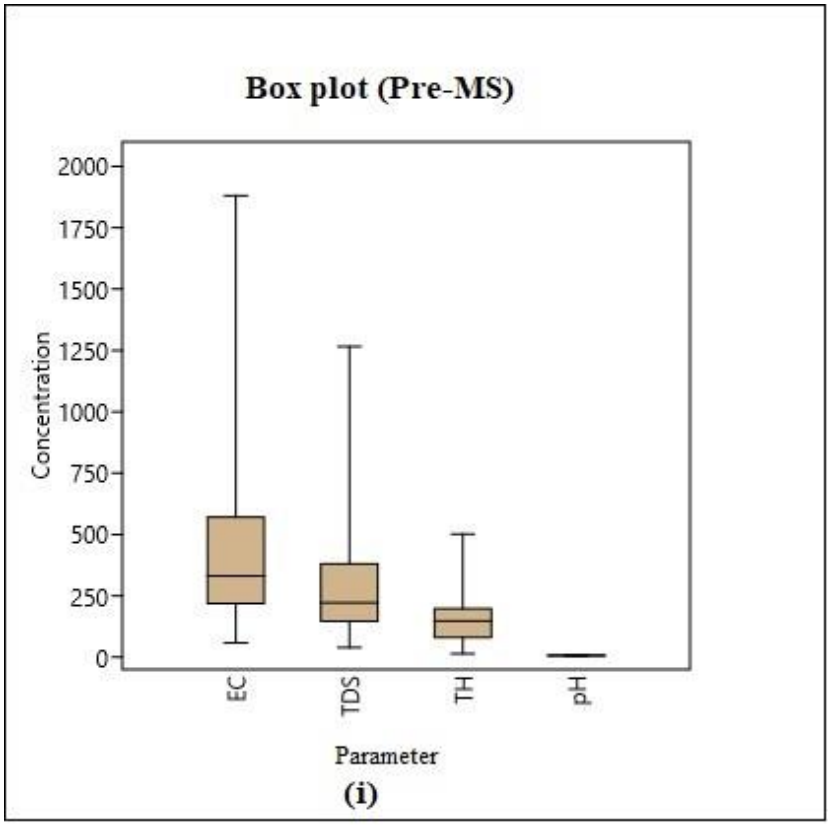
Box plot (Pre-MS)
2000
1750
1500
1250
1000
750
500
250
0
Concentration
EC
TDS
TH
pH
Parameter

(i)

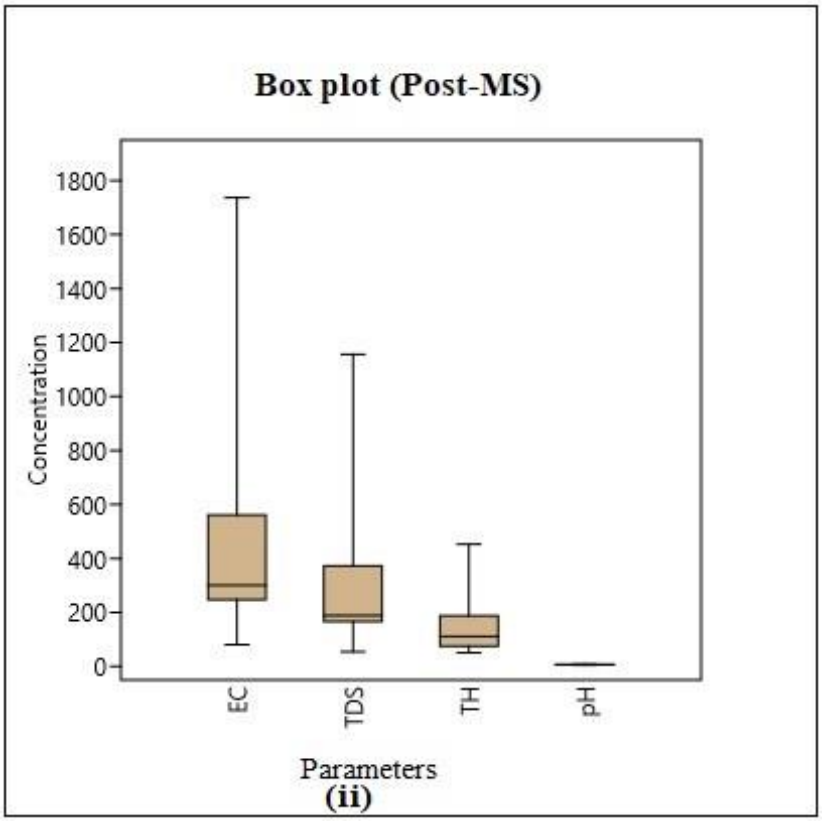
Box plot (Post-MS)
1800
1600
1400
1200
1000
800
600
400
200
0
Concentration
EC
TDS
TH
pH
Parameters

(ii)

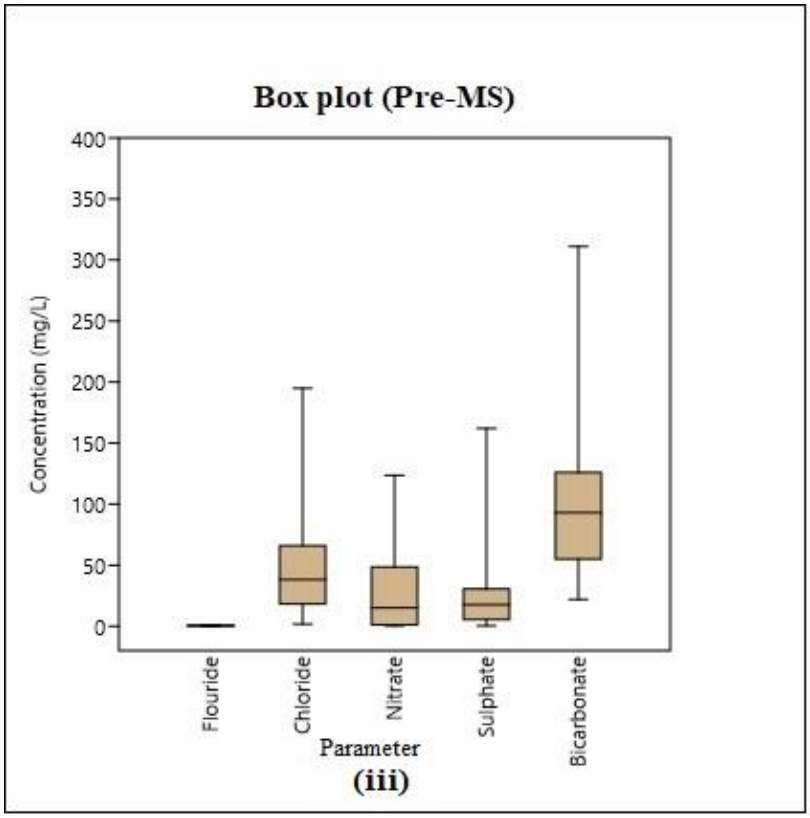
Box plot (Pre-MS)
Concentration (mg/L)
400
350
300
250
200
150
100
50
0
Flouride
Chloride
Nitrate
Sulphate
Bicarbonate
Parameter

(iii)

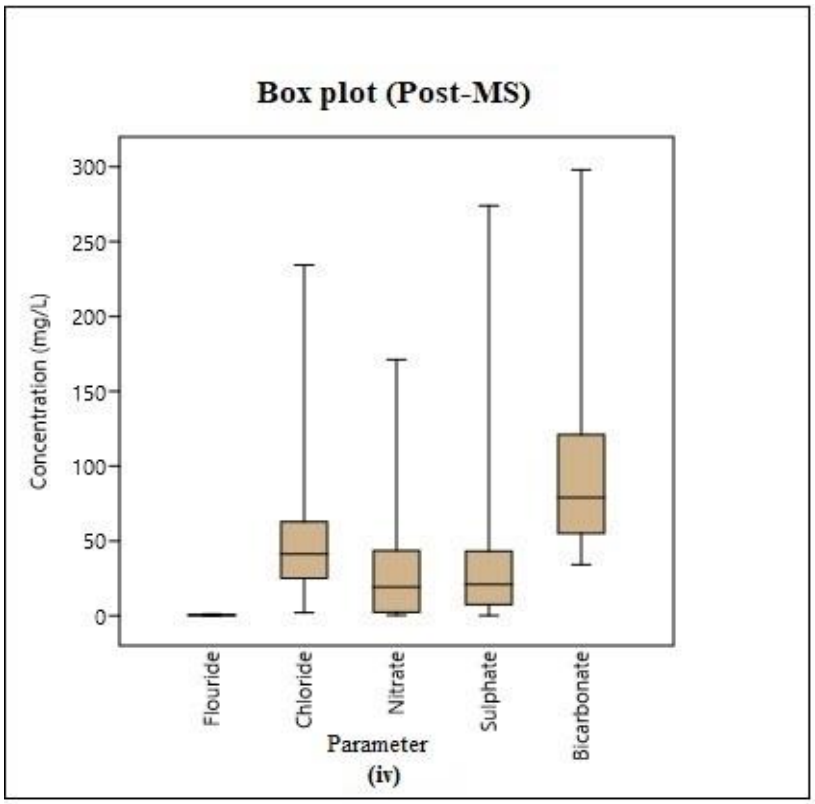
Box plot (Post-MS)
Concentration (mg/L)
300
250
200
150
100
50
0
Flouride
Chloride
Nitrate
Sulphate
Bicarbonate
Parameter

(iv)

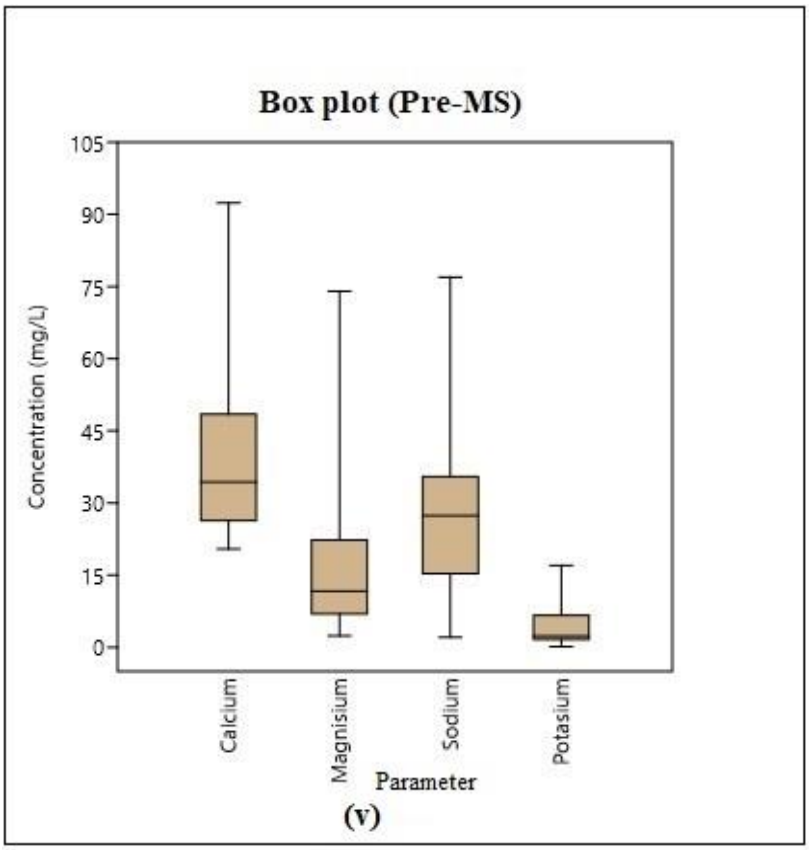

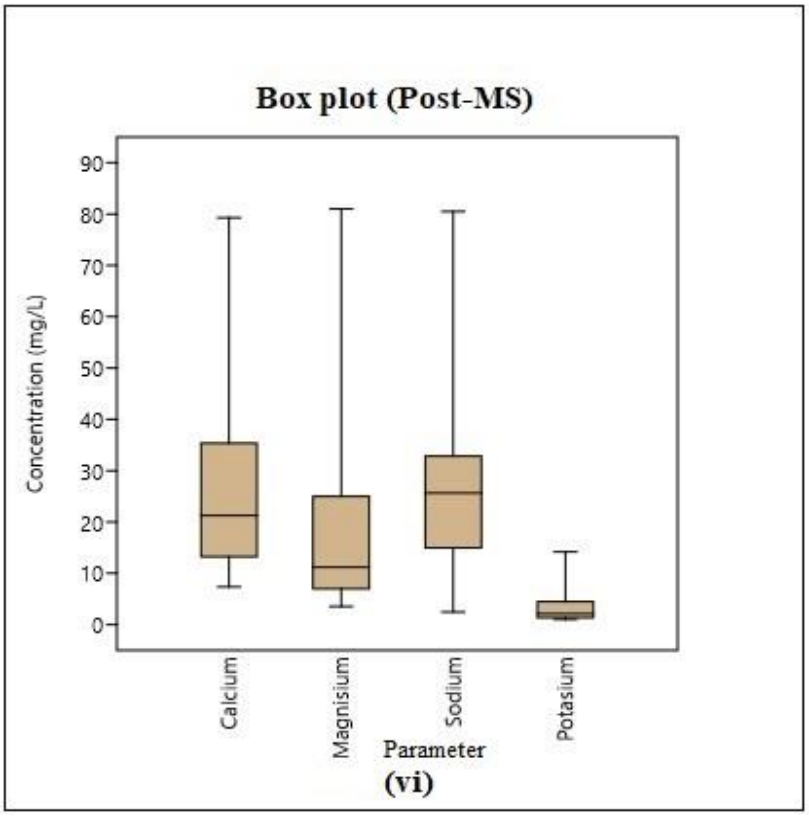

Fig.5.38 (i) to **(vi)** Box plot of physicochemical parameters in pre & post monsoon season

Table.5.7 CCME WQI value and its category in groundwater during pre-monsoon season

Sample code	Sampling locations	CCME WQI	Description
GW-1	Jhabar hand pump water	100	Excellent
GW-2	Batari Dugwell water	93.69	Good
GW-3	Tiverta hand pump water	89.64	Good
GW-4	Ratija borewell water	100	Excellent
GW-5	Chainpur bore well water	87.42	Good
GW-6	Binjhari bore well water	100	Excellent
GW-7	Andikachhar bore well water	93.62	Good
GW-8	Renki bore well water	92.69	Good
GW-9	Suwabhondi borewell water	100	Excellent
GW-10	Suberpara handpunp water	48.63	Marginal
GW-11	Malgaon borewell water	93.71	Good
GW-12	Haldibazar borewell water	100	Excellent
GW-13	Raliya bore well water	93.34	Good
GW-14	Mahowadih borewell water	100	Excellent
GW-15	Keshla hand pump water	100	Excellent
GW-16	Bhilaibazar borewell water	79.08	Fair
GW-17	Bethora dug well water	100	Excellent
GW-18	Mangaon borewell water	100	Excellent
GW-19	Durena borewell water	93.68	Good
GW-20	Durena dugwell water	100	Excellent
GW-21	Rohina borewell water	100	Excellent
GW-22	Bhairotal borewell water	100	Excellent
GW-23	Balkikhar dugwell water	100	Excellent
GW-24	Barpali borewell water	87.39	Good
GW-25	Hasdev power plant bore water	100	Excellent
GW-26	Durpa handpump water	86.83	Good
GW-27	Patel Nagar borewell water	74.54	Fair
GW-28	Sitamadi borewell water	100	Excellent
GW-29	Kuchaina mod borewell water	93.72	Good
GW-30	Awadh Nagar road borewell water	100	Excellent
GW-31	Vijay Nagar handpump water	100	Excellent
GW-32	Dhara chauk Dipka borewell water	100	Excellent
GW-33	Gevra basti hand pump water	93.48	Good
GW-34	Salora handpump water	100	Excellent
GW-35	Rishdi borewell water	100	Excellent
GW-36	Ghanadabri borewell water	100	Excellent
GW-37	Padhania borewell water	100	Excellent
GW-38	Chandra nagar handpump water	100	Excellent
GW-39	Sonpuri borewell water	93.71	Good
GW-40	Mudhali handpump water	100	Excellent
GW-41	Bamhanikona borewell water	100	Excellent
GW-42	Ratija ka para dugwell	100	Excellent
GW-43	Vikash Nagar borewell water	100	Excellent

Table.5.8 CCME WQI value and its category during post monsoon season

Sample code	Sampling locations	CCME WQI	Description
GW-1	Jhabar hand pump water	100	Excellent
GW-2	Batari Dugwell water	100	Excellent
GW-3	Tiverta hand pump water	91.23	Good
GW-4	Ratija borewell water	100	Excellent
GW-5	Chainpur bore well water	87.42	Good
GW-6	Binjhari bore well water	100	Excellent
GW-7	Andikachhar bore well water	93.71	Good
GW-8	Renki bore well water	93.43	Good
GW-9	Suwabhondi borewell water	100	Excellent
GW-10	Suberpara handpunp water	86.44	Good
GW-11	Malgaon borewell water	93.25	Good
GW-12	Haldibazar borewell water	100	Excellent
GW-13	Raliya bore well water	93.36	Good
GW-14	Mahowadih borewell water	100	Excellent
GW-15	Keshla hand pump water	100	Excellent
GW-16	Bhilaibazar borewell water	72.79	Fair
GW-17	Bethora dug well water	100	Excellent
GW-18	Mangaon borewell water	100	Excellent
GW-19	Durena borewell water	100	Excellent
GW-20	Durena dugwell water	100	Excellent
GW-21	Rohina borewell water	100	Excellent
GW-22	Bhairotal borewell water	100	Excellent
GW-23	Balkikhar dugwell water	100	Excellent
GW-24	Barpali borewell water	93.6	Good
GW-25	Hasdev power plant bore water	100	Excellent
GW-26	Durpa handpump water	80.88	Good
GW-27	Patel Nagar borewell water	82.92	Good
GW-28	Sitamadi borewell water	100	Excellent
GW-29	Kuchaina mod borewell water	93.54	Good
GW-30	Awadh Nagar road borewell water	100	Excellent
GW-31	Vijay Nagar hand pump water	100	Excellent
GW-32	Dhara chauk Dipka borewell water	87.39	Good
GW-33	Gevra basti handpump water	100	Excellent
GW-34	Salora handpump water	100	Excellent
GW-35	Rishdi borewell water	100	Excellent
GW-36	Ghanadabri borewell water	87.14	Good
GW-37	Padhania borewell water	100	Excellent
GW-38	Chandra nagar handpump water	100	Excellent
GW-39	Sonpuri borewell water	93.71	Good
GW-40	Mudhali handpump water	100	Excellent
GW-41	Bamhanikona borewell water	100	Excellent
GW-42	Ratija ka para dugwell	100	Excellent
GW-43	Vikash Nagar borewell water	100	Excellent

5.1.4.3 Hierarchical Cluster Analysis

Hierarchical Cluster Analysis (HCA) is a method that divides observations into clusters by considering their similarities or dissimilarities. This process intends to achieve a high level of homogeneity within each cluster and a high level of variation across different clusters (Singh et al. 2005). Cluster analysis is a statistical method that is used to group elements together based on their attribute values (Simeonova et al. 2003). The primary objective of cluster analysis is to categorise different entities based on a selected criterion that exhibits a significant level of homogeneity within each cluster and a substantial level of heterogeneity among the clusters. HCA is the most commonly used method for determining the association between samples and data sets (McKenna et al. 2003). The HCA results of two monsoon samples were shown using dendrograms with Ward's linkage method of Squared Euclidean distance which serving as a measure of similarity.

The sampling points might be clustered based on chemical and CCME WQI similarity in collected samples from different locations (Shreshtha and Kazama, 2006). The water samples are categorised based on similar observation sites in terms of chemical composition using HCA or dendrogram. The HCA is being utilised in this study to cluster the 43 sampling locations based on CCME WQI throughout both seasons separately. This is being done with the purpose of spatially evaluating the pattern of the water quality index during selected seasons.

The results of the study revealed that the total of 43 sites were categorised into three distinct clusters. Among these clusters, Cluster-I exhibited the highest number of sampling sites, comprising 27 sites (GW-42, GW-43, GW-41, GW-40, GW-38, GW-37, GW-36, GW-35, GW-34, GW-32, GW-31, GW-30, GW-28, GW-25, GW-23, GW-22, GW-21, GW-20, GW-18, GW-17, GW-15, GW-14, GW-12, GW-9, GW-6, GW-4, GW-1) from the study region in pre monsoon season. According to the descriptive data, it can

be observed that Cluster-I exhibits the highest value of CCME WQI in the pre-monsoon season, with a maximum value of 100.

Whereas, Cluster-II is made up of 15 sampling sites (GW-16, GW-27, GW-2, GW-19, GW-11, GW-39, GW-29, GW-7, GW-13, GW-33, GW-8, GW-5, GW-24, GW-26, GW-3) based on CCME WQI similarity. Cluster-II has a moderate CCME WQI score in comparison to the Clusters-I based on the analysed data. Cluster II has a maximum value of 86.83, as per the calculated CCME WQI statistics. Moreover, Cluster-III comprised a single sample site (GW-10) that exhibited distinct behavioural characteristics compared to the preceding clusters (Cluster-I and Cluster-II). The CCME WQI statistics shows that cluster-III has the lowest CCME WQI value of 48.63 as shown in Fig.5.39.

However, Cluster-I comprises the large number of 28 sample sites (GW-42, GW-43, GW-41, GW-40, GW-38, GW-37, GW-35, GW-34, GW-33, GW-31, GW-30, GW-28, GW-25, GW-23, GW-22, GW-20, GW-19, GW-18, GW) in post monsoon season. Based on the descriptive data, it can be observed that Cluster-I exhibits the highest value of CCME WQI during the post-monsoon season, reaching a maximum value of 100.

Similarly, Cluster-II consists of 14 sampling sites (GW-8, GW-13, GW-11, GW-7, GW-39, GW-24, GW-29, GW-3, GW-5, GW-32, GW-36, GW-10, GW-26, GW-27). According to the estimated WQI statistics, Cluster-II has a maximum value of 80.88. In addition, Cluster-III contained a single sample site (GW-16), representing the minimum number of sites included in this cluster. Cluster-III has the lowest CCME WQI score, of 72.79 as shown in Fig.5.40.

The HCA technique makes it easier to categorise the calculated CCME WQI for the area in which, water quality declines from Cluster-I to Cluster-III in both seasons.

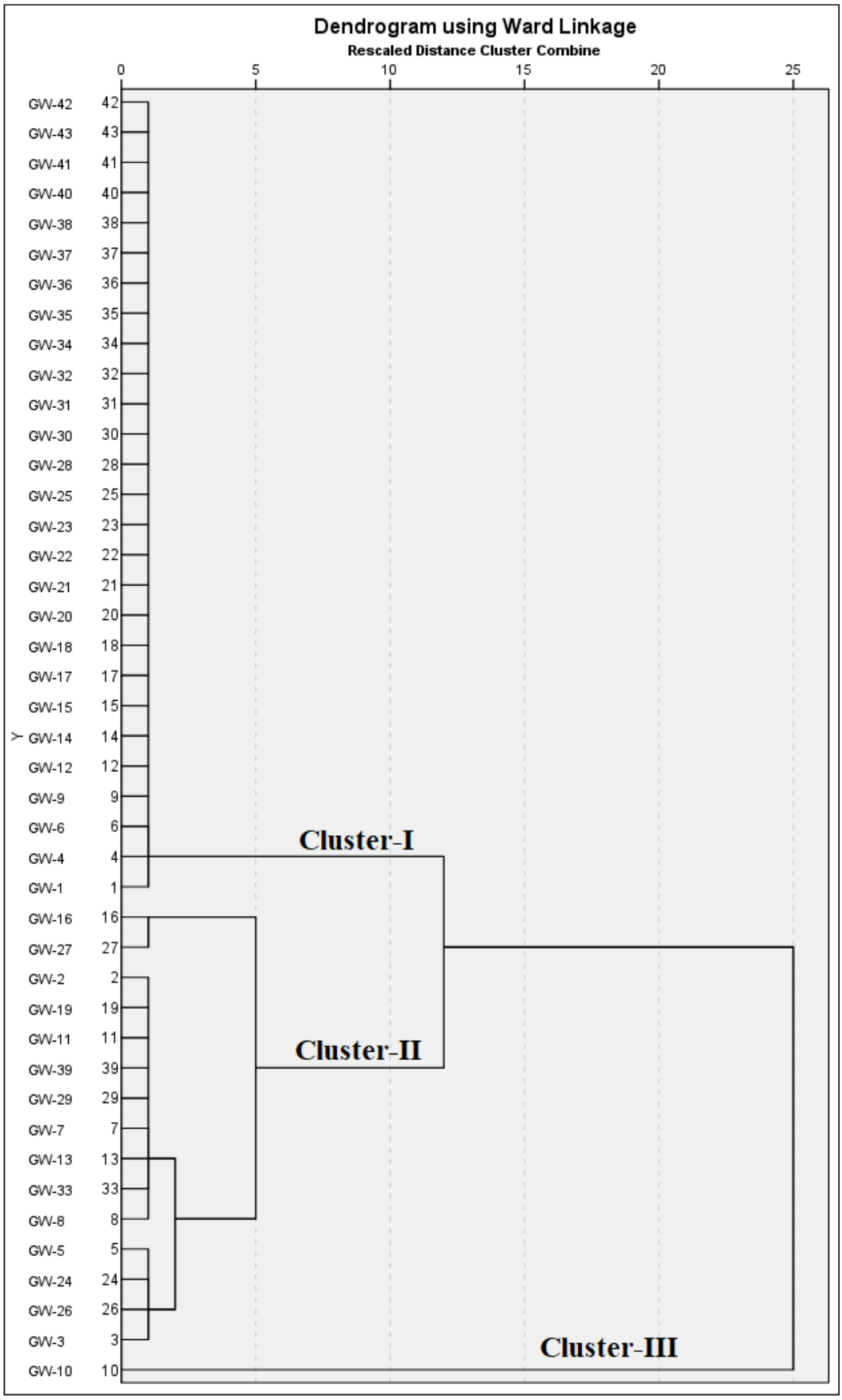

Fig.5.39 Dendrogram of HCA based on WQI of sampling sites in pre monsoon season

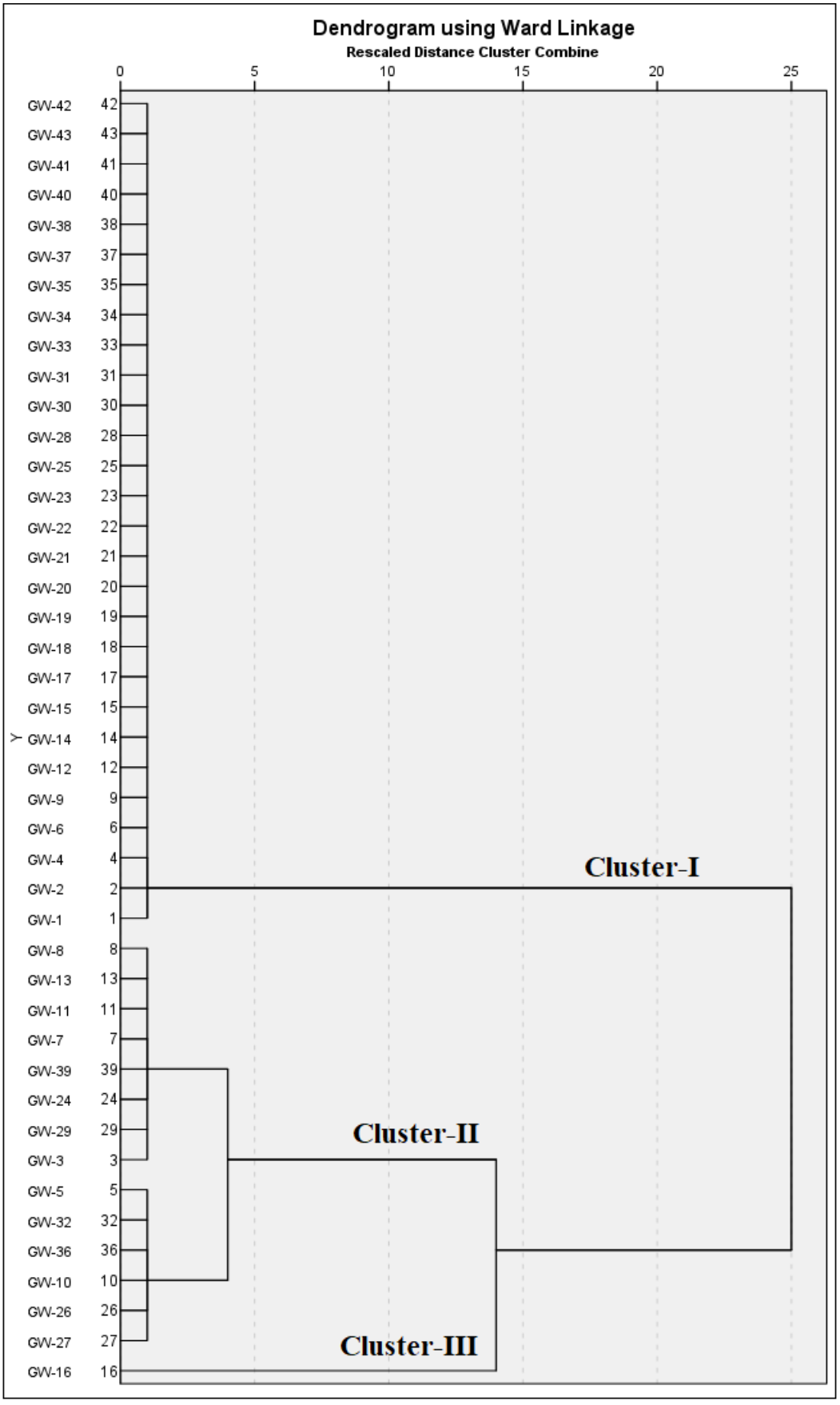

Fig.5.40 Dendrogram of HCA based on WQI of sampling sites in post monsoon season

5.1.5 Hydrogeochemical facies of the groundwater samples

5.1.5.1 Piper Diagram

The major cation and anion are typically plotted in trilinear plots to depict the hydro geochemistry regime of groundwater (Piper, 1953). Piper plots are widely utilised in hydrogeological and water analysis. These plots are applied to visually represent the relative abundance of common ions found in water samples. Piper plots possess distinctive and significant characteristics as they allow for the simultaneous plotting of many samples. Consequently, this enables the grouping of water samples according to groundwater facies and other relevant properties. This diagram displays the similarities and dissimilarities between the water samples since those with similar traits prefer to group together (Todd 1980). Piper plot makes it possible to show the cation and anion content among several samples on just a single graph, making it possible to spot major patterns in the data visually (Freeze and Cherry, 1979).

In order to facilitate the interpretation of the diamond plot within the Piper diagram, it is observed that samples located in the upper quadrant are indicative of gypsum groundwater and mines drainage. However, samples situated in the left quadrant are representative of shallow fresh groundwater, characterised by calcium bicarbonate water. On the other hand, samples found in the right quadrant are reflective of marine groundwater, denoted by sodium chloride water. Lastly, samples positioned in the lower quadrant are indicative of deep groundwater influenced by acid rain, as evidenced by sodium bicarbonate water.

Piper diagram was employed in this study, effectively illustrates the prevailing hydrogeochemical facies in the region throughout both pre and post monsoon seasons as shown in Fig.5.41 and Fig.5.42 respectively. The trilinear diagram displays significant cations such as Ca^{2+}, Mg^{2+}, Na^{+}, and K^{+} and major anions such as HCO_3^{-}, Cl^{-}, and SO_4^{2-}.

A plot with a diamond shape as well as two plots with triangular shapes form the majority of the Piper diagram.

In pre-monsoon season, only 23.26% of the acquired samples are of the calcium type as per the cationic triangle, whereas the other 76.74% samples do not fit into any particular dominating type. However, in the anion facies, 25.58% of the samples were bicarbonate type, 34.88% were chloride type, and the rest 39.54% were of no prominent type. The diamond shaped section of the data reveals that 27.91% of the samples belong to the CaMg-HCO3 group, indicating the occurrence of percolation and dissolution processes involving minerals such as calcite and dolomite, which are significant in the geological context of the studied area. Approximately 72.09% of the samples were classified into the Ca-Mg-Cl-SO4 group, suggesting the presence of anthropogenic activities, such as current mining operations and the existence of thermal power plants in the region. Consequently, the aforementioned information is supported by Fig.5.41, which illustrates the Piper diagram used to represent the variation in hydrogeochemical facies in the pre monsoon season.

In post monsoon season, based on cationic triangle analysis, it was observed that only 4.65% of the samples exhibit characteristics of the magnesium type. Additionally, 9.30% of the samples are categorised as sodium or potassium types, while 16.28% are identified as calcium types. The remaining 69.77% of the samples do not exhibit a dominating type within the analysed cationic triangle context. Furthermore, it was seen that 4.65% of the samples belonging to the anion facies exhibit characteristics of the sulphate type, while 16.28% are classified as bicarbonate type, 46.51% as chloride type, and the remaining 32.56% do not exhibit a dominating type. Moreover, within this particular diamond shaped section, 16.28% of the samples can be classified as belonging to the CaMg-HCO3 group. Additionally, 74.42% of samples can be categorised as falling within the Ca-Mg-

Cl-SO4 group. Furthermore, the remaining 9.30% of the groundwater samples can be classified as falling under the NaCl-SO4 category. This particular finding suggests the occurrence of small mineral dissolution processes within the studied area. As a result, the aforementioned findings are supported by Fig.5.42, expressing the hydrogeochemical facies fluctuation in post monsoon season.

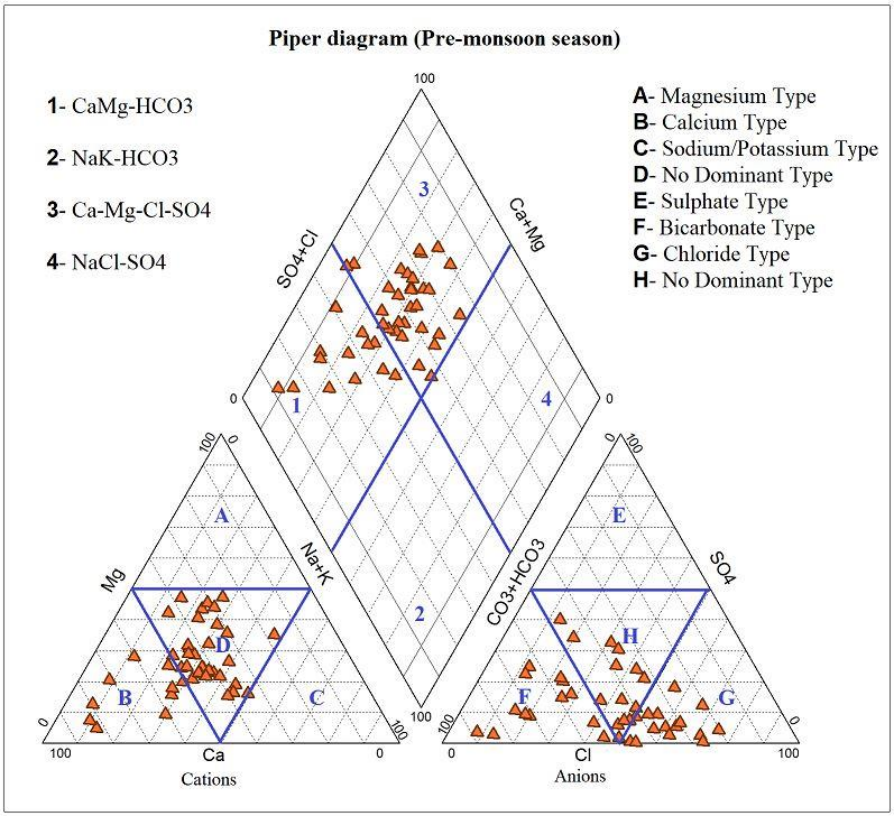

Fig.5.41 Piper diagram for describing hydrogeochemical facies in pre monsoon season

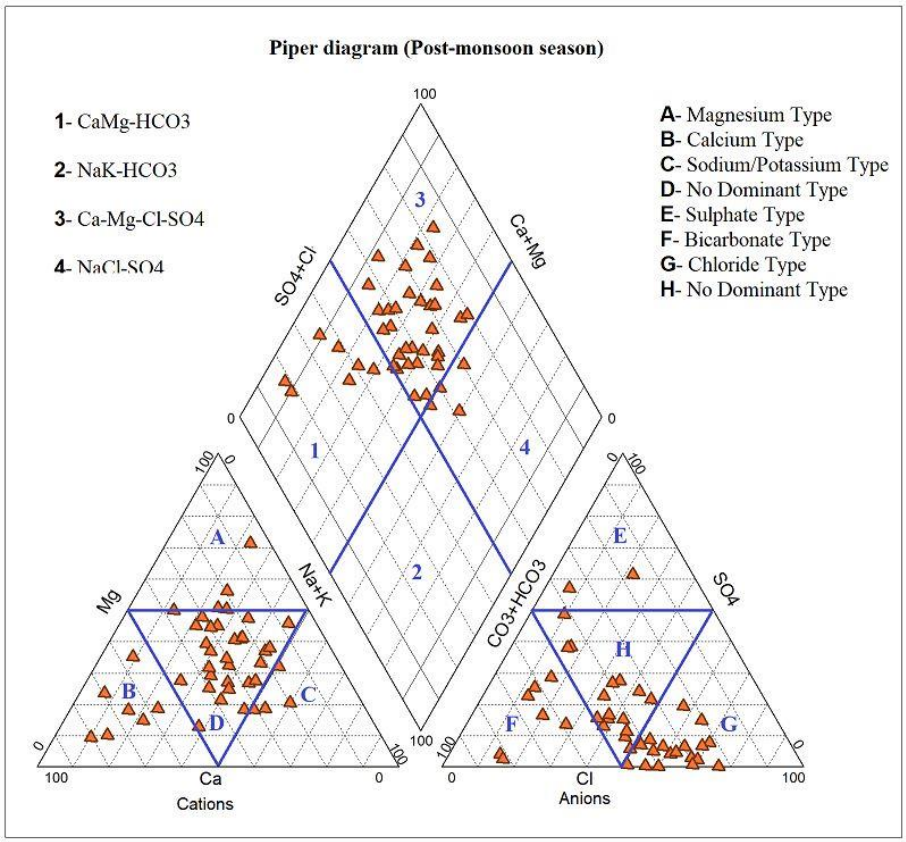

Fig.5.42 Piper diagram for describing hydrogeochemical facies in post monsoon season

5.1.5.2 Gibbs Diagram

It is necessary to explore this relationship in order to understand how the environment and water interact to reveal the specific chemistry of water (Egbueri et al. 2019). The Gibbs plot is used to determine the relation between lithology, hydrologic processes, and water chemistry of an aquifer. In the Gibbs plot, the weight proportions for cations and anions, such as $Na^+/ (Na^+ + Ca^{2+})$ and $Cl^-/ (Cl^- + HCO_3^-)$, are shown on the abscissa, while the variation in TDS is shown on the ordinate. It is well-organized concept which serve as a general approach for a discussion of the various mechanisms that influence global water chemistry (Gibbs, 1970). The evaporation crystallisation, rock dominance and atmospheric precipitation are the three major processes that govern global groundwater chemistry.

According to the Gibbs diagram, the majority of groundwater samples collected during both the pre and post monsoon seasons exhibit characteristics of rock water dominance and evaporation crystallisation in terms of both cation and anion composition. This suggests that the quality of groundwater in the area is influenced by the dominance of rock minerals and the process of evaporation crystallisation as shown in Fig.5.43 and Fig.5.44 respectively.

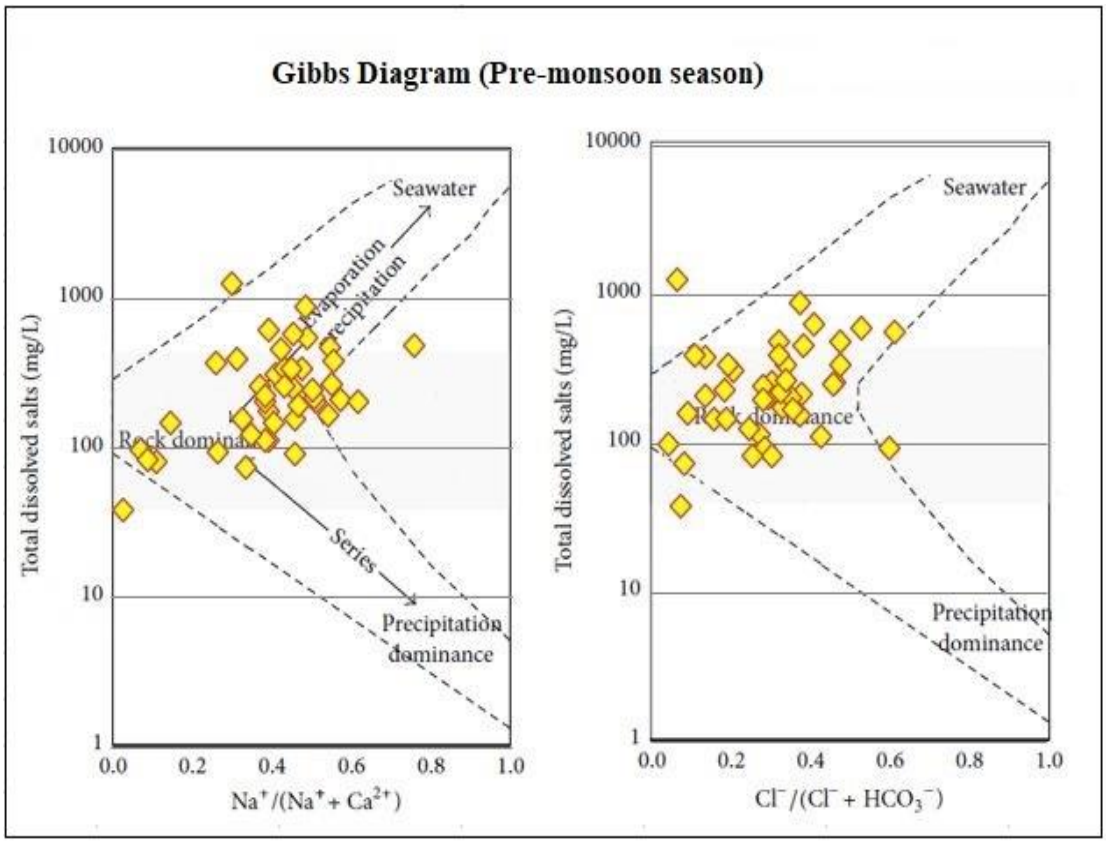

Fig.5.43 Gibbs diagram for groundwater in pre monsoon season a)-cation and b)-anion

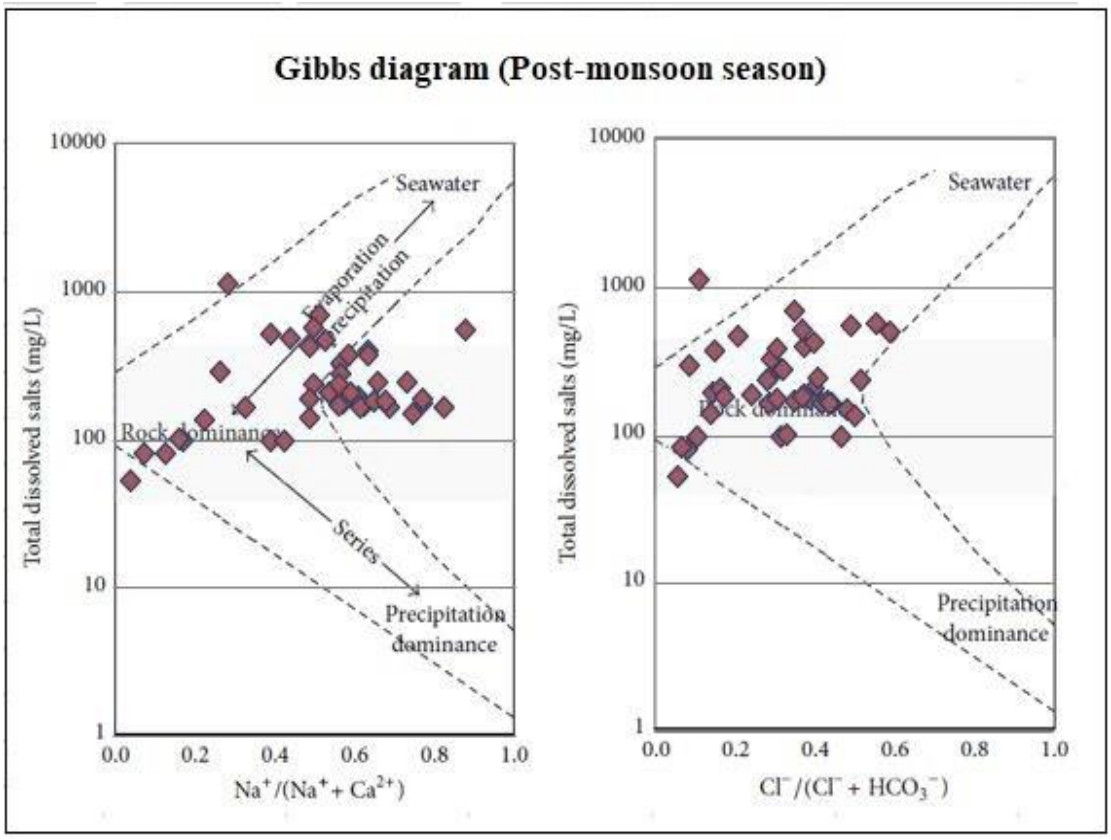

Fig.5.44 Gibbs diagram for groundwater in post monsoon season a)-cation and b)-anion

5.1.6 Water Assessment Suitability for Irrigational Uses

The acceptable use of groundwater for irrigation is mostly determined by the mineral content in the water as well as the potential impacts that the water may have on soils as well as plants. An elevated concentration of salt in irrigation water leads to an increase in osmotic pressure within the soil solution. Salts can have an indirect impact on plant growth in addition to having a direct impact by altering the structure, permeability, and aeration of the soils (Todd and Mays, 2005). In general, it stops water from getting to different plant parts, which reduces agricultural output (Rao et al. 2013). For long-term production, it's important to know how to use water quality for irrigation and what management changes are needed (Srinivasamoorthy et al. 2014). The suitability of irrigation water was evaluated using a variety of indices, including SAR, %Na, KI, PI, and MH, as tabulated in Table.5.14, Table.5.15, Table.5.16 and Table.5.17 respectively.

5.1.6.1 Sodium Absorption Ratio (SAR)

The USSL proposes the utilisation of the SAR as a means to evaluate the alkalinity or sodium-related risks associated with using water for irrigation (U.S Salinity Laboratory, 1954). The osmotic pressure in the soil solution increases when irrigation water has high salt in it. It is calculated by dividing the Na^+ content by the sum of squares root of one-half of the (Ca^{2+} + Mg^{2+}) concentrations as given by equation no. 4.8 in previous chapter. SAR values ranged from 0.35 to 14.51 meq/L, with an average value of 2.86 meq/L in pre monsoon season while from 0.45 to 15.49 meq/L, with an average value of 6.03 meq/L in post monsoon season respectively.

According to the SAR (Richard, 1954) classification, the majority of groundwater samples, specifically 97.7% samples in pre monsoon and 90.7% samples in post monsoon seasons respectively, can be categorised as low. The remaining samples, 9.3% in the pre and 2.3% samples in post monsoon seasons respectively, fall into the medium

category, indicating their suitability for irrigation purposes as given in Table.5.9 respectively.

Based on the SAR map, the groundwater samples may be classified into three distinct groups, namely C1-S1, C2-S1, and C3-S1, for both seasons, respectively as shown in Fig.5.45 and Fig.5.46. This means that the majority of groundwater samples (69.77% in pre and 74.42% in post monsoon) fall into the C2-S1 class, (18.60 % in pre monsoon and 13.95% in post monsoon) of samples fall under C1-S1 class and the rest (11.63% in pre monsoon and 11.63% in post monsoon) of samples under C3-S1 are suitable for irrigation.

Table.5.9 Classification of samples showing their suitability for irrigation based on SAR in pre and post monsoon season

Parameter	**Range**	**Classification**	**No. of samples (Pre-MS)**	**No. of samples (Post-MS)**
SAR	<10	Low	42 samples (97.7%)	39 samples (90.7%)
	10 – 18	Medium	1 sample (2.3%)	4 samples (9.3%)
	18 – 26	High	0	0
	> 26	Very High	0	0

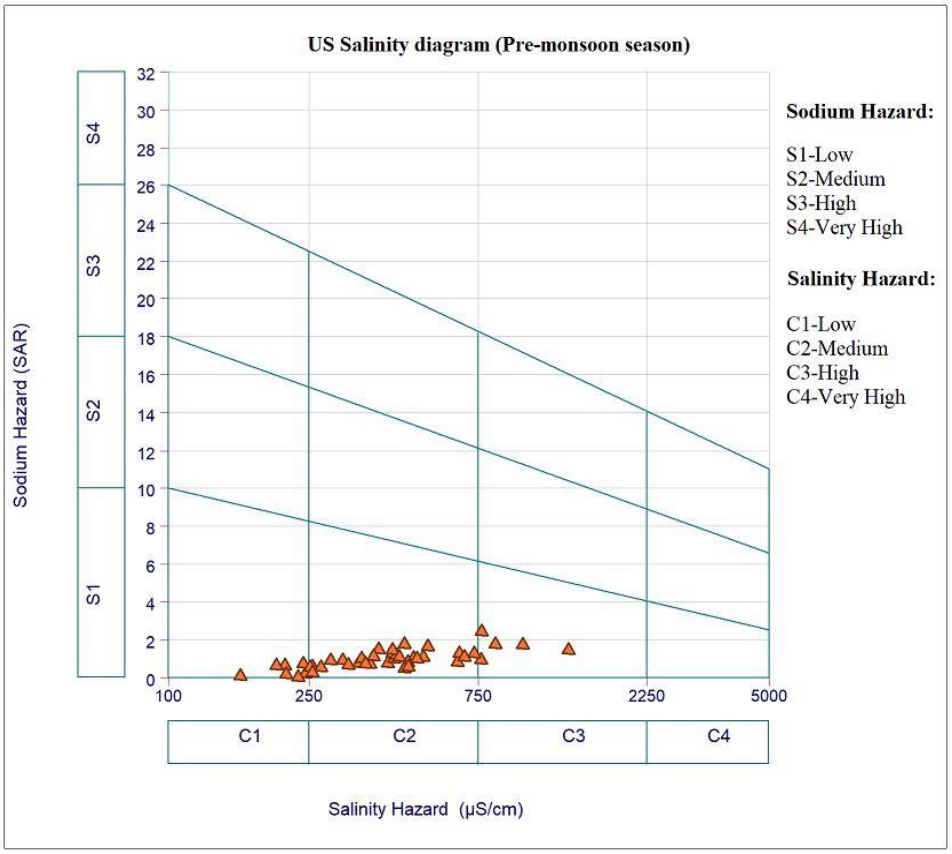

Fig.5.45 US Salinity diagram for irrigation water classification in pre monsoon season

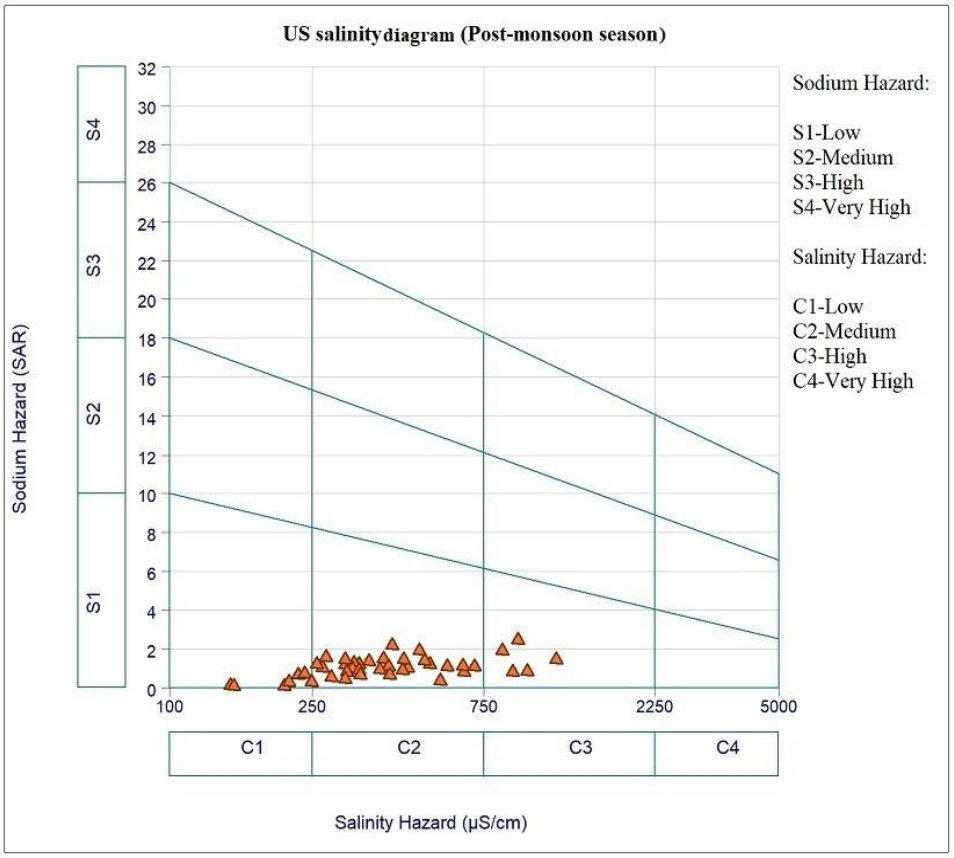

Fig.5.46 US Salinity diagram for irrigation water classification in post monsoon season

5.1.6.2 Percent Sodium

Sodium plays a crucial role in crop production; however, higher concentrations of sodium can lead to the deterioration of soil structure, thus resulting in a decrease in crop yield (Adimalla and Venkatayogi, 2018). The percent sodium is often used to determine the suitability of water quality for irrigation purposes (Wilcox 1955). The presence of excessive sodium in water leads to a decrease in soil permeability, resulting in poor internal drainage of the soil due to the exchange of sodium ions in water with calcium ions and magnesium ions in the soil. Consequently, in the presence of moisture, the movement of air and water inside the soil is restricted, leading to the frequent hardened of such soils upon drying (Collins and Jenkins 1996; Saleh et al. 1999). Indian Standard (BIS 1991) specifies a maximum sodium level of 60% in irrigation water. The percent sodium is calculated with formula as given by equation no. 4.9 in previous chapter. A Wilcox plot is commonly drawn with sodium percentage on the y-axis and electrical conductivity on the x-axis Wilcox (1955). The percent sodium ranged from 10.13% to 58.53%, with an average value of 35.96% in pre monsoon while from 10.04% to 68.44%, with an average value of 41.65% in post monsoon season respectively as shown in Table.5.10.

The Wilcox plots Wilcox (1948) proposed for this analysis for both seasons as shown in Fig.5.47 and Fig.5.48 respectively. The five categories of irrigation water quality based on percent sodium are given in Table.5.10. Based on the %Na classification, it is observed that a significant proportion of groundwater samples (67.43% in pre-monsoon and 46.53% in post-monsoon) may be categorised as the excellent to a good class. Additionally, a notable percentage of samples (32.6% in pre-monsoon and 37.32% in post-monsoon) fall within the permissible class, indicating their suitability for irrigation

purposes. The rest 16.3% of post monsoon samples belongs to doubtful class which cannot be used for irrigation.

Table.5.10 Classification of samples showing their suitability for irrigation based on %Na in pre and post monsoon season

Parameter	Range	Classification	No. of samples (Pre-MS)	No. of samples (Post-MS)
%Na	<20	Excellent	5 samples (11.63%)	5 samples (11.63%)
	20 – 40	Good	24 samples (55.8%)	15 samples (34.9%)
	40 – 60	Permissible	14 samples (32.6%)	16 samples (37.2%)
	60 - 80	Doubtful	0	7 samples (16.3%)
	>80	Unsuitable	0	0

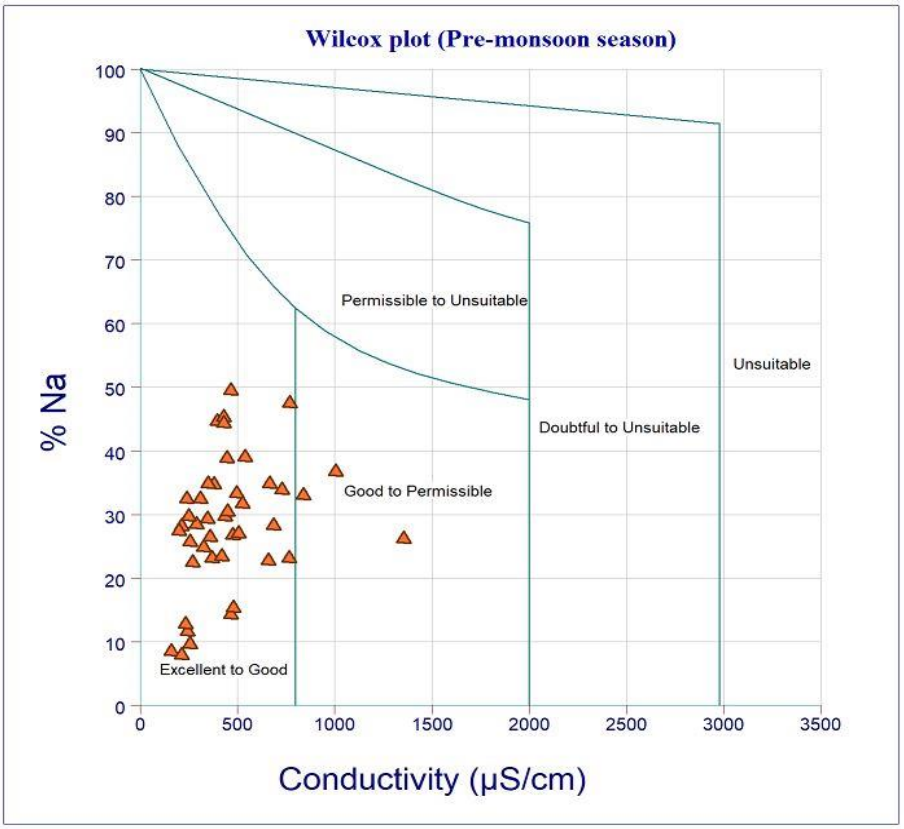

Fig.5.47 Wilcox plot for classification of irrigation water in pre monsoon season

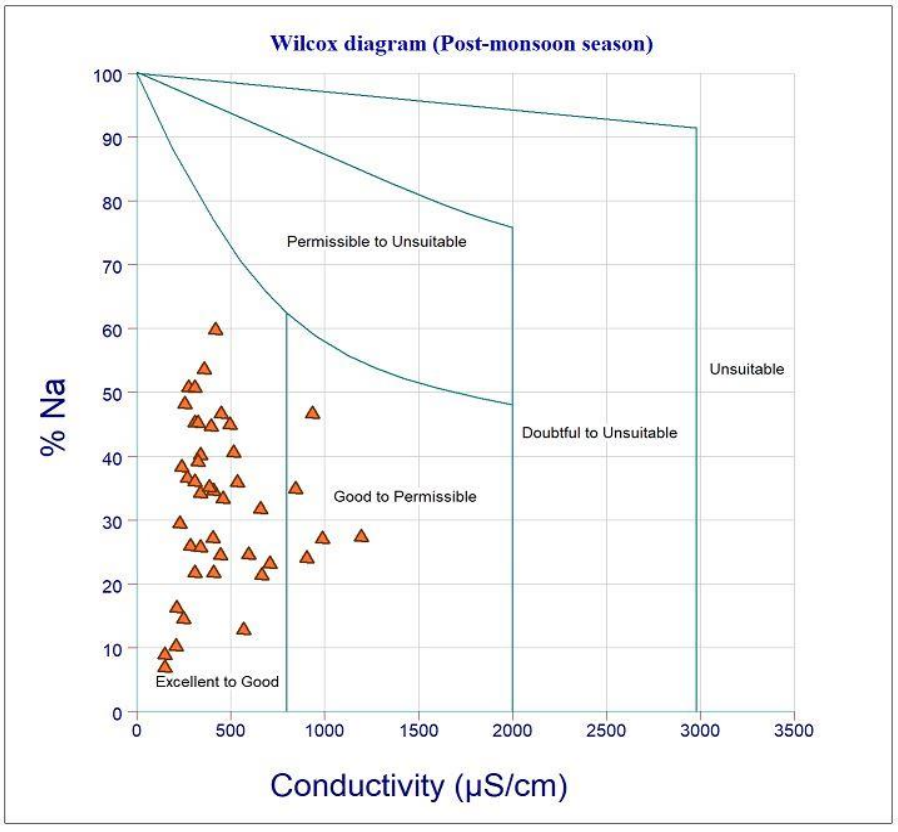

Fig.5.48 Wilcox plot for classification of irrigation water in post monsoon season

5.1.6.3 Kelly Index (KI)

The KI is an essential method employed in the categorization of water for the purpose of irrigation. The KI > 1.0 is sodium-rich and should not be used for irrigation whereas KI < 1.0 is only considered suitable for irrigation (Kelley 1946 and Paliwal 1967). Kelly index is calculated using the formula given by equation 4.10 in previous chapter.

The calculated KI values ranged from 0.03 to 1.39, with an average value of 0.29 in pre monsoon whereas it is ranged from 0.04 to 2.06, with an average value of 0.72 in post monsoon season respectively. The majority of the samples (93.02% in pre monsoon and 74.40% in post monsoon) fall into the suitable class while the remaining (6.98% in pre monsoon and 25.60% in post monsoon) of samples fall into the unsuitable class as tabulated in Table.5.11.

Table.5.11 Classification of samples showing their suitability for irrigation based on KI in pre and post monsoon season

KI	Water quality	No. of samples (Pre-MS)	No. of samples (Post-MS)
<1	Suitable	40 samples (93.02%)	32 samples (74.40%)
>1	Unsuitable	3 samples (6.98%)	11 samples (25.60%)

5.1.6.4 Permeability Index

The use of irrigated water induces changes in soil permeability over a period of time, leading to consequential effects on agricultural productivity. Consequently, it becomes essential to assess the suitability of water for irrigation based on its permeability index. Permeability index is an important measure for assessing bicarbonate and carbonate risks in groundwater. According to the classification proposed by (Doneen in 1964), groundwater can be categorised into three classes based on its potential irrigation suitability. Class I represents groundwater with a PI >75%, indicating its suitability for irrigation purposes. Class II signifies groundwater that is considered good for irrigation when the PI value falls between 25% and 75%. Lastly, Class III denotes groundwater that is unsuitable for irrigation when the PI value is < 25%.

The calculated Permeability index values varied from 8.50% to 84.15% with an average value of 17.0% in pre monsoon while it varied from 11.93% to 88.62% with an average value of 17% in post monsoon season. The majority of the samples (6.98% in pre monsoon and 6.98% in post monsoon) belonged to Class I, while significance proportion of samples (81.4% in pre monsoon and 79.1% in post monsoon) belong to Class II, showing that this groundwater was suitable for irrigation application. The remaining samples, accounting for (11.6% in pre monsoon and 14% of post monsoon) belong to Class III is not suitable for irrigation as tabulated in Table.5.12.

Table.5.12 Classification of samples showing their suitability for irrigation based on PI in pre and post monsoon season

Parameter	Range	Classification	No. of samples (Pre-MS)	No. of samples (Post-MS)
Permeability Index	>75	Excellent	3 samples (6.98%)	3 samples (6.98%)
	25 – 75	Good	35 sample (81.4%)	34 samples (79.1%)
	<25	Permissible	5 samples (11.6%)	6 samples (14%)

5.1.6.5 Magnesium Hazard

The excess concentration of magnesium in groundwater changes the soil's quality and makes it alkaline. The crops yield gets decreased as a result, poor agricultural returns. Hence, it can be concluded that when MR >50, it is deemed unsuitable for irrigation as it leads to a decrease in crop yield. However, when the MR< 50, it is considered ideal for irrigation purposes (Szaboles et al. 1964).

The calculated MH values varied from 3.39 to 54.99 meq/L with an average value of 12.06 meq/L in pre monsoon while it varied from 6.62 to 88.67 meq/L with an average value of 39.33 meq/L in post monsoon season respectively. The MH values indicated that (95.3% in pre monsoon and 74.4% in post monsoon) belonged to excellent category (MH < 50), indicating that suitable for irrigation use. The remaining samples (4.7% in pre monsoon and 25.6% in post monsoon) belonged to unsuitable class (MH > 50), which is not suitable for irrigation as tabulated in Table.5.13.

Table.5.13 Classification of samples showing their suitability for irrigation based on MH in pre and post monsoon season

Parameter	Range	Classification	No. of samples (Pre-MS)	No. of samples (Post-MS)
MH	<50	Suitable	41 samples (95.35%)	32 samples (74.4%)
	>50	Unsuitable	2 sample (4.65%)	11 samples (25.6%)

Table.5.14 Table showing calculated SAR, %Na, KI values in pre monsoon season

Sample code	SAR	Status	%Na	Status	KI	Status
GW-1	1.28	Low	16.55	Excellent	0.13	Suitable
GW-2	8.36	Low	37.97	Good	1.02	Unsuitable
GW-3	9.60	Low	71.19	Doubtful	0.71	Suitable
GW-4	4.34	Low	29.80	Good	0.39	Suitable
GW-5	9.41	Low	58.93	Permissible	0.83	Suitable
GW-6	5.90	Low	40.49	Permissible	0.57	Suitable
GW-7	5.61	Low	47.52	Permissible	0.38	Suitable
GW-8	4.60	Low	26.17	Good	0.46	Suitable
GW-9	4.61	Low	26.79	Good	0.44	Suitable
GW-10	8.69	Low	81.33	Unsuitable	0.49	Suitable
GW-11	3.43	Low	16.22	Excellent	0.45	Suitable
GW-12	5.05	Low	22.82	Good	0.62	Suitable
GW-13	4.26	Low	19.51	Excellent	0.52	Suitable
GW-14	6.46	Low	35.04	Good	0.67	Suitable
GW-15	0.35	Low	20.99	Good	0.03	Suitable
GW-16	4.53	Low	37.90	Good	0.33	Suitable
GW-17	7.46	Low	40.87	Permissible	0.72	Suitable
GW-18	5.72	Low	29.56	Good	0.60	Suitable
GW-19	6.11	Low	31.06	Good	0.60	Suitable
GW-20	3.57	Low	18.73	Excellent	0.47	Suitable
GW-21	3.79	Low	18.89	Excellent	0.43	Suitable
GW-22	3.12	Low	16.64	Excellent	0.36	Suitable
GW-23	9.80	Low	42.04	Permissible	1.24	Unsuitable
GW-24	6.88	Low	49.22	Permissible	0.81	Suitable
GW-25	4.88	Low	34.94	Good	0.43	Suitable
GW-26	9.91	Low	78.11	Doubtful	0.64	Suitable
GW-27	14.51	Medium	76.94	Doubtful	1.39	Unsuitable
GW-28	6.68	Low	37.59	Good	0.75	Suitable
GW-29	4.00	Low	26.55	Good	0.52	Suitable
GW-30	2.90	Low	31.67	Good	0.33	Suitable
GW-31	0.60	Low	9.82	Excellent	0.07	Suitable
GW-32	2.79	Low	18.96	Excellent	0.23	Suitable
GW-33	7.15	Low	47.87	Permissible	0.63	Suitable
GW-34	3.52	Low	24.78	Good	0.26	Suitable
GW-35	1.32	Low	8.29	Excellent	0.12	Suitable
GW-36	3.34	Low	16.35	Excellent	0.45	Suitable
GW-37	0.90	Low	6.36	Excellent	0.09	Suitable
GW-38	7.99	Low	34.65	Good	0.99	Suitable
GW-39	6.09	Low	37.01	Good	0.52	Suitable
GW-40	5.94	Low	32.49	Good	0.56	Suitable
GW-41	6.33	Low	41.85	Permissible	0.56	Suitable
GW-42	5.42	Low	26.19	Good	0.67	Suitable
GW-43	4.08	Low	23.78	Good	0.44	Suitable

Table.5.15 Table showing calculated MH and PI values in pre monsoon season

Sample code	MH	Status	PI	Status
GW-1	21.97	Suitable	21.1	Unsuitable
GW-2	23.99	Suitable	47.0	Good
GW-3	25.29	Suitable	72.1	Good
GW-4	43.92	Suitable	34.5	Good
GW-5	31.75	Suitable	63.5	Good
GW-6	25.40	Suitable	43.5	Good
GW-7	40.35	Suitable	49.8	Good
GW-8	23.28	Suitable	34.7	Good
GW-9	47.07	Suitable	34.7	Good
GW-10	47.34	Suitable	84.1	Excellent
GW-11	30.06	Suitable	26.9	Good
GW-12	25.83	Suitable	35.6	Good
GW-13	19.28	Suitable	34.0	Good
GW-14	25.41	Suitable	44.7	Good
GW-15	3.39	Suitable	8.5	Unsuitable
GW-16	22.77	Suitable	45.2	Good
GW-17	41.53	Suitable	53.6	Good
GW-18	42.34	Suitable	40.1	Good
GW-19	21.06	Suitable	45.8	Good
GW-20	24.22	Suitable	31.1	Good
GW-21	30.67	Suitable	33.8	Good
GW-22	25.96	Suitable	32.5	Good
GW-23	22.16	Suitable	55.1	Good
GW-24	20.77	Suitable	43.7	Good
GW-25	14.66	Suitable	34.1	Good
GW-26	23.32	Suitable	82.6	Excellent
GW-27	54.99	Unsuitable	84.1	Excellent
GW-28	24.97	Suitable	44.3	Good
GW-29	23.45	Suitable	31.5	Good
GW-30	8.51	Suitable	26.2	Good
GW-31	14.97	Suitable	18.3	Unsuitable
GW-32	36.94	Suitable	31.6	Good
GW-33	23.21	Suitable	50.9	Good
GW-34	43.04	Suitable	34.3	Good
GW-35	5.09	Suitable	16.6	Unsuitable
GW-36	16.46	Suitable	29.2	Good
GW-37	8.87	Suitable	16.2	Unsuitable
GW-38	18.69	Suitable	49.5	Good
GW-39	28.54	Suitable	47.2	Good
GW-40	52.53	Unsuitable	43.5	Good
GW-41	34.46	Suitable	42.0	Good
GW-42	23.44	Suitable	39.8	Good
GW-43	28.31	Suitable	36.8	Good

Table.5.16 Table showing calculated SAR, %Na, KI values in post monsoon season

Sample code	SAR	Status	%Na	Status	KI	Status
GW-1	6.77	Low	47.94	Permissible	0.86	Suitable
GW-2	9.01	Low	35.70	Good	1.22	Unsuitable
GW-3	5.06	Low	36.28	Good	0.46	Suitable
GW-4	5.55	Low	31.58	Good	0.55	Suitable
GW-5	10.95	Medium	58.47	Permissible	1.10	Unsuitable
GW-6	3.08	Low	25.56	Good	0.36	Suitable
GW-7	4.81	Low	38.70	Good	0.35	Suitable
GW-8	5.89	Low	27.91	Good	0.67	Suitable
GW-9	5.91	Low	23.69	Good	0.81	Suitable
GW-10	8.76	Low	76.65	Doubtful	0.53	Suitable
GW-11	7.24	Low	27.15	Good	1.22	Unsuitable
GW-12	7.57	Low	31.46	Good	1.15	Unsuitable
GW-13	5.62	Low	21.33	Good	0.86	Suitable
GW-14	5.59	Low	31.51	Good	0.52	Suitable
GW-15	0.46	Low	15.64	Excellent	0.04	Suitable
GW-16	4.38	Low	36.86	Good	0.33	Suitable
GW-17	7.24	Low	33.27	Good	0.83	Suitable
GW-18	6.96	Low	25.65	Good	1.17	Unsuitable
GW-19	7.98	Low	38.29	Good	0.90	Suitable
GW-20	9.43	Low	30.71	Good	1.56	Unsuitable
GW-21	5.26	Low	24.56	Good	0.73	Suitable
GW-22	3.93	Low	16.99	Excellent	0.57	Suitable
GW-23	12.48	Medium	41.26	Permissible	2.06	Unsuitable
GW-24	7.80	Low	48.71	Permissible	1.19	Unsuitable
GW-25	1.76	Low	16.87	Excellent	0.18	Suitable
GW-26	10.64	Medium	79.50	Doubtful	0.72	Suitable
GW-27	15.49	Medium	82.07	Unsuitable	1.49	Unsuitable
GW-28	8.54	Low	37.49	Good	1.17	Unsuitable
GW-29	4.77	Low	24.14	Good	0.76	Suitable
GW-30	3.95	Low	33.96	Good	0.55	Suitable
GW-31	0.82	Low	6.45	Excellent	0.11	Suitable
GW-32	2.23	Low	15.15	Excellent	0.20	Suitable
GW-33	2.34	Low	21.23	Good	0.26	Suitable
GW-34	6.64	Low	45.47	Permissible	0.50	Suitable
GW-35	1.78	Low	11.93	Excellent	0.18	Suitable
GW-36	7.16	Low	50.15	Permissible	0.53	Suitable
GW-37	0.59	Low	6.50	Excellent	0.07	Suitable
GW-38	8.05	Low	27.28	Good	1.34	Unsuitable
GW-39	6.52	Low	36.09	Good	0.63	Suitable
GW-40	6.78	Low	32.02	Good	0.81	Suitable
GW-41	4.03	Low	26.49	Good	0.38	Suitable
GW-42	5.58	Low	23.64	Good	0.75	Suitable
GW-43	4.04	Low	18.48	Excellent	0.50	Suitable

Table.5.17 Table showing calculated MH and PI values in post monsoon season

Sample code	MH	Status	PI	Status
GW-1	25.19	Suitable	41.5	Good
GW-2	54.81	Unsuitable	48.0	Good
GW-3	41.41	Suitable	42.3	Good
GW-4	57.68	Unsuitable	39.5	Good
GW-5	36.51	Suitable	64.7	Good
GW-6	26.38	Suitable	29.3	Good
GW-7	44.95	Suitable	42.7	Good
GW-8	32.09	Suitable	38.8	Good
GW-9	38.86	Suitable	37.1	Good
GW-10	49.53	Suitable	80.1	Excellent
GW-11	58.09	Unsuitable	38.1	Good
GW-12	47.79	Suitable	42.6	Good
GW-13	32.64	Suitable	39.2	Good
GW-14	63.73	Unsuitable	43.7	Good
GW-15	6.62	Suitable	11.9	Unsuitable
GW-16	16.44	Suitable	43.8	Good
GW-17	51.52	Unsuitable	51.0	Good
GW-18	24.86	Suitable	42.8	Good
GW-19	30.16	Suitable	51.3	Good
GW-20	53.04	Unsuitable	46.1	Good
GW-21	49.47	Suitable	41.4	Good
GW-22	39.87	Suitable	36.2	Good
GW-23	38.18	Suitable	56.0	Good
GW-24	28.95	Suitable	41.9	Good
GW-25	14.22	Suitable	19.6	Unsuitable
GW-26	27.69	Suitable	84.6	Excellent
GW-27	78.65	Unsuitable	88.6	Excellent
GW-28	39.29	Suitable	49.4	Good
GW-29	52.42	Unsuitable	36.4	Good
GW-30	13.69	Suitable	32.2	Good
GW-31	27.52	Suitable	23.2	Unsuitable
GW-32	44.79	Suitable	28.2	Good
GW-33	12.50	Suitable	23.9	Unsuitable
GW-34	55.40	Unsuitable	53.8	Good
GW-35	7.51	Suitable	20.3	Unsuitable
GW-36	88.67	Unsuitable	53.6	Good
GW-37	16.99	Suitable	17.5	Unsuitable
GW-38	26.40	Suitable	45.2	Good
GW-39	34.40	Suitable	47.3	Good
GW-40	61.42	Unsuitable	45.6	Good
GW-41	48.69	Suitable	29.8	Good
GW-42	40.64	Suitable	42.6	Good
GW-43	47.41	Suitable	34.7	Good

5.1.7 Qualitative Analysis of Surface Water

The analysis of water quality is an essential approach applied in examining surface water, serving to monitor and determine the presence and levels of contaminants that impact a specific region. Since water is one of the most essential resources for supporting life on Earth therefore its quality needs to be regularly monitored (Li et al. 2018a). The utilisation of surface water from the pre monsoon and post monsoon seasons of 2022 was undertaken to examine the effects of mining activities on surface water within the identified study area. Geostatistical tools are the most efficient approaches available while attempting to illustrate the changes that occur between distinct physicochemical properties over different seasons. The significance of surface water as a vital water resource is attributed to its role in meeting both agricultural and industrial water demands. The objective of this study is to utilise ArcGIS software in order to evaluate the quality of surface water by analysing physicochemical parameters.

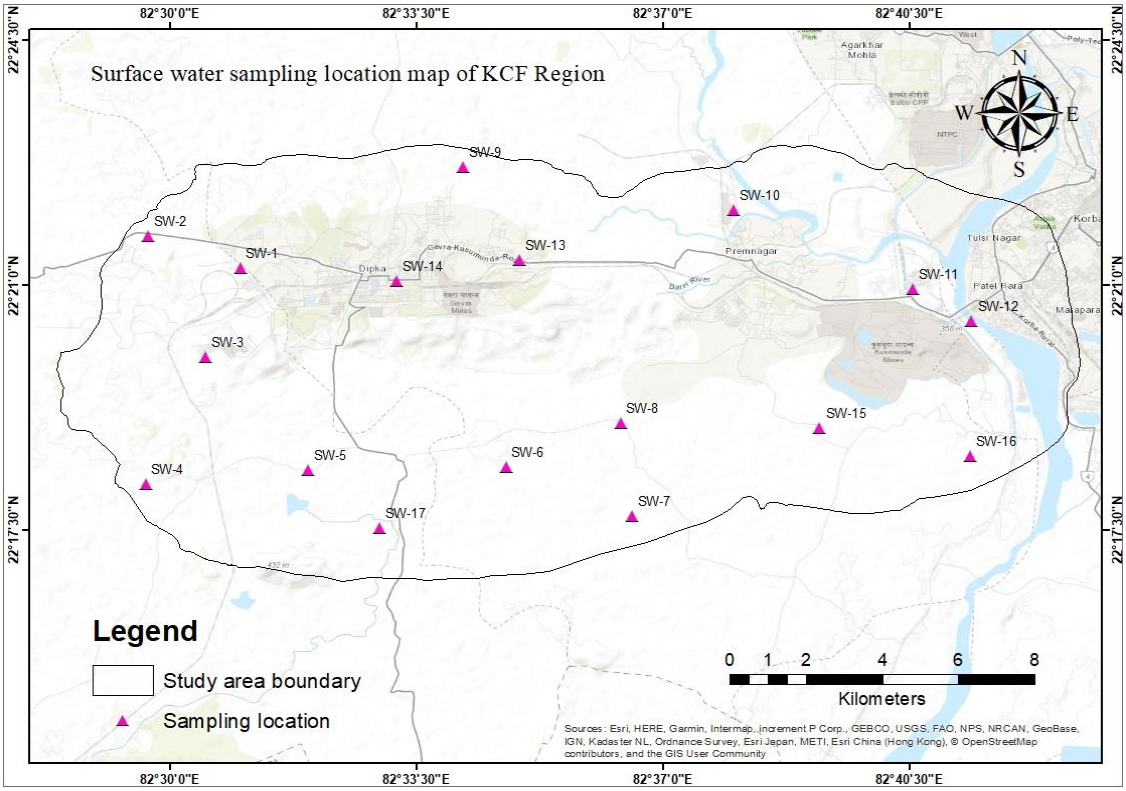

Fig.5.49 Sampling locations map for surface water in KCF region

The data sets used in this analysis were collected from 34 distinct sites within the mining region, encompassing data from both seasons. The ultimate goal is to generate a comprehensive water quality index map based on the findings. A total of 34 surface water samples were collected from various ponds during the pre monsoon and post monsoon seasons of 2022 as shown in Fig.5.49. Thirteen significant physicochemical parameters, namely pH, EC, TDS, Total Hardness, Calcium, Magnesium, Sodium, Potassium, Bicarbonate, Fluoride, Chloride, Sulphate, and Nitrate, were analysed for these samples (Table.5.18). The surface water samples were examined to determine their suitability for domestic and irrigation usage. The water samples were collected using 400 ml polypropylene bottles that were washed and rinsed twice with distilled water. Prior to conducting physicochemical parameter measurement, the water samples were filtration using a 0.22 m Nylon syringe filter.

Table.5.18 Sampling locations details of surface water samples

Sample code	Sampling locations	Latitude	Longitude
SW-1	Sirki Khurd pond water	22.35414	82.51663
SW-2	Tiverta pond water	22.3616	82.49478
SW-3	Chainpur pond water	22.33282	82.50842
SW-4	Andikachhar pond water	22.30262	82.4942
SW-5	Suwabhondi pond water	22.30597	82.53274
SW-6	Ralia pond water	22.30666	82.57948
SW-7	Mahowadih pond water	22.29502	82.60928
SW-8	Bhathora SECL pond water	22.31709	82.60657
SW-9	Chakadhamna pond water	22.37801	82.56934
SW-10	Surakchhar pond water	22.36784	82.63339
SW-11	Durpa pond water	22.34914	82.67577
SW-12	Patel para pond water	22.3415	82.68958
SW-13	Shakti Nagar Dhurena pond water	22.35607	82.58254
SW-14	Urja Nagar pond water	22.35099	82.55361
SW-15	Khodri pond water	22.31589	82.65367
SW-16	Khairbhawna pond water	22.30934	82.6892
SW-17	Bamhanikona pond water	22.29223	82.54957

The pH, TDS, and EC parameters were concurrently assessed immediately after sampling using a calibrated multiparameter device known as the ISO-TECH System. The Ion-Chromatography (IC) technique was applied in order to determine the presence of cations and anions within every surface water sample in CIF, IIT (BHU). The physicochemical parameters result from laboratory are listed and given in Appendix A.7 to Appendix A.12 respectively. The fast growth of mining and thermal power plants in the study region has resulted in the degradation of water quality and other resources. The stated objective was achieved through a comparative analysis of the data obtained throughout both seasons, in accordance with the drinking water quality standards established by the (WHO, 2011).

5.1.7.1 Physiochemical parameter characteristics of surface water

Surface water samples were examined for physicochemical parameters such as pH, EC, TDS, Total Hardness, Calcium, Magnesium, Sodium, Potassium, Bicarbonate, Fluoride, Chloride, and Nitrate. As we observed that the surface water samples are having better quality because of more suspended impurities and less concentration of parameters in it while groundwater quality depends on the geochemistry of aquifers and the overlying soil. The groundwater, being more isolated and slow-moving, tends to accumulate contaminants over time, making it more susceptible to quality degradation from mining industry. The measured physicochemical parameter values for both pre and post monsoon seasons were compared to standard guidelines values as per (WHO 2011), which are tabulated in Table 5.19 & Table 5.20 respectively.

5.1.7.1.1 pH

The measurement of pH in surface water serves as an essential indicator for determining the prevailing acidity or alkalinity of the water. Once the pH is < 7, water is considered acidic, pH > 7 indicates basic, and pH is equal to 7 at 25 °C, indicating neutral water

solution. The acceptable pH range for drinking water should be between 6.5 and 8.5 WHO (2011).

The measured pH values ranged from 6.25 to 8.66, with an average of 7.84 in the pre monsoon, and from 6.35 to 8.23, with an average of 7.66 in the post monsoon season. The pH level in surface water was significantly higher than the WHO (2011) recommended limit at few locations studied in the pre monsoon, while it was slightly lower than pre monsoon at several sites in the post monsoon season. This data shows that both pre and post monsoon surface water are of a slightly acidic to alkaline in nature and can be used for different uses.

Table.5.19 Statistical summary of physicochemical parameters of surface water in pre-monsoon season compared with WHO (2011) standards

S No.	Parameters	Minimum	Maximum	Std dev	Median	WHO (2011)
1.	pH	6.25	8.66	0.69	7.84	6.5-8.5
2.	EC	98.00	962.00	193.92	370.06	1400
3.	TDS	64.00	643.00	131.24	245.59	500
4.	Calcium (Ca^{2+})	20.96	74.64	13.09	34.03	75
5.	Magnesium (Mg^{2+})	3.29	81.43	19.70	18.20	50
6.	Sodium (Na^{+})	10.33	46.65	9.97	23.49	50
7.	Potassium (K^{+})	1.65	13.35	3.51	5.11	15
8.	Fluoride (F^{-})	0.39	1.10	0.20	0.68	1.5
9.	Chloride (Cl^{-})	10.84	131.96	29.67	34.28	250
10.	Nitrate (NO_3^{-})	0.36	14.56	4.08	3.68	45
11.	Sulphate (SO_4^{2-})	4.19	282.09	74.80	59.61	150
12.	Bicarbonate (HNO_3^{-})	29.00	193.00	43.65	105.06	200
13.	Total Hardness	50.77	304.04	68.83	142.17	500

Table.5.20 Statistical summary of physicochemical parameters of post-monsoon season compared with WHO (2011) standards.

S No.	Parameters	Minimum	Maximum	Std dev	Median	WHO (2011)
1.	pH	6.35	8.23	0.44	7.66	6.5-8.5
2.	EC	82.00	712.00	158.23	273.94	1400
3.	TDS	63.00	465.00	103.56	180.76	500
4.	Calcium (Ca^{2+})	7.85	78.36	17.39	23.49	75
5.	Magnesium (Mg^{2+})	2.00	40.45	10.15	11.40	50
6.	Sodium (Na^{+})	2.64	28.42	7.73	13.05	50
7.	Potassium (K^{+})	0.20	11.20	3.29	3.34	15
8.	Fluoride (F^{-})	0.38	0.92	0.14	0.56	1.5
9.	Chloride (Cl^{-})	2.81	51.71	13.54	17.90	250
10.	Nitrate (NO_3^{-})	0.00	124.73	30.03	8.45	45
11.	Sulphate (SO_4^{2-})	3.76	128.94	33.98	28.44	150
12.	Bicarbonate (HNO_3^{-})	26.00	121.00	27.04	73.41	200
13.	Total Hardness	34.07	254.77	66.91	105.59	500

All parameters are expressed in mg/l except pH, EC (µS/cm)

5.1.7.1.2 Electrical conductivity

The EC is an important variable for calculating the ionic concentrations in a water bodies. The higher EC concentration may also lead to increased salinity and total dissolved concentration as well. The measuring of EC in water often relies on the measurement of TDS, as EC and TDS exhibit a direct correlation. Consequently, an increase in TDS leads to a corresponding increase in EC, and conversely, a decrease in TDS results in a decrease in EC (Rusydi 2018).

The observed EC values ranged from 98 µS/cm to 960 µS/cm, with an average of 370 µS/cm in the pre monsoon, and from 82 µS/cm to 712 µS/cm, with an average of 273 µS/cm in the post monsoon season respectively. These findings indicate that all samples collected during both seasons fell considerably below the permissible range recommended by the WHO (2011). Consequently, these samples can be deemed suitable for various applications.

5.1.7.1.3 Total dissolved solid

The measuring of TDS concentration in surface water is of extreme significance for the evaluation of water quality. This assessment is crucial in determining the suitability of water for both drinking and agricultural purposes. TDS levels < 600 mg/L are generally considered acceptable to human health, whereas those >1000 mg/L are considered unpleasant WHO (2011). Elevated TDS concentrations in water have been associated with a variety of health diseases such as arthritis, kidney and gallstone formation, joint stiffness, and several other issues.

The measured TDS levels varied from 64 mg/L to 643 mg/L in the pre monsoon, whereas it ranged from 63 mg/L to 465 mg/L with an average of 180 mg/L in the post monsoon season. These findings demonstrate that one sample (SW-13) surpassed the WHO (2011) recommended limits in the pre monsoon season. On the other hand, all surface water

samples taken in the post monsoon season were considerably below the recommended allowable limit of 500 mg/L.

5.1.7.1.4 Calcium

The calcium and magnesium levels of water are frequently used to classify its suitability. The calcium is necessary for the proper functioning of our skeletal system, nervous system, muscles, and blood clotting system. The calcium carbonate content in water increases due to the process of weathering of limestone and dolomite. The calcium ions are formed in higher concentrations by the calc-silicate minerals amphibole, pyroxene, and plagioclase in water (Hem, 1989).

The measured calcium values ranged from 20.96 mg/L to 74.64 mg/L, with its mean value of 34.03 mg/L in the pre monsoon, while it ranged from 7.85 mg/L to 78.36 mg/L with its mean value of 23.49 mg/L in the post monsoon season. These findings show that no samples exceeded the permissible limits in the pre monsoon season. One sample (SW-12) exceeded the WHO (2011) guideline limits in the post monsoon season, however the remaining samples were significantly under the limit of 75 mg/L.

5.1.7.1.5 Magnesium

Magnesium has a substantial impact on the amount of water hardness. it is obtained from several sources, such as the ferromagnesian minerals olivine, biotite, diopside, augite, and hornblende. It is also present in significant quantities within natural water systems. Magnesium salts have the potential to cause severe health problems for humans, including cathartic and diuretic changes, as well as a laxative influence (CPCB 2008).

The measured magnesium concentration ranged from 3.29 mg/L to 81.43 mg/L, with its mean value of 18.20 mg/L in pre monsoon, whereas it ranged from 2.0 mg/L to 40.45 mg/L, with its mean value of 11.40 mg/L, in the post monsoon season. The findings demonstrate that one sample (SW-13) was exceeded the standards guidelines in the pre

monsoon. Whereas, all samples in the post monsoon season were well below the suggested allowable limit of 50 mg/L WHO (2011).

5.1.7.1.6 Sodium

Sodium has been the most essential nutrient. The sodium level of the water must be taken into consideration when assessing the quality of water for irrigation since higher sodium concentrations result in harder and more permeable soil (Tijani 1994). The utilisation of water with elevated sodium levels is not recommended for irrigation or domestic applications.

The measured sodium concentration ranged from 10.33 mg/L to 46.65 mg/L, with its mean value of 23.49 mg/L in pre monsoon, while it ranged from 2.64 mg/L to 28.42 mg/L, with its mean value of 13.05 mg/L in post monsoon season respectively. The surface water samples collected throughout both seasons were found to be within acceptable limits and showed much lower levels compared to the allowed limit of 50 mg/L established by the WHO (2011). These findings suggest that the water samples could be potentially utilised for various purposes.

5.1.7.1.7 Potassium

The potassium ion concentration is important in assessing water quality. The primary factor behind the elevated levels of potassium ions in the water is the process of rock weathering in the vicinity, with the weathering of potash silicate minerals serving as the principal cause for the observed increase in potassium concentration within the water (Murkute, 2014). The potassium ion limit in water is < 15 mg/L, as per WHO (2011) standards. The potential cause of this phenomenon may be attributed to the release of pollutants originating from the chemical industry or the effluent of agricultural fertilisers into adjacent surface water bodies.

The concentration of potassium values ranged from 1.65 mg/L to 13.35 mg/L, with its mean value of 5.11 mg/L in pre monsoon. However, it ranged from 0.2 mg/L to 11.20 mg/L, with its mean value of 3.34 mg/L in post monsoon season. The surface water samples collected during both seasons were substantially below the permissible limit of 15 mg/L WHO (2011), which indicates that they might be used for a variety of applications. Based on the results obtained from this investigation, there was a significant decrease in the potassium concentration within the designated study region while comparing the pre monsoon and post monsoon seasons.

5.1.7.1.8 Fluoride

Fluoride is the most common kind of fluorine which is a naturally occurring water pollutant. The water containing < 0.5 mg/l of fluoride can result in dental cavities and weak bones, whereas water containing >1.5 mg/l of fluoride can result in physiological disorder, skeletal and dental fluorosis, hormonal imbalance, and failing kidneys BIS (2012). The fluoride in water samples is therefore safe for human consumption at levels of 0.5 to 1.5 mg/l. The anthropogenic increase in fluoride levels can be attributed to the discharge of industrial wastewater into adjacent water bodies, resulting in elevated concentrations of fluoride (Kumar et al. 2019). The potential rise in fluoride concentrations can be attributed to the process of fluoride-rich mineral leaching, specifically from minerals such as fluorspar and biotite, which are commonly found in rocks.

The measured fluoride values ranged from 0.39 mg/L to 1.11 mg/L, with an average of 0.68 mg/L in pre monsoon, while it ranged from 0.38 mg/L to 0.92 mg/L, with an average of 0.56 mg/L in the post-monsoon season respectively. The fluoride content in water was significantly lower than the recommended limits of 1.5 mg/L WHO (2011) in all water samples during both seasons, making the water safe for different uses.

5.1.7.1.9 Chloride

The process of weathering leads to the dissolution of chloride ions derived from distinct rock formations into the surrounding soil and water bodies. Chloride is commonly used as an indicator for assessing water pollution due to its ability to impart a saline taste to water and induce laxative effects when found in high concentrations. The maximum allowable concentration of chloride in drinkable water should not exceed 200 mg/L, although it may be necessary to increase this level to 600 mg/L in order to meet international standards (WHO, 2008).

The measured concentration of Chloride varied from 10.84 mg/L to 131.96 mg/L with an average of 34.28 mg/L in pre monsoon, while it varied from 2.81 mg/L to 51.71 mg/L with an average of 17.90 mg/L in the post monsoon season. The chloride concentration in the water samples collected from both seasons was under the recommended threshold of 250 mg/L as stated by the (WHO, 2011). This finding suggests that the water can be considered suitable for consumption.

5.1.7.1.10 Nitrate

Nitrate is one of the contaminants that can be found in agricultural water almost anywhere in the world (Adimalla and Li, 2018). The primary source of nitrate in the aquatic environment is derived from terrestrial runoff, along with industrial discharge. The significance of an increase in nitrate levels lies in its association with several chronic conditions, such as stomach cancer, cardiovascular disease, and the "blue baby syndrome" that affects newborns (Raju et al. 2009). The observed elevated concentrations of nitrates in the study region can potentially be attributed to both sewage discharges and agricultural practices.

The observed nitrate concentration ranged from 0.36 mg/L to 14.56 mg/L, with an average of 3.68 mg/L in pre monsoon, while, it ranged from 0.0 mg/L to 124.73 mg/L,

with an average of 8.45 mg/L in post monsoon season. The nitrate concentration in surface water was found to be consistently below the recommended limit of 45 mg/L (WHO, 2011) in almost all samples examined over both seasons, indicating that the water is suitable for different uses. According to these findings, the nitrate level in the area decreased significantly in post monsoon than pre monsoon season.

5.1.7.1.11 Sulphate

The presence of sulphate concentrations in mining regions is commonly attributed to the process of sulphide-containing minerals (such as pyrite, anhydrite, arsenopyrite, and gypsum) undergoing oxidation. This phenomenon is recognised as the principal factor contributing to the occurrence of acid mine drainage (Singh et al. 2011). The potential increase in sulphate contents within the aquifer materials and groundwater samples could be attributed to the process of sulphide oxidation occurring within the aquifer materials. Elevated levels of sulphate in potable water have the potential to cause respiratory problems in human individuals.

The observed sulphate concentration ranged from 4.19 mg/L to 282.09 mg/L with an average of 59.61 mg/L in the pre monsoon, while it ranged from 3.76 mg/L to 128.94 mg/L with an average of 28.44 mg/L in the post monsoon season. This finding indicates that two samples (SW-3 and SW-13) collected in the pre monsoon exceeded the recommended permissible limit of 250 mg/L (WHO, 2011). The sulphate concentrations were significantly lower than the suggested allowed limit of 150 mg/L in the post monsoon season. Based on the data acquired, there was a notable decline in sulphate concentration within the area from pre to post monsoon season.

5.1.7.1.12 Bicarbonate

The regulation of freshwater alkalinity is regulated by the presence of bicarbonate ions. Furthermore, bicarbonate exerts a substantial influence on the concentration of electrical

conductivity in the given region (Tiwari et al. 2016). The assessment of bicarbonate hazard commonly involves the evaluation of residual sodium carbonate, a significant parameter that significantly influences the suitability of water for agricultural use. The presence of an excessive amount of bicarbonate in agricultural soil and its subsequent interaction with plants can have adverse physical and chemical consequences, ultimately leading to a decrease in productivity (Adhikary et al. 2011).

The measured bicarbonate concentration ranged from 29 mg/L to 193 mg/L with an average of 105.06 mg/L in the pre monsoon while it ranged from 26 mg/L to 121 mg/L with an average of 73.41 mg/L in the post monsoon season, indicating that all samples collected from both seasons were well within the permissible limit of 200 mg/L (WHO, 2011). The data collected indicates a considerable reduction in bicarbonate concentration within the area from pre monsoon to post monsoon season.

5.1.7.1.13 Total Hardness

Water hardness refers to its ability to generate soap lather, with calcium and magnesium being the primary minerals responsible for influencing water hardness in various water samples. The classification of water hardness encompasses four distinct categories: soft, moderately soft, hard, and extremely hard. Soft water is characterised by a mineral content of < 75 mg/L, while moderately soft water was within the range of 76 to 150 mg/L. Hard water is defined as having a mineral content between 151 and 300 mg/L, whereas extremely hard water is identified by a mineral content >300 mg/L (Sawyer and McCarty, 1967).

The total hardness concentrations ranged from 50.77 mg/L to 304.04 mg/L in the pre monsoon, with an average of 142.17 mg/L while it ranged from 34.07 mg/L to 254.77 mg/L, with an average of 105.59 mg/L in post monsoon season. Total Hardness concentration in the area decreased significantly from pre to post monsoon season based

on obtained data. Total Hardness concentrations in surface water was significantly lower than the recommended limits of 500 mg/L (WHO, 2011) in almost all samples in both seasons which makes the water safe for different uses.

5.1.8 Major Ion Chemistry

The predominant dissolved ions detected in aqueous solutions are major ions, which include cations and anions possessing positive and negative charges, respectively. The major ions of surface water samples were statistically analysed. This finding shows that calcium and sodium were the two most abundant cations in the pre monsoon and bicarbonate was most abundant anion in surface water samples in the post monsoon seasons, respectively.

5.1.8.1 Cation Chemistry

Calcium was the most abundant cation, accounting for 42.10% and 45.8% among cation in the pre monsoon and post monsoon seasons, respectively. Sodium was the second most abundant cation, accounting for 29.06% and 25.4% of total cations in the pre monsoon and post monsoon seasons. Only magnesium was a less dominating cation accounting for 22.51% and 22.2% in both pre monsoon and post monsoon seasons. Potassium was the least abundant cation accounting only 6.32% and 6.5% of the total cation in the pre monsoon and post monsoon seasons.

The order of mean abundance of major cations is $Ca^{2+} > Na^{+} > Mg^{2+} > K^{+}$ in both seasons. The concentrations of potassium are typically lower than those of Na^{+}, Ca^{2+}, and Mg^{2+} in an aquifer system. The percentage contribution and box plot diagram of individual cations in pre and post monsoon season were shown in Fig.5.50, Fig.5.51 and Fig.5.52, Fig.5.53 respectively.

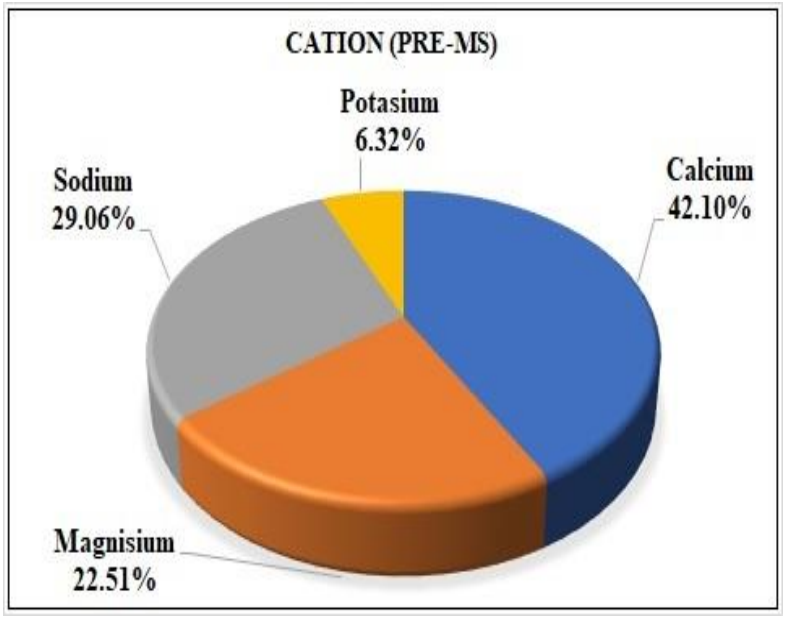

Fig.5.50 Percentage contribution of major cations in pre monsoon season

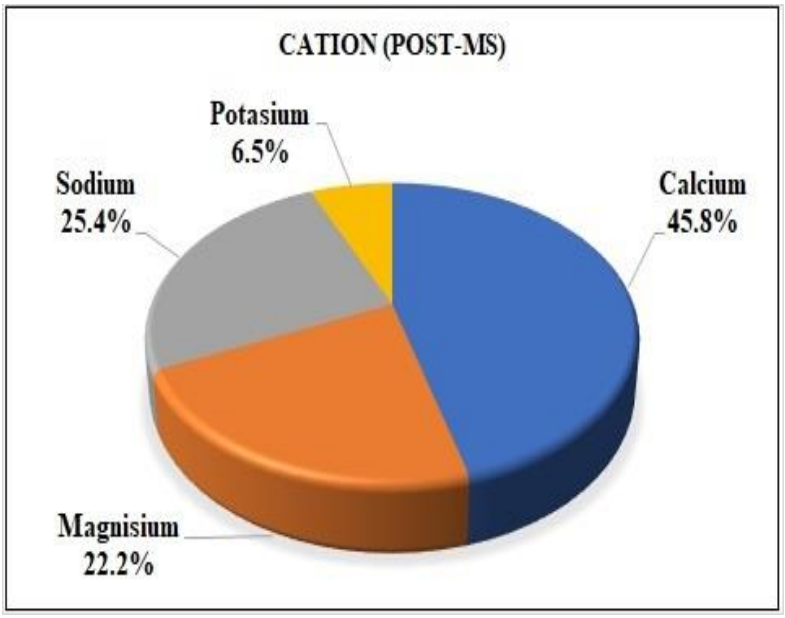

Fig.5.51 Percentage contribution of major cations in post monsoon season

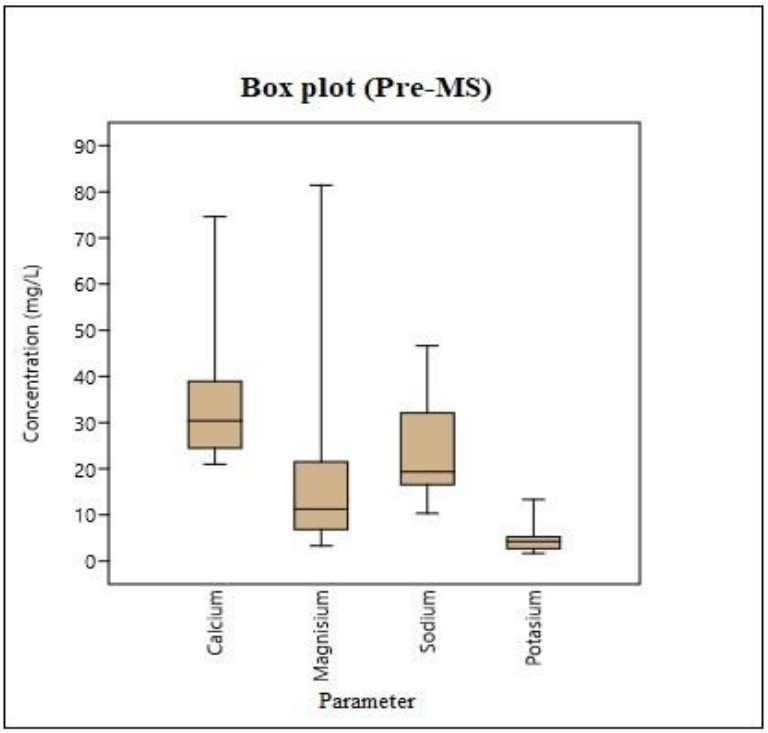

Fig.5.52 Box plot of cations of surface water in pre monsoon season

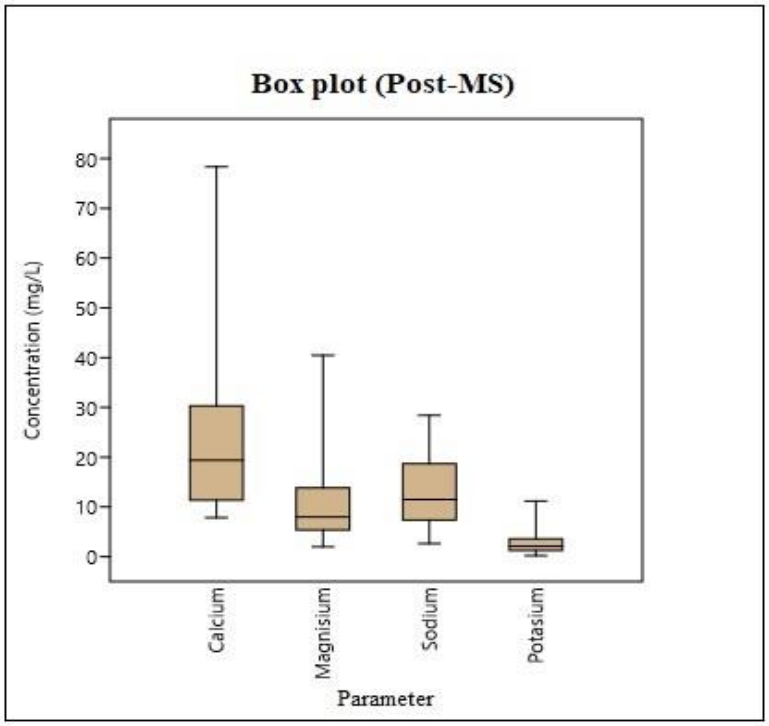

Fig.5.53 Box plot of cations of surface water in post monsoon season

5.1.8.2 Anion Chemistry

The most abundant anion was bicarbonate, that consist 51.68% and 57.01% of all anions in the pre monsoon and post monsoon seasons, respectively. The second most abundant

anion was sulphate, accounting for 29% and 22.08% among anions in the pre monsoon and post monsoon seasons. On the other hand, Chloride was a less dominant anion, accounting about 16.86% and 13.90% in the pre monsoon and post monsoon seasons. While nitrate was the least common anion, it accounted 1.8% and 6.56% of the total anion in the pre monsoon and post monsoon seasons. Fluoride ions appeared to be the only anions to pass in both seasons with approximately 0% of contribution.

The order of mean abundance of major anions was HCO_3^- > SO_4^{2-} > Cl^- > NO_3^- > F^- in both seasons respectively. The percentage contribution and box plot diagram of individual anions in pre and post monsoon season were shown in Fig.5.54, Fig.5.55 and Fig.5.56, Fig.5.57 respectively.

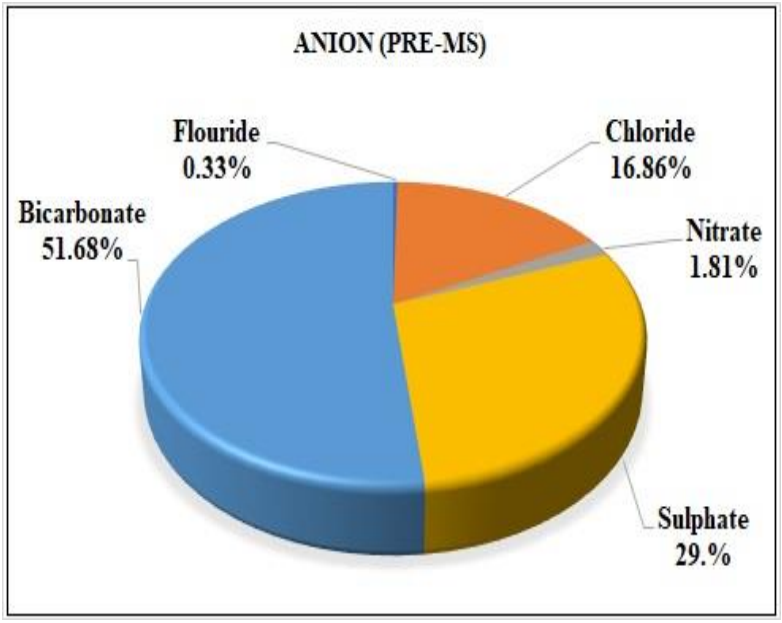

Fig.5.54 Percentage contribution of major anions in pre monsoon season

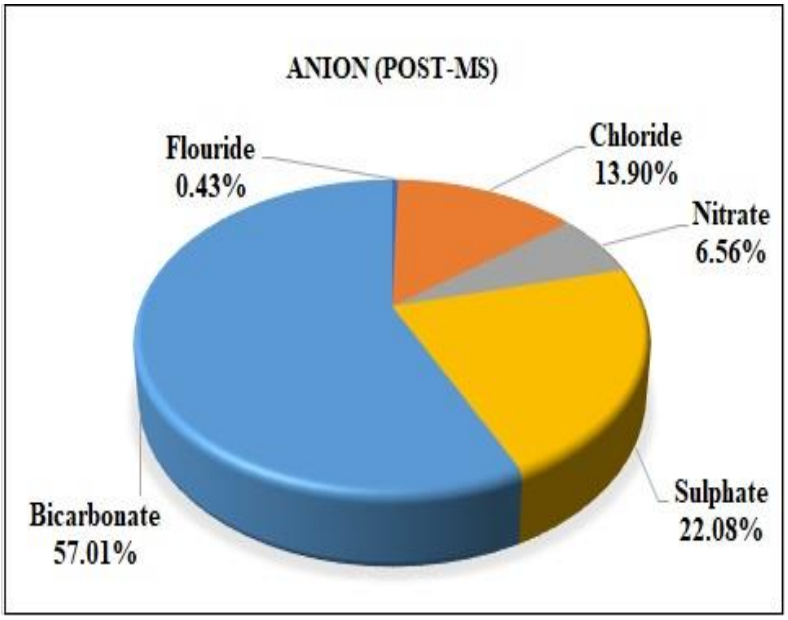

Fig.5.55 Percentage contribution of major anions in post monsoon season

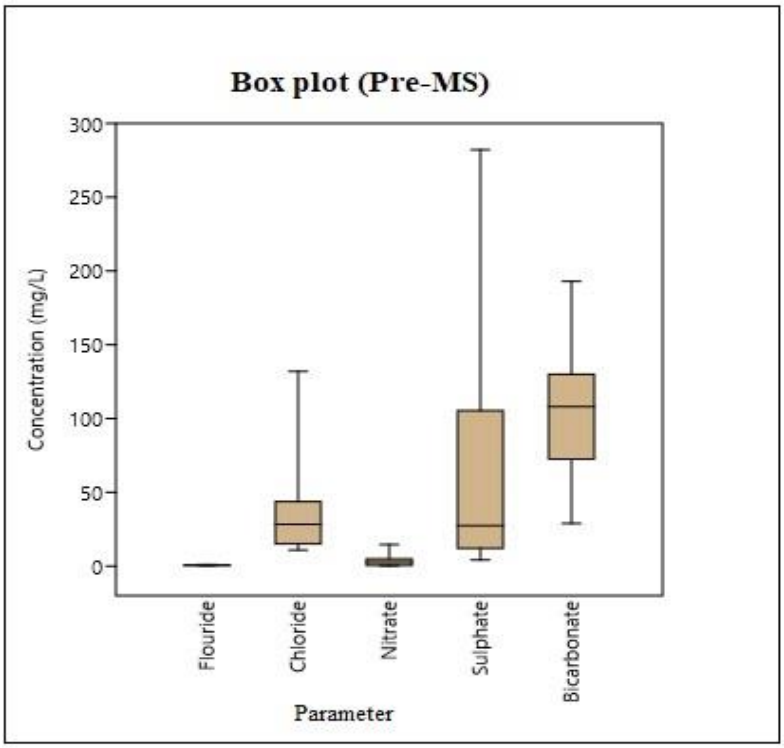

Fig.5.56 Box plot of Anions of surface water in pre monsoon season

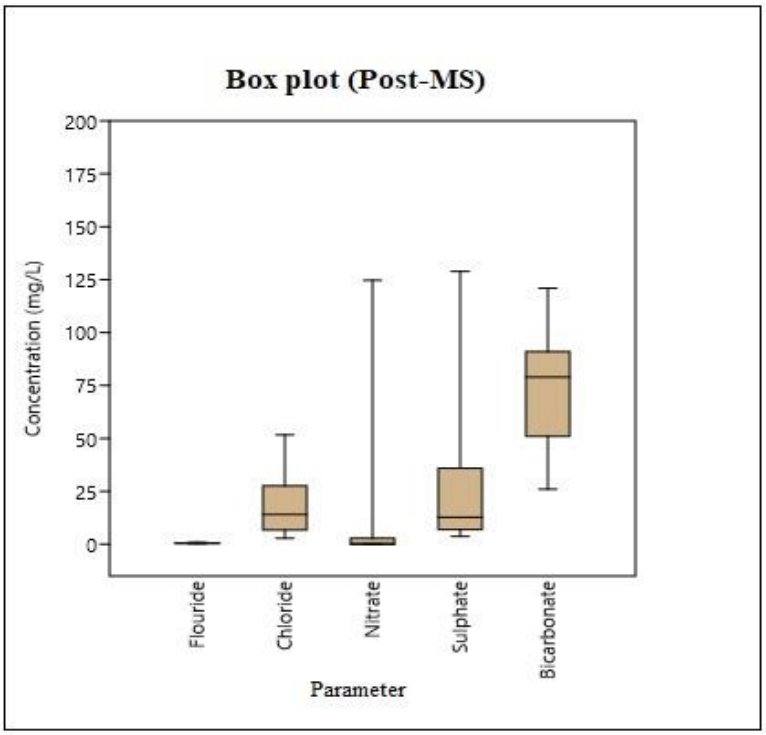

Fig.5.57 Box plot of Anions of surface water in post monsoon season

5.1.9 Statistical correlation

This technique depicts the statistical correlation among two or more independent variables, facilitating in the identification of the key processes that caused the current water chemistry. Furthermore, the correlation analysis assists in measuring the extent of correlation between the two parameters and in establishing a general concept of their relationship (Peat et al 2009). Pearson correlation coefficient values ranging from 0.9 to 1 are considered strongly correlated, while values between 0.9 and 0.5 are moderately correlated and < 0.5 are poorly correlated (Tirkey et al., 2017).

The correlation coefficients (r) between thirteen water parameters were determined during both seasons and their numerical values are tabulated in Tables.5.21 and Table.5.22. Out of the total of 91 correlation coefficients, it was seen that 12 of them exhibited negative correlations, while the remaining 79 coefficients demonstrated positive correlations. Here, significantly strong to moderately positive correlation were observed between various pair of parameters in pre monsoon season such as EC and TDS

(r = 0.998), EC and TH (r = 0.852), EC and HCO_3^- (r = 0.862), TDS and TH (r = 0.846), TH and Mg^{2+} (r = 0.828), Mg and SO_4^{2-} (r = 0.801), whereas a negative correlation observed between pH and EC (r = -0.287), pH and TDS (-0.288), Mg^{2+} and K^+ (r = -0.222), K^+ and SO_4^{2-} (r = -0.303) respectively.

It was observed that of the 91 correlation coefficients examined in the post monsoon season, 13 exhibited negative correlations while 78 had positive correlations. The significant strong to moderately positive correlations were identified between EC and TDS (r = 0.991), EC and SO_4^{2-} (0.873), TDS and SO_4^{2-} (r = 0.873), Na^+ and Cl^- (r = 0.910), whereas a negative correlation identified between pH and TH (r = -0.274), pH and Ca^{2+} (r = -0.498), K^+ and SO_4^{2-} (r = -0.195) and F^- and NO_3^- (-0.252) respectively. Additional correlations were found, but they had no statistical significance. The significant positive correlations between the combinations made it evident that the variables were related to one another and might have come from the same origins within the examined area (Mohamed et al. 2003).

Table.5.21 Correlation coefficient matrix of surface water in pre-monsoon season

	pH	EC	TDS	TH	Ca^{+}	Mg^{2+}	Na^{+}	K^{+}	F^{-}	Cl^{-}	NO_3^{-}	SO_4^{2+}	HCO_3^{-}
pH	1.000												
EC	-0.287	1.000											
TDS	-0.288	0.998	1.000										
TH	-0.104	0.852	0.846	1.000									
Ca^{2+}	0.269	0.208	0.205	0.168	1.000								
Mg^{2+}	-0.175	0.779	0.769	0.808	0.108	1.000							
Na^{+}	0.036	0.496	0.497	0.709	0.152	0.157	1.000						
K^{+}	0.061	0.084	0.099	0.026	0.175	-0.222	0.310	1.000					
F^{-}	0.199	0.014	0.025	-0.062	0.344	-0.125	0.045	0.388	1.000				
Cl^{-}	0.081	0.406	0.419	0.478	0.226	0.024	0.772	0.538	-0.020	1.000			
NO_3^{-}	0.237	0.106	0.112	0.019	0.389	0.054	-0.033	0.530	0.098	0.251	1.000		
SO_4^{2+}	0.107	0.494	0.498	0.698	0.304	0.801	0.210	-0.303	-0.162	0.117	0.041	1.000	
HCO_3^{-}	-0.017	0.862	0.862	0.787	0.327	0.660	0.529	-0.095	0.095	0.399	0.003	0.560	1.000

Table.5.22 Correlation coefficient matrix of surface water in post-monsoon season

	pH	EC	TDS	TH	Ca^{+}	Mg^{2+}	Na^{+}	K^{+}	F^{-}	Cl^{-}	NO_3^{-}	SO_4^{2+}	HCO_3^{-}
pH	1.000												
EC	0.181	1.000											
TDS	0.194	0.991	1.000										
TH	-0.274	0.523	0.535	1.000									
Ca^{2+}	-0.498	0.178	0.191	0.794	1.000								
Mg^{2+}	0.078	0.653	0.659	0.776	0.232	1.000							
Na^{+}	0.098	0.551	0.574	0.487	0.261	0.508	1.000						
K^{+}	0.362	-0.012	0.027	0.307	0.124	0.362	0.106	1.000					
F^{-}	0.070	0.049	0.094	0.158	0.357	-0.117	-0.042	-0.074	1.000				
Cl^{-}	0.346	0.514	0.532	0.351	0.159	0.397	0.918	0.197	-0.119	1.000			
NO_3^{-}	0.081	0.062	0.059	0.558	0.162	0.725	0.272	0.619	-0.252	0.183	1.000		
SO_4^{2+}	-0.039	0.867	0.873	0.390	0.100	0.521	0.463	-0.195	0.076	0.354	-0.140	1.000	
HCO_3^{-}	-0.015	0.566	0.538	0.452	0.264	0.450	0.439	-0.071	0.234	0.319	0.198	0.361	1.000

5.1.10 CCME Water Quality Index (WQI) of surface water samples

The CCME WQI of surface water samples ranged from 80.79 to 100 in the pre monsoon season. Based on the findings of the CCME WQI analysis, it was found that a total of 3 (17.65%) of the surface water samples, specifically SW-5, SW-10, and SW-14, were classified as excellent. The other fourteen (82.35%) of the samples were classed as good. No sample was assigned to the fair to poor class of CCME WQI.

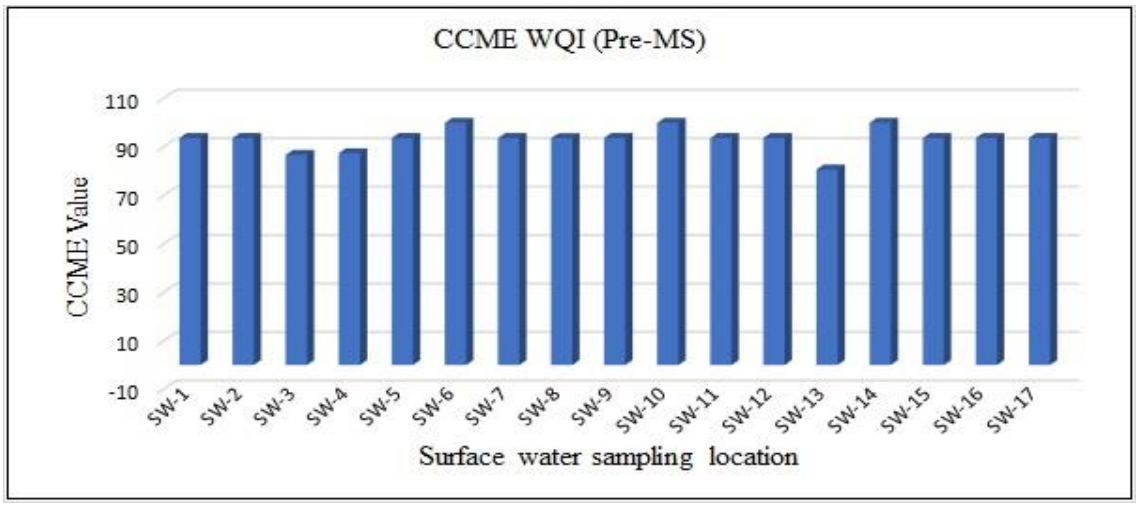

Fig.5.58 Graphical representation of CCME WQI during pre-monsoon season

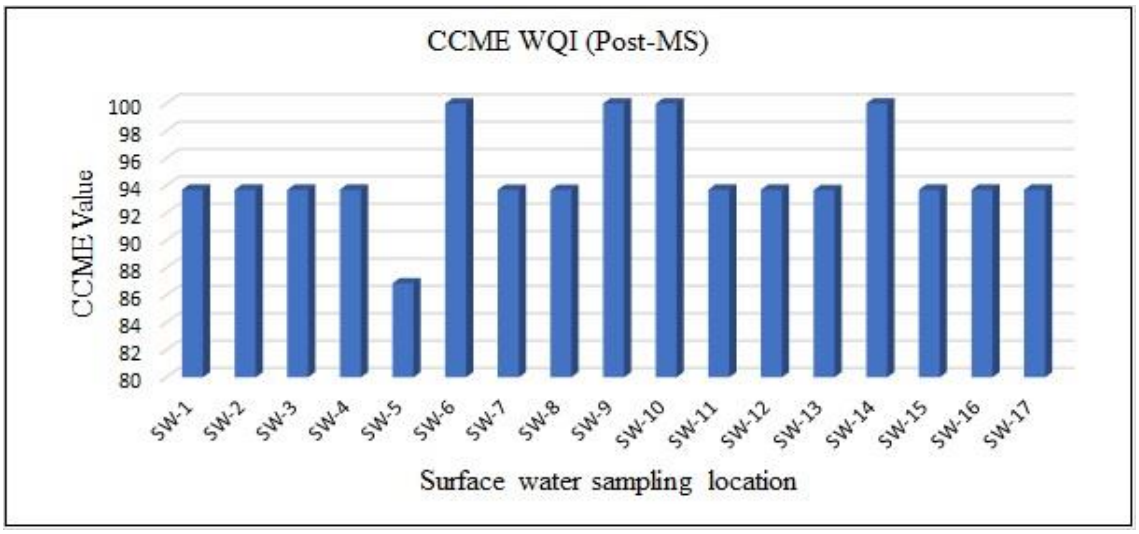

Fig.5.59 Graphical representation of CCME WQI during post monsoon season

The spatial map of CCME WQI values demonstrates that the north and western sides of the area had lower CCME WQI values, whereas east, north western, and south regions, had higher CCME WQI values which indicates the surface water safe for domestic uses

in the pre monsoon season. The bar chart and spatial distribution map of CCME WQI in pre monsoon season has been shown in Fig.5.58 and Fig.5.60 respectively.

The CCME WQI ranged from 86.87 to 100 in the post monsoon season. CCME WQI analysis determined that 4 (23.53%) samples such as SW-6, SW-9, SW-10, and SW-14 were excellent and rest 13 (76.47%) samples were good category in post monsoon season. The spatial map of the CCME WQI shows that the whole area had higher CCME WQI values than the south western sides, indicating that the surface water was safe for domestic uses in the post monsoon season. The bar chart and spatial map of CCME WQI in post monsoon season has been shown in Fig.5.59 and Fig.5.61 respectively.

The lower value of the CCME WQI was attributed to a larger concentration of physicochemical constituents in the surface water, which directly affects the quality of the surface water. As a consequence of this, the quality of the water improved during the post-monsoon season as compared to the pre-monsoon season depending on the physicochemical characteristic that played a crucial role in defining water quality. These changes in the quality of the water samples could be related to a dilution of the pollution that was induced by the considerable rainfall that occurred in the region during the monsoon season. The CCME WQI values and the status of surface water quality for the pre and post monsoon seasons are provided in Tables.5.23 and Table.5.24 respectively.

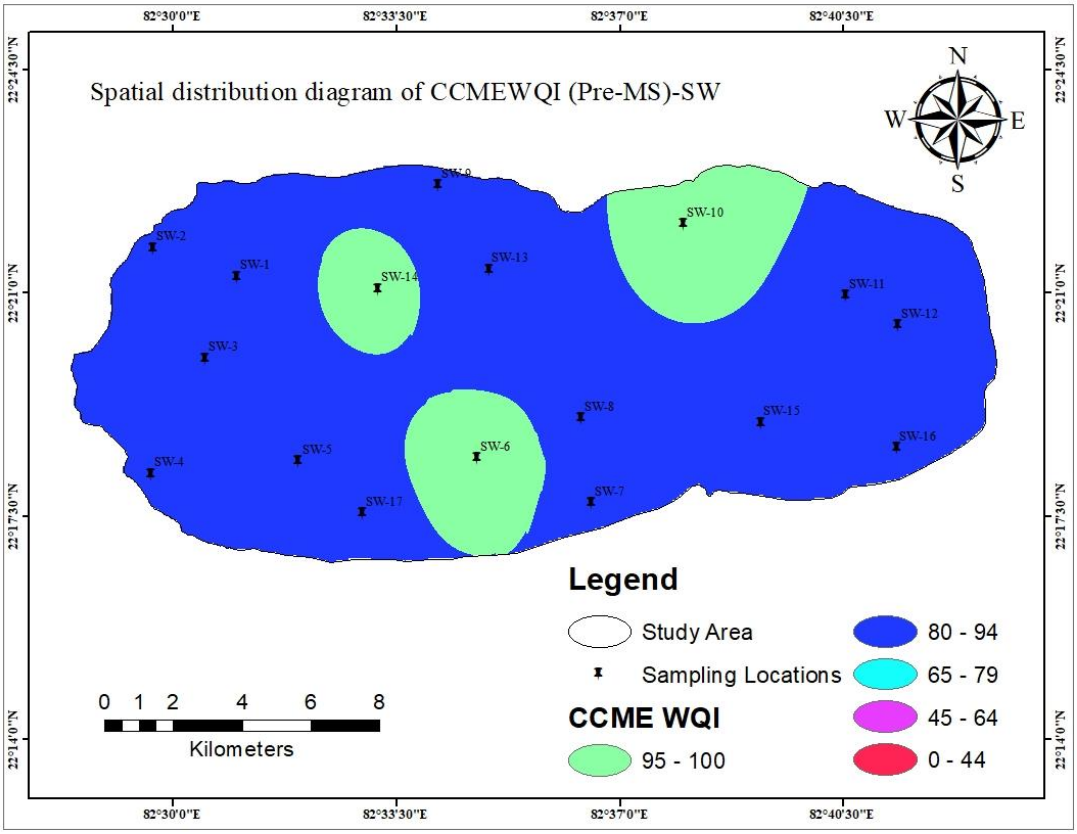

Fig.5.60 Spatial map of CCME WQI of surface water during pre-monsoon season

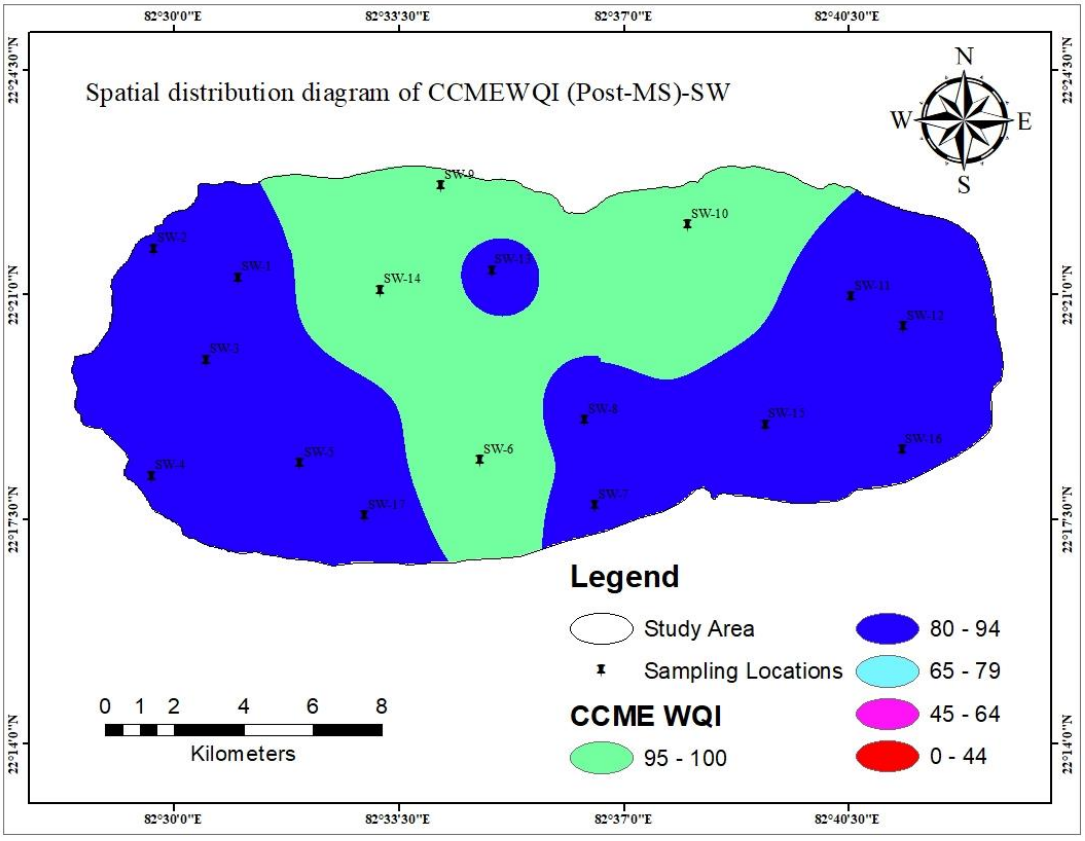

Fig.5.61 Spatial map of CCME WQI of surface water during post-monsoon season

Table.5.23 CCME WQI value and its category in surface water during pre-monsoon

Sample code	Sampling locations	CCME WQI	Description
SW-1	Sirki Khurd pond water	93.7	Good
SW-2	Tiverta pond water	93.7	Good
SW-3	Chainpur pond water	86.75	Good
SW-4	Andikachhar pond water	87.43	Good
SW-5	Suwabhondi pond water	93.71	Good
SW-6	Ralia pond water	100	Excellent
SW-7	Mahowadih pond water	93.7	Good
SW-8	Bhathora SECL pond water	93.68	Good
SW-9	Chakadhamna pond water	93.71	Good
SW-10	Surakchhar pond water	100	Excellent
SW-11	Durpa pond water	93.71	Good
SW-12	Patel para pond water	93.72	Good
SW-13	Shakti Nagar pond water	80.69	Good
SW-14	Urja Nagar pond water	100	Excellent
SW-15	Khodri pond water	93.71	Good
SW-16	Khairbhawna pond water	93.71	Good
SW-17	Bamhanikona pond water	93.71	Good

Table.5.24 CCME WQI value and its category in surface water during post monsoon

Sample code	Sampling locations	CCME WQI	Description
SW-1	Sirki Khurd pond water	93.71	Good
SW-2	Tiverta pond water	93.71	Good
SW-3	Chainpur pond water	93.71	Good
SW-4	Andikachhar pond water	93.71	Good
SW-5	Suwabhondi pond water	86.87	Good
SW-6	Ralia pond water	100	Excellent
SW-7	Mahowadih pond water	93.7	Good
SW-8	Bhathora SECL pond water	93.7	Good
SW-9	Chakadhamna pond water	100	Excellent
SW-10	Surakchhar pond water	100	Excellent
SW-11	Durpa pond water	93.71	Good
SW-12	Patel para pond water	93.71	Good
SW-13	Shakti Nagar pond water	93.68	Good
SW-14	Urja Nagar pond water	100	Excellent
SW-15	Khodri pond water	93.71	Good
SW-16	Khairbhawna pond water	93.71	Good
SW-17	Bamhanikona pond water	93.71	Good

5.1.11 Surface water Assessment Suitability for Irrigational Uses

The suitability of surface water for irrigation is assessed based on its mineral content and the potential effects it may have on soils and plants. The presence of a high sodium concentration in the irrigation water leads to an increase in the osmotic pressure that is present within the soil. Salts can have a direct impact on plant growth and an indirect impact by altering the permeability, aeration, and structure of the soils (Todd and Mays, 2005). It generally restricts water from reaching different plant segments, which reduces crop yields (Rao et al. 2013). Several indices, including SAR, %Na, and KI, were used to determine irrigation water suitability as tabulated in Table.5.28 and Table.5.29 respectively.

5.1.11.1 Sodium Absorption Ratio (SAR)

The USSL suggests that employing the SAR to assess the alkalinity or sodium hazard of available water for irrigation purposes (U.S Salinity laboratory, 1954). It is calculated by dividing the Na^+ content by the sum of squares root of one-half of the (Ca^{2+} + Mg^{2+}) concentrations.

The calculated SAR values for surface water ranged from 2.53 meq/L to 9.35 meq/L, with an average value of 4.80 meq/L in pre monsoon season while it ranged from 2.53 meq/L to 9.35 meq/L, with an average value of 4.80 meq/L in post monsoon season respectively. According to the SAR (Richard, 1954) classification, all surface water samples from both seasons were classified as low, indicating that the water samples were suitable for irrigation purposes. as given in Table.5.25. Based on SAR map, water samples fall into three groups: C1-S1, C2-S1, and C3-S1 as shown in Fig.5.62 and Fig.5.63 respectively. This means that the majority of surface water samples (70.59% in pre monsoon and 52.94% in post monsoon) fall into the C2-S1, (17.65% in pre monsoon and 47.06% in

post monsoon) of samples fall under C1-S1 categories and rest 11.76% samples only in pre monsoon season lied under C3-S1 are suitable for irrigation.

Table.5.25 Classification of samples showing their suitability for irrigation based on SAR in pre and post monsoon season

Parameter	Range	Classification	No. of samples (Pre-MS)	No. of samples (Post-MS)
SAR	<10	Low	17 samples (100%)	17 samples (100%)
	10 – 18	Medium	0	0
	18 – 26	High	0	0
	> 26	Very High	0	0

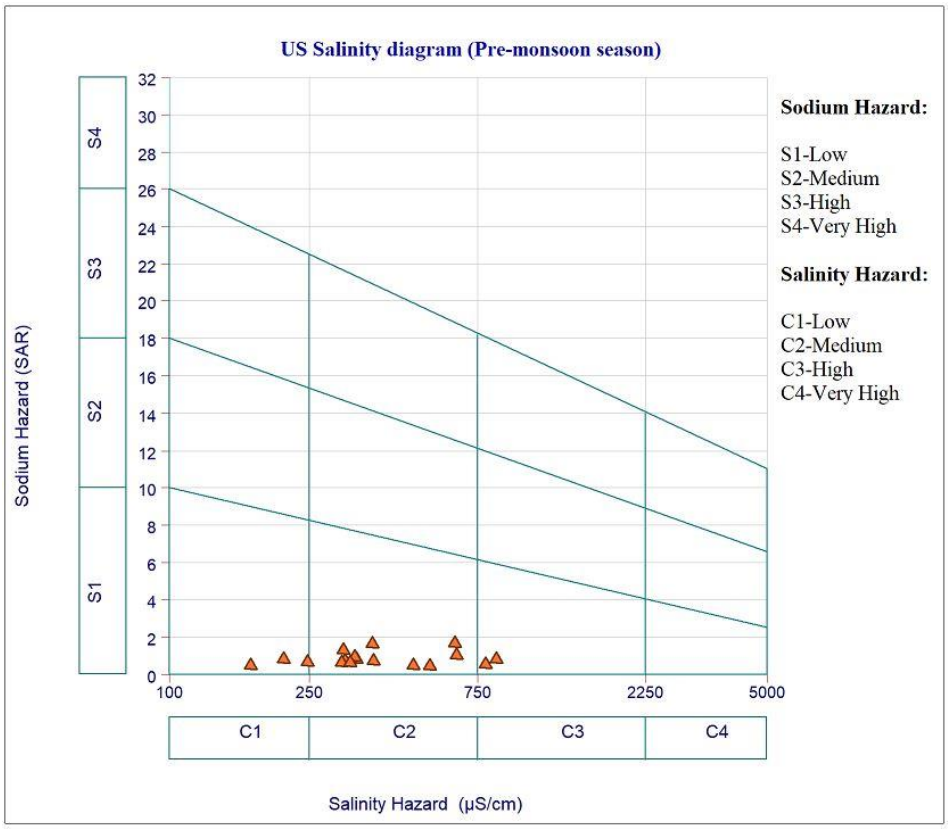

Fig.5.62 US Salinity diagram for irrigation water classification in pre monsoon season

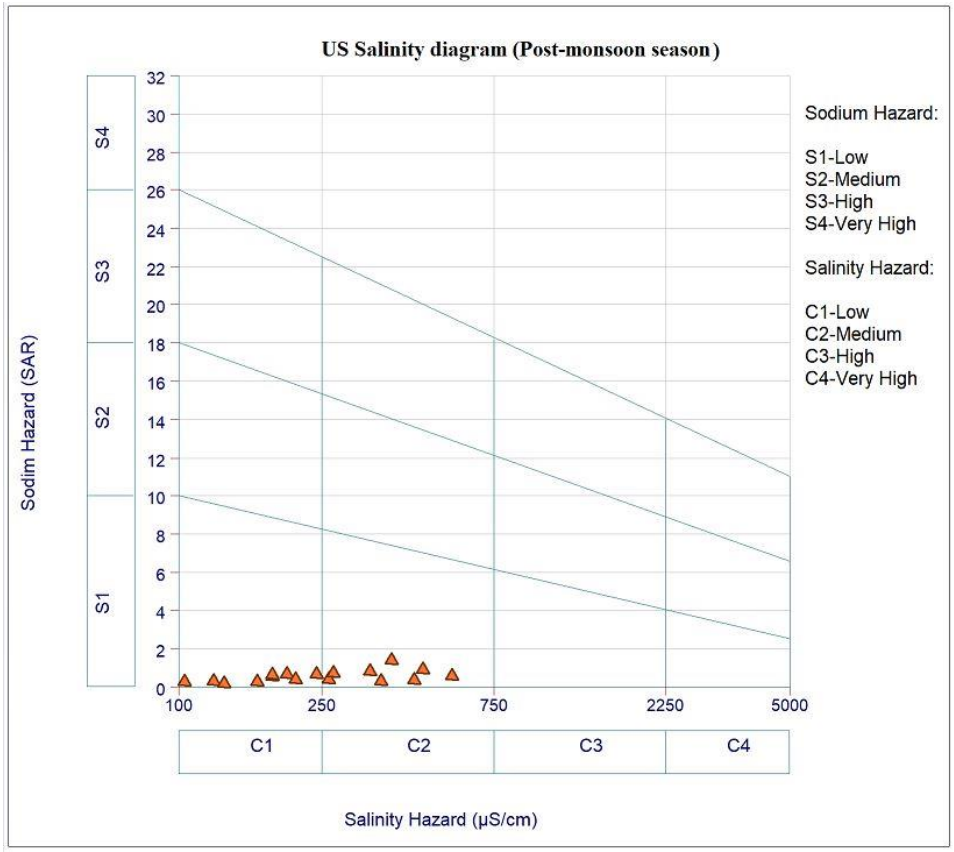

Fig.5.63 US Salinity diagram for irrigation water classification in post monsoon season

5.1.11.2 Sodium Content (%Na)

The percent sodium is frequently used to measure the suitability of irrigation water quality (Wilcox 1955). The presence of sodium in irrigation water leads to an exchange process with calcium ions and magnesium ions in the soil, resulting in reduced permeability and impaired internal drainage of the soil. The maximum sodium level allowed is 60% as per the Indian Standard (BIS 1991).

The soluble sodium percentage ranged from 19.32% to 56.45%, with an average value of 36.62% in pre monsoon while, it ranged from 14.05% to 57.53%, with an average value of 33.32% in post monsoon season as mentioned in Table.5.26. Wilcox (1948) proposed the classification depicted in Fig.5.64 and Fig.5.65 respectively. The five categories of irrigation water quality based on percent sodium are given in Table 5.26. According to Wilcox plot, (70.58% in pre monsoon and 88.2% in post monsoon) of surface water samples are excellent to good, while (29.4% in pre monsoon and 11.8% in post monsoon) of surface water samples are permissible category, allowing them to be used for irrigation.

Table.5.26 Classification of samples showing their suitability for irrigation based on %Na in pre and post monsoon season

Parameter	Range	Classification	No. of samples (Pre-MS)	No. of samples (Post-MS)
%Na	<20	Excellent	1 sample (5.88%)	1 sample (5.88%)
	20 – 40	Good	11 samples (64.7%)	14 samples (82.4%)
	40 – 60	Permissible	5 samples (29.4%)	2 samples (11.8%)
	60 - 80	Doubtful	0	0
	>80	Unsuitable	0	0

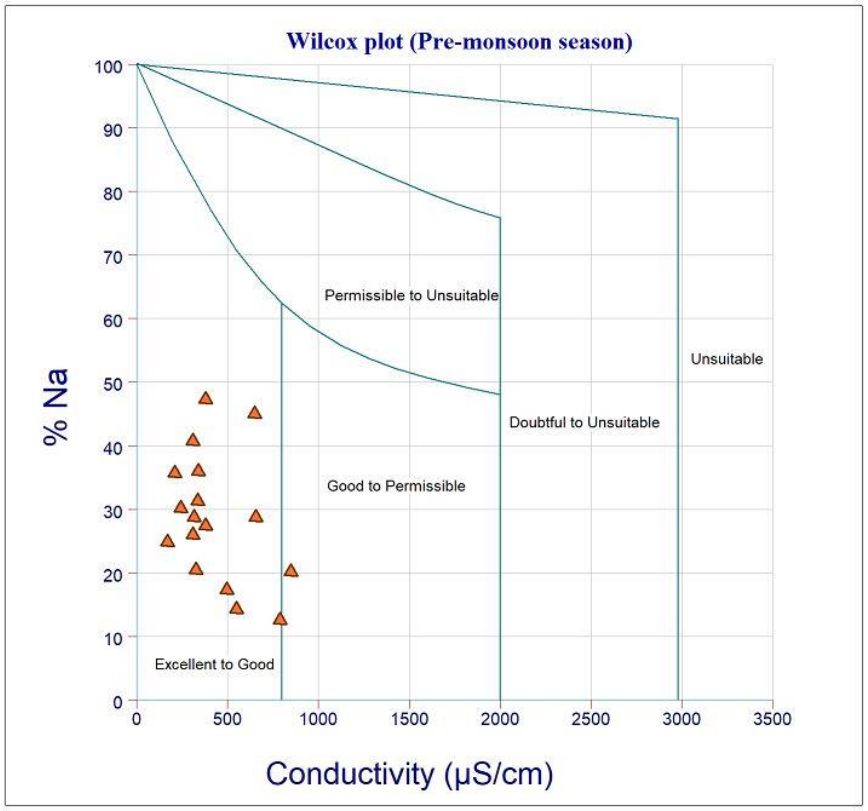

Fig.5.64 Wilcox plot for classification of irrigation water in pre monsoon season

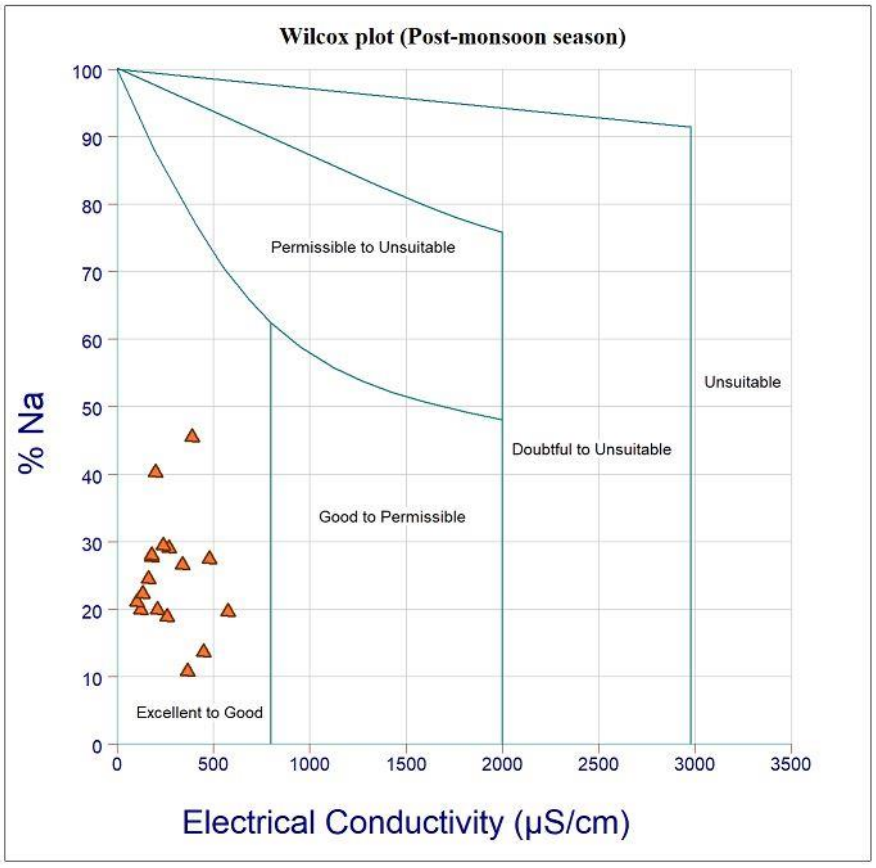

Fig.5.65 Wilcox plot for classification of irrigation water in post monsoon season

5.1.11.3 Kelly Index (KI)

The KI is a valuable approach for the classification of water intended for irrigation purposes. Additionally, it serves as a means to categorise irrigation water. The water with KI > 1.0 is sodium-rich and should not be utilised for irrigation, but water with KI < 1.0 is acceptable for irrigation (Kelley 1946; Paliwal 1967).

KI ranged from 0.18 to 1.14, with an average value of 0.51 in pre monsoon while, it ranged from 0.13 to 1.26, with an average value of 0.42 in post monsoon season respectively. Based on the KI classification, it can be observed that approximately 94.10% of the samples are categorised as acceptable for irrigation in both seasons. However, the remaining 5.9% of the samples are classified as unsuitable for irrigation in both seasons as given in Table.5.27.

Table.5.27 Classification of samples showing their suitability for irrigation based on KI in pre and post monsoon season

KI	Water quality	No. of samples (Pre-MS)	No. of samples (Post-MS)
<1	Suitable	16 samples (94.10%)	16 samples (94.10%)
>1	Unsuitable	1 sample (5.9%)	1 sample (5.9%)

Table.5.28 Values of SAR, %Na and KI of surface water samples in pre monsoon season

Sample code	SAR	Status	%Na	Status	KI	Status
GW-1	4.66	Low	47.58	Permissible	0.56	Suitable
GW-2	4.07	Low	36.34	Good	0.49	Suitable
GW-3	5.00	Low	28.72	Good	0.38	Suitable
GW-4	4.30	Low	42.96	Permissible	0.62	Suitable
GW-5	8.95	Low	52.49	Permissible	0.86	Suitable
GW-6	2.99	Low	24.93	Good	0.28	Suitable
GW-7	5.38	Low	38.62	Good	0.59	Suitable
GW-8	6.09	Low	37.22	Good	0.52	Suitable
GW-9	2.59	Low	31.50	Good	0.33	Suitable
GW-10	4.18	Low	35.80	Good	0.49	Suitable
GW-11	3.54	Low	32.75	Good	0.39	Suitable
GW-12	2.53	Low	19.32	Excellent	0.18	Suitable
GW-13	3.28	Low	20.78	good	0.22	Suitable
GW-14	7.44	Low	50.42	Permissible	0.89	Suitable
GW-15	3.69	Low	39.42	Good	0.40	Suitable
GW-16	9.35	Low	56.45	Permissible	1.14	Unsuitable
GW-17	3.61	Low	27.30	Good	0.34	Suitable

Table.5.29 Values of SAR, %Na and KI of surface water samples in post monsoon season

Sample code	SAR	Status	%Na	Status	KI	Status
GW-1	3.83	Low	53.93	Permissible	0.63	Suitable
GW-2	2.98	Low	36.52	Good	0.47	Suitable
GW-3	4.41	Low	32.37	Good	0.45	Suitable
GW-4	1.87	Low	28.99	Good	0.33	Suitable
GW-5	3.56	Low	30.43	Good	0.29	Suitable
GW-6	2.42	Low	25.71	Good	0.31	Suitable
GW-7	3.47	Low	35.63	Good	0.50	Suitable
GW-8	5.14	Low	35.26	Good	0.48	Suitable
GW-9	1.55	Low	27.50	Good	0.26	Suitable
GW-10	4.50	Low	39.28	Good	0.64	Suitable
GW-11	3.64	Low	36.21	Good	0.49	Suitable
GW-12	1.72	Low	14.05	Excellent	0.13	Suitable
GW-13	2.25	Low	21.13	Good	0.22	Suitable
GW-14	8.47	Low	57.53	Permissible	1.26	Unsuitable
GW-15	1.54	Low	35.01	Good	0.22	Suitable
GW-16	1.06	Low	31.97	Good	0.21	Suitable
GW-17	2.35	Low	24.94	Good	0.30	Suitable

5.2 Heavy Metal Analysis to evaluate the groundwater

Water is a fundamental necessity for the survival of all organisms living on the earth. Consequently, it is imperative to regularly assess the quality of water in terms of heavy metals. The phenomenon of sudden fluctuations in the demand for drinking water has been noted to be mostly attributed to the scarcity of groundwater resources and substantial population expansion. The people mostly use groundwater for drinking and residential purposes, therefore water contamination from mining is a major issue (Tiwari et al. 2017). The mining process, the disposal of overburden, and the washing of coal are all factors that have an impact on the quality of the groundwater. Therefore, surrounding area is experiencing an increase in the amount of chemical contamination (Singh et al. 2008). In addition to this, the quality of groundwater has seen degradation due to the discharge of untreated sewage and the over exploitation of groundwater resources. The utilisation of groundwater samples collected throughout the pre and post monsoon seasons of 2022 has been used to evaluate the effects of these heavy metal contamination in the groundwater around the area of study. Groundwater is prone to heavy metal contamination, which can arise from various sources, including both anthropogenic or naturals (Adaikpoh et al. 2005; Reza and Singh, 2010). The metal content in the majority of native habitats is incredibly low and mainly originates from the process of geological formations and mineral weathering (Karbassi et al. 2008; Charles et al. 1994; Reiners et al. 1975). The issue of non-biodegradable metal pollution is of the highest priority due to its ability to adversely affect several human body systems, including the nervous system and internal organs, leading to substantial harm and damage (Lee et al. 2007; Adams et al. 2008; Lohani et al. 2008).

5.2.1 Water sampling and its analysis

A total of seventy (70) groundwater samples were taken from various sites, including bore wells (46 samples), hand pumps (18 samples), and dug wells (6 samples), during both the pre and post monsoon seasons of 2022 (Fig.5.66 & Table.5.30). An analysis was conducted on a set of 10 heavy metals, including aluminium (Al), barium (Ba), cadmium (Cd), chromium (Cr), copper (Cu), iron (Fe), manganese (Mn), lead (Pb), nickel (Ni), and zinc (Zn), utilising an ICP-MS instrument. All of the water samples were passed through a 0.22 m Nylon syringe filter before the heavy metals were tested.

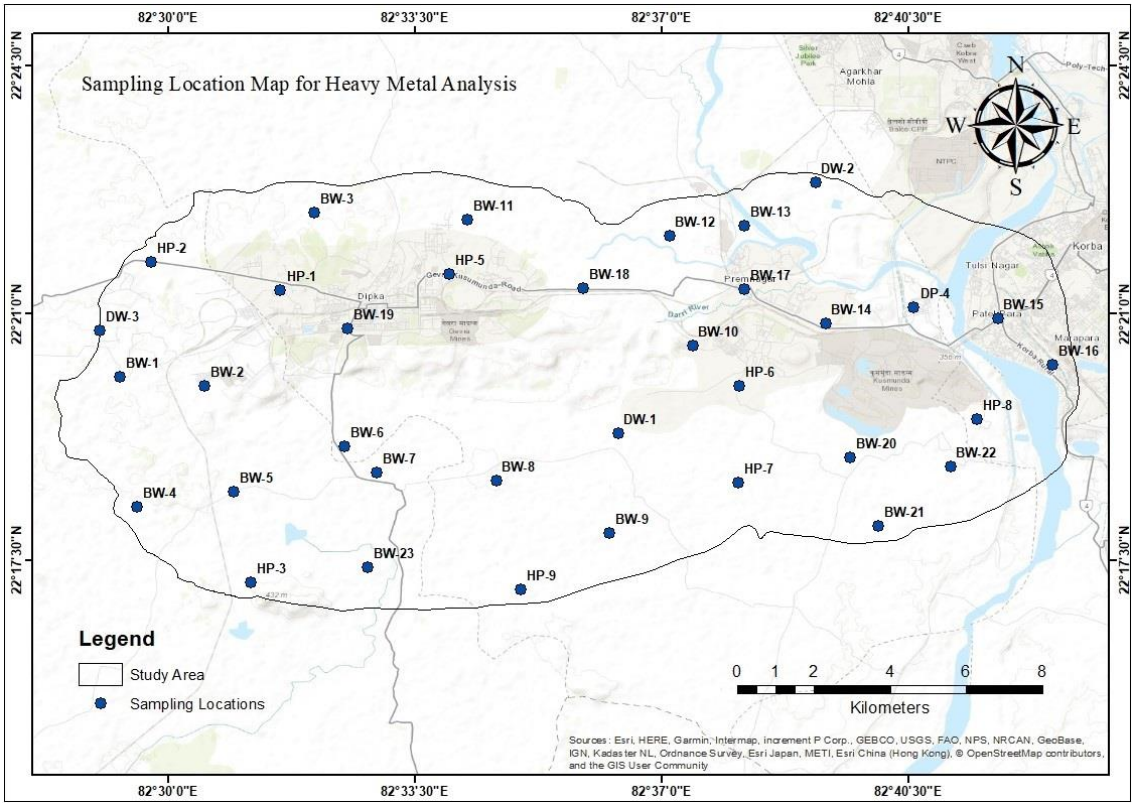

Fig.5.66 Sampling locations map for heavy metal analysis in KCF region

The utilisation of an integrated approach, encompassing the heavy metal pollution index (HPI), heavy metal evaluation index (HEI), and metal index (MI), holds significant importance in the evaluation of groundwater quality with respect to heavy metal contamination. The measurement of heavy metals has been conducted in the Central Instrument Facility (CIF) IIT (BHU), Varanasi. The summarized result of all heavy

metals for both seasons are given in Appendix A.13 to Appendix A.16 respectively. The primary goal of this chapter is to use GIS to analyse groundwater quality in terms of heavy metals for both pre and post monsoon seasons, and to create a distinct map for pollution indices.

Table.5.30 Sampling locations details of surface water samples

Sample code	Sampling locations	Latitude	Longitude
GW-1	Jhabar hand pump water	22.3555	82.5265
GW-2	Tiverta hand pump water	22.3620	82.4958
GW-3	Ratija borewell water	22.3349	82.4885
GW-4	Chainpur bore well water	22.3328	82.5086
GW-5	Binjhari bore well water	22.3737	82.5345
GW-6	Andikachhar bore well water	22.3041	82.4925
GW-7	Renki bore well water	22.3078	82.5154
GW-8	Suberpara handpump water	22.2864	82.5195
GW-9	Malgaon borewell water	22.3186	82.5416
GW-10	Haldibazar borewell water	22.3122	82.5493
GW-11	Raliya bore well water	22.3104	82.5775
GW-12	Mahowadih borewell water	22.2981	82.6042
GW-13	Bethora SECL dug well water	22.3217	82.6063
GW-14	Mangaon borewell water	22.3422	82.6240
GW-15	Durena dug well water	22.3720	82.5706
GW-16	Rohina borewell water	22.3682	82.6185
GW-17	Bhairotal borewell water	22.3706	82.6363
GW-18	Balkikhar dug well water	22.3810	82.6530
GW-19	Vaishali Nagar borewell water	22.3476	82.6554
GW-20	Durpa handpump water	22.3514	82.6763
GW-21	Patel Nagar /Korba borewell water	22.3488	82.6961
GW-22	Sitamadi Korba borewell water	22.3377	82.7091
GW-23	Kuchaina mod borewell water	22.3556	82.6362
GW-24	Awadh Nagar road borewell water	22.3560	82.5981
GW-25	Vijay Nagar Dhurena handpump water	22.3592	82.5664
GW-26	Dhara chauk Dipka borewell water	22.3464	82.5424
GW-27	Gevra basti handpump water	22.3327	82.6350
GW-28	Salora handpump water	22.3100	82.6348
GW-29	Rishdi borewell water	22.3158	82.6612
GW-30	Ghanadabri borewell water	22.2996	82.6679
GW-31	Padhania borewell water	22.3138	82.6849
GW-32	Chandra Nagar handpump water	22.3250	82.6912
GW-33	Mudhali handpump water	22.2848	82.5832
GW-34	Bamhanikona borewell water	22.2899	82.5471
GW-35	Ratija ka para dug well	22.3458	82.4838

5.2.2 Heavy metal characteristics and their spatial contour mapping

Heavy metals are a group of metallic chemical elements, such as Al, Ba, Cd, Cr, Cu, Fe, Mn, Pb, Ni, and Zn, among others. These elements possess a relatively high density and exhibit toxicity or adverse effects even at low concentrations. Therefore, it is crucial to regularly evaluate both the quantity and quality of it. Several pollution indices, such as HPI, HEI and MI, have been used to evaluate the suitability of groundwater for drinking and domestic usage. The computed HPI and HEI show the overall water quality in terms of heavy metals, whereas metal index (MI) measures the degree to which heavy metals have an adverse effect on human health. The application of pollution evaluation indicators is highly beneficial in the identification and assessment of trends related to water quality, specifically in relation to the quantitative aspects of water composition.

The present study examines ten heavy metals in order to evaluate the suitability of groundwater for drinking purposes. The concentrations of these heavy metals are compared to the standard values established by the WHO (2006) and BIS (2012). The statistical summary of metal concentration, including the minimum, maximum, mean, and standard deviation, in the groundwater samples for both seasons can be found in Table 5.31 and Table 5.32, respectively. For a better understanding, ArcGIS 10.8 version programme were employed to prepare the spatial contour distribution map for all selected elements.

Table.5.31 Summary statistic of various elements in pre monsoon season with WHO (2006) and BIS (2012) standards

Metals	Min	Max	Mean	Std dev	WHO (2006)	BIS 2012 (IS 10500)	
						Reqd.	Per. limits
Al	0.00	176.57	12.40	30.03	100-200	30	200
Ba	38.94	660.39	168.16	149.65	300	700	No relaxation
Cd	0.00	1.49	0.15	0.29	3	3	No relaxation
Cr	0.00	2.641	1.194	0.954	50	50	No relaxation
Cu	0.00	50.71	5.06	10.66	2000	50	1500
Fe	0.00	2892.06	125.53	485.61	300	300	No relaxation
Mn	17.53	367.68	87.85	86.31	100	100	300
Pb	0.00	7.37	1.25	1.82	10	10	No relaxation
Ni	0.00	69.87	11.37	17.24	20	20	No relaxation
Zn	0.00	11766.92	485.01	2059.60	4000	5000	15000

Table.5.32 Summary statistic of various elements in post monsoon season with WHO (2006) and BIS (2012) standards

Metals	Min	Max	Mean	Std dev	WHO (2006)	BIS 2012 (IS 10500)	
						Reqd.	Per. limits
Al	0.000	153.214	11.372	25.927	100-200	30	200
Ba	32.654	243.321	121.047	65.925	300	700	No relaxation
Cd	0.008	0.864	0.107	0.197	3	3	No relaxation
Cr	0.000	2.252	0.936	0.798	50	50	No relaxation
Cu	0.000	34.351	3.973	7.659	2000	50	1500
Fe	0.000	289.621	38.977	55.808	300	300	No relaxation
Mn	15.025	183.651	57.597	39.448	100	100	300
Pb	0.000	5.261	0.908	1.219	10	10	No relaxation
Ni	0.000	52.364	10.046	12.864	20	20	No relaxation
Zn	0.000	9866.35	401.761	1717.14	4000	5000	15000

5.2.2.1 Aluminium

Aluminium has a low acute toxicity. The presence of elevated levels of aluminium in various water bodies has been observed as a consequence of acid rain (Schecher and Driscoll, 1988). Aluminium has the ability to leach into any water supply, and this ability is possessed by rock and soil. The presence of aluminium has been detected in drinking water, which caused concerns about potential health implications due to its potential relationship with dialysis encephalopathy or Alzheimer's disease (Jekel, 1991). One of the challenges associated with water distribution is the formation of a hydrous aluminium precipitate, which has the potential to increase turbidity levels. This issue occurs due to an increase in the concentration of aluminium in treated water (Costello, 1984). Although extended exposure is rare, Al appears to interfere with phosphorus absorption and cause weakness, bone discomfort, and anorexia.

The observed Al concentration ranged from 0 µg/L to 176.57 µg/L with an average of 12.40 µg/L in the pre monsoon, while it ranged from 0 µg/L to 153.21 µg/L with an average of 11.37 µg/L in the post monsoon season. This result indicates that two samples (GW-4 and GW-29) collected in both pre and post monsoon season exceeded the recommended required limit of 30 µg/L (BIS, 2012). This excess of Al content in groundwater could indeed originate from sandstone, shale, sedimentary clays, and coal-bearing sediments (Finkelman 1981). Apart from this, not a single sample from either season went over the suggested maximum amount of 200 µg/L as per BIS and WHO. However, Al concentrations in groundwater samples collected in post monsoon were significantly lower than those collected in the pre monsoon seasons. The spatial map of the Al concentration demonstrates that a spot in south east side had higher concentrations throughout both seasons. The spatial distribution map of Al concentration for both the pre and post monsoon seasons is shown in Fig.5.67 and Fig.5.68, respectively.

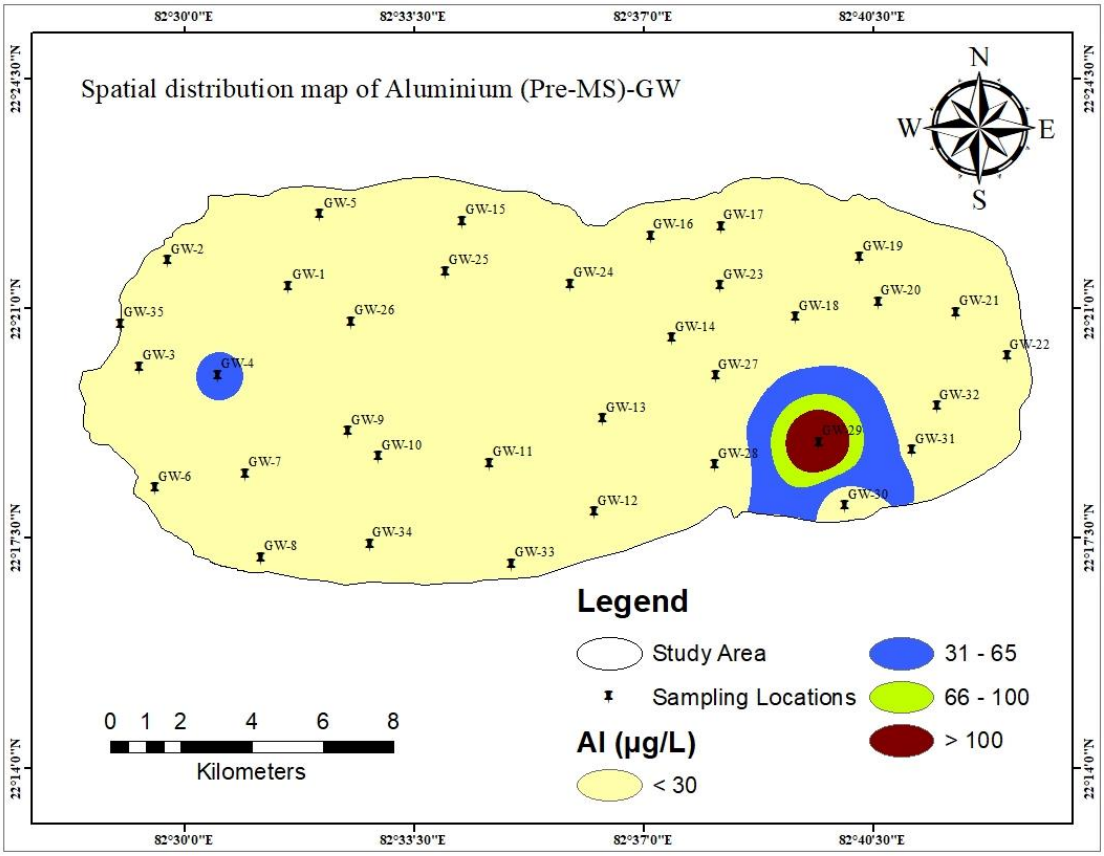

Fig.5.67 Spatial map of Aluminium during pre-monsoon season in study region

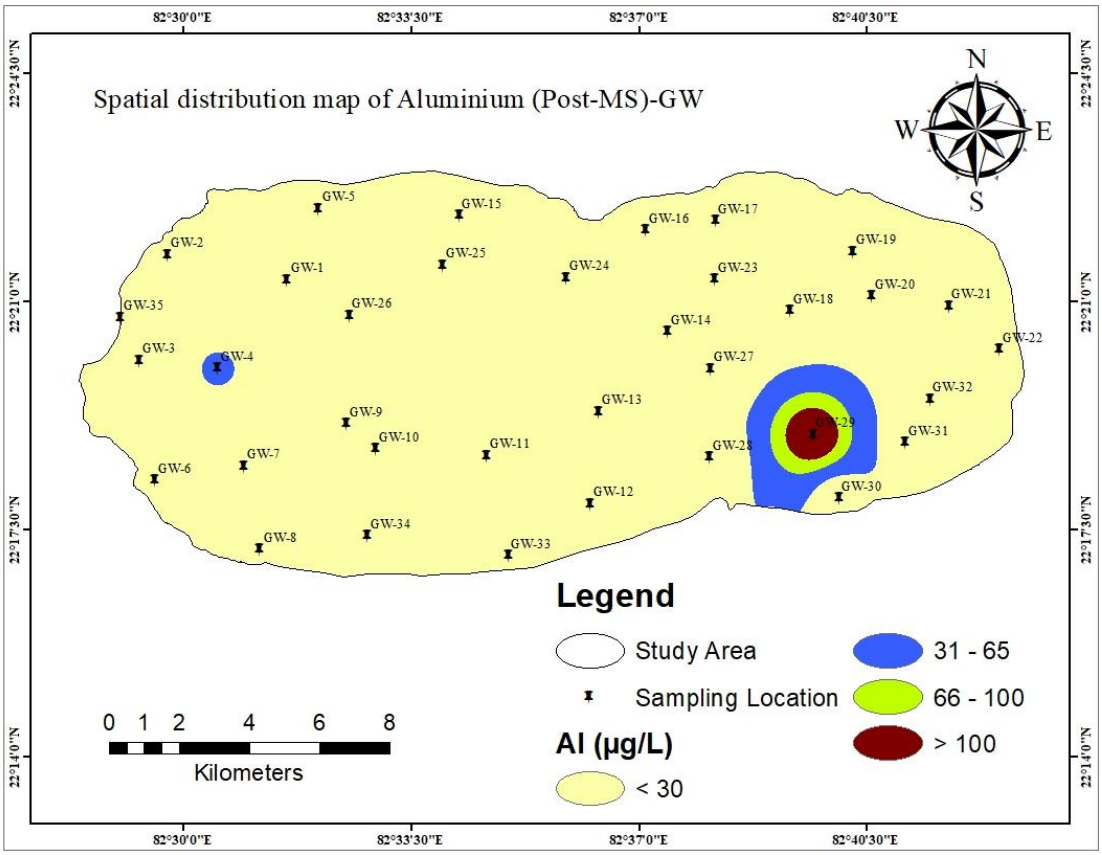

Fig.5.68 Spatial map of Aluminium during post-monsoon season in study region

5.2.2.2 Barium

The process of weathering or leaching occurring in sedimentary rocks facilitates the entering of barium into both groundwater and surface water bodies. The source of public drinking water with elevated barium concentrations is derived from deep rock and drift boreholes. The ingestion of barium in an acute manner has been shown to exert significant effects on smooth, striated, and cardiac muscle (Roza et al. 1971). Barium is regarded to be a trace element that is not required for humans; however, very little is known about its metabolic activities in bone or soft tissue (Schroeder et al. 1972). Barium is associated with a range of adverse effects, including headache, vomiting, abdominal cramps, diarrhoea, respiratory complications, alterations in blood pressure, facial numbness, and muscle weakness.

The observed Ba concentration ranged from 38.94 µg/L to 660.39 µg/L with an average of 168.16 µg/L in the pre monsoon, while it ranged from 32.65 µg/L to 243.32 µg/L with an average of 121.05 µg/L in the post monsoon season. The concentration of Ba was exceeded the permissible limit of 300 µg/L (WHO, 2006) at 3 locations during pre monsoon season. These excess Ba content in groundwater is likely a result of geological processes and anthropogenic activities associated with mining operations. Moreover, all sample from either season were well below the recommended required limits of 700 µg/L (BIS, 2012). However, the concentrations of barium in the groundwater samples that were obtained in post monsoon seasons were noticeably lower than the barium concentrations that were collected in pre monsoon seasons. The spatial map of Ba concentration indicates that the higher concentrations were found in the west, north central side in the pre monsoon and west to central part of the area in the post monsoon season. The spatial map of Ba concentration for both the pre and post monsoon seasons is shown in Fig.5.69 and Fig.5.70.

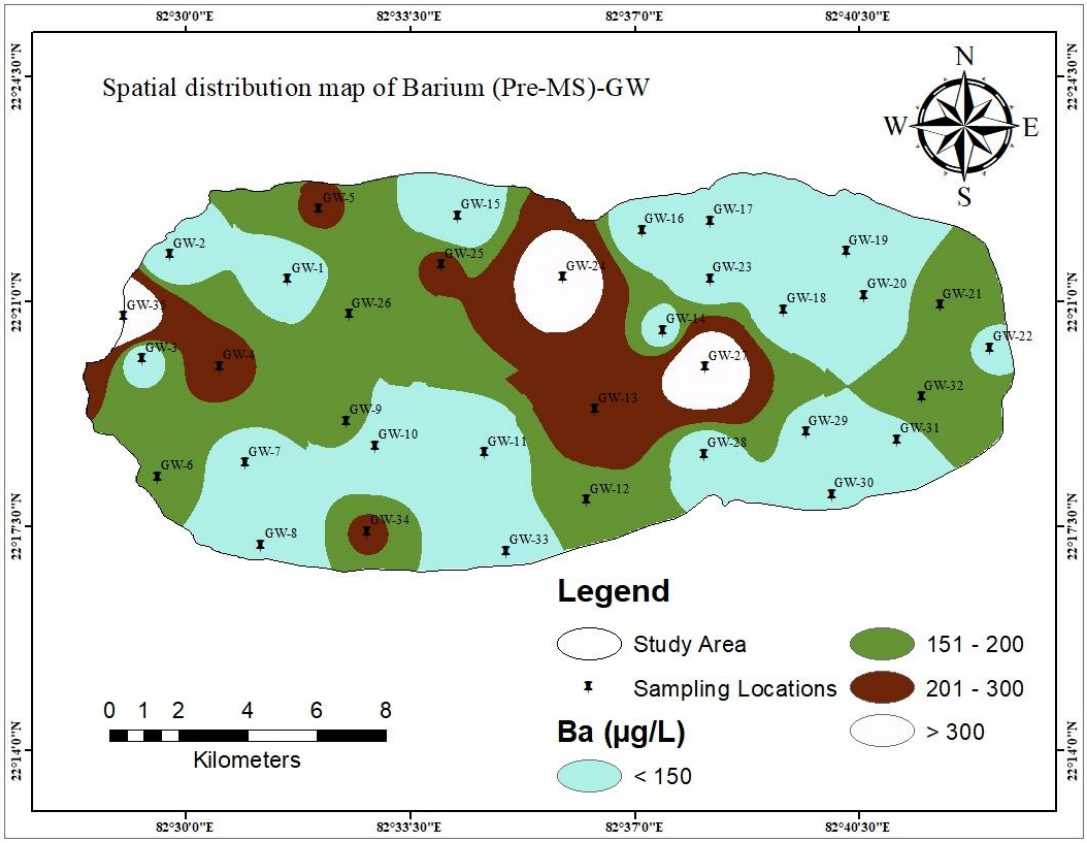

Fig.5.69 Spatial map of Barium during pre-monsoon season in study region

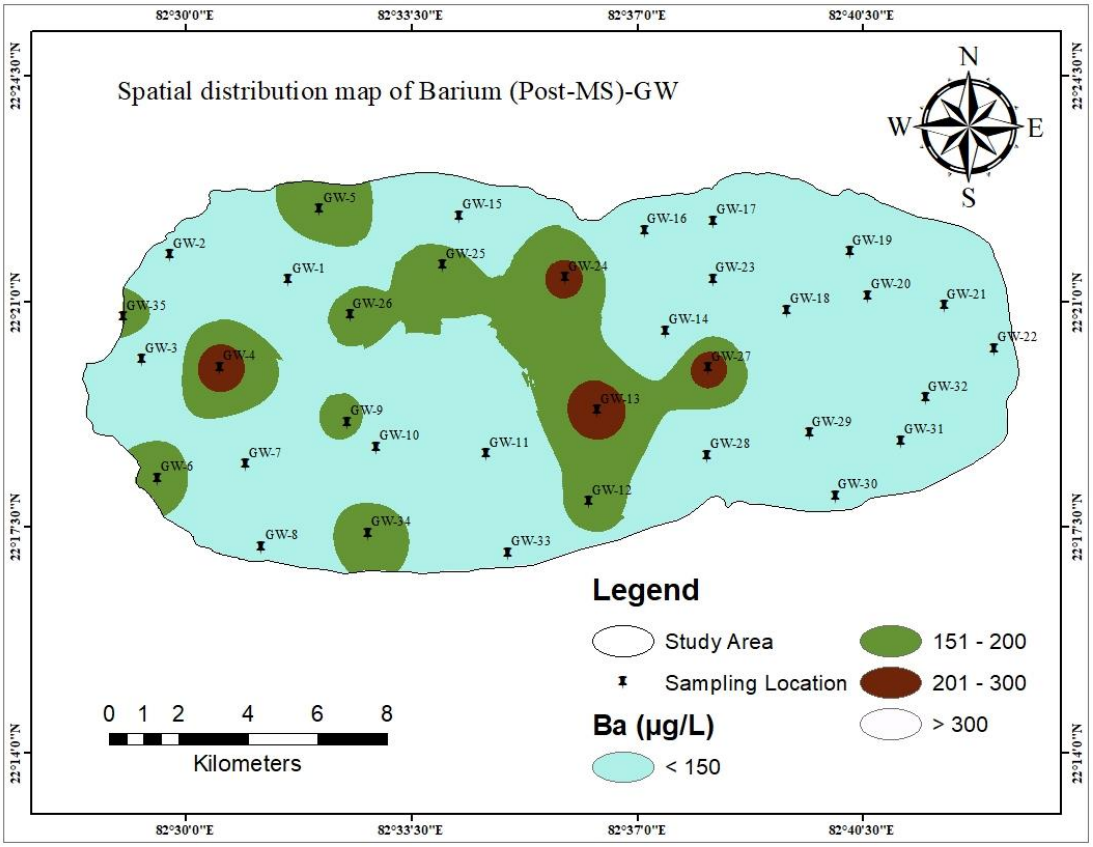

Fig.5.70 Spatial map of Barium during post-monsoon season in study region

5.2.2.3 Cadmium

Cadmium (Cd), a trace metallic element, occurs naturally in water. The extensive utilisation of cadmium compounds in batteries leads to the release of cadmium into the environment via wastewater. Additionally, diffuse pollution of cadmium occurs as a result of contamination from fertilisers, landfill activities, mining operations, and regional air pollutants. It is widely recognised that human health can be negatively affected by exposure to certain concentrations and amounts of cadmium. Cadmium exposure causes both acute and long-term effects on living organism mainly kidney and bone issues. An experimental study conducted on both humans and animals has indicated that exposure to cadmium in individuals can potentially lead to the development of cancer (IARC 1993). Cadmium contamination in water arises from anthropogenic activities, such as industrial discharge, including mining operations, and thermal power plants. Additionally, a natural source of cadmium pollution comes from the erosion and weathering of sedimentary rocks in close proximity (Agrawal et al 2011).

The concentration of Cd varied from 0 µg/L to 1.49 µg/L with an average value of 0.15 µg/L in the pre monsoon while it varied from 0 µg/L to 0.864 µg/L with an average value of 0.107 µg/L in the post monsoon season. This data shows that all sample taken throughout both seasons was well below the standard limit of 3 µg/L recommended by BIS and WHO. However, the Cd contents in the post monsoon were significantly lower than the pre monsoon seasons due to the occurrence of rainy season before the time of samples collection. Here, it is suggested that groundwater of the area is safe for drinking. The maximum Cd concentration is observed in east and north western part of the area in both seasons. The spatial map of Cd concentration for both pre and post monsoon seasons is shown in Fig.5.71 and Fig.5.72.

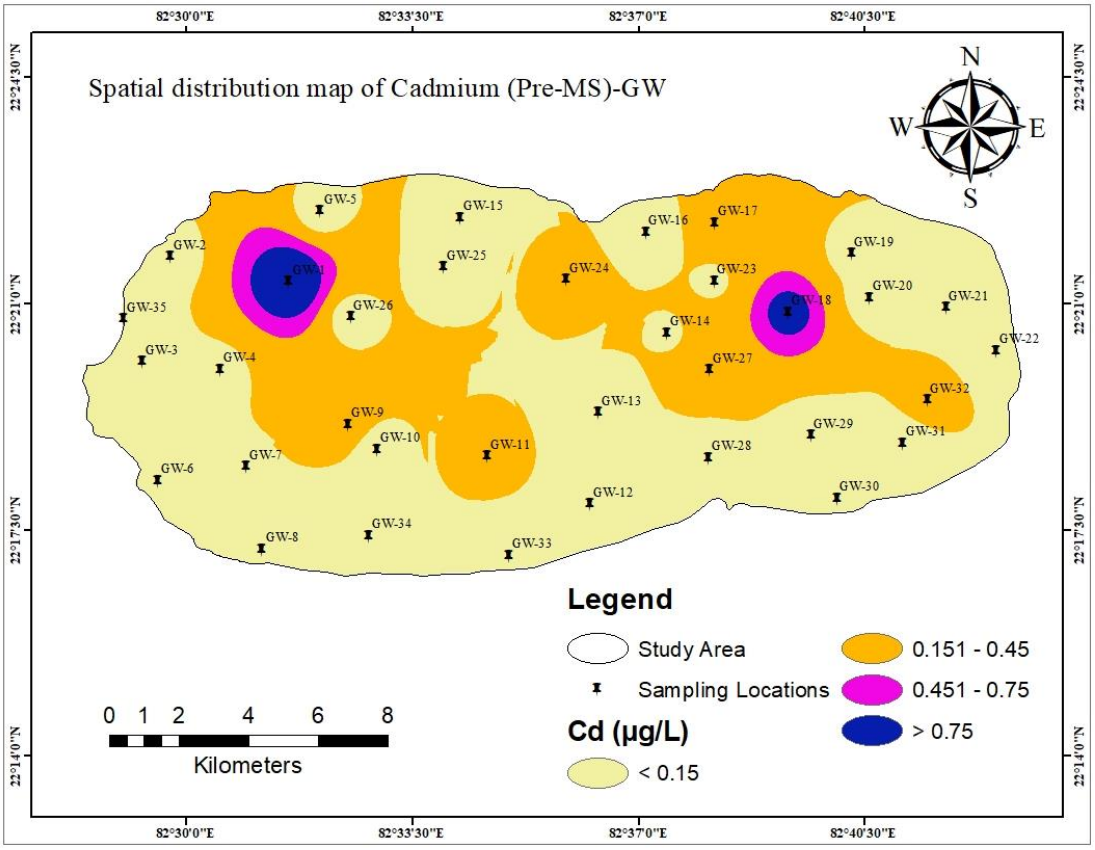

Fig.5.71 Spatial map of Cadmium during pre-monsoon season in the region

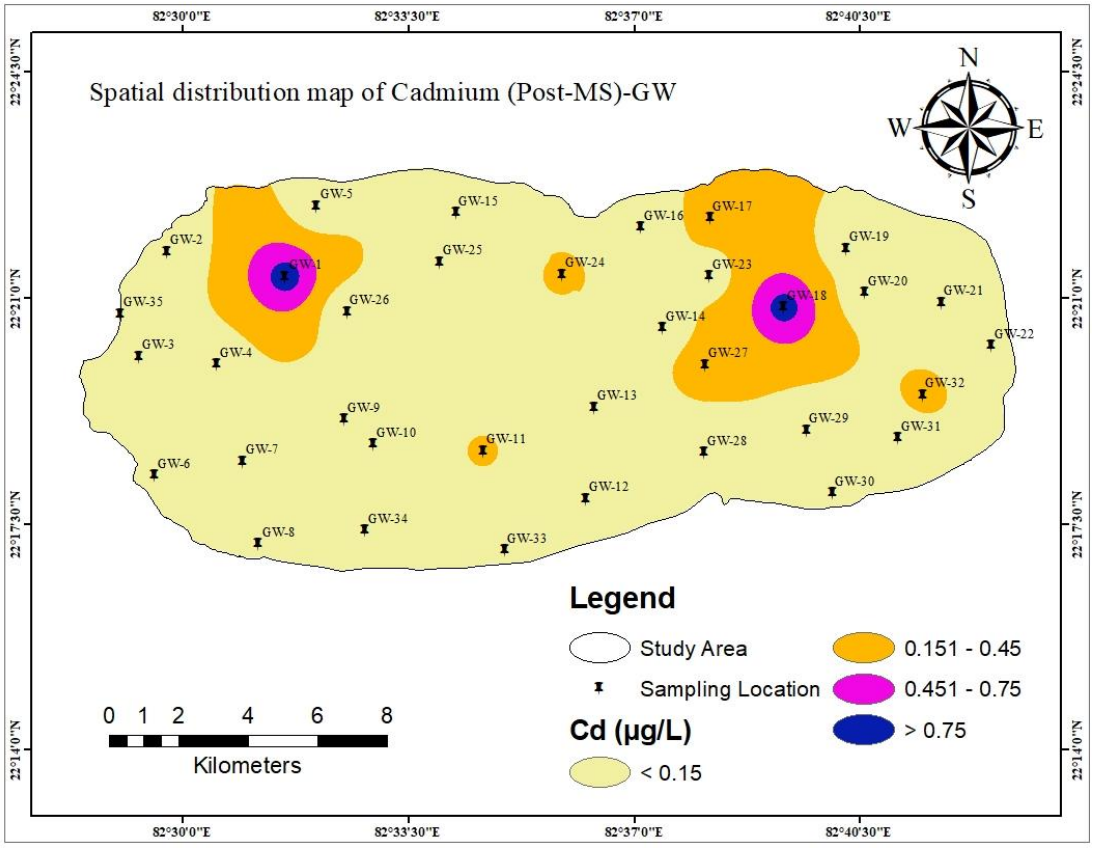

Fig.5.72 Spatial map of Cadmium during post-monsoon season in the region

5.2.2.4 Chromium

Chromium is a commonly occurring chemical element that is naturally present in several geological formations, including rocks, plants, soil, volcanic dust, animals, and gases (Dernbach, 2008). The environment commonly contains two main valence states of chromium, namely trivalent chromium (Cr (III)) and hexavalent chromium (Cr (VI)). Additionally, in comparison to hexavalent chromium (Cr (VI)), trivalent chromium (Cr (III)) exhibits significantly reduced levels of risk (USEPA, 2000). It functions as an important micronutrient in the body, collaborating with various enzymes to transfer sugar, protein, as well as fat. The soluble Cr (III) compounds might irritate the eyes and skin, this impact is typically caused by their acidic nature. Cr (VI) is recognised to have a number of negative health impacts. The utilisation of leather items can cause allergic responses, such as the arising of a skin rash. Chromium, a metallic element found abundantly in the Earth's crust, ranks as the 21st most prevalent metal. It is significant because the United States Environmental Protection Agency has identified chromium as one of the 126 priority pollutants (EPA) (USEPA 2014; Emsley 2001).

The observed Cr concentration varied from 0 µg/L to 2.64 µg/L with an average value of 1.194 µg/L in pre-monsoon while it ranged from 0 µg/L to 2.25 µg/L with an average value of 0.936 µg/L in the post monsoon season. This shows that all sample from both seasons were well below the standard limit of 50 µg/L (WHO, 20006). However, the slight decline in Cr content in the post-monsoon season might be attributed to water dilution by rainfall during the preceding rainy season. The observed low concentration of Cr in water implies that the indices measuring heavy metal pollution remain unaffected, indicating that the water is safe for drinking and domestic uses. The spatial map of Cr concentration for both the pre and post monsoon seasons is shown in Fig.5.73 and Fig.5.74.

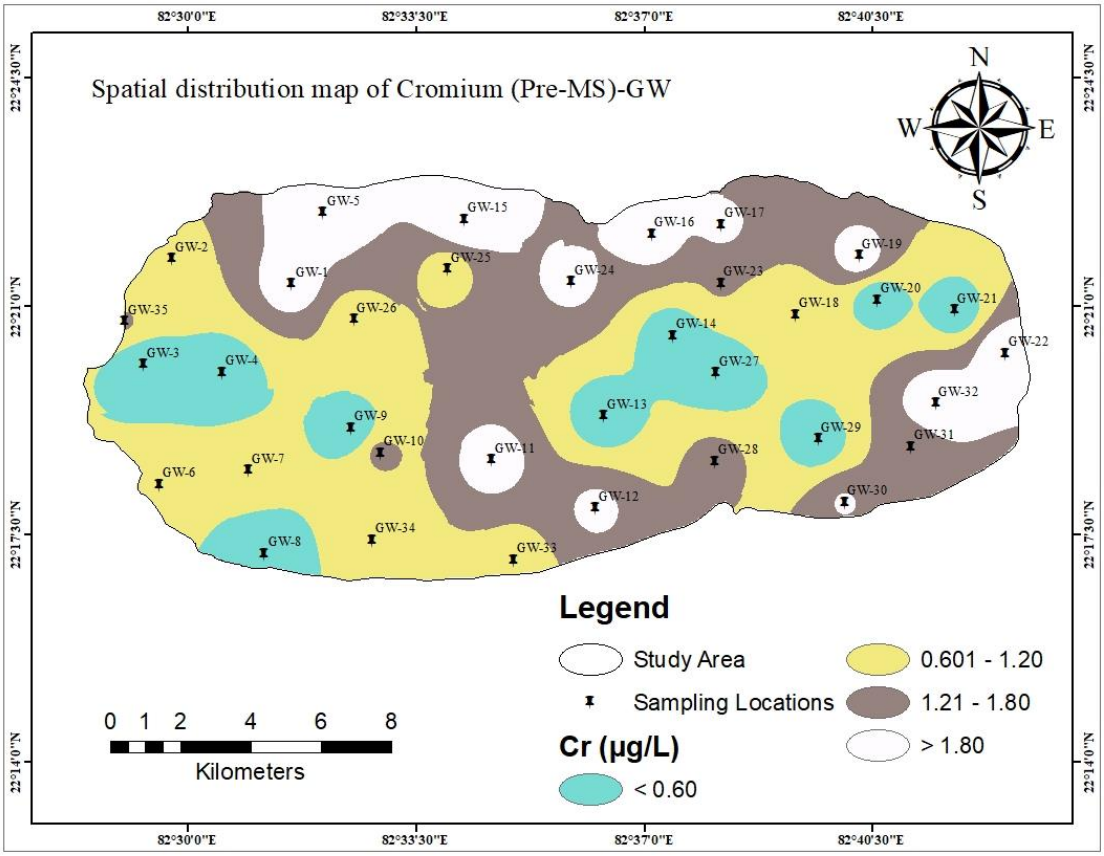

Fig.5.73 Spatial map of Chromium during pre-monsoon season in study region

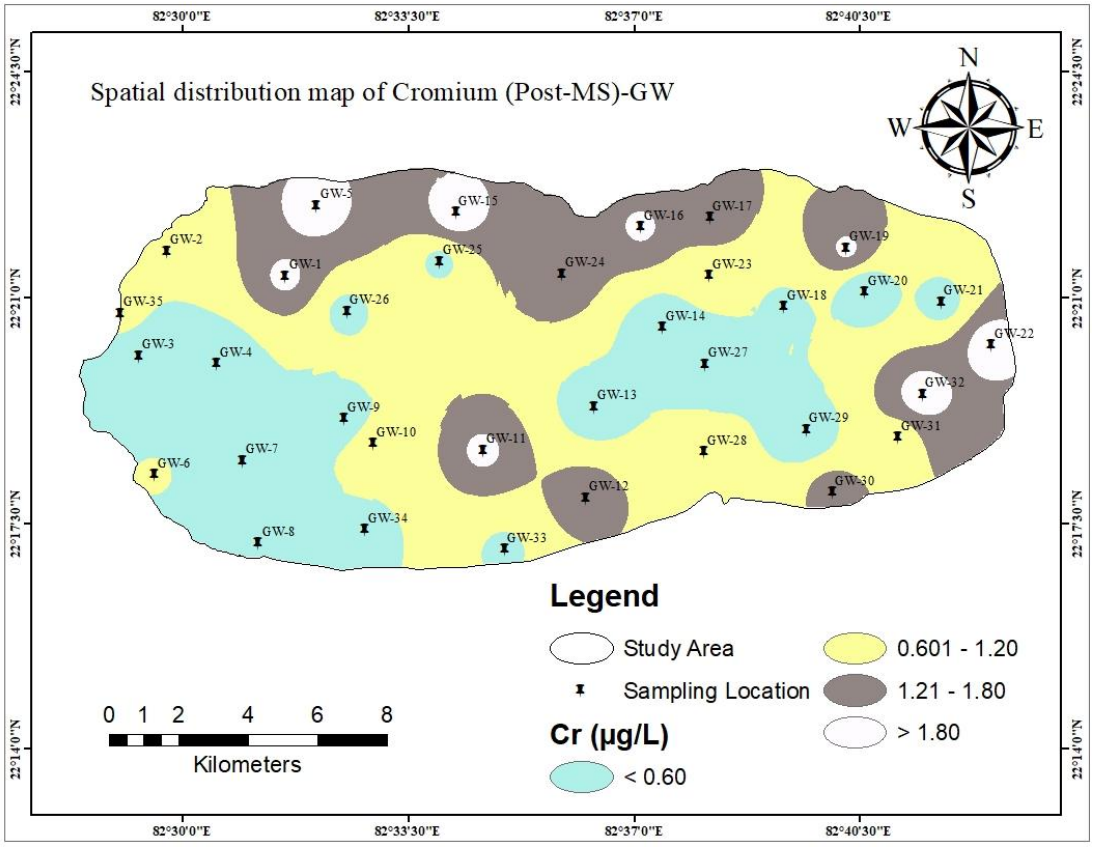

Fig.5.74 Spatial map of Chromium during post-monsoon season in study region

5.2.2.5 Copper

Copper, a malleable metallic element, is frequently utilised as an electrical conductor, similar to the usage of bronze and brass. The accumulation of copper (Cu) content in water is attributed to industrial activities such as steel production, plastic manufacturing, and blast furnace operations. Agricultural chemicals and trash landfills are two other significant sources of copper. The quantity of copper in drinking water is often found to be at a few micrograms per litre. However, the presence of copper plumbing systems can considerably elevate the content of copper in the water. Copper poses a significant risk to both ecological systems and human health when present in elevated concentrations (WHO 1993). Several genetic diseases, such as Menkes Syndrome, can be attributed to a deficiency in zinc, whereas Wilson disease is associated with an excessive amount of zinc (Wazir et al. 2017). Copper and zinc in high amounts may harm the thyroid, kidneys, and liver over time. They can also lower lipoprotein cholesterol levels (ATSDR 2004).

The observed Cu concentration varied from 0 µg/L to 50.68 µg/L with an average value of 5.06 µg/L in the pre monsoon while it varied from 0 µg/L to 34.34 µg/L with an average value of 3.973 µg/L in the post monsoon season respectively. This data shows that all sample taken throughout both seasons was well below the standard limit of 1500 µg/L (WHO, 2006). However, Copper concentrations from the post monsoon were considerably lower than those from the pre monsoon season. However, these decrease in Cu content in the post-monsoon season might be attributed to the fact that Cu variations in water are primarily caused by pH and hardness variations that occur throughout the rainy season (Sengupta et al. 2002). The maximum concentration of copper is observed in eastern part of the study area in both seasons. The spatial map of Cu element for both the pre and post monsoon seasons is shown in Fig.5.75 and Fig.5.76.

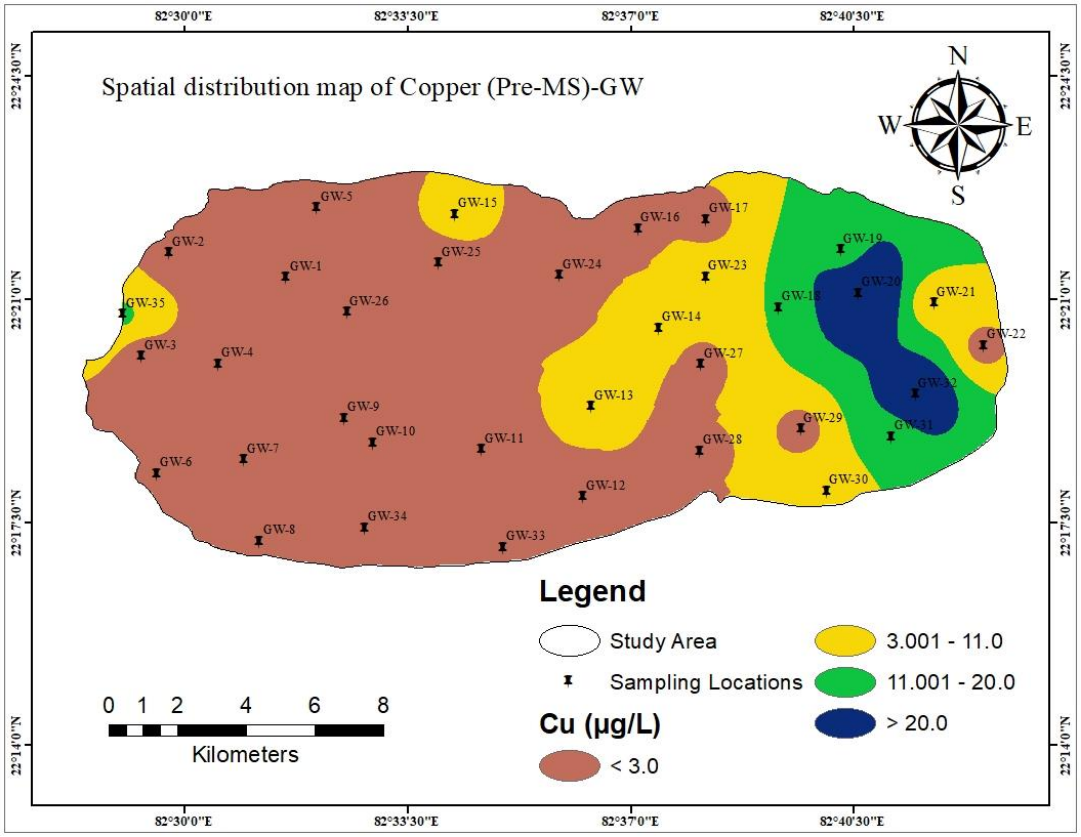

Fig.5.75 Spatial map of Copper during pre-monsoon season in the region

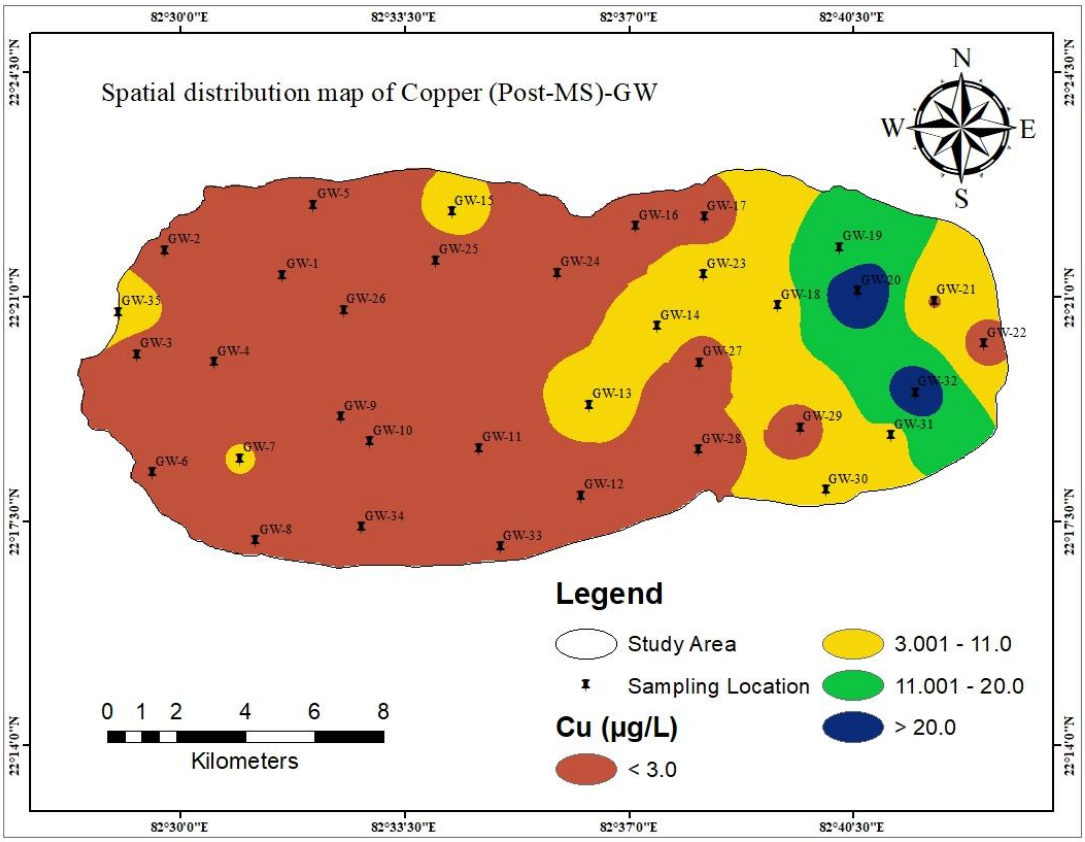

Fig.5.76 Spatial map of Copper during post-monsoon season in the region

5.2.2.6 Iron

Iron is the most abundant element in the earth's crust after oxygen, silicon, and aluminium, although it is the most important metal in metallic minerals and rocks (Anderson 1983). The occurrence of iron in the water samples, which might be typically found in nature in the form of its oxides, has been generally indicated by the yellowish colour of the water (Elinder, 1986). Its analysis is necessary since its excess leads to diseases like hemosiderosis, while its deficiency leads to anaemia and poor brain development in neonates (Baskar et al. 2010). The presence of iron in water is seen undesirable due to its tendency to change the taste and colour of the water, resulting in a visible rusty appearance. A mine can also cause a number of iron pollution issues in groundwater (Mink, 1972).

The observed Fe concentration ranged from 0 µg/L to 2889.74 µg/L with an average value of 125.53 µg/L in the pre monsoon, while it ranged from 0 µg/L to 289.49 µg/L with an average value of 38.977 µg/L in the post monsoon season respectively. The data suggests that out of all the samples obtained, only two samples (GW-20 and GW-32) exceeded the standard limit in the pre-monsoon season. The increased iron level is attributed to a geogenic source, most likely leachates from coal mine overburden dumps caused by adjacent mine drainage and effluent discharge (Singh et al 2017). However, all samples collected in the post-monsoon season were found to be under the recommended allowable range of 300 µg/L, as recommended by BIS and WHO. The iron contents in groundwater samples from the post monsoon seasons, however, were significantly lower than those from the pre monsoon season. The spatial map of the Fe content revealed that the eastern side of both seasons exhibited elevated levels of iron as shown in Fig.5.77 and Fig.5.78, respectively.

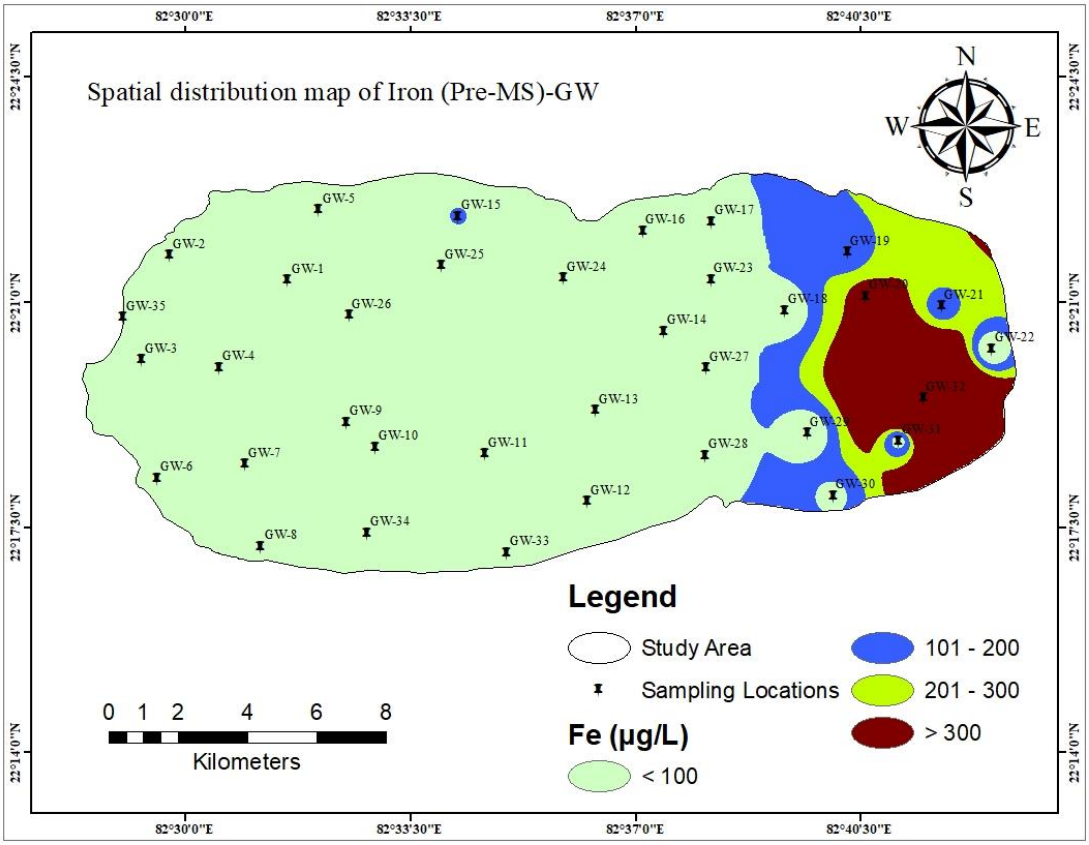

Fig.5.77 Spatial map of Iron during pre-monsoon season in the region

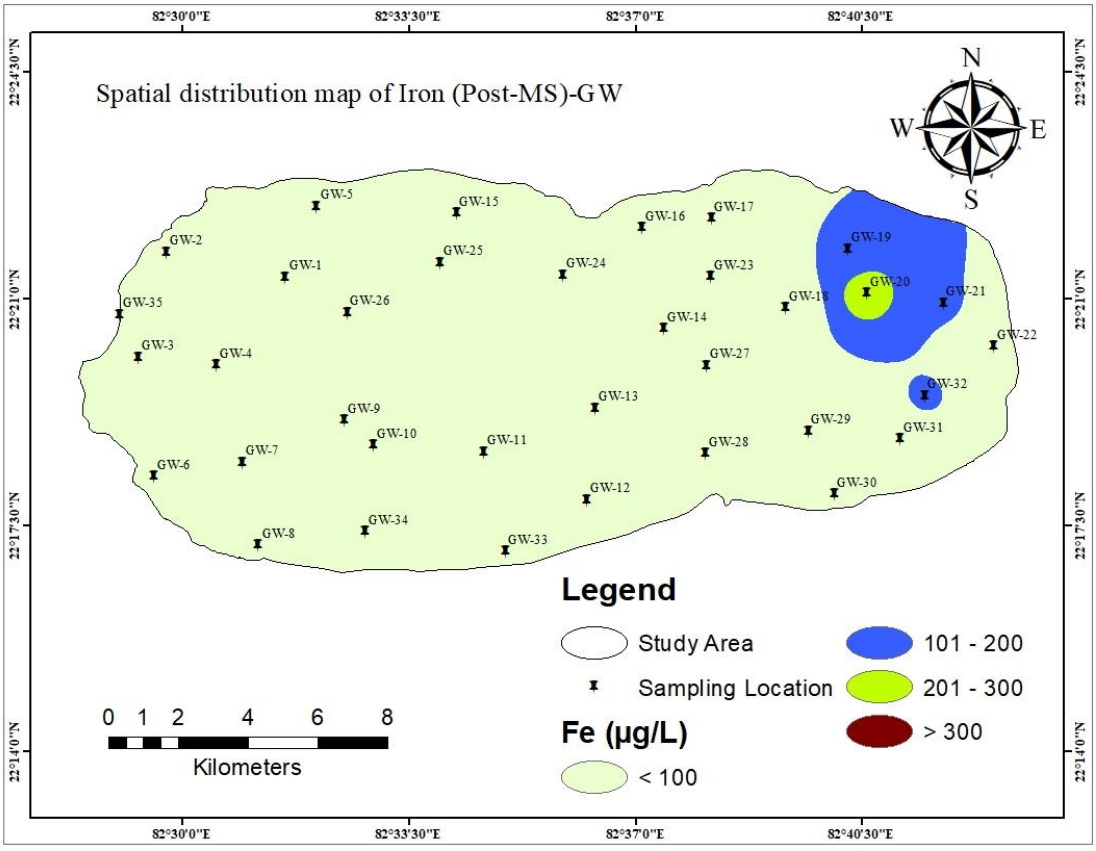

Fig.5.78 Spatial map of Iron during post-monsoon season in the region

5.2.2.7 Manganese

Manganese is a common component in impounded water and many well waters (Griffin,1958). It leaves stains on clothes and pipes and turns water black. It leads to significant economic losses in industrial supplies by discolouring things, leaving specks in finished commodities, and lowering pipeline carrying capacities. It enters in the water through biological and chemical processes. The presence of manganese in stored water is attributed to a combination of biological and chemical processes. However, it is widely accepted that the predominant source of Mn in groundwater is chemical reactions (Flentje, 1960). Manganese is a well-known occupational toxin that can lead to memory loss, neurological disorder, and dopamine depletion that resembles Parkinson's disease. Although being essential for human nourishment, high exposure levels have been linked to negative health effects.

The observed Mn concentration ranged from 17.53 µg/L to 3687.68 µg/L with an average of 87.88 µg/L in pre monsoon season, while it ranged from 15.03 µg/L to 183.65 µg/L with an average of 57.59 µg/L in post monsoon season respectively, indicating that ten samples from pre monsoon and five samples from post monsoon season exceeded the recommended required limit of 100 µg/L as per BIS and WHO. In addition, only two sample (GW-24 and GW-32) from pre monsoon and no samples from post monsoon season exceeded the recommended permissible level of 300 µg/L BIS (2012). The concentrations of Mn in water samples exhibited a considerable decrease in the post monsoon season compared to the pre monsoon season which are representative of superficial aquifers, are discerned to be of anthropogenic origin and the most likely source is the adjacent thermal power plants. The Mn spatial map demonstrates that the east and north sides had higher Mn concentrations during the pre-monsoon season, whereas the north western side in the post monsoon season as shown in Fig.5.79 and Fig.5.80.

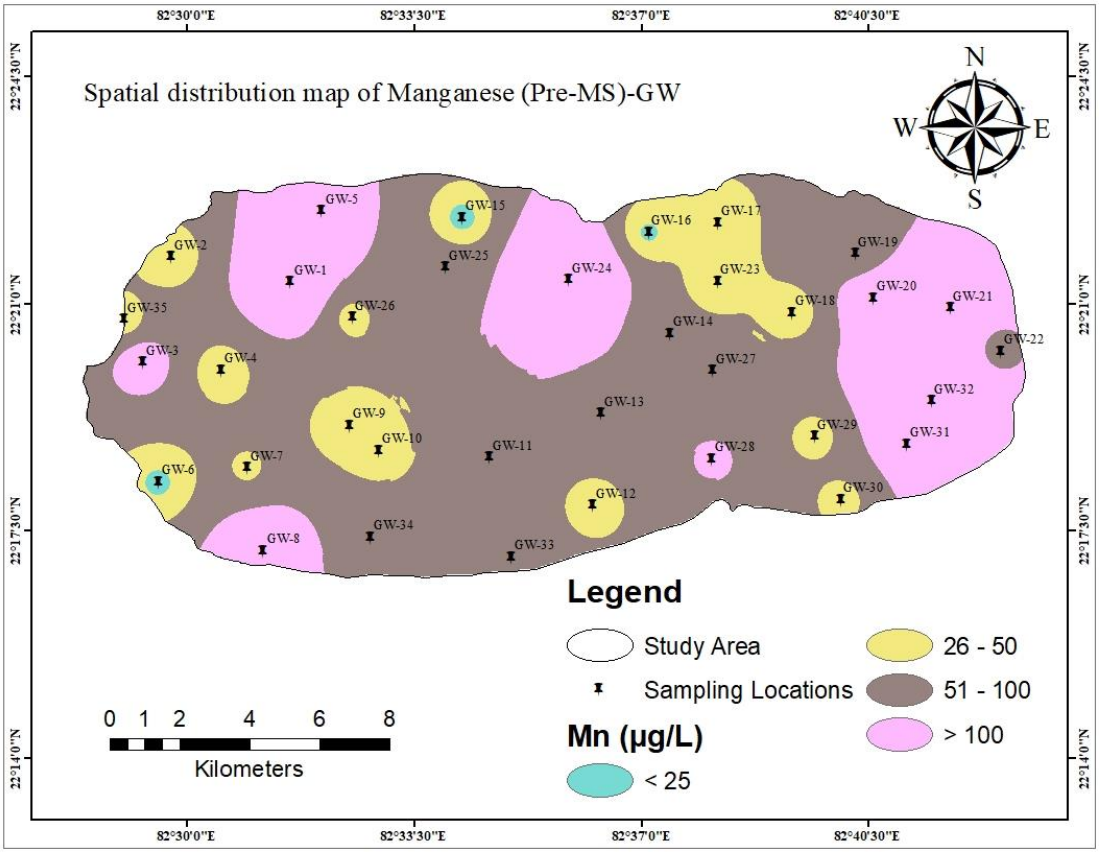

Fig.5.79 Spatial map of Manganese during pre-monsoon season in the region

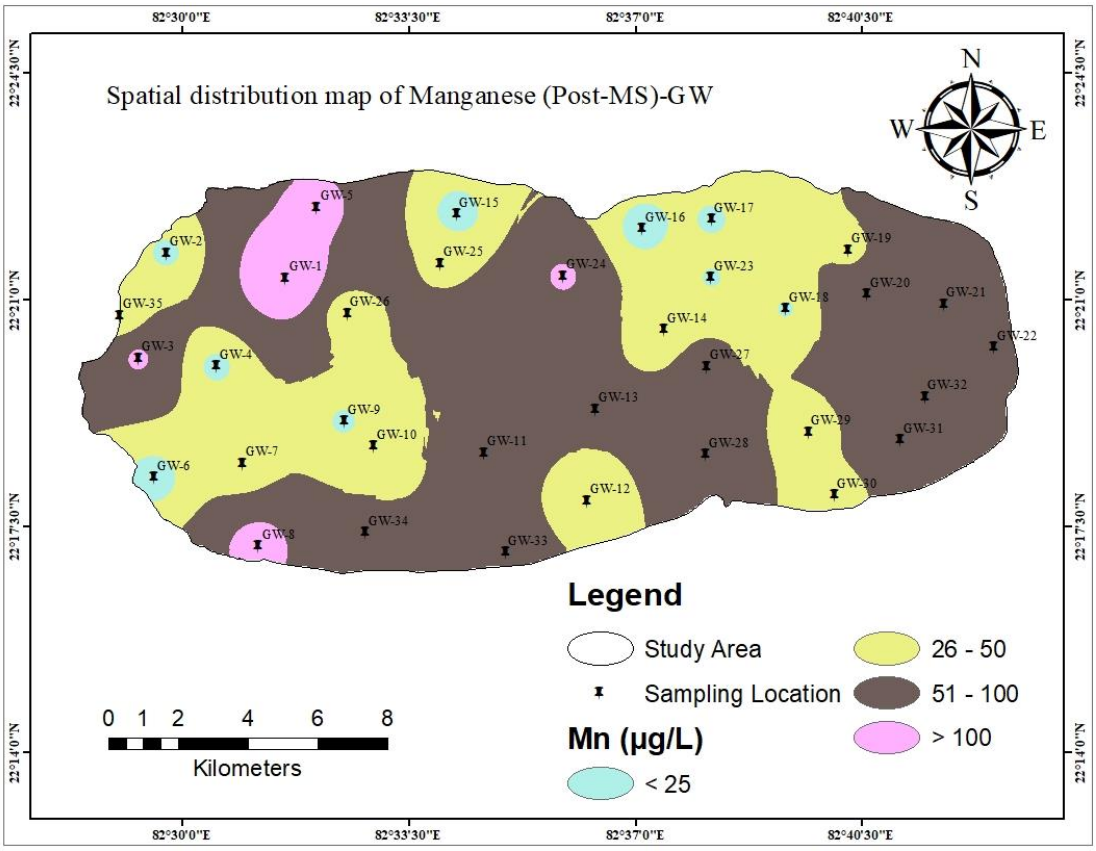

Fig.5.80 Spatial map of Manganese during post-monsoon season in the region

5.2.2.8 Lead

Lead is a carbon-based heavy metal that is primarily used in the manufacture of lead acid storage batteries. Lead can also be discharged into the environment during the casting process, through the fumes of automobile exhaust, and corrosion of lead pipes (Gowd and Govil 2008). The presence of lead in tap water is rarely due to natural degradation processes. However, it is predominantly observed in domestic plumbing systems that utilise lead pipes, solder, fittings, and service connections (WHO 1993). Lead is a very harmful substance that is carcinogenic to people which causes significant serious diseases including brain tumours, itchiness, hypertension, kidney, stomach, and nerve damage (Keshav Krishna and Mohan 2016). Excessive lead exposure may result in complex health problems such as dementia and behavioural disorders.

The observed Pb concentration ranged from 0 µg/L to 7.36 µg/L with an average value of 1.25 µg/L in pre monsoon season, while it ranged from 0 µg/L to 5.26 µg/L with an average value of 0.908 µg/L in post monsoon season. This data demonstrates that all samples collected from both seasons were well below the recommended permissible limits of 10 µg/L (WHO, 2006). However, the Pb contents in the groundwater samples from the post monsoon seasons were significantly lower than the pre monsoon seasons which indicates that the local geology may be contributing to the increasing few Pb content in the groundwater (Das et al. 2018). The spatial map for Lead demonstrates that east and south sides of pre monsoon whereas south side in post monsoon season were high Pb concentrations shown in Fig.5.81 and Fig.5.82.

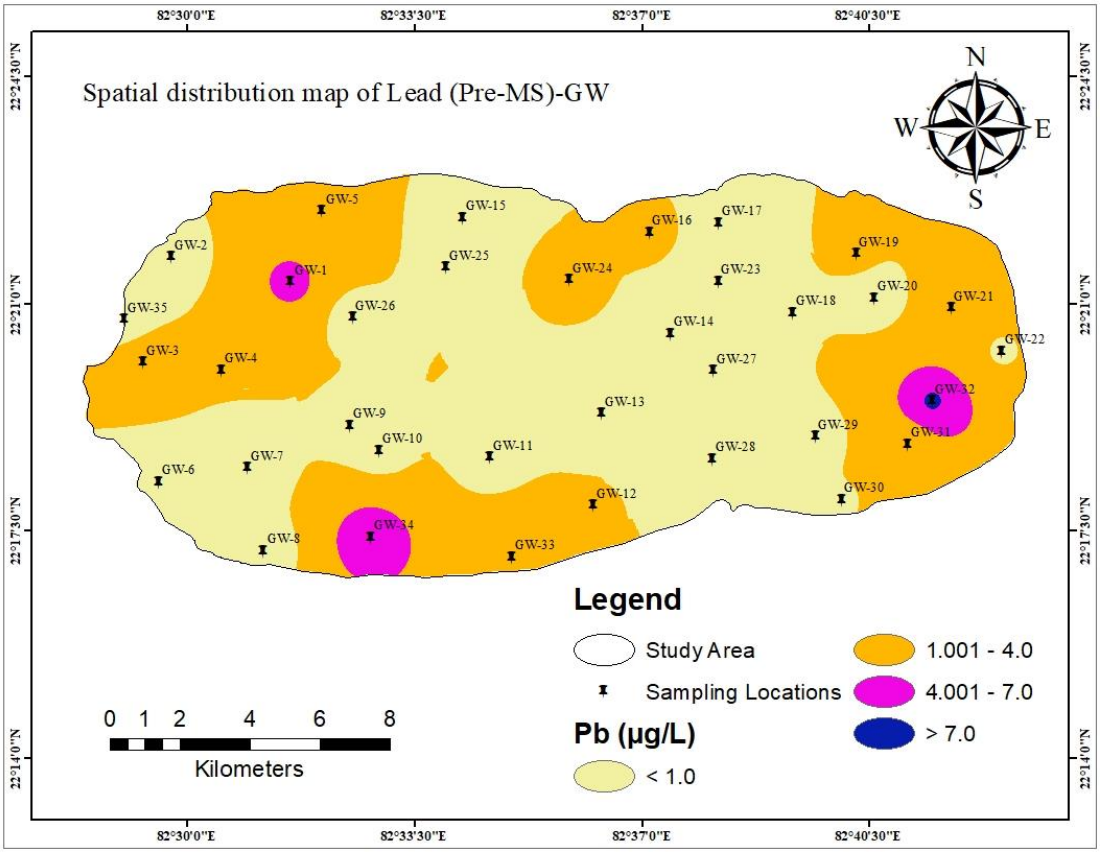

Fig.5.81 Spatial map of Lead during pre-monsoon season in the region

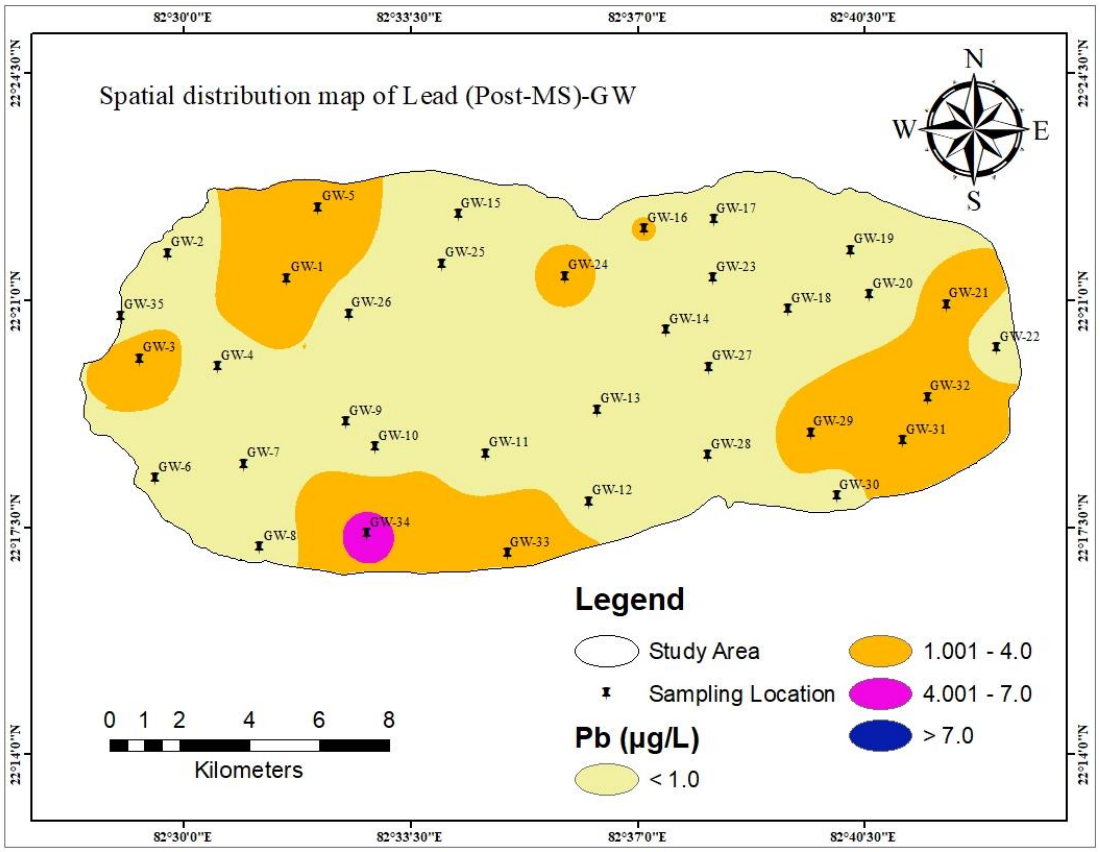

Fig.5.82 Spatial map of Lead during post monsoon season in the region

5.2.2.9 Nickel

Nickel in groundwater is naturally released from soils and rocks which can harm humans. The soil type, pH, and sampling depth affect nickel content (Lehr et al. 2005; WHO 2005). However, the primary sources of Ni contents are direct combustion of fossil fuels from thermal power plants and coal washing directly into surface waters. The most prevalent disorders induced by Nickel consumption are lung cancer and nasal tumour moreover nickel is also carcinogenic in nature, inducing changes in the structure of NDA (Guo et al 2019).

The observed Ni concentration ranged from 0 µg/L to 69.87 µg/L with an average of 11.37 µg/L in the pre monsoon, while, it ranged from 0 µg/L to 52.36 µg/L with an average of 10.05 µg/L in post monsoon season, indicating that only six sample (GW-23, 24, 25, 27, 28, 32) collected in the pre monsoon and four samples (GW-25, 28, 29, 33) collected in post monsoon season exceeded the recommended permissible limit of 20 µg/L as per BIS and WHO. However, Nickel contents in groundwater samples from the post monsoon were significantly lower than pre monsoon season due to dilution effect (decrease) and dissociation (increase) effect (Mahapatra et al. 2020). The spatial map of the research region shows that the east and north to south sides had higher Ni content in both seasons as shown in Fig.5.83 and Fig.5.84.

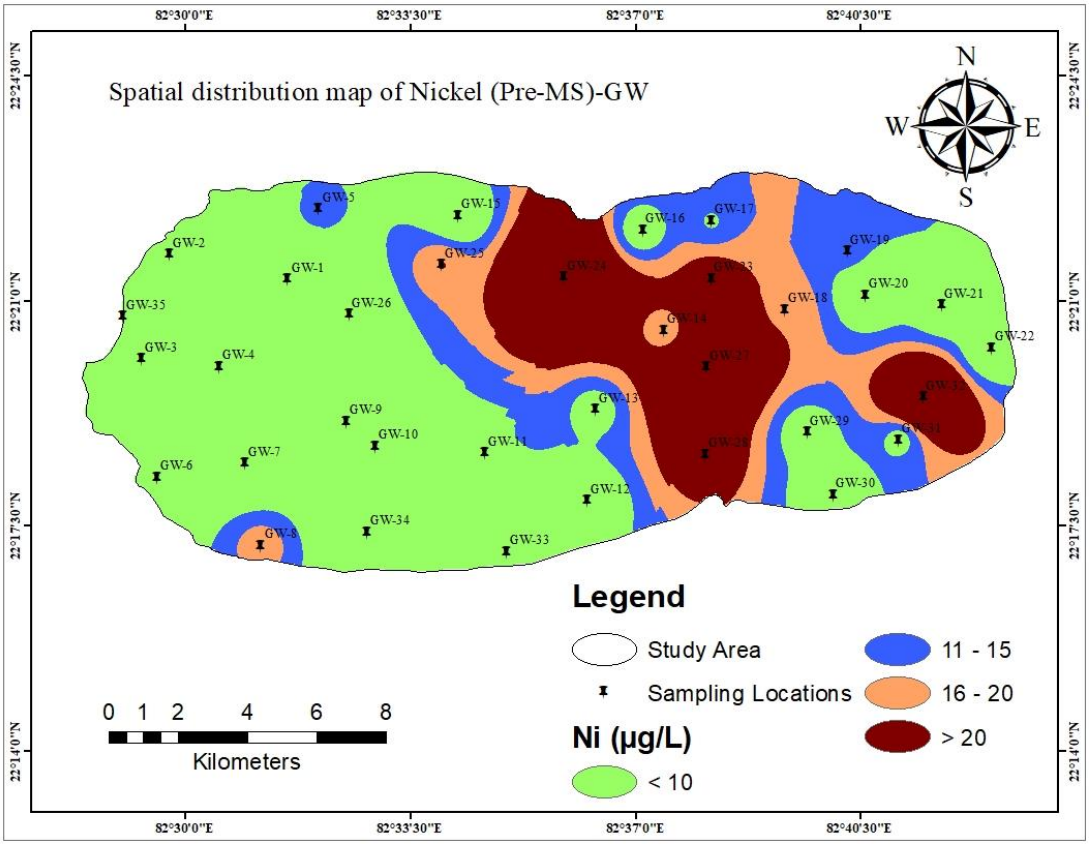

Fig.5.83 Spatial map of Nickel during pre-monsoon season in the region

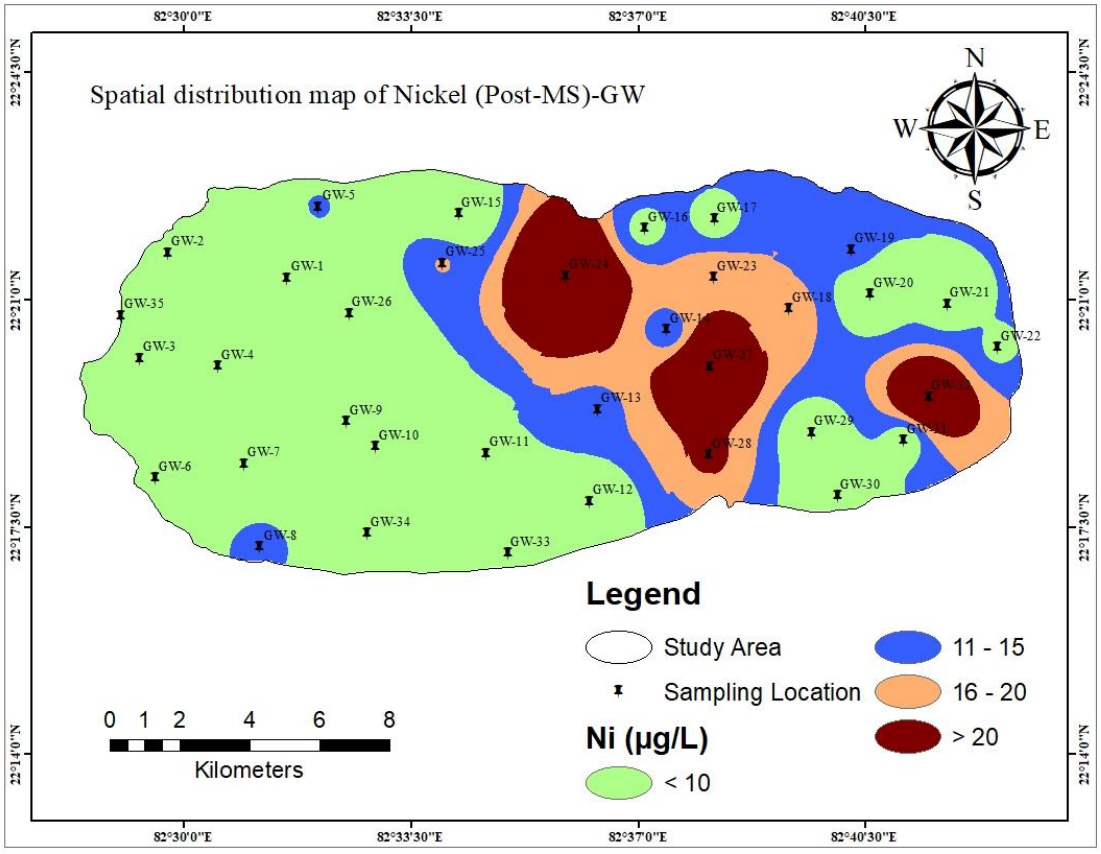

Fig.5.84 Spatial map of Nickel during pre-monsoon season in the region

5.2.2.10 Zinc

Zinc is a vital trace element that may be found in practically all foods and beverages in the form of salts or other chemical complexes. The diet is the main source of zinc. On the other hand, consumer might not be willing to drink water with zinc concentrations higher than 3 mg/L. The maximum Zn concentration limit in drinking water is 4000 µg/L as per WHO (2006) guidelines. Zinc is one of the most toxic substances which also found in igneous rocks with less quantity (WHO, 2004). Zinc contamination makes water physically unfit for human consumption by producing a milky turbid appearance with unpleasant taste. Zinc pollution in water is mostly caused by runoff from nearby waste dumps, weathering, and pollution from power plants and mining companies (Sengupta et al 2002). Although zinc is an essential micronutrient for both plants and humans, elevated quantities of this element can have negative effects on the environment and public health. The long-term high zinc intake may cause anaemia, pancreatic damage, liver and kidney damage, and decrease in HDL cholesterol levels (ATSDR 2004).

The observed Zn concentration ranged from 0 g/L to 11766.92 µg/L with an average of 485.01 µg/L in pre monsoon season, while it ranged from 0 µg/L to 9866.35 µg/L with an average of 401.76 µg/L in post monsoon season. This data indicates that one sample (GW-32) collected in both seasons exceeded the recommended permissible limit of 4000 µg/L WHO (2006). However, Zn concentrations in groundwater samples collected in post monsoon seasons were significantly lower than those collected in pre monsoon season. However, these decline in Zn content during the post monsoon, which may be related to an increase in groundwater hardness caused by the addition of suspended particles and other components to water during the rainy season at particular sites (Chakraborty et al. 2019). The spatial map of Zn content demonstrates that the east side had higher concentrations throughout both seasons shown in Fig.5.85 and Fig.5.86.

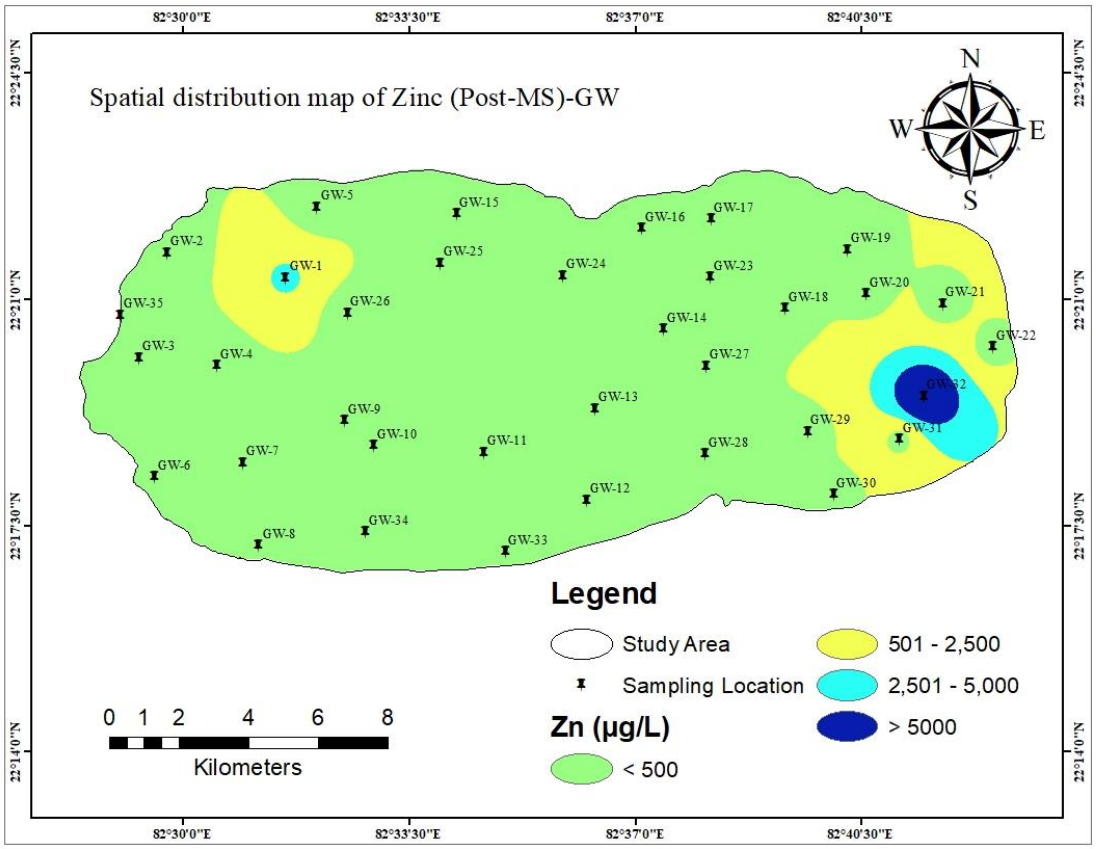

Fig.5.85 Spatial distribution map of Zinc during pre-monsoon season in the region

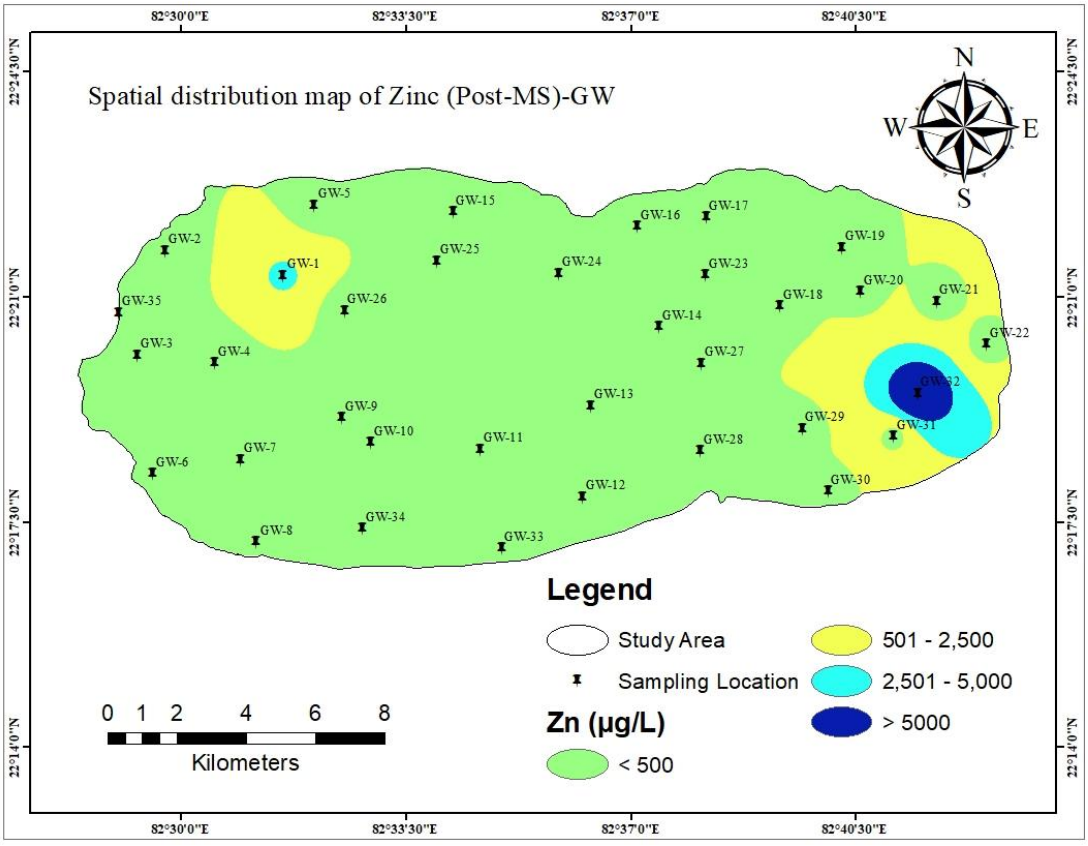

Fig.5.86 Spatial distribution map of Zinc during post-monsoon season in the region

5.2.3 Heavy metal pollution index (HPI)

The HPI is an assessment method that provides insight into the collective impact of individual heavy metals on the overall water quality. The rating system employs a random value ranging from 0 to 1, with the selection of the rating being dependent upon the relative significance attributed to several quality concerns (Horton 1965; Mohan et al. 1996). The critical pollution index of the HPI value for drinking water is 100 (Prasad and Bose, 2001). The value of HPI is estimated with formula (Prasad and Bose 2001) given by Equation (4.14) in previous chapter. It was found that the higher HPI value was the result of increasing concentrations of related metals in groundwater, which has a direct impact on the quality of groundwater. The HPI values with their quality status are shown in Tables.5.33 for the pre monsoon seasons and Table.5.34 for post monsoon seasons.

The values of the HPI for groundwater samples ranged from 0.79 to 53.59 in the pre monsoon season. It has been found that 30 (86.71%) groundwater samples were classified as low and the remaining 5 (14.28%) samples as high category of pollution. No samples were assigned to the medium category of HPI indices. It has been found that five samples (GW-1, GW-18, GW-24, GW-27, and GW-32) have high levels of HPI, making them unfit for human consumption and necessitating minor treatment before consumption. The spatial distribution of the HPI reveals that the eastern, western, and southern regions of the area exhibited comparatively lower HPI values. Conversely, certain locations in the east and northern parts displayed greater HPI values, suggesting that the groundwater in these areas necessitates minor treatment prior to use. The bar chart and spatial map of HPI in pre monsoon season has been shown in Fig.5.87 and Fig.5.89.

While in the post monsoon season, HPI of groundwater samples ranged from 0.79 to 31.72. The examination of the HPI reveals that 30 (85.71%) groundwater samples were classified as low, 4 (11.45%) samples were categorised as medium, and the remaining 1

(2.86%) sample classified into the high category of HPI. The analysis revealed that a one sample (GW-25) had high levels of HPI, making it unsuitable for human consumption and requiring significant treatment prior to consumption. However, the remaining 34 (97.14%) samples are considered to be drinkable. The spatial distribution map of the HPI reveals that the eastern, southern, and western areas of the study region exhibit lower HPI values. However, one spot in the north region displays higher HPI values, suggesting that the groundwater of these sites requires only minor treatment prior to consumption. The bar chart and spatial map of HPI in post monsoon season has been shown in Fig.5.88 and Fig.5.90.

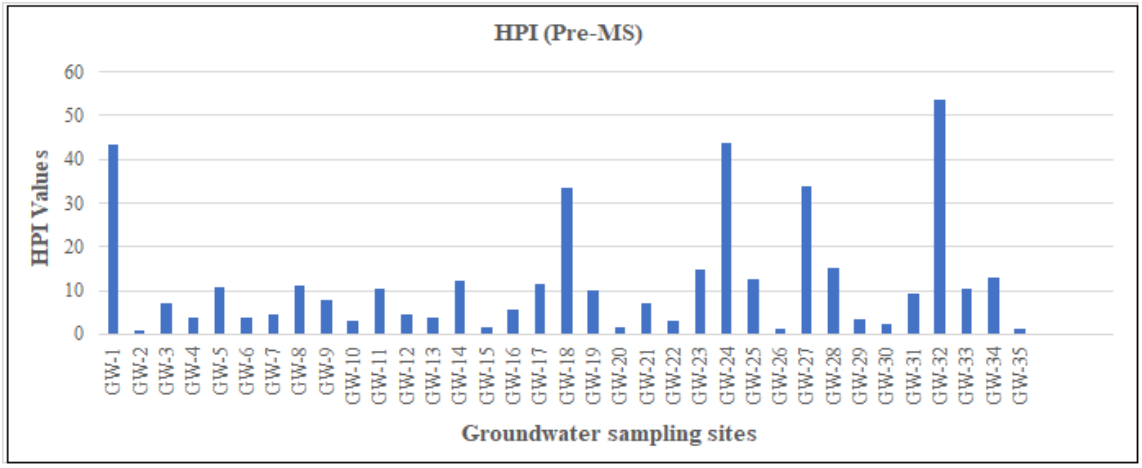

Fig.5.87 Graphical representation of HPI during pre-monsoon season

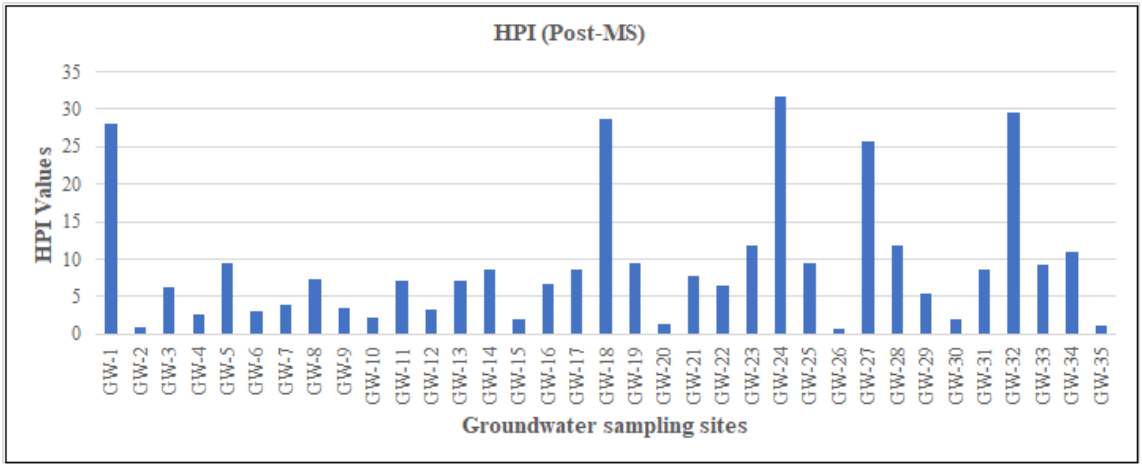

Fig.5.88 Graphical representation of HPI during post monsoon season

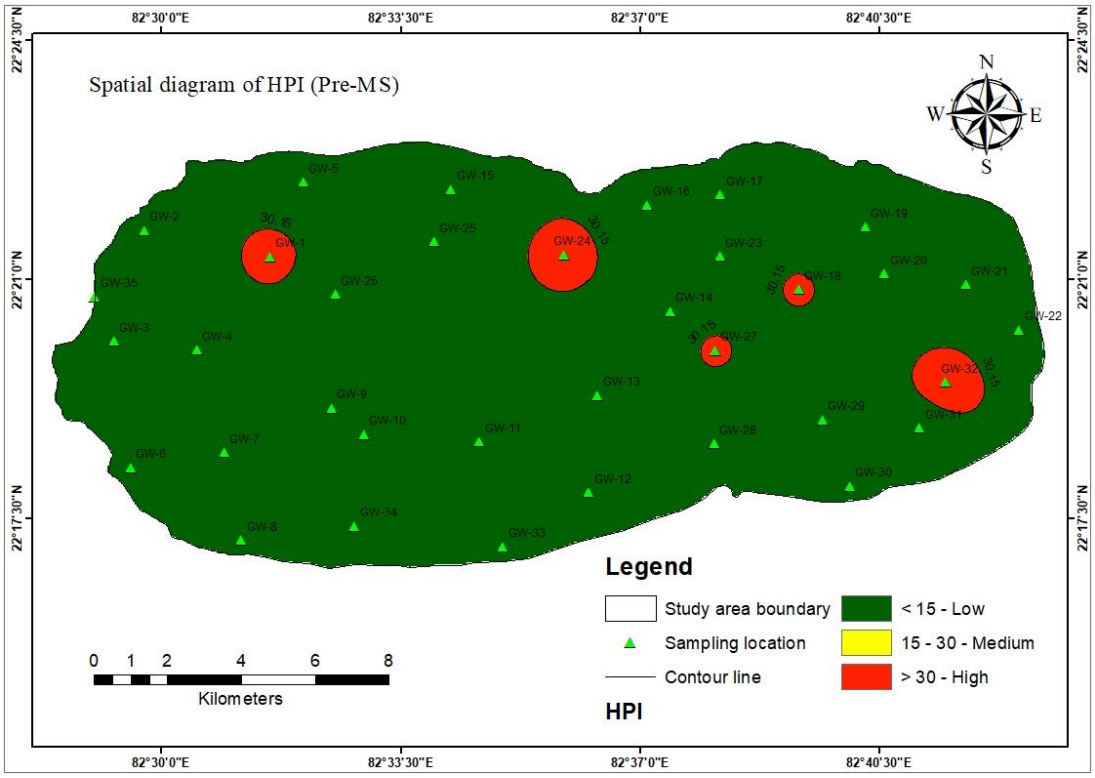

Fig.5.89 Spatial map of HPI during pre-monsoon season in study region

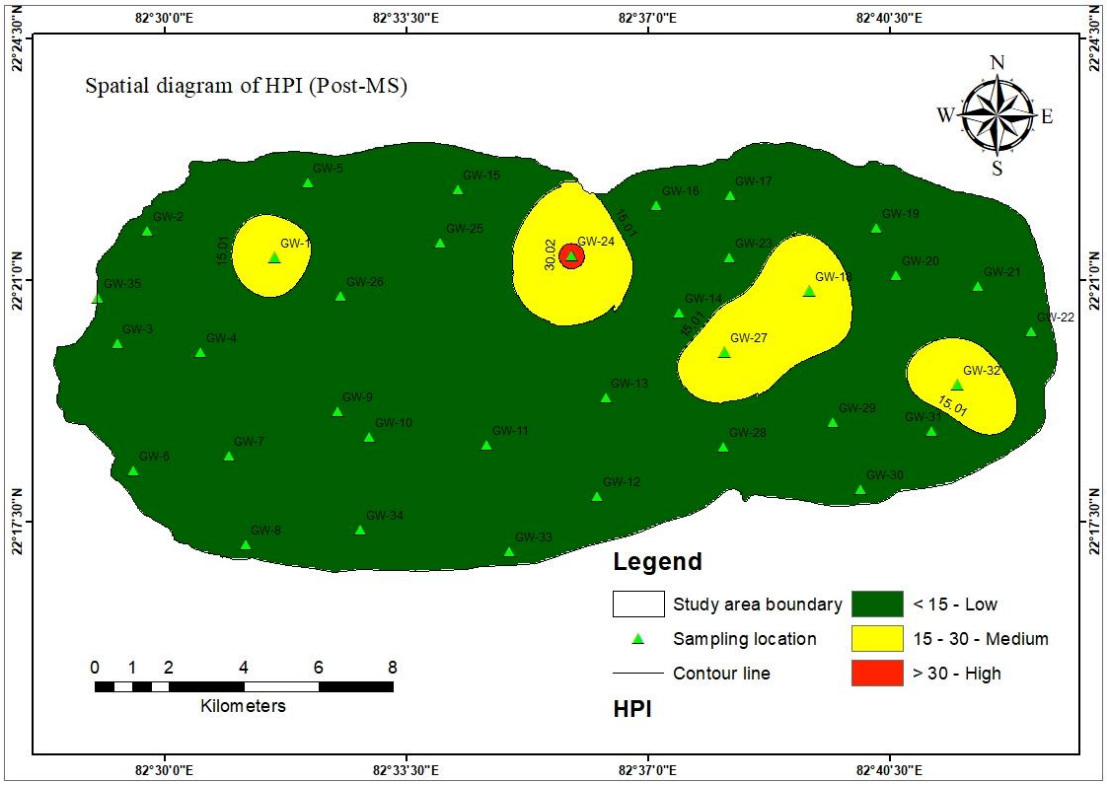

Fig.5.90 Spatial map of HPI during post-monsoon season in study region

5.2.4 Heavy metal evaluation index (HEI)

The HEI is a scientific approach used to evaluate the quality of water, with a specific focus on the presence of heavy metals in drinking water. Edet and Offiong 2002, HEI index proposed as an alternative to the HPI index for evaluating the occurrence of heavy metals in existing water sources. This HEI method is employed to simplify the analysis of heavy metal contamination levels in groundwater samples, hence facilitating the interpretation of pollution classes (Prasanna et al. 2012). HEI is expressed by Equation 4.16 as given in previous chapter. It also has three classes based on the computed HEI value, as given in Table.5.33.

The HEI values of the groundwater samples in the pre-monsoon season varied from 0.53 to 20.25. Among the groundwater samples, 16 (45.71%) were classified as low HEI, 14 (40.0%) sample fell into the medium HEI category, and the remaining 5 (14.29%) samples were categorised as high HEI. Five samples, namely GW-1, GW-24, GW-27, GW-29 and GW-32, were found to exhibit elevated levels of HEI, considering them unsuitable for human consumption. These samples require minor treatment prior to usage. Conversely, the remaining 30 (85.71%) samples are considered safe for drinking purposes. The spatial map of HEI shows that the eastern and north of the area had high HEI values, indicating that the groundwater required minor treatment before consumption. The bar chart and spatial map of HEI of study area in pre monsoon season has been shown in Fig.5.91 and Fig.5.93 respectively.

The groundwater samples collected in the post monsoon season showed HEI values, ranging from 0.41 to 5.87. Analysis of these data indicated that a majority of the samples, specifically 33 (94.29%), were classified as having low to medium levels of pollution. The remaining 2 (5.71%) samples were categorised as having high levels of pollution.

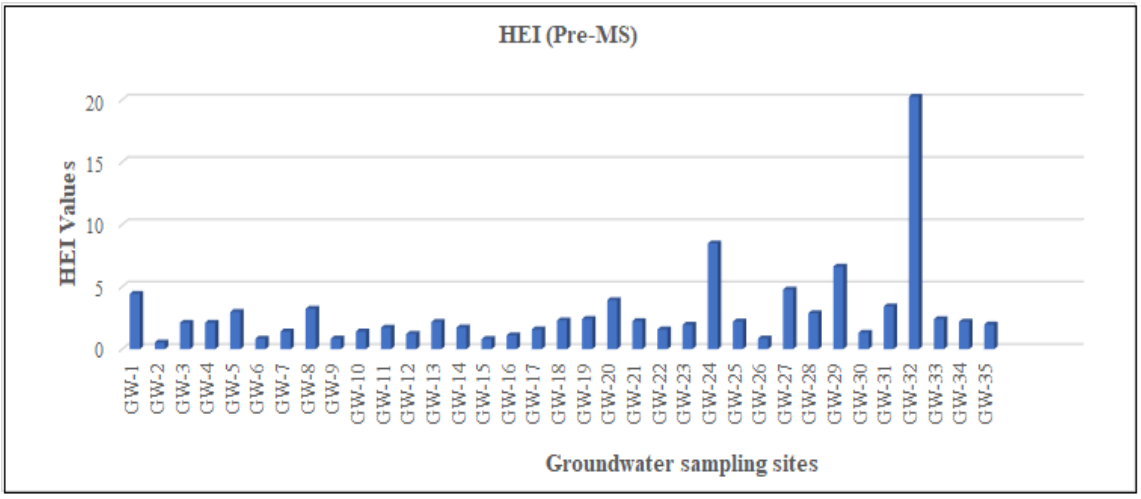

Fig.5.91 Graphical representation of HEI during pre-monsoon season

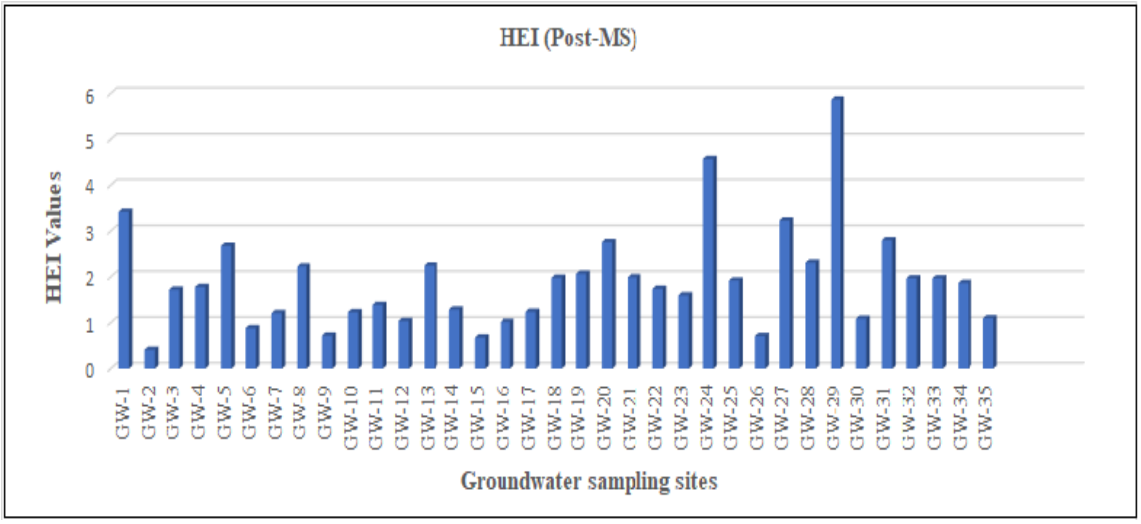

Fig.5.92 Graphical representation of HEI during post-monsoon season

The analysis revealed that the HEI levels observed in all of the samples varied between low and medium, indicating that they are appropriate for human consumption. The east, west, and south of the study area had lower HEI values, although some spots in the east and north had medium HEI values, indicating that the groundwater of this area is safe for consumption. The bar chart and spatial map of HEI of the area in post monsoon season has been shown in Fig.5.92 and Fig.5.94.

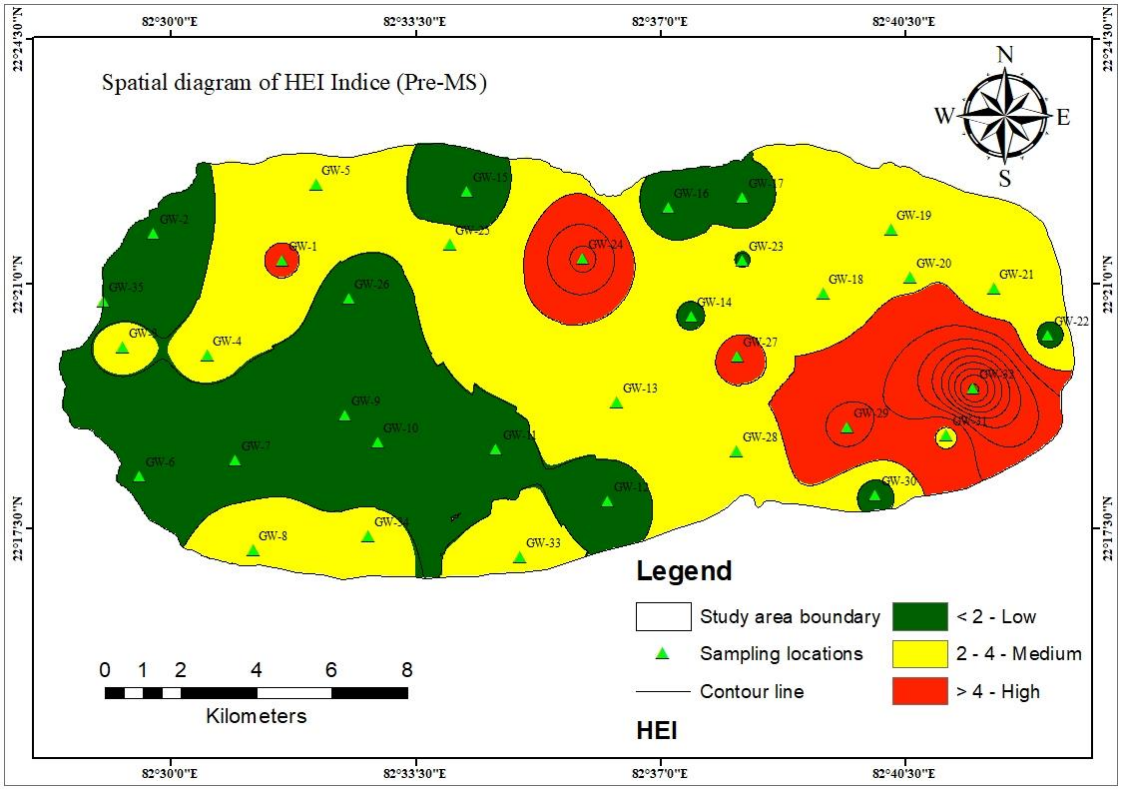

Fig.5.93 Spatial map of HEI during pre-monsoon season in study region

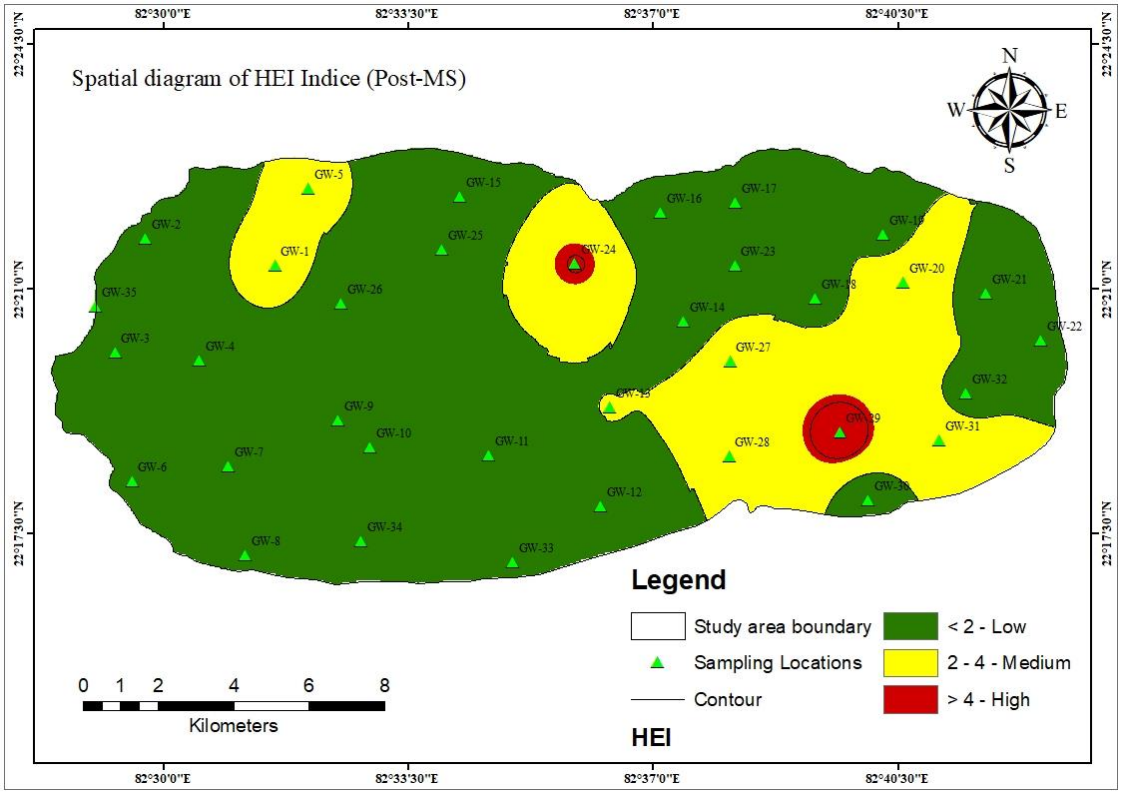

Fig.5.94 Spatial map of HEI during post monsoon season in study region

5.2.5 Metal Index

The Metal Index (MI) evaluates the degree to which heavy metals pose a threat to human health, as well as the overall quality of water intended for drinking, domestic, and other purposes (Balakrishnan and Ramu, 2016). The presence of higher metal concentrations related to the maximum allowable concentration (MAC) serves as an indicator of poor water quality. A higher MI score indicates that the water poses a higher risk to human health and is unsuitable for a variety of other applications as well. MI is expressed by Equation 4.17 as mentioned in previous chapter. Balakrishnan and Ramu, 2016 divided the MI index into six categories as given by Table.5.33.

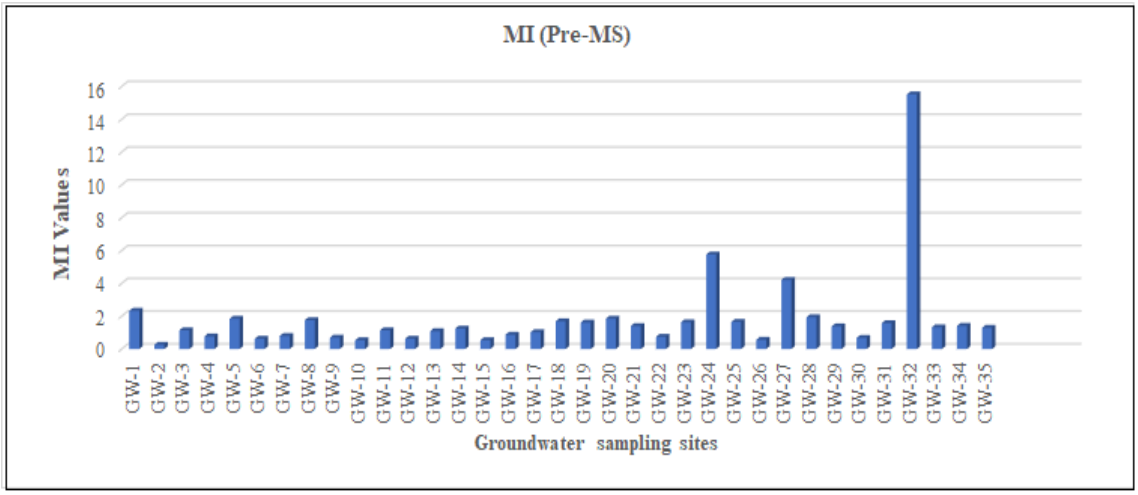

Fig.5.95 Graphical representation of MI during pre-monsoon season

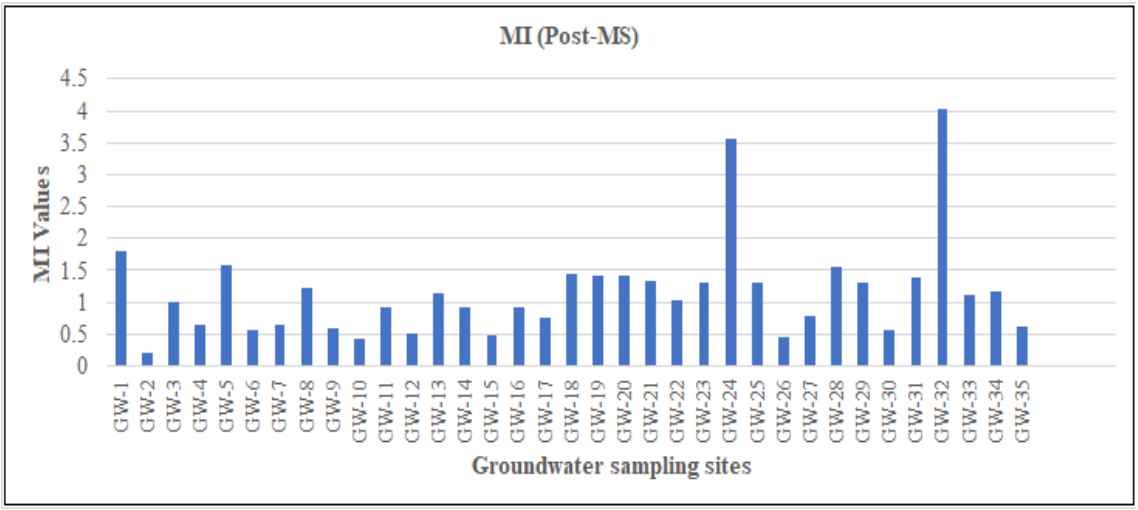

Fig.5.96 Graphical representation of MI during post-monsoon season

The MI of groundwater samples ranged from 0.26 to 15.52 in the pre-monsoon season from which 1 (2.86%) sample (GW-2), was categorised as very pure, while 11 (31.43%) samples were pure and safe for drinking. Furthermore, it was observed that 19 (54.29%) samples were slightly affected, 1 (2.86%) sample was moderately affected, 2 (5.71%) samples were strongly affected, and the remaining 1 (2.86%) sample was seriously affected which makes them unsafe for drinking. Overall, 88.57% of total samples belong to very pure to slightly affected, making them safe to drink while rest 11.43% of samples in the moderately to seriously affected class are unsafe to consume. The spatial map of MI revealed that the western region exhibited lower MI values, while the east and north regions displayed higher MI values which suggest that the groundwater in the area requires minor treatment prior to use. The bar chart and spatial map of MI of the area in pre monsoon season has been shown in Fig.5.95 and Fig.5.97 respectively.

MI of groundwater samples in the post monsoon season ranged from 0.195 to 4.04 from which 1 (2.86%) groundwater sample (GW-2) was assessed to be very pure, while 14 (40.0%) samples were pure and suitable for drinking. Furthermore, 19 (54.29%) samples were slightly, 1 (2.86%) sample was moderately and 1 (2.86%) sample was strongly affected class. No samples were belonging to the seriously affected class of MI indices. Overall, 97.14% of the samples fall into the very pure to slightly affected MI class, making them suitable for drinking purposes while the remaining 2.86% of samples classified as the moderately affected to strongly affected class which are unsafe to consumption. The spatial map of MI revealed that few spots in the east and north had moderate MI values, indicating groundwater needed some minor treatment before use whereas the remaining samples ware suitable for drinking. The bar chart and spatial map of MI of the area in post monsoon season has been shown in Fig.5.96 and Fig.5.98 respectively.

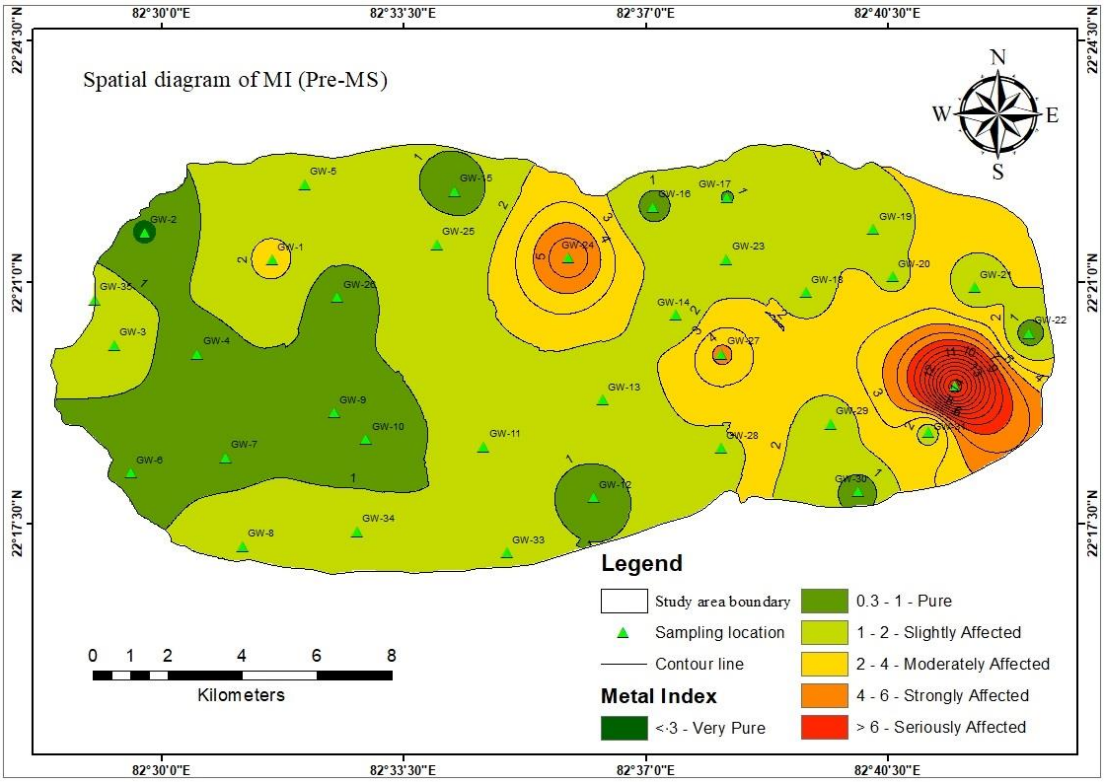

Fig.5.97 Spatial map of MI during pre-monsoon season in the region

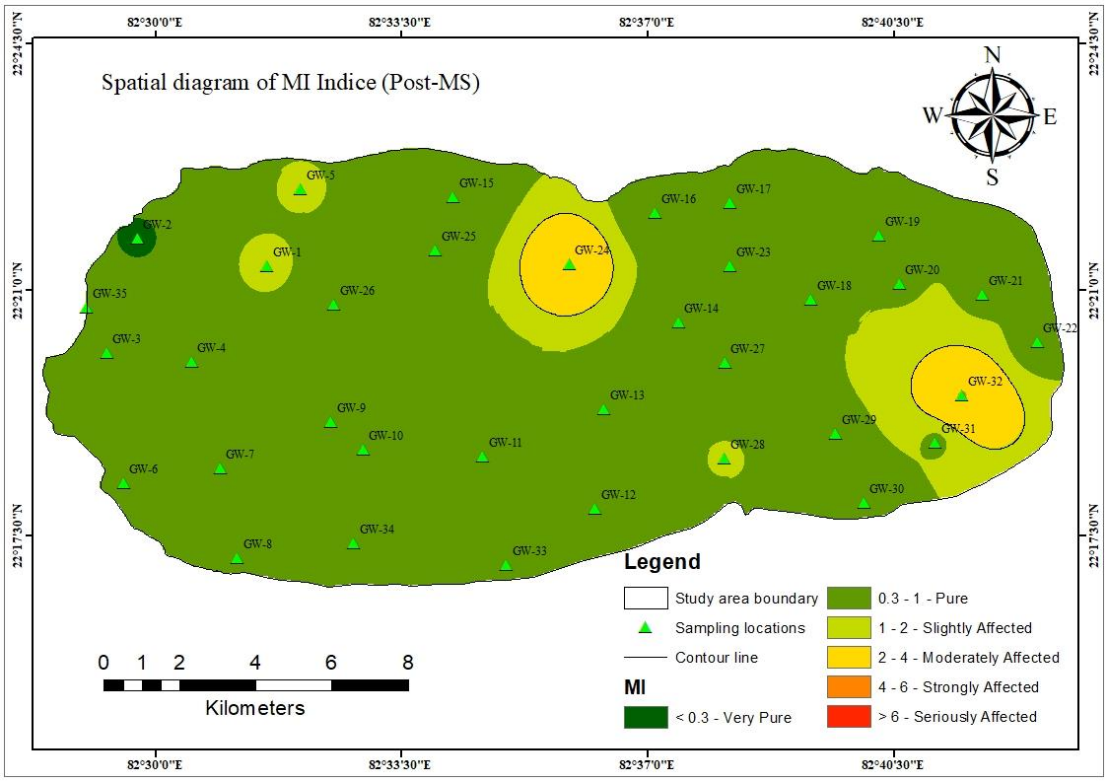

Fig.5.98 Spatial map of MI during post-monsoon season in the region

Here, Table.5.37 and Table.5.38 are showing calculated HPI, HEI and MI values of groundwater samples in pre and post monsoon season respectively.

Table.5.33 Water quality classification of pre-MS base on pollution indices categories

Indices methods	Category	Degree of pollution	Number of samples	Percentage (%)
Heavy metal pollution index	<15	Low	30	85.71%
	15-30	Medium	0	0%
	>30	High	5	14.29%
Heavy metal evaluation index	<2	Low	16	45.71%
	2-4	Medium	14	40%
	>4	High	5	14.29%
Metal Index	<0.3	Very pure	1	2.86%
	0.3-1	Pure	11	31.43%
	1-2	Slightly affected	19	54.29%
	2-4	Moderately affected	1	2.86%
	4-6	Strongly affected	2	5.71%
	>6	Seriously affected	1	2.86%

Table.5.34 Water quality classification of post-MS base on pollution indices categories

Indices methods	Category	Degree of pollution	Number of samples	Percentage (%)
Heavy metal pollution index	<15	Low	30	85.71%
	15-30	Medium	4	11.43%
	>30	High	1	2.86%
Heavy metal evaluation index	<2	Low	25	71.43%
	2-4	Medium	8	22.86%
	>4	High	2	5.71%
Metal Index	<0.3	Very pure	1	2.86%
	0.3-1	Pure	14	40%
	1-2	Slightly affected	19	54.29%
	2-4	Moderately affected	1	2.86%
	4-6	Strongly affected	0	0
	>6	Seriously affected	0	0

5.2.6 Exploratory data analysis

5.2.6.1 Scatter plot analysis

The utilisation of scatter plots is known to be more effective in identifying significant correlations across several indices, including HPI, HEI, and MI. The different indices represent different correlation with R^2 value. In order to conduct a more comprehensive analysis, a scatter plot was generated to explore the relationship between the HPI, HEI, and MI in the pre monsoon season represented in Fig.5.99 a, b, and c. Based on the analysis of the scatter plot, it has been observed that there exists a strong correlation between HEI and MI with (R^2 = 0.9348). Conversely, a moderate correlation is evident between the HPI and HEI, with (R^2 = 0.5306). Similarly, a comparable moderate correlation is observed between HPI and MI, with (R^2 =0.5929), in the pre monsoon season. Therefore, selection of either the HEI or MI indices, or both for sample classification may be a better option in this study. Here, the MI indices have been chosen as the appropriate metric for assessing the extent of pollution, in accordance with previous research conducted in the vicinity (Al-Ami et al. 1987 and Jahanshahi and Zare 2015).

Consequently, a thematic map has been generated utilising the metal index (MI), showcasing both the spatial map of pollutant levels and the temporal variations in different water sources within the examined area as shown in Fig.5.97 and Fig.5.98. It has been observed from Fig. 5.97, the water sample (GW-32) from the pre monsoon exhibit the highest pollution level (MI = 15.52) in the east side of the area. The elevated levels of pollution observed at this particular site can potentially be attributed to the influence of mining activities, as it is situated in close proximity to an active mining area known as the southern boundary of the Kushmunda mine. Furthermore, sample GW-24 (MI=5.76) from the north side and sample GW-27 (MI=4.21) from the centre side of the study area are strongly affected (MI between 4 to 6) zones, while sample GW-1 (MI=2.33) are

moderately affected (MI between 2 to 4), and the rest are less contaminated (MI between 0.3 to 1). The presence of elevated Fe, Mn, Ni, and Ba concentrations in the water is principally responsible for the higher pollution index detected at the respective locations. These metallic elements typically originate from geogenic sources, where hinterland formations consist of alumino-silicates with pyrite as an accompanying mineral. Through a process of water-rock interaction, they are released into groundwater as leachate (Stallard and Edmond 1983).

However, a scatter plot was generated to examine the relationship between HPI, HEI, and MI in the post monsoon season represented in Fig.5.100 a, b, and c. A strong correlation between HEI and MI (R^2 = 0.8128), and moderate correlation between HPI and HEI (R^2 = 0.3763), and HPI and MI (R^2 = 0.5228) have been found. Therefore, only 2 samples from east, and north parts of the area such as GW-24 (MI=3.56), and GW-32 (MI=4.04), from the post monsoon season plot in a moderately zone (MI between 2 and 4) to strongly affected zone (MI between 4 and 6), while all other samples plot in a less contaminated zone (i.e., MI between 0.3 to 1) as shown in Fig.5.98.

The post monsoon season exhibits a lower level of metal index (MI) in comparison to the pre monsoon season. The metal load exhibits seasonal variations as a consequence of the "dilution effect" caused by intense regional rainfall, measuring 1438 mm. This rainfall mostly occurs (80%) in the monsoon season. Percolated rainfall rejuvenates the water table after the monsoon season, diluting metal concentrations and facilitating their migration (Tiwari et al. 2016). Hence, groundwater recharge in the post monsoon season dilutes heavy metal concentrations, lowering the metal index (MI) in groundwater.

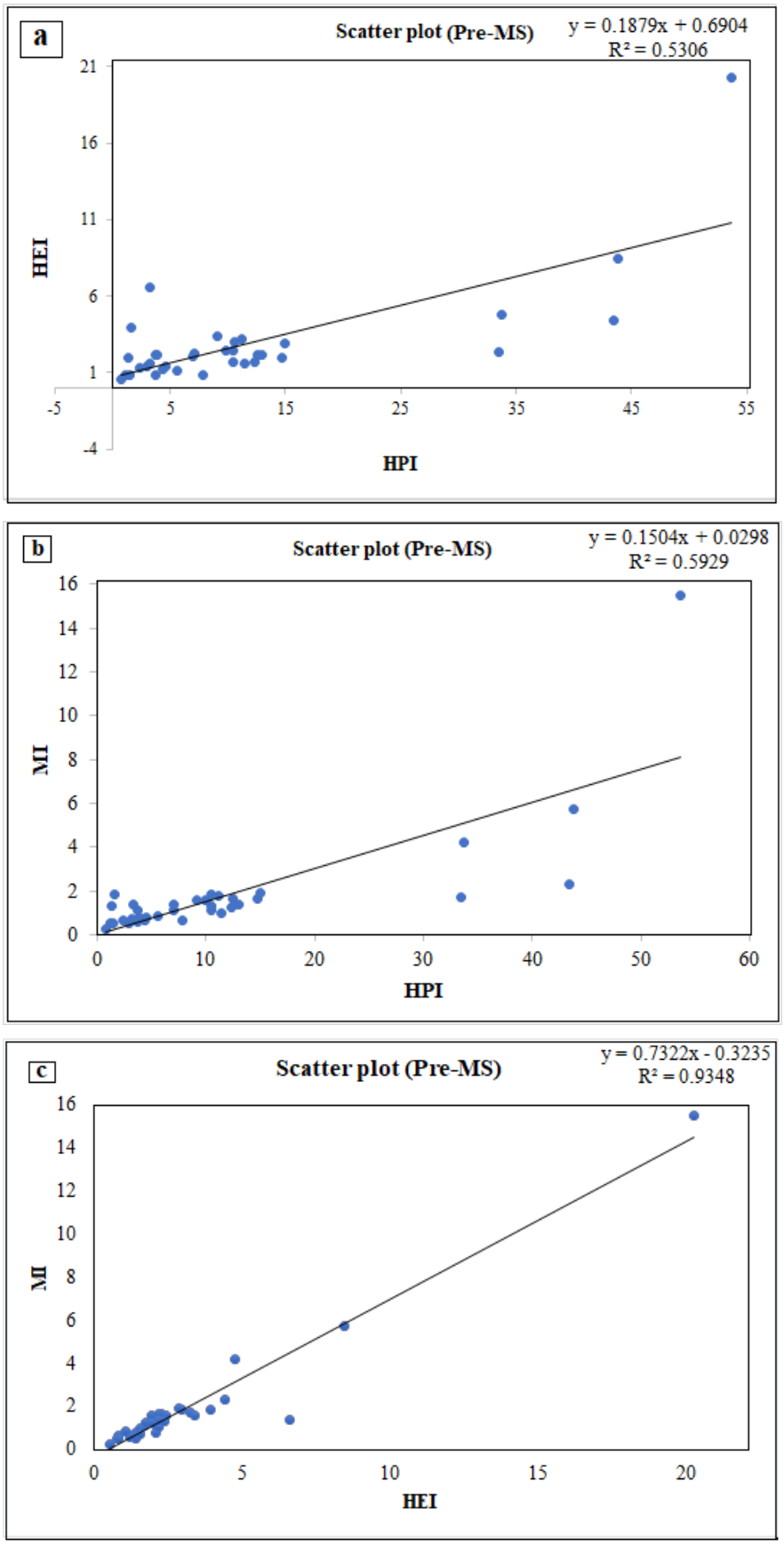

Fig.5.99 Scatter plot of (**a**) HPI versus HEI (**b**) HPI versus MI (**c**) HEI versus MI and their correlation of determination in pre monsoon season

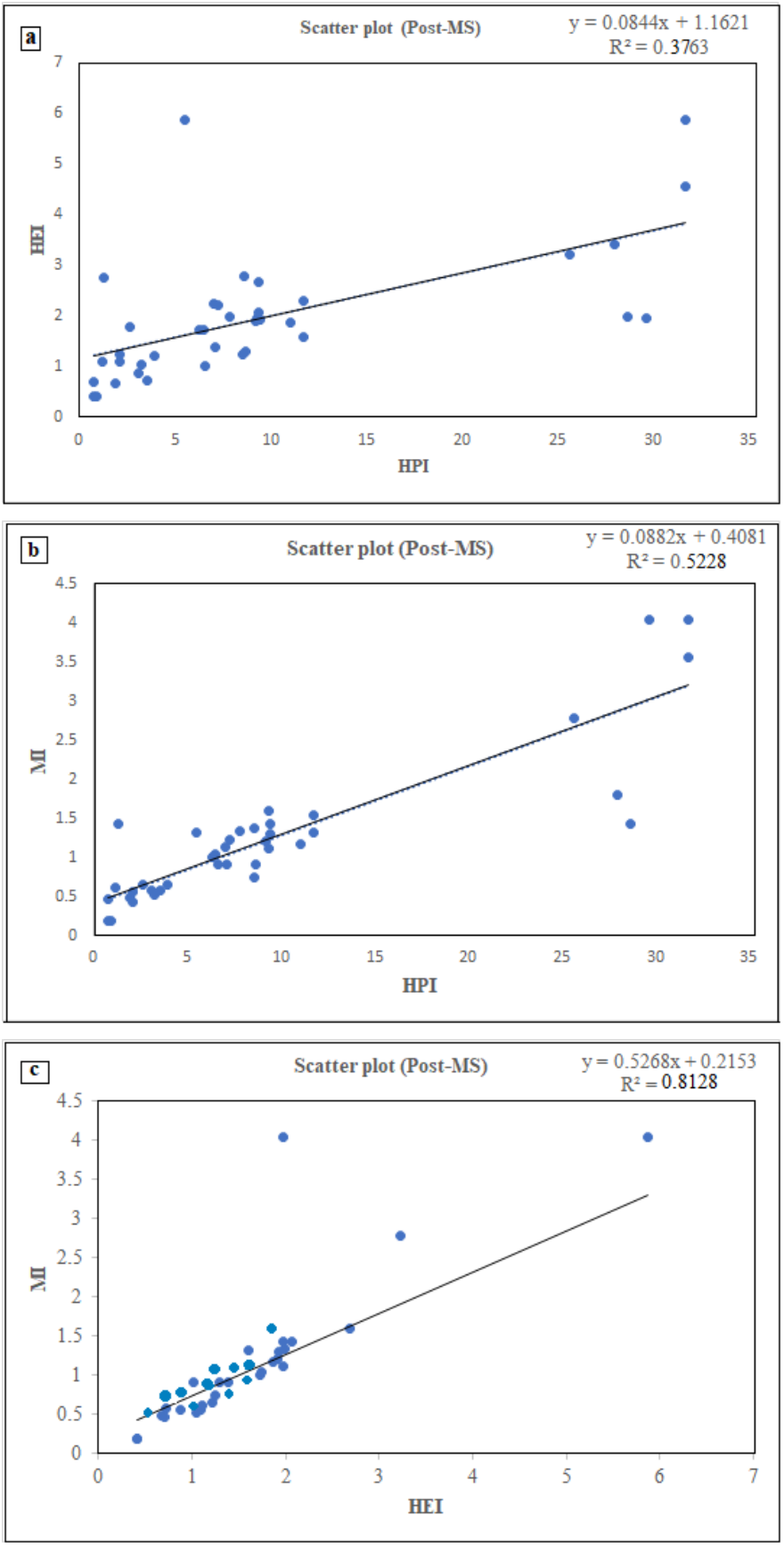

Fig.5.100 Scatter plot of (**a**) HPI versus HEI (**b**) HPI versus MI (**c**) HEI versus MI and their correlation of determination in post monsoon season

5.2.6.2 Principal component analysis

PCA technique was employed to facilitate the interpretation of elemental data and identify the cluster of metals having the same source. It indicates the association of variables, lowering the dimensionality of the dataset. PCA with the covariance function should be used only if all elements have the same units of measurement (Costa et al. 2009). There were 35 monitoring points and 10 measured variables in the data matrix considered for classification in both seasons. The important gradients in the dataset are determined PC and its eigenvalues. Here, the most significant components were identified in the first three principal components (PCs), which accounted for 65.39% of the total variance in water quality (PC1: 37.71%, PC2: 14.98%, and PC3: 12.69%) in pre monsoon season and 57.14% of the total variance in water quality (PC1: 25.70%, PC2: 18.18%, and PC3: 13.26%) in post monsoon season, respectively as illustrated in Table.5.35 and Table.5.36 respectively. The three factors with eigenvalues >1 in both seasons was extracted from principal factor matrix after varimax rotation.

First component (PC1), its parameters were most essential to identify changes in water quality due to its large positive loadings of Fe (0.453), Mn (0.422), and Zn (0.478), accounted for the highest total variation of 37.7% in pre monsoon season while 25.7% of highest total variation, contains high positive loadings of Zn (0.494), Cu (0.416), and Mn (0.410) in post monsoon season respectively. The PCA results for pre monsoon and post monsoon seasons are given in Table.5.35 and Table.5.36. The first factor (PC1) exhibits a discernible correlation with the composition of the earth's crust and the geological structure of the region (Tiwari et al. 2016). Considering second component (PC2), contributed 14.98% of the variance with large positive loading of Ba (0.699) and Ni (0.537) in pre monsoon season while PC2 comprised high negative loadings of Cu (-0.440), Fe (-0.589), accounting for 18.18% of the total variance in post monsoon season.

It can be inferred that PC2 was associated to nearby mining operations. The origins of such metallic elements can be attributed primarily to the discharge of mining waste and the leaching of water from coal overburden deposits (Tiwari 2001; Bhuiyan et al. 2010). However, PC3 contributed 14.98% of the variation exhibited large positive loadings of Cd (0.518), Cr (0.401) and high negative loadings of Cr (-0.509) in pre monsoon while 13.26% of the variance shows high positive loading of Ba (0.668) and Ni (0.428) in post monsoon season. The third component PC3 appears to have come from other anthropogenic sources, like pollution from industry and vehicles (Mahato et al. 2016).

A scree plot is an approach for determining the number of significant factors by looking for a sharp change in the magnitude of the eigenvalues, which causes the slope of the plot to change from very steep to shallow as shown in Fig.5.101 (a) for pre monsoon and Fig.5.101 (b) for post monsoon season. The slope of the plot changes from steep to shallow after considering the initial three factors.

Table.5.35 PC loadings (varimax normalized) for the metals in groundwater during pre-monsoon season

Element	PC1	PC2	PC3
Al	-0.116	0.093	-0.363
Ba	0.051	**0.699**	0.126
Cd	0.175	-0.160	**0.518**
Cr	0.194	-0.330	**0.401**
Cu	0.278	-0.038	**-0.509**
Fe	**0.453**	-0.060	-0.317
Mn	**0.422**	0.163	0.100
Pb	0.374	-0.195	0.069
Ni	0.294	**0.537**	0.198
Zn	**0.478**	-0.103	-0.119
Eigen value	3.772	1.498	1.269
% of Variance	37.71%	14.98%	12.69%
Cumulative	37.71%	52.70%	65.39%

Table.5.36 PC loadings for the metals in groundwater during post-monsoon season

Element	PC1	PC2	PC3
Al	-0.218	0.110	0.123
Ba	-0.093	0.280	**0.668**
Cd	0.262	0.301	-0.358
Cr	0.279	0.096	-0.288
Cu	**0.416**	**-0.440**	0.267
Fe	0.302	**-0.589**	0.068
Mn	**0.410**	0.230	-0.125
Pb	0.233	0.305	-0.137
Ni	0.281	0.337	**0.428**
Zn	**0.494**	0.098	0.187
Eigen value	2.569	1.818	1.326
% of Variance	25.70%	18.18%	13.26%
Cumulative	25.70%	43.88%	57.14%

Large loading having an absolute value ≥ 0.40 are highlighted in boldface

Once move from factor 2 to factor 3, the eigenvalues of the studied data likewise fall below one. This indicates that a three-component solution that accounts for the total variance of 65.39% in pre monsoon and 57.14% in post monsoon seasons may be the right choice.

Almost all variables are distributed in the first (upper right) and fourth (lower right) quadrants, as per the loadings plot of the first two PCs (PC1 and PC2) in pre and post monsoon season as shown in Fig. 5.103 (a) and Fig.5.103 (b) respectively. The lines joining the variables and intersecting at the origin in the factor loadings plot depict the influence of the variables on the samples. The proximity of lines for two variables indicates the strength of their reciprocal association (Qu and Kelderman 2001). The loading plot reveals a significant positive connection between the variables grouped as (Ba, Ni, Mn; Cu, Fe, Zn and Pb, Cd, Cr) in the pre monsoon, and (Pb, Ni, Cd; Mn, Cr, Zn and Cu, Fe) in the post monsoon season.

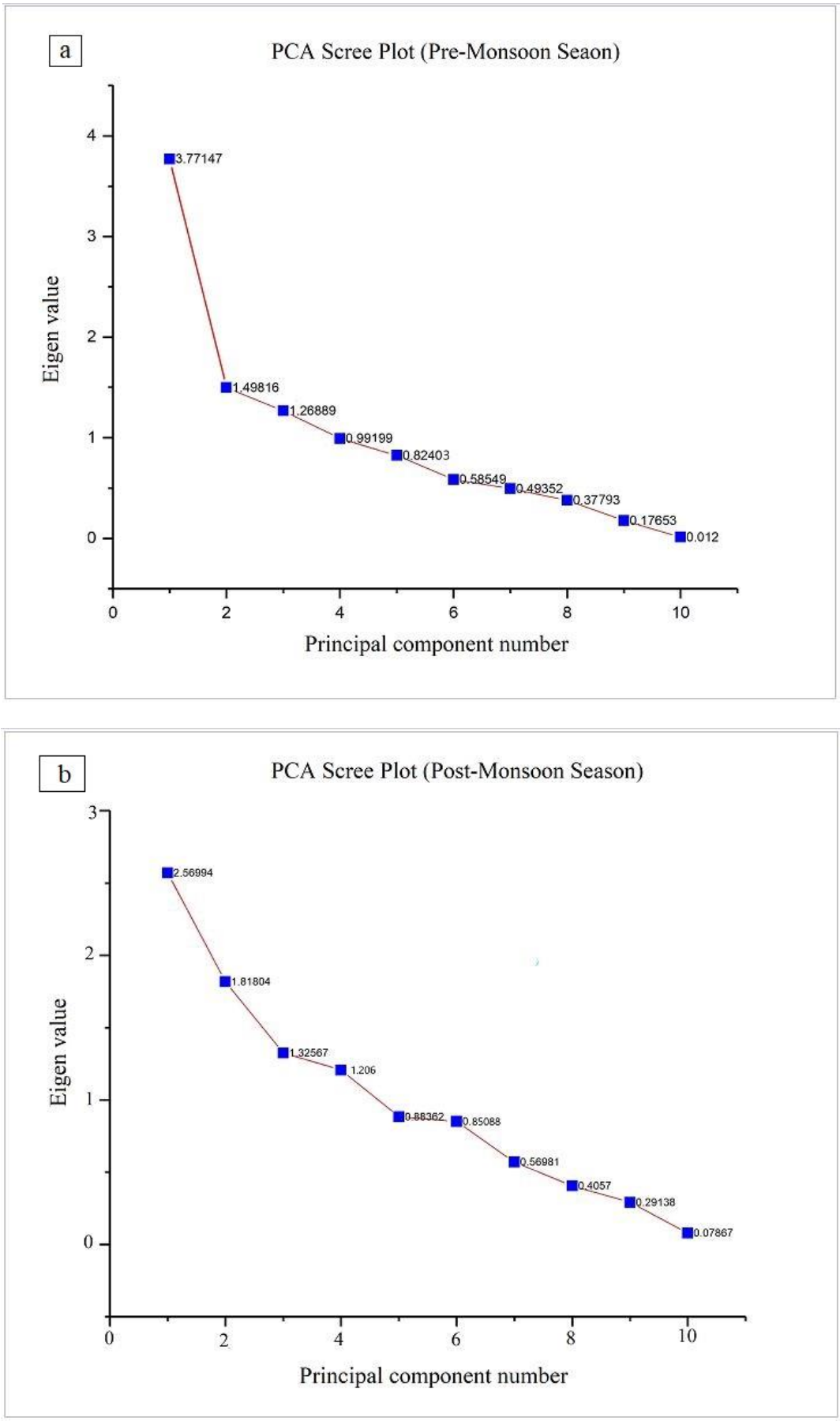

Fig.5.101 PCA scree plot of the eigen value **(a)** in pre and **(b)** post monsoon season

PCs score plots are charts that show the characteristics of samples and provide information about their spatial distribution. The PCs scores plot for both seasons created with the help of PC1 and PC2 components verifies the clustering of site-specific samples in area and their spatial distribution as shown in Fig.5.103 (a) and Fig.5.103 (b).

It has been observed from Fig.5.102 (a) that samples located in the upper quadrants exhibit a higher concentration of Al, Ba, Ni, and Mn. Conversely, samples situated in the lower quadrants demonstrate a lower concentration of Cu, Fe, Zn, Pb, Cd, and Cr in the pre monsoon season. In contrast, the analysis of Figs.5.102 (b), reveal that the upper quadrants exhibit higher concentrations of elements such as Al, Ba, Pb, Cd, Ni, Mn, Cr, and Zn. However, the lower quadrants mostly include Cu and Fe, specifically in the post monsoon season.

The distribution of the samples is mixed based on both score plots for groundwater from the study area as illustrated in Fig.5.103 (a) and Fig.5.103 (b) respectively. Most of the samples exhibit significant grouping in the upper left and lower left quadrants, while the upper right and lower right quadrants clearly display dispersed loading.

Finally, it was found that the three principal components, PC1, PC2, and PC3, which accounted for 37.71%, 14.98%, and 12.69% of the total variance in pre monsoon season and 25.70%, 18.18%, and 13.26% of the total variance in post monsoon season, are principally responsible of governing the concentrations of metals in groundwater (Ravikumar & Somashekar 2017). This phenomenon can be attributed to the fact that a significant proportion of the elements examined in the area, specifically 70% in the pre monsoon season and 50% in the post monsoon season, exhibit large loading (≥ 0.40) and fall under three principal components which governs the metal concentrations in groundwater.

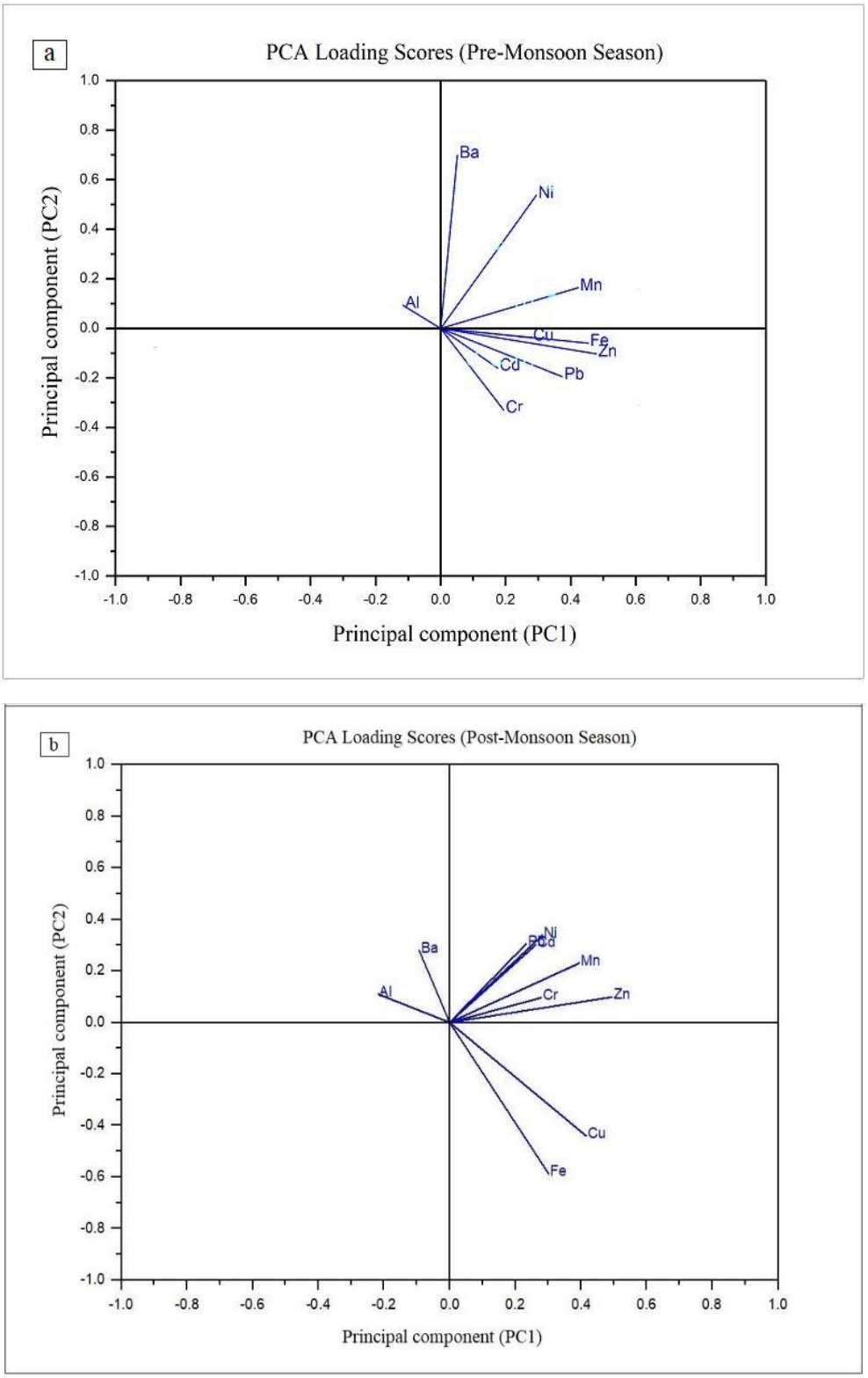

Fig.5.102 Plots of PCA loadings scores for datasets of water samples (**a)** in pre and **(b)** for post-monsoon season

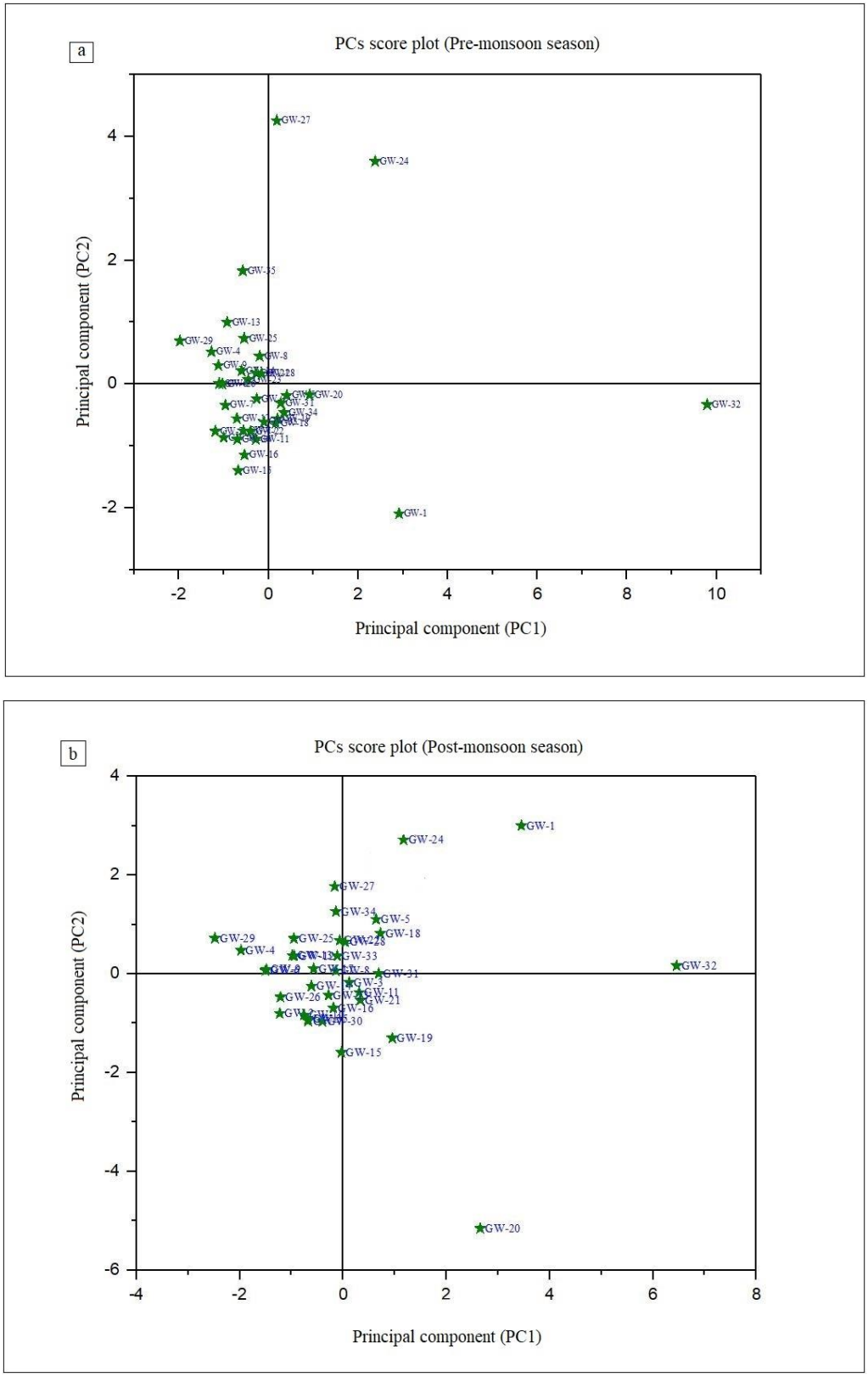

Fig.5.103 PCs score plot for datasets of water samples **(a)** in pre and **(b)** for post monsoon season respectively

Table.5.37 HPI, HEI and MI values of groundwater samples in pre monsoon season

Sample code	HPI	Status	HEI	Status	MI	Status
GW-1	43.42	High	4.44	High	2.33	Moderately Affected
GW-2	0.79	Low	0.53	Low	0.26	Very Pure
GW-3	7.01	Low	2.11	Medium	1.14	Slightly Affected
GW-4	3.86	Low	2.12	Medium	0.77	Pure
GW-5	10.57	Low	2.98	Medium	1.84	Slightly Affected
GW-6	3.73	Low	0.83	Low	0.62	Pure
GW-7	4.57	Low	1.42	Low	0.79	Pure
GW-8	11.17	Low	3.24	Medium	1.76	Slightly Affected
GW-9	7.91	Low	0.85	Low	0.69	Pure
GW-10	2.95	Low	1.41	Low	0.53	Pure
GW-11	10.47	Low	1.72	Low	1.14	Slightly Affected
GW-12	4.35	Low	1.22	Low	0.63	Pure
GW-13	3.71	Low	2.18	Medium	1.09	Slightly Affected
GW-14	12.38	Low	1.74	Low	1.24	Slightly Affected
GW-15	1.52	Low	0.81	Low	0.54	Pure
GW-16	5.61	Low	1.1	Low	0.87	Pure
GW-17	11.42	Low	1.58	Low	1.02	Slightly Affected
GW-18	33.46	High	2.31	Medium	1.69	Slightly Affected
GW-19	9.91	Low	2.42	Medium	1.61	Slightly Affected
GW-20	1.62	Low	3.93	Medium	1.85	Slightly Affected
GW-21	7.09	Low	2.25	Medium	1.4	Slightly Affected
GW-22	3.21	Low	1.58	Low	0.74	Pure
GW-23	14.69	Low	1.96	Low	1.63	Slightly Affected
GW-24	43.79	High	8.48	High	5.76	Strong Affected
GW-25	12.55	Low	2.21	Medium	1.65	Slightly Affected
GW-26	1.16	Low	0.86	Low	0.56	Pure
GW-27	33.73	High	4.78	High	4.21	Strong Affected
GW-28	14.99	Low	2.88	Medium	1.93	Slightly Affected
GW-29	3.28	Low	6.62	High	1.38	Slightly Affected
GW-30	2.37	Low	1.32	Low	0.68	Pure
GW-31	9.12	Low	3.43	Medium	1.57	Slightly Affected
GW-32	53.59	High	20.25	High	15.52	Seriously Affected
GW-33	10.46	Low	2.41	Medium	1.32	Slightly Affected
GW-34	13.02	Low	2.2	Medium	1.41	Slightly Affected
GW-35	1.41	Low	1.97	Low	1.29	Slightly Affected

Table.5.38 HPI, HEI and MI values of groundwater samples in post monsoon season

Sample code	HPI	Status	HEI	Status	MI	Status
GW-1	27.97	Medium	3.42	Medium	1.81	Slightly Affected
GW-2	0.94	Low	0.41	Low	0.195	Very Pure
GW-3	6.32	Low	1.72	Low	1.01	Slightly Affected
GW-4	2.63	Low	1.78	Low	0.66	Pure
GW-5	9.37	Low	2.68	Medium	1.59	Slightly Affected
GW-6	3.08	Low	0.88	Low	0.57	Pure
GW-7	3.93	Low	1.21	Low	0.65	Pure
GW-8	7.28	Low	2.23	Medium	1.23	Slightly Affected
GW-9	3.59	Low	0.72	Low	0.58	Pure
GW-10	2.11	Low	1.23	Low	0.44	Pure
GW-11	7.14	Low	1.39	Low	0.91	Pure
GW-12	3.28	Low	1.04	Low	0.52	Pure
GW-13	7.05	Low	2.25	Medium	1.13	Slightly Affected
GW-14	8.69	Low	1.29	Low	0.91	Pure
GW-15	1.91	Low	0.68	Low	0.49	Pure
GW-16	6.61	Low	1.02	Low	0.91	Pure
GW-17	8.58	Low	1.24	Low	0.75	Pure
GW-18	28.66	Medium	1.98	Low	1.44	Slightly Affected
GW-19	9.41	Low	2.07	Medium	1.43	Slightly Affected
GW-20	1.31	Low	2.76	Low	1.43	Slightly Affected
GW-21	7.84	Low	1.99	Low	1.34	Slightly Affected
GW-22	6.53	Low	1.74	Low	1.04	Slightly Affected
GW-23	11.72	Low	1.6	Low	1.32	Slightly Affected
GW-24	31.72	High	4.57	High	3.56	Moderately Affected
GW-25	9.43	Low	1.92	Low	1.31	Slightly Affected
GW-26	0.79	Low	0.71	Low	0.46	Pure
GW-27	25.64	Medium	3.23	Medium	0.79	Slightly Affected
GW-28	11.72	Low	2.31	Medium	1.55	Slightly Affected
GW-29	5.52	Low	5.87	High	1.32	Slightly Affected
GW-30	2.09	Low	1.09	Low	0.56	Pure
GW-31	8.61	Low	2.8	Medium	1.38	Slightly Affected
GW-32	29.65	Medium	1.97	Low	4.04	Strongly Affected
GW-33	9.33	Low	1.97	Low	1.11	Slightly Affected
GW-34	11.03	Low	1.87	Low	1.17	Slightly Affected
GW-35	1.18	Low	1.1	Low	0.61	Pure

5.3 Land Use/ Land Cover change analysis (2001 to 2021)

The LULC is a significant method for classifying the area into many classes to know the exact located area under study. The LULC map was generated through the use of the unsupervised classification technique over three distinct temporal intervals, utilising the ERDAS 15 software platform. The most frequent way for representing LULC classes is through satellite imagery, which is acquired, improved, processed, and digitalized to generate False Colour Composition (FCC). Multiband raster images have been used to examine LULC with the help of imagery classification and interpretation (Li et al. 2014). This study involved the classification of six land use and land cover (LULC) classifications, namely Forest area, Habitation, Water bodies/River, Mining area, Crop land/Vegetation, and Fallow land as presented in the Table 5.39. Land Use and Land Cover (LULC) assessments were conducted for three distinct temporal intervals, specifically the years 2001, 2011, and 2021, respectively.

Table.5.39 Scheme of LULC classification

Classes	**Descriptions**
Forest	This category includes coniferous vegetation scattered throughout surrounding mountains.
Habitation	Residential area, commercial building, industries, road and another paved surface included in this category.
Water bodies /River	This category includes lakes, rivers, and permanent ponds.
Mining Area	Area covered with mines and dumps.
Crop Land/ Vegetation	Land used for cultivation of Rabi and Kharif crops.
Fallow Land	This class includes bare land, rock strewn, and other soil surfaces that are free of vegetation throughout the year.

5.3.1 Land use/ land cover analysis of year 2001

The LULC map for the year 2001 was created with a satellite image acquired by the Landsat 5 Thematic Mapper (TM) sensor as shown in Fig.5.104. According to the map that had been created, it was shown that the research region had a forest area cover of around 16.033 km^2, which is comparable to approximately 7.08% of the total area (226.604 km^2) of the study region. The second notable category is Habitation, encompassing an estimated area of 10.902 km^2, constituting approximately 4.81% of the total land. The third category in terms of area is water bodies, which covered approximately 11.57 km2 and account for 5.11% of the overall area. This generally refers to the sump, ponds, rivers, and the tributaries of those rivers in the investigated area. The mining area is comprising about 12.737 Km^2 or 5.62% of the total area under consideration. Furthermore, it is worth noting that the categories of follow land and crop land encompass the most extensive regions, accounting for around 86.142 km^2 (28.01%) and 98.22 km^2 (39.37%) of the overall area, respectively. These classes statistics from LULC map of 2001 is illustrated in Table.5.40 and Fig.5.105 respectively.

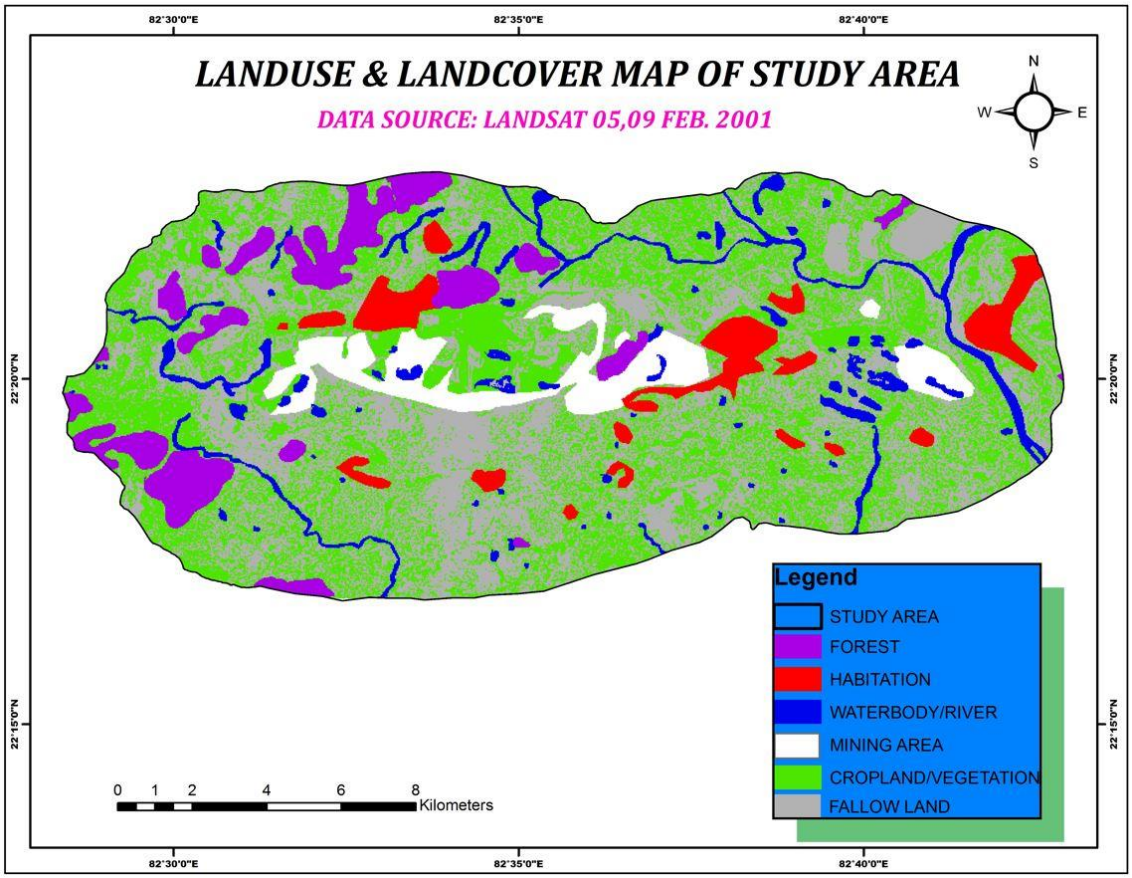

Fig.5.104 Land Use/Land Cover map for study area in 2001

Table.5.40 LULC statistics for year 2001

LULC Classes (2001)	**Area (Km^2)**	**Area (%)**
Forest	16.033	7.08
Habitation	10.902	4.81
Water bodies/ River	11.57	5.11
Mining Area	12.737	5.62
Crop Land/ Vegetation	89.22	39.37
Fallow Land	86.142	38.01
Total	**226.604**	**100.00**

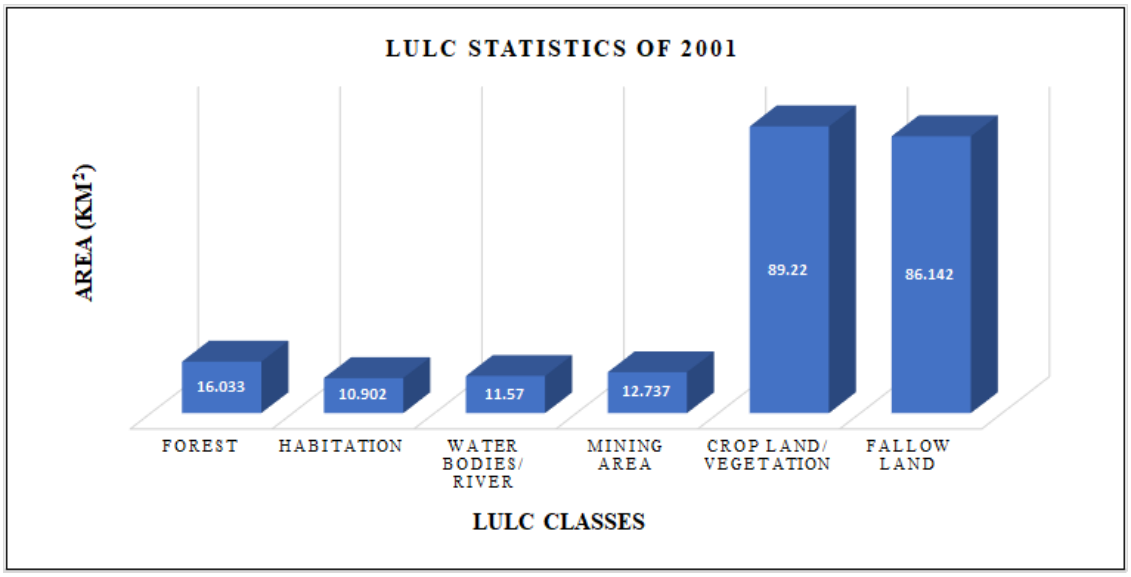

Fig.5.105 Graph shows LULC statistic for year 2001

5.3.2 Land use/ land cover analysis of year 2011

The LULC map for 2011 was created using a Landsat 5 TM satellite image, as seen in Fig.5.106. Based on the available LULC map for the year 2011, it has been observed that water bodies constituted the smallest proportion of land, occupying around 9.186 km^2, which corresponds to 4.05% of the total land area. Another important class was habitation, which covered approximately 13.304 km^2 (5.87%) of the total area. The Mining area encompasses around 12.737 km^2, accounting for 5.62% of the entire area being studied. Meanwhile, the Forest area covers 14.899 km^2, representing 6.57% of the total area being analysed. Furthermore, the two LULC classes, namely fallow land and agricultural land, constituted the most extensive spatial coverage of area. These two LULC classifications accounted for approximately 80.634 Km^2 (35.58%) and 87.445 Km^2 (38.59%) of the total area that was taken into account for LULC in 2011. The LULC classes statistics from LULC map of 2011 is shown in Table.5.41 and Fig.5.107 respectively.

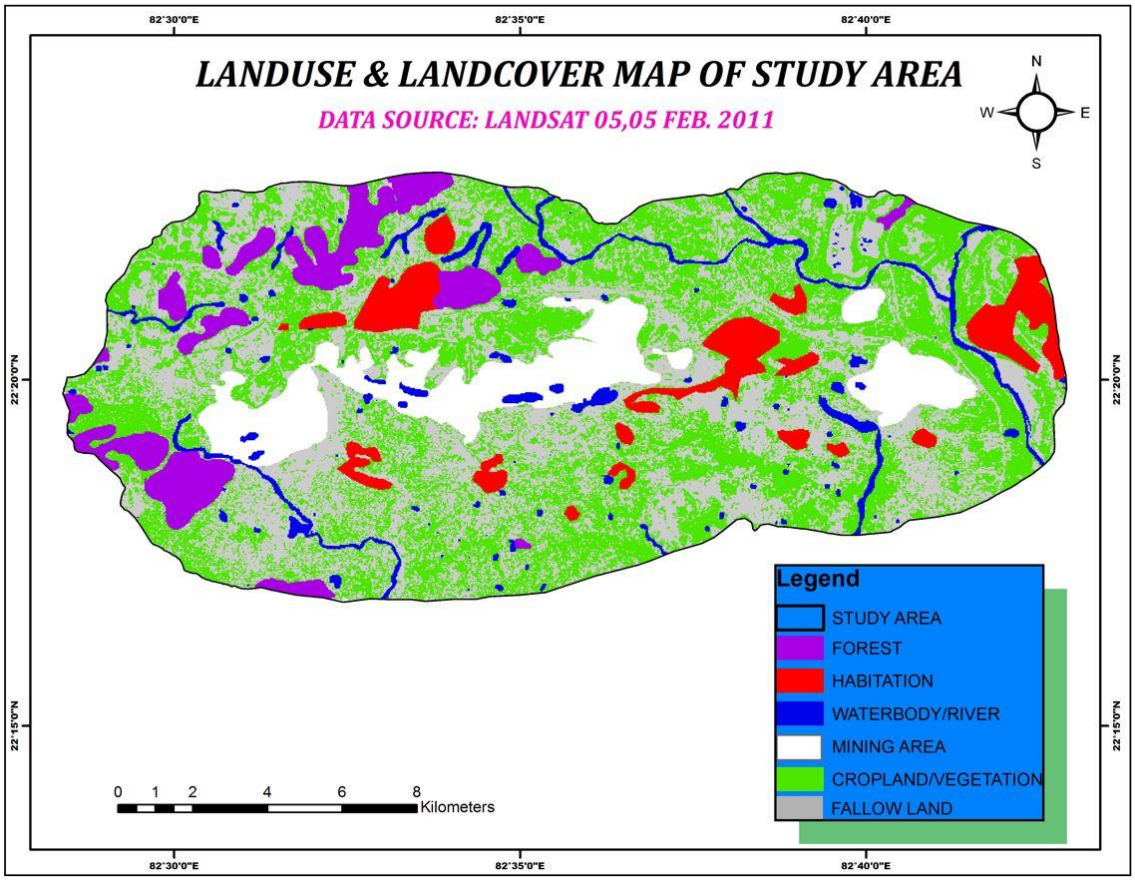

Fig.5.106 Land Use/Land Cover map for study area in 2011

Table.5.41 LULC statistics for year 2011

LULC Classes (2011)	**Area (Km^2)**	**Area (%)**
Forest	14.899	6.57
Habitation	13.304	5.87
Water bodies/ River	9.186	4.05
Mining Area	21.136	9.33
Crop Land/ Vegetation	87.445	38.59
Fallow Land	80.634	35.58
Total	**226.604**	**100.00**

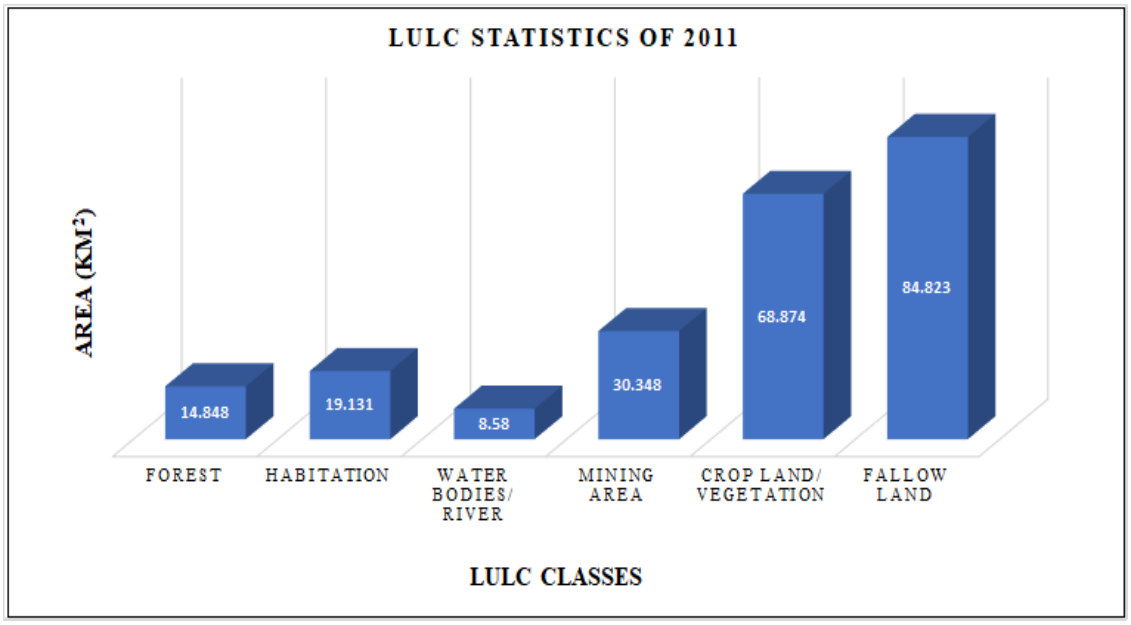

Fig.5.107 Graph shows LULC statistic for year 2011

5.3.3 Land use/ land cover analysis of year 2021

The LULC map for the year 2021 was generated by utilising a satellite image acquired by the Landsat 8 Operational Land Imager (OLI) and Thermal Infrared Sensor (TIRS) as seen in Fig.5.108. According to the LULC data for the year 2021, Water bodies seen in the analysed area predominantly comprised wetland areas, ponds, rivers, and their tributaries. These water bodies constituted a very small portion of the overall land area, accounting around 8.58 km^2, which corresponds to 3.79% of the entire area under study. Whereas, Forest area is having approximately 14.848 km^2 (6.55%) of the total area. Habitation is the third-smallest class in terms of area, with 19.131 Km^2 (8.44%) of the total area. The Mining area accounts for 30.348 Km^2 (13.39%) of the total area which follows the increasing trend continuously. Furthermore, it should be noted that in the year 2021, the predominant land cover types were Cropland and Fallow land, encompassing a considerable extent of around 68.874 km^2 (30.39%) and 84.823 km^2 (37.43%) respectively, out of the total area that was evaluated for LULC analysis. The classes statistics from LULC (2021) map is shown in Table.5.42 and Fig.5.109 respectively.

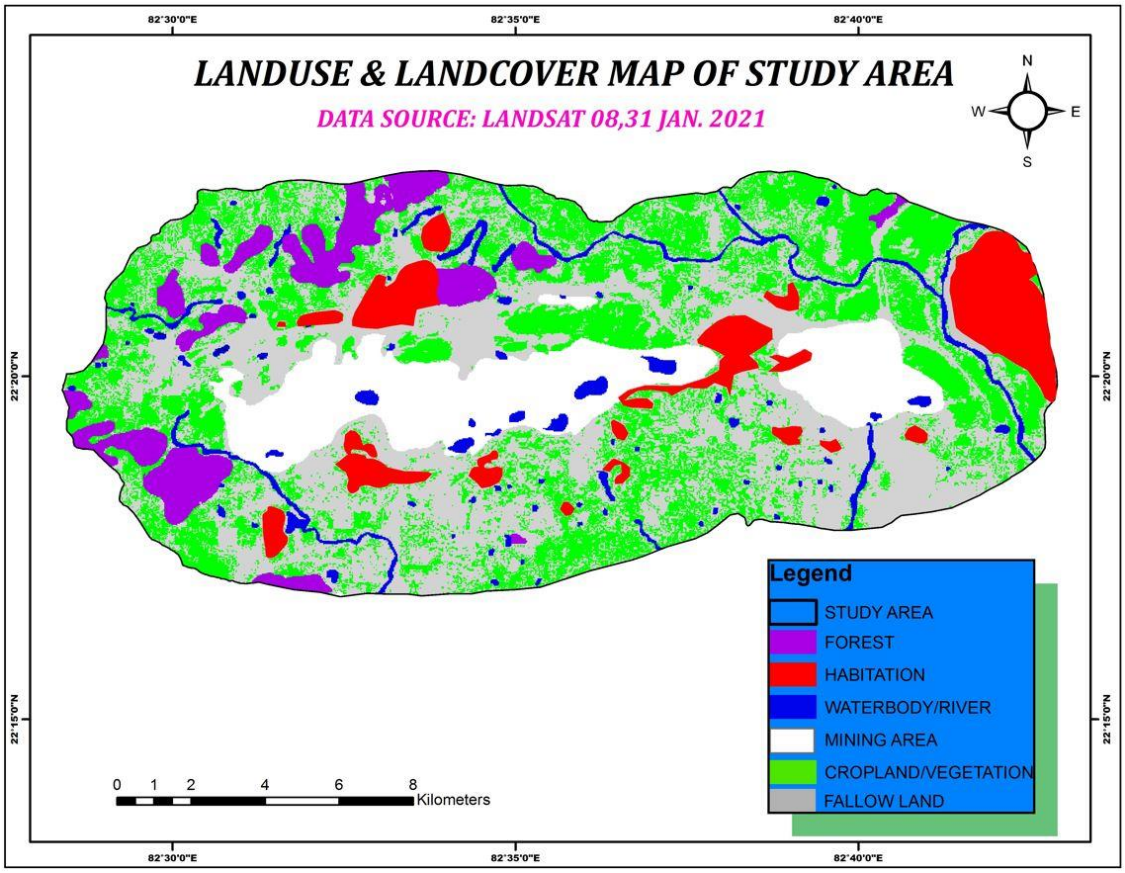

Fig.5.108 Land Use/Land Cover map for study area in 2021

Table.5.42 LULC statistics for year 2021

LULC Classes (2021)	**Area (Km^2)**	**Area (%)**
Forest	14.848	6.55
Habitation	19.131	8.44
Water bodies/ River	8.58	3.79
Mining Area	30.348	13.39
Crop Land/ Vegetation	68.874	30.39
Fallow Land	84.823	37.43
Total	**226.604**	**100.00**

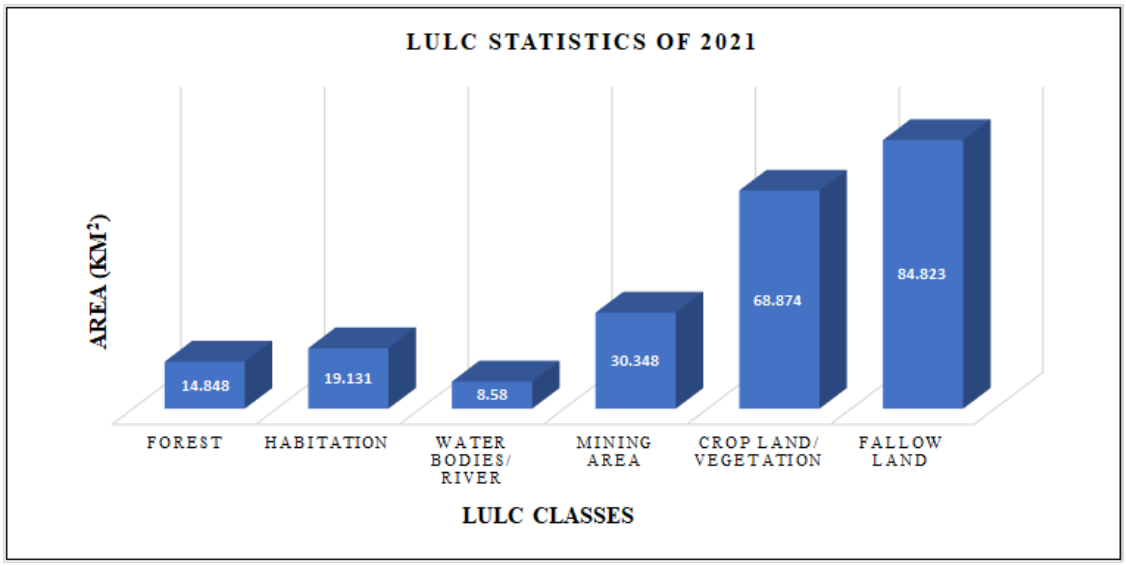

Fig.5.109 Graph shows LULC statistic for year 2021

5.3.4 Areal expansions of LULC and its comparison statistics

The unsupervised classification method has been used to create the LULC map for the year 2001, 2011, and 2021 in this study as shown in Fig.5.104, Fig.5.106 and Fig.5.108 respectively. The area statistics and area in percentage for each LULC class are given in Table. 5.43. The Cropland/vegetation and Fallow land were more dominant throughout the studied area, as per the results obtained from the LULC study.

Forest area is one of the important classes of LULC which shows a declining trend continuously from 2001 to 2021, which covers an area of 16.033 km^2 (7.08%) in 2001, 14.899 km^2 (6.57%) in 2011, and 14.848 km^2 (6.55%) in 2021 respectively. The decline in forest coverage can be attributed to the installation of thermal power plants and the expansion of mine blocks, given that a significant number of mine blocks are situated in close proximity to forested areas of the studied region. Similarly, the total area occupied by Habitation in the area was found to be 10.902 km^2 (4.81%) in 2001, 13.304 km^2 (5.87%) in 2011, and 19.131 km^2 (8.44%) in 2021, following continuously increasing trend in the selected tenure from 2001 to 2021. The increase in Habitation in this area can be attributed to the process of urbanisation and the ongoing growth of the population.

Moreover, Water bodies/Rivers are a third important LULC class that have been on the declining trend from 2001 to 2021, which covered an area of 11.570 km^2 (5.11%) in 2001, 9.186 km^2 (4.05%) in 2011, and 8.580 km^2 (3.79%) in 2021 respectively. The majority of the water body has been harmed by the expansion of mining blocks in the area. The mining area expanded steadily over the selected time period from 2001 to 2021, occupies an area of 12.737 km^2 (5.62%) in the year 2001, 21.136 km^2 (9.33%) in the year 2011, and 30.348 km^2 (13.39%) in the year 2021 respectively. The region has experienced a significant expansion of the mining field, with a growth rate of 138.27%. This expansion can be attributed to the expansion of opencast coal mines and overburden dumps.

Table.5.43 Arial statistics of each LULC class from 2001-2021

LULC Classes	**Area in 2001**		**Area in 2011**		**Area in 2021**	
	Area (Km^2)	Area (%)	Area (Km^2)	Area (%)	Area (Km^2)	Area (%)
Forest	16.033	7.08	14.899	6.57	14.848	6.55
Habitation	10.902	4.81	13.304	5.87	19.131	8.44
Water Bodies /River	11.57	5.11	9.186	4.05	8.58	3.79
Mining Area	12.737	5.62	21.136	9.33	30.348	13.39
Crop Land/ Vegetation	89.22	39.37	87.445	38.59	68.874	30.39
Fallow Land	86.142	38.01	80.634	35.58	84.823	37.43
Total Area (Km^2)	**226.604**		**226.604**		**226.604**	

The Crop land/vegetation area has declined with the area being 89.220 km^2 (39.37%) in 2001, 87.445 km^2 (38.59%) in 2011, and 68.874 km^2 (30.39%) in 2021 respectively. The area used for Crop land was seen to be continuous declining during the study period, primarily as a result of the expansion of the mining area. Moreover, it has been found that Fallow land shows mix trends over the given period of time which firstly decreased from an area of 86.142 Km^2 (38.01%) in 2001 to 80.634 Km^2 (35.58%) in 2011, and then increased from 80.634 Km^2 (35.58%) in 2011 to 84.823 Km^2 (37.43%) in 2021

respectively. The study region was largely characterised by fallow land, which encompassed a significant portion of the total area, equal to 37.43% as shown in Fig.5.110.

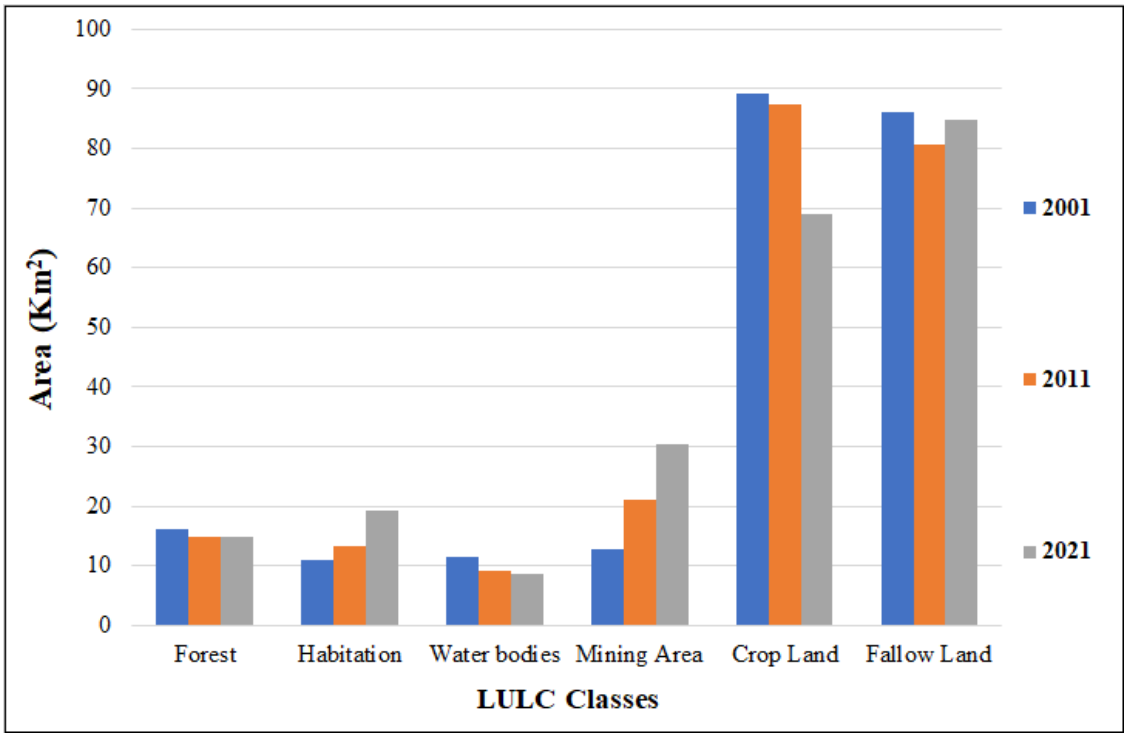

Fig.5.110 Bar chart showing LULC area distribution of the study region

5.3.5 LULC Change analysis

The prepared LULC shows major changes from 2001 to 2011 and from 2011 to 2021, including net changes, change patterns, percent changes, and rate of change using Landsat 4-5 TM of 2001, 2011 and Landsat 8-9 OLI/TIRS data of year 2021 respectively. Therefore, it has been observed from three distinct LULC map that only two LULC classes shows a positive net change, while all other four classes showed a negative net change. The LULC class such as Mining area, shows the highest net positive change of 17.61 km^2 followed by the Habitation class of 8.23 km^2 from 2001 to 2021. Furthermore, Crop land has the highest net negative changes of -20.35 km^2 while next by water bodies of -2.33 km^2 from 2001 to 2021. The remaining classes such as Fallow land and Forest area have had the least net negative changes of -1.32 km^2 and -1.19 km^2

respectively as illustrated in Table.5.44. The bar chart showing LULC classes of the study region from 2001 to 2021 as shown in Fig.5.111.

Table.5.44 Change in arial extend (km^2) of each LULC classes

LULC Classes (Km^2)	Net change (2001-2011)	Net change (2011-2021)	Net change (2001-2021)
Forest	-1.13	-0.05	-1.19
Habitation	2.40	5.83	8.23
Water Bodies /River	-2.38	-0.61	-2.99
Mining Area	8.40	9.21	17.61
Crop Land/ Vegetation	-1.78	-18.57	-20.35
Fallow Land	-5.51	4.19	-1.32

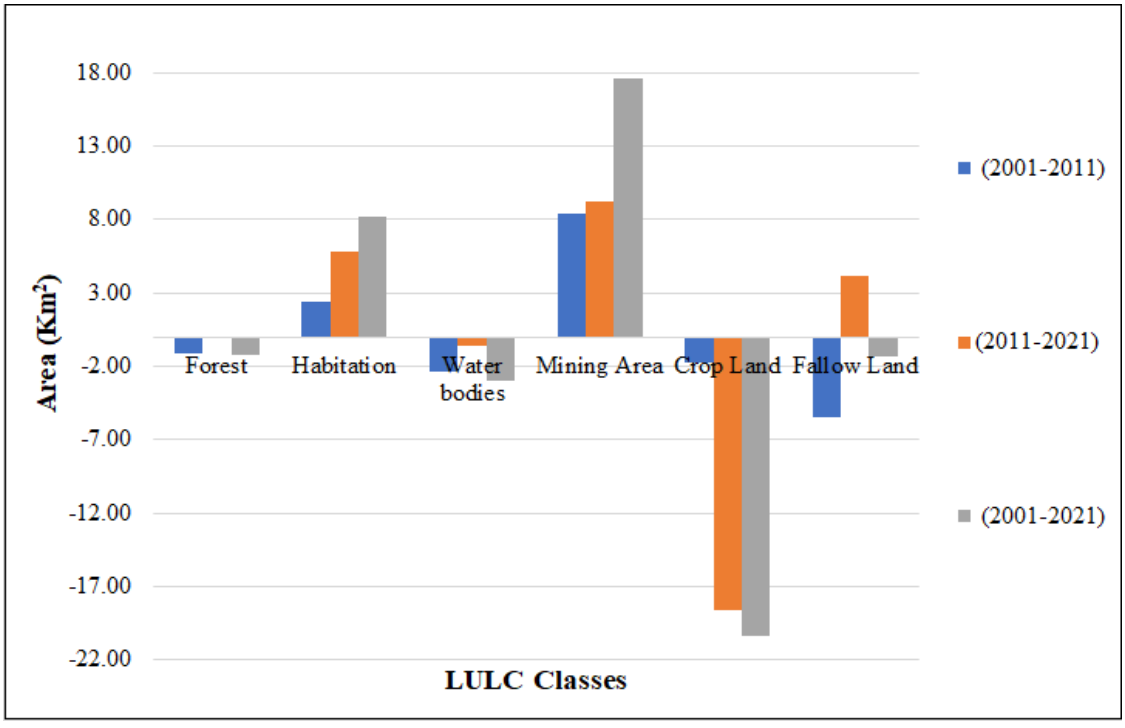

Fig.5.111 Bar chart showing LULC classes of the study region from 2001 to 2021

5.3.5.1 Percentage change calculation

The formula depicted in equation 4.18, as introduced in the preceding chapter, is suitable for calculating the percentage change in Land use and Land cover. The Mining area and

Habitation have the highest net positive changes of 138.27% and 75.48% between 2001 and 2021, whereas the Water bodies and Crop land area have observed the highest negative changes of -25.84% and -22.80% respectively. The maximum increased in Mining area is a direct consequence of decline in the total area of Crop land, and Water bodies as listed in Table.5.45. The Fallow land also shows the negative change of -1.53% from 2001 to 2021. This is induced by the expansion of coal mining operations and the rise in habitations in the area under study.

Table.5.45 Percentage change in ariel extend of each LULC class

LULC Classes	**Change in % (2001-2011)**	**Change in % (2011-2021)**	**Change in % (2001-2021)**
Forest	-7.07	-0.34	-7.39
Habitation	22.03	43.80	75.48
Water Bodies /River	-20.61	-6.60	-25.84
Mining Area	65.94	43.58	138.27
Crop Land/ Vegetation	-1.99	-21.24	-22.80
Fallow Land	-6.39	5.20	-1.53

5.3.5.2 Rate of LULC change

The derived formula (equation 4.19) is presented in previous chapter and utilised to compute the rate of change within land use/cover. The rate of LULC change was computed for three session such as years 2001-2011, 2011-2021 and 2001-2021 as listed in Table.5.46. It was observed that the Forest area shows decreasing rate of change of -0.06 km^2/year during 2001-2021 session. The rate of change in Habitation area is increasing continuously, with a net rate of change of 0.41 km^2/year during the study period while it is highest with 0.58 km^2/year during 2011-2021 session. The net negative rate of change of water bodies was of -0.15 km^2/year for study tenure while it was highest with -0.24 km^2/year during 2001-2011 session.

The rate of change in Mining area class has been observed to be expanding continually, with a net change rate of 0.88 km^2/year throughout the study period as given in Table.5.46. However, it has been assessed with maximum change rate of 0.94 km^2/year during 2011-2021 and minimum change rate of 0.84 km^2/year during 2001-2011 session respectively. Moreover, the net negative change rate of crop land is of -1.02 km^2/year for the study period while it is more with -1.86 km^2/year during 2011-2021 session. The net negative rate of change of Fallow land is of -0.07 km^2/year for 2001-2021 while it has positive change rate of 0.42 km^2/year during 2011-2021 session. It means that deforestation was quite low in 2011-2021 than 2001-2011 session. As a result, it has been observed that the expansion of mining activities through time has a major impact on many natural resources, including water bodies, agricultural land, forested areas, and fallow land.

Table.5.46 Rate of change in each LULC class

LULC Classes	**Rate of change (2001-2011)**	**Rate of change (2011-2021)**	**Rate of change (2001-2021)**
Forest	-0.11	-0.01	-0.06
Habitation	0.24	0.58	0.41
Water Bodies /River	-0.24	-0.06	-0.15
Mining Area	0.84	0.92	0.88
Crop Land/ Vegetation	-0.18	-1.86	-1.02
Fallow Land	-0.55	0.42	-0.07

5.3.5.3 Accuracy Assessment

The accuracy of the created map for the years 2001, 2011, and 2021 has been evaluated using an error matrix. The accuracy assessment of all land use and land cover (LULC) maps were conducted using the stratified random sample approach. The assessment of accuracy for a created LULC map can be conducted using several key ways. These

include overall accuracy (as defined by equation 4.20), user accuracy (equation 4.21), producer accuracy (equation 4.22), and Kappa coefficient accuracy (equation 4.23). These approaches provide valuable insights into the validity and accuracy of the LULC map. The accuracy assessment is one of the most significant steps in the classification process.

The primary objective of accuracy assessment is to conduct a quantitative evaluation of the extent to which pixels have been correctly assigned to their respective land cover class. Furthermore, the use of high-resolution Landsat imagery, Google Earth, and Google maps have been employed as the principal means of reference for ensuring correctness in the process of pixel selection during the assessment. The classified image of the study region for the years 2001, 2011, and 2021 had 210, 229, and 217 points (locations) accordingly.

The accuracy assessment cell array reference column has been filled with the best guess of each reference point. The rows of the confusion matrix depict the assigned classes of the pixels in images, whereas the columns represent the classes of pixels in the validation set (ground truth) correspond. The correctly classified pixels are shown on the diagonal in the table. The utilisation of a stratified random sample approach has been employed to conduct accuracy assessments for all LULC maps.

Accuracy assessment was also done in parallel to user and producer accuracy calculations. According to the computed data, the generated Land Use and Land Cover (LULC) map exhibits overall accuracy values of 90.41%, 92.14%, and 94.50% for the years 2001, 2011, and 2021, respectively. Additionally, the Kappa coefficient accuracy values for the same years are determined to be 88.19%, 90.53%, and 92.50% as given in Table.5.47, Table.5.48 and Table.5.49 respectively.

Table.5.47 Accuracy assessment LULC classes of the year 2001

LULC Classes	Fallow Land	Habitation	Crop Land	Forest Area	Mining Area	Water Bodies	Total (User)	User accuracy	Koppa Coeff.
Fallow Land	48	1	2	0	2	0	53	90.6%	88.2%
Habitation	1	14	0	1	1	1	18	77.8%	
Crop Land	1	0	50	2	1	0	54	92.6%	
Forest Area	0	1	1	27	0	0	29	93.1%	
Mining Area	1	0	0	0	31	2	34	91.2%	
Water Bodies	0	0	1	0	1	20	22	90.9%	
Total (Producer)	51	16	54	30	36	23	210		
Producer accuracy	94.1%	87.5%	92.5 %	90%	86.1%	86.9%			
Overall accuracy	90.5%								

Table.5.48 Accuracy assessment LULC classes of the year 2011

LULC Classes	Fallow Land	Habitation	Crop Land	Forest Area	Mining Area	Water Bodies	Total (User)	User accuracy	Koppa Coeff.
Fallow Land	38	0	1	0	0	0	39	97.4%	90.5%
Habitation	1	33	0	1	1	1	37	89.2%	
Crop Land	1	0	38	2	0	0	41	92.7%	
Forest Area	0	1	2	33	1	0	37	89.2%	
Mining Area	1	1	0	1	42	2	47	89.4%	
Water Bodies	0	0	0	0	1	27	28	96.4%	
Total (Producer)	41	35	41	37	45	30	229		
Producer accuracy	92.7%	94.3%	92.7 %	89.2%	93.3%	90%			
Overall accuracy	92.1%								

Table.5.49 Accuracy assessment LULC classes of the year 2021

LULC Classes	Fallow Land	Habitation	Crop Land	Forest Area	Mining Area	Water Bodies	Total (User)	User accuracy	Koppa Coeff.
Fallow Land	37	0	1	0	0	0	38	97.3%	93.3%
Habitation	0	31	0	0	1	0	32	96.9%	
Crop Land	1	1	36	1	0	0	39	92.3%	
Forest Area	0	0	1	33	0	0	34	97.1%	
Mining Area	1	1	1	1	41	1	46	89.1%	
Water Bodies	0	0	0	0	1	27	28	96.4%	
Total (Producer)	39	33	39	35	43	28	217		
Producer accuracy	94.8%	93.9%	92.3 %	94.3%	95.4%	96.4%			
Overall accuracy	94.5%								

5.3.6 Post LULC Change Estimation

The present study commenced by conducting an analysis of land use and land cover (LULC) map categorization for three distinct time periods. Subsequently, the process of image overlaying was performed using ERDAS software in order to eliminate spatial changes in LULC between the years 2001 and 2021.

The change detection involves distinguishing an entity at different periods to identify dissimilarities. This technique entails the comprehensive estimation of temporal impacts through the use of datasets. The analysis of changes in LULC over a twenty-year period is made possible by the change detection technique. It is a useful tool for monitoring environmental changes, such as damage assessment, LULC analysis, changing agricultural and vegetation, crop stress detection, disaster monitoring, and evaluation of deforestation (Adeniyi 1980). However, there are two approaches to computing change detection, which are referred as pre classification change detection and post classification change detection. Here, the post classification change detection method has been used. This approach involves the comparison of distinct classified images obtained at distinct time intervals. By employing this method, subsequent analysis successfully facilitated the characterization of changes within the selected area, depending on "From-to" statistical data derived from six distinct classes over two distinct maps representing different years.

A change detection map was also created for the area by making use of the ARDAS software. The purpose of this map was to know the significant changes and land transformations that occurred in the area in last two decade (2001- 2021) as shown in Fig.5.112. It has been observed that a majority of the vegetation was observed in years 2001 and 2021, with just a small fraction being observed exclusively in the year 2011. Similarly, major fractions of other classes (Habitations, Crop land, Fallow land, water bodies, vegetations) were covered by the mining area. The small portion of the

Habitations were being found in years 2001, with a major portion of it distributed in the year of 2011 and 2021. Moreover, the majority of water bodies was observed in years 2001 and 2021, with a small proportion being identified in the year 2011. A small region of mining area was happened in the year of 2001 while large area of it covered by years 2011 and 2021 demonstrating that mining area was seen to be steadily expanded in last two decade.

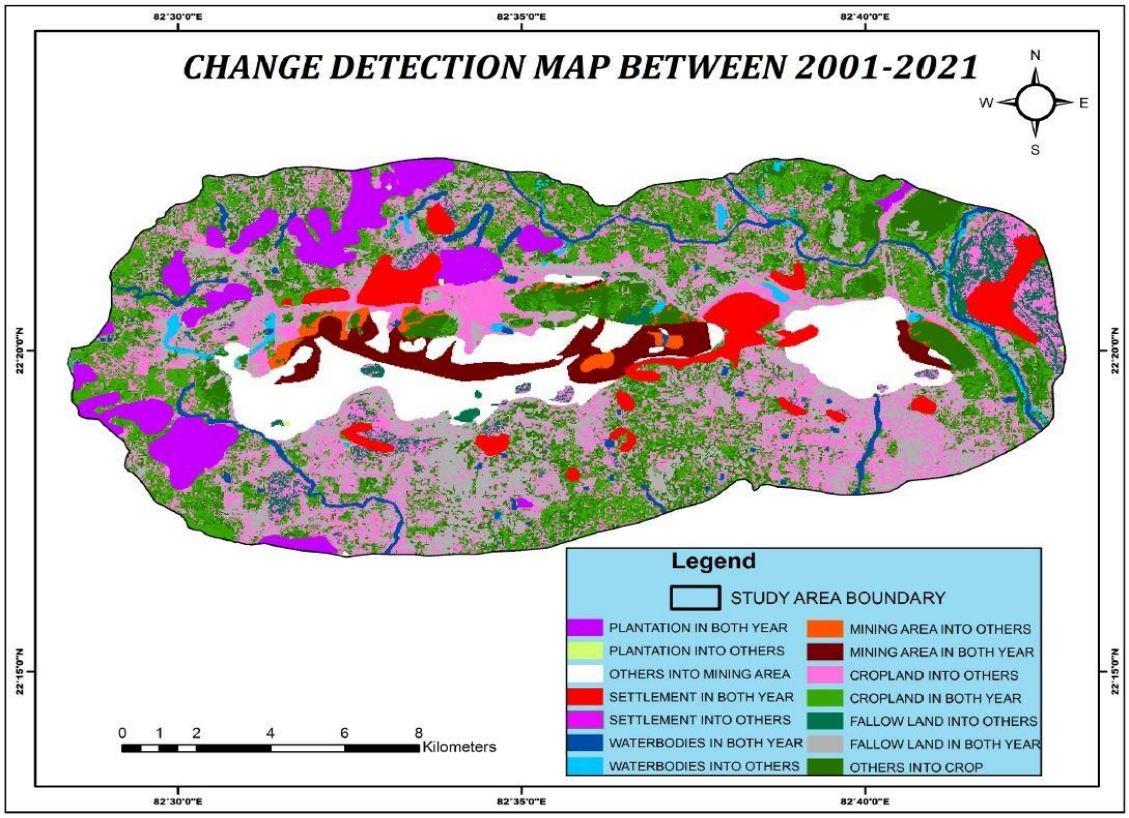

Fig.5.112 Change detection map of study area from 2001 to 2021

The remaining LULC classes like Crop land and Fallow land, encompassed a major portion of the total area, accounting for about 68% of the total land in the area. The major portion of Cropland was seen in the initial year 2001 however, a relatively smaller extent was observed in years 2011 and 2021. Similarly, Fallow land covered major portion of the area in the year 2001 while comparatively less were covered in years 2011 and 2021. Moreover, other classes were covered by crop land based on change detection map of LULC as shown in Fig.5.112.

5.4 Estimation of Land Surface Temperature (LST)

The rising temperatures are a pressing concern in many parts of the world. The surface temperature is a broad term that refers to the overall temperature of all the elements that comprise the present surface. The maintenance of land surface temperature (LST) is influenced by various factors, including incoming solar radiation, longwave radiation, outgoing terrestrial infrared radiation, sensible heat flow, latent heat flux, and ground flux (Li et al. 2013). The energy balance at the earth's surface is significantly influenced by this essential factor.

The surface temperature plays a crucial role in the physical processes taking place on both regional and global scales on the Earth's surface, as well as in the interaction between the Earth and its atmosphere (Hu et al. 2015). Thermal infrared remote sensing images derived from satellite observations offer a rapid and convenient means of acquiring extensive surface temperature data. Moreover, these data are regularly updated at a relatively affordable expense. Consequently, surface temperature extraction heavily relies on the utilisation of thermal infrared remote sensing data (Zheng and Zeng, 2011).

The mono-window approach has been used as described by (Qin et al. 2001 and Guha et al. 2017, 2018, 2019), to extract land surface temperature from multi-temporal Landsat satellite data. In order to calculate the Land Surface Temperature using the mono-window approach, three essential characteristics must be considered: ground emissivity, atmospheric transmittance, and effective mean atmospheric temperature. The methods for estimating land surface temperature through the utilisation of mathematical equations are outlined in the preceding chapter. The completion of all Land Surface Temperature phases was achieved using the Raster calculator tool within the Arc toolbox of the ArcGIS 10.8 software. The calculation of Land Surface Temperature has been

performed using equation (4.23) for Landsat 5 and 7 data, and equation (4.29) for Landsat 8 OLI data, as described in the preceding chapter.

5.4.1 Impact of coal mining activities on surface temperatures

The extraction of coal generates a significant amount of heat. Consequently, the combination of the corresponding industries characterised by high energy consumption and high heat generation has led to an increase in localised heating inside the urban area (Hu, Zhao and Dong, 2010). The continuous economic expansion of mining regions has resulted in a simultaneous rise in population density and heat generation from urban infrastructure. The opencast coal mines, dumps, and industrial regions all produce bigger contributions to regional warming, depending on certain assessments of different disruptions somewhere in the interior of mining fields (Xie et al. 2011; Liu, 2016). Other studies have shown similar findings, noting that bigger land areas designated for building purposes exhibit uniform development, elevated land surface temperatures, and more pronounced heat island effects (Yu, 2006; Fu, 2001). The rapid increase in temperature is observed when coal and coal gangue are exposed, however, it is significant that piles of coal gangue hills exhibit a higher vulnerability to heat and subsequent spontaneous combustion (Hao, 2011). Consequently, an abundance of factors contributes to the elevated temperatures experienced throughout mining sites.

5.4.2 Estimated LST from the year 2001 to 2021

Here, LST for Landsat 5 TM, Landsat 7 ETM+ data were derived by using calculation of spectral radiance based on its mathematical expression. In contrast, LST for Landsat 8 OLI/TIRS data was also calculated by converting radiance to satellite brightness temperature and spectral emissivity (equation 4.29). The estimated LST for April in the year 2001, 2006, 2011, 2016 and 2021 images were shown in Fig.5.113 to Fig.5.117 respectively. The LST map was generated for the last 21 years and makes use of satellite

data in order to illustrate the variance in surface temperature. The temporal satellite data were acquired and utilised for the calculation of Land Surface Temperature (LST). A comprehensive overview of the dataset, including its characteristics, is given in Table.4.5 of the preceding chapter. The Land surface temperature for the specified year, together with its corresponding mean and standard deviation values, were presented in Table.5.50. All of these observations were conducted utilising temporal datasets obtained from satellites.

The utilisation of image processing techniques on the thermal bands of the five acquired images proved to be helpful in identifying the spatial distribution and fluctuations in surface temperature inside the designated area. The minimum, maximum, and average LST values for each of the five years under consideration are likewise plotted in Fig.5.118. According to the statistics provided, there has been a continuous increase in surface temperature from the year 2001 to 2021.

The land surface temperatures for the years 2001, 2006, 2011, 2016, and 2021, as depicted in the imagery, exhibit distinct values for the minimum, mean, and maximum temperatures. Specifically, the minimum, mean, and maximum land surface temperatures for these years are as follows: 18.83 °C, 28.40 °C, 41.46 °C for 2001; 19.73 °C, 29.62 °C, 42.59 °C for 2006; 21.06 °C, 29.98 °C, 43.33 °C for 2011; 26.39 °C, 37.06 °C, 45.41 °C for 2016; and 27.99 °C, 38.27 °C, 48.13 °C for 2021 as given in Table.5.50. The observed increase in surface temperature from one period to another may potentially be attributed to the land use and land cover (LULC) changes in the area. The high spatial resolution of the imagery facilitated the clear differentiation between vegetation, water bodies, and impermeable surfaces. The land surface temperature exhibited an increase in areas characterised by impermeable surfaces throughout the course of twenty years while seeing a decline in areas dominated by vegetation.

According to the analysis of all five LST maps, it has been observed that the north, north-west, and north-east parts of the region exhibited comparatively lower temperatures. This can be attributed to the substantial coverage of cropland and vegetation in these areas. Conversely, the central, south, and eastern parts of the region had higher surface temperatures. This can be attributed to the existence of mines and barren land in these regions. The observed occurrence could potentially be attributed to the varying land cover types seen within the region. The regions with high land surface temperature exhibit impermeable surfaces, such as mines and bare land, which hinder the infiltration of water. Conversely, regions with low LST are characterised by the presence of vegetated and permeable land uses. Therefore, LST images from multiple years are compared, they show considerable changes in the spatial distribution of surface temperature throughout the area.

The data collected in the years 2001, 2006, 2011, 2016, and 2021 consistently indicate elevated surface temperatures in regions where anthropogenic activities, such as coal mining and thermal power plant operations, are prominent. Consequently, there was an increase in the mean land surface temperature of the entire region from 28.40°C to 38.27°C (9.87°C) throughout the period covering from 2001 to 2021. Moreover, it has been observed from this analyses that the KCF region has been characterised by open barren land and residential area. The year wise comparative analysis of Land Surface Temperature has been carried out as given below.

Table.5.50 Spatiotemporal variation of LST (°C) distribution (2001-2021)

Date of acquisition	LST (minimum)	LST (maximum)	LST (mean)	LST (standard deviation)
22 April 2001	18.83	41.46	28.40	1.92
28 April 2006	19.73	42.59	29.62	2.09
26 April 2011	21.06	43.33	29.98	1.98
23 April 2016	26.39	45.41	37.06	2.14
05 April 2021	27.99	48.13	38.27	2.25

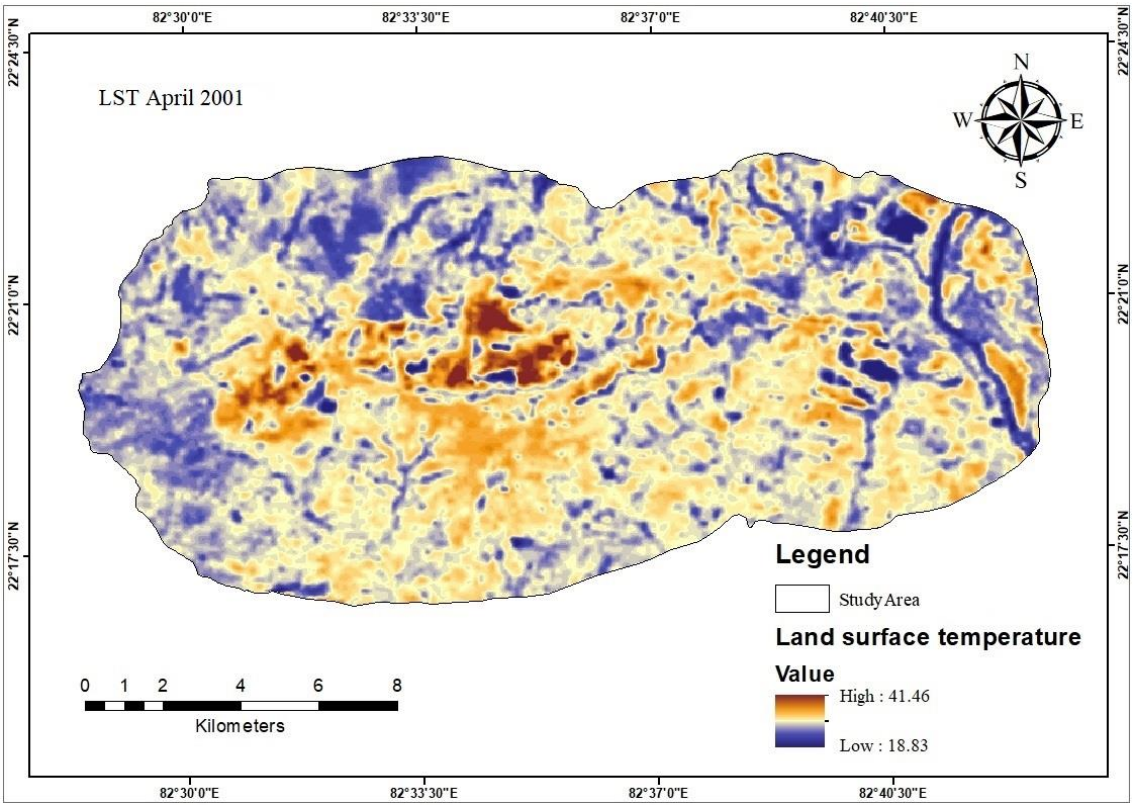

Fig.5.113 LST map for the year 2001

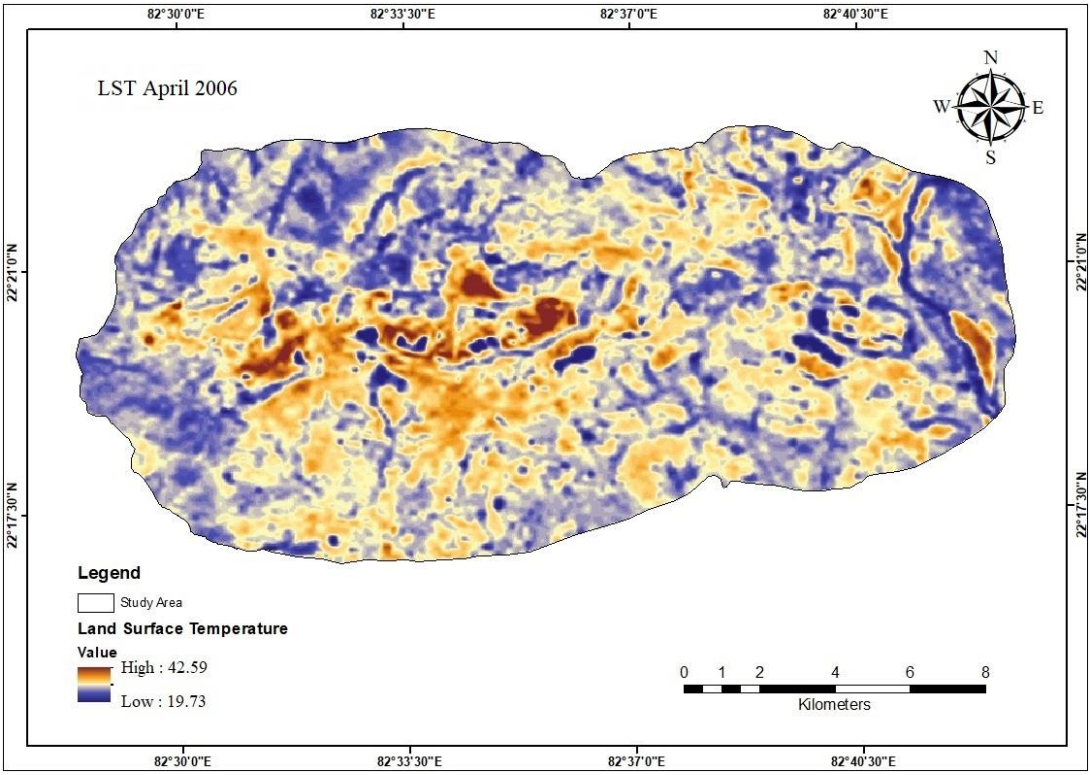

Fig.5.114 LST map for the year 2006

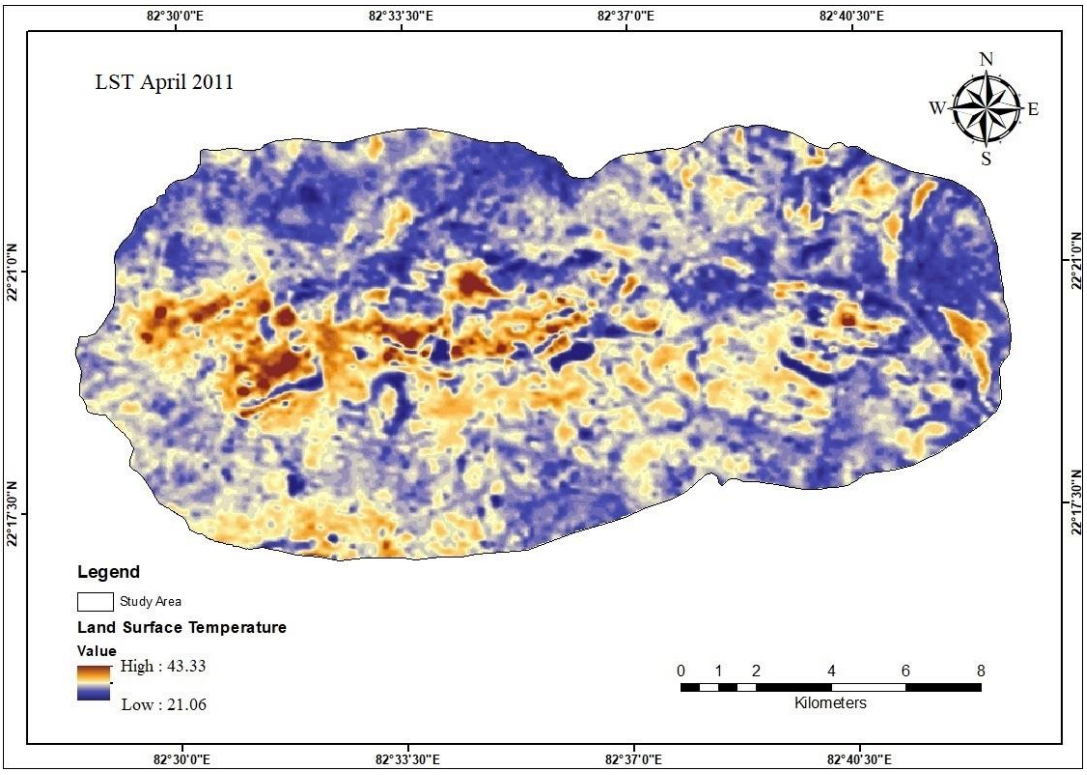

Fig.5.115 LST map for the year 2011

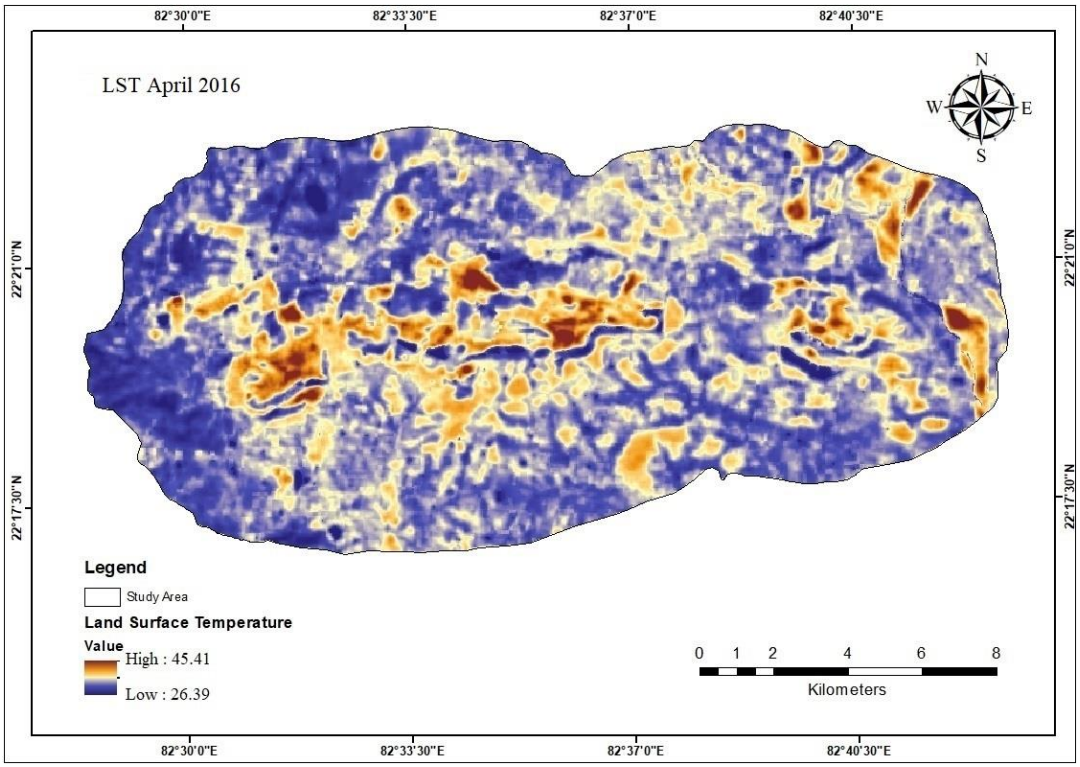

Fig.5.116 LST map for the year 2016

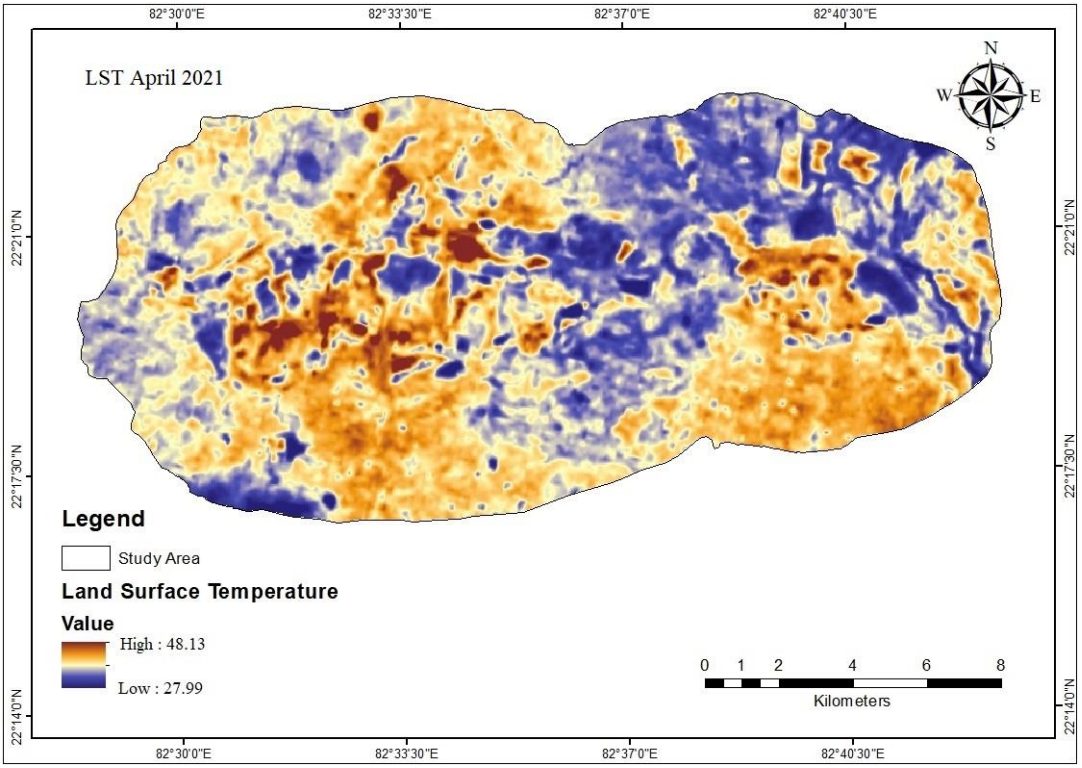

Fig.5.117 LST map for the year 2021

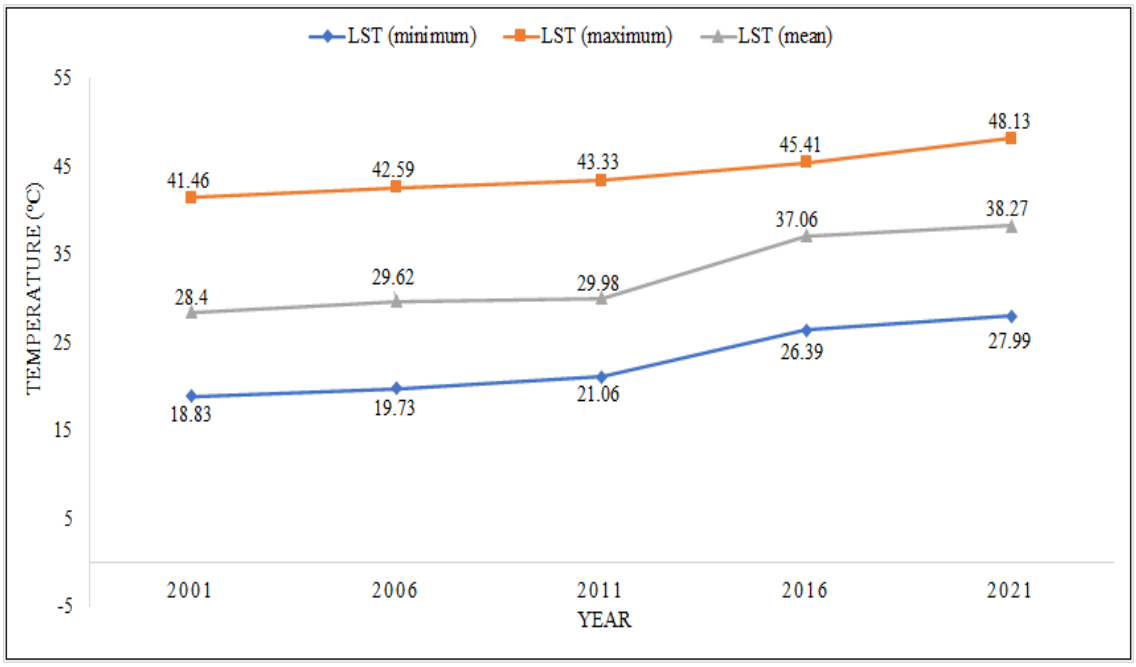

Fig.5.118 Graphical plot of the min, max, mean values of LST from 2001 to 2021

5.4.3 Normalized Difference Vegetation Index (NDVI) Estimation

The Normalized Difference Vegetation Index is a vegetation proportion index. It is a term used in satellite imagery to emphasize open water features, allowing a body of water to "stand out" against the land and vegetation. It quantifies the disparity between the near-infrared region of the electromagnetic spectrum, which is highly reflected by green vegetation, and the red component of the spectrum, which is absorbed by vegetation. The Normalized Difference Vegetation Index (NDVI) is a widely used technique that utilises the reflectance of red and near-infrared wavelengths to estimate the extent of green vegetation present above the earth's surface.

According to the principle of NDVI, plants that are considered "green" have the ability to absorb light within the red wavelength range (640–670 nm) as a result of the presence of chlorophyll pigments. Conversely, these plants scatter light throughout the near-infrared wavelength range (700–1100 nm) due to the internal structure of the leaf. Meanwhile, bare soil has less reflection in the near-infrared spectrum while displaying higher reflectivity in the red spectrum. The NDVI scale exhibits a range from -1 to +1,

demonstrating a linear correlation with vegetative factors such as biomass or Leaf Area Index (LAI) (Mróz & Sobieraj, 2004).

This index was widely used as an indication of green vegetation by numerous scholars worldwide. The calculation of the NDVI for Landsat 5 and 7 involved the utilisation of bands 3 and 4. However, for Landsat 8, the NDVI calculation was performed using bands 4 and 5. The NDVI value ranges from -1 to +1 respectively. The -1 represents a non-vegetated area, whereas a +1 represents a vegetated area. The calculation of NDVI has been performed using equation (4.30) for Landsat 5 and 7 data, and equation (4.31) for Landsat 8 OLI data, as described in the preceding chapter. The NDVI was computed using the Raster calculator tool within the Arc toolbox of the ArcGIS 10.8 software.

All of the NDVI maps that have been made for the years 2001, 2006, 2011, 2016, and 2021 are shown in Fig.5.119 to Fig.5.123. The NDVI value with its mean value for each selected year calculated as given in Table.5.51. The presence of bare soil or artificial surfaces is indicated by low NDVI values, while the presence of dense vegetation is represented by high NDVI values (Barbieri et al. 2018). An Increased vegetation cover was observed in the years 2001 and 2006, with maximum NDVI values of 0.55 and 0.51 correspondingly. Furthermore, there was a notable decline in vegetation intensity between 2001 and 2006, with a fall from 0.55 in 2001 to 0.51 in 2006. Subsequently, there was an increase in vegetation intensity from 2006 to 2011, with a rise from 0.51 in 2006 to 0.54 in 2011. However, this positive trend was reversed, and vegetation intensity experienced a decline from 2011 to 2021, with values of 0.54 in 2011, 0.49 in 2016, and 0.45 in 2021.

According to the analysis of all five NDVI maps, it has been observed that the northern and northwestern regions of the area exhibited higher NDVI values. This can be attributed to the substantial presence of forests and vegetation in these areas. However, the centre and eastern sections of the study region had the lower NDVI values. This can be attributed

to the prevalence of mining activities and the presence of barren land in these areas. The analysis of NDVI maps from different times indicates that the study region has experienced a decline in vegetation cover and a corresponding increase in non-vegetated areas over the course of the past 20 years. High NDVI values were expected to be found in forest areas, whereas low NDVI values were found in mining as well as urban areas.

Furthermore, for the whole duration of the study period, extensive mining activity was seen in the area, encompassing the establishment of new mining operations as well as the expansion of existing ones. The mining activity were expanded more considerably between 2016 and 2021 as a result of increased demand. The rate of conversion of vegetated lands to open-pit mines were increased throughout this time period. The aforementioned theories might account for the observed decline in NDVI levels for the period ranging from 2001 to 2021. The region continues to experience a notable decline in vegetation coverage, resulting in elevated surface temperatures and contributing to the occurrence of urban heat islands.

This is essential in context with the ongoing expansion in large-scale mining activities, which are converting considerable areas of vegetated lands into mining sites. These extensive mining operations may potentially function as rocky deserts, hence increasing land surface temperature (LST) within the designated area. The year wise comparative analysis of NDVI has been carried out as given below.

Table.5.51 Spatiotemporal variation of NDVI distribution in area from 2001 to 2021

Date of acquisition	NDVI (minimum)	NDVI (maximum)	NDVI (mean)	NDVI (standard deviation)
22 April 2001	-0.51	0.55	0.09	0.07
28 April 2006	-0.53	0.51	0.07	0.08
26 April 2011	-0.50	0.54	0.06	0.09
23 April 2016	-0.17	0.49	0.04	0.05
05 April 2021	-0.18	0.45	0.03	0.06

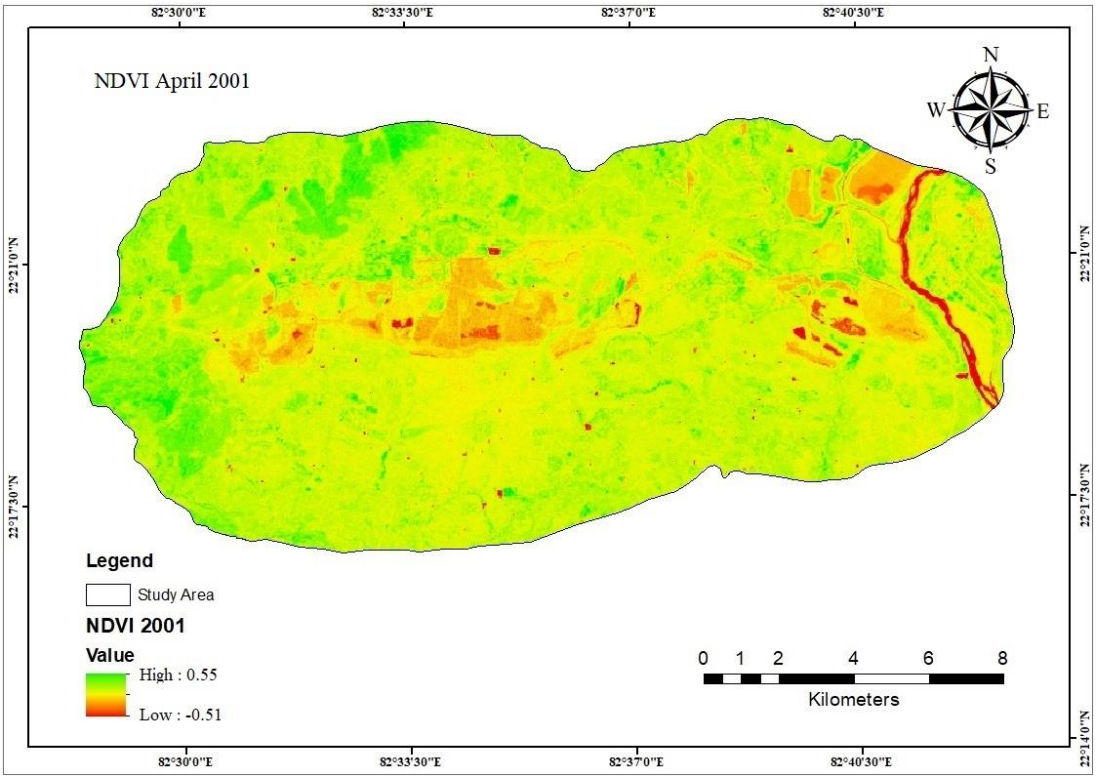

Fig.5.119 NDVI map for the year 2001

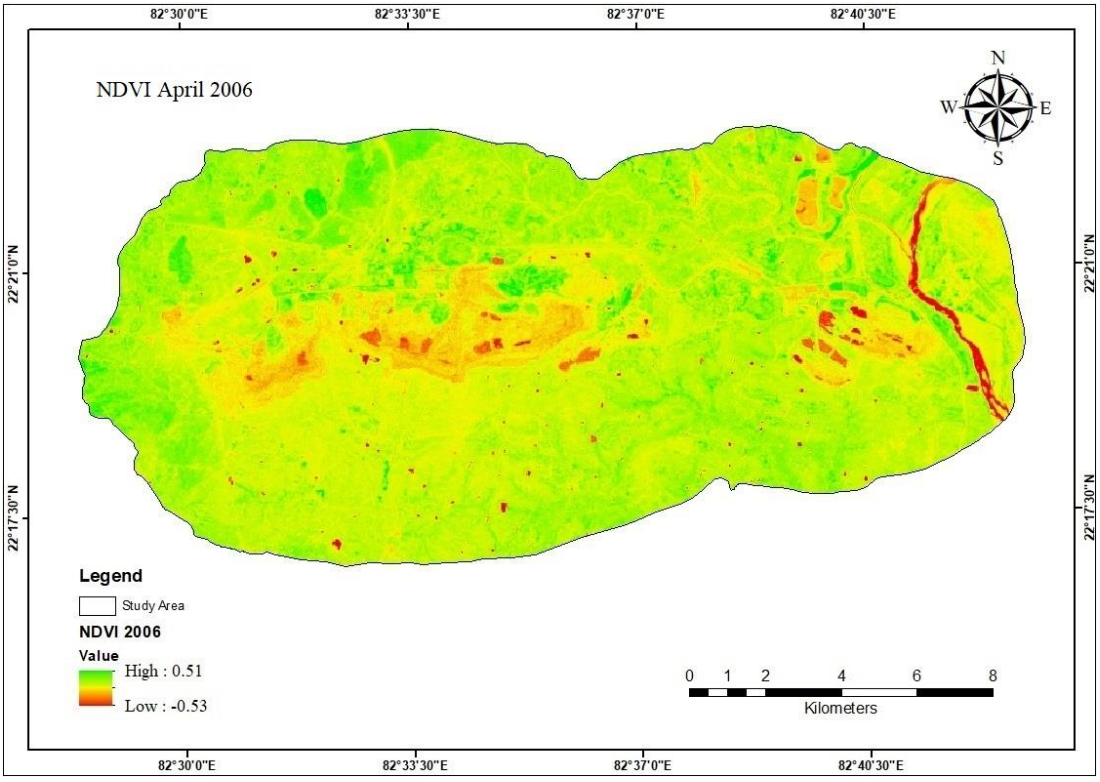

Fig.5.120 NDVI map for the year 2006

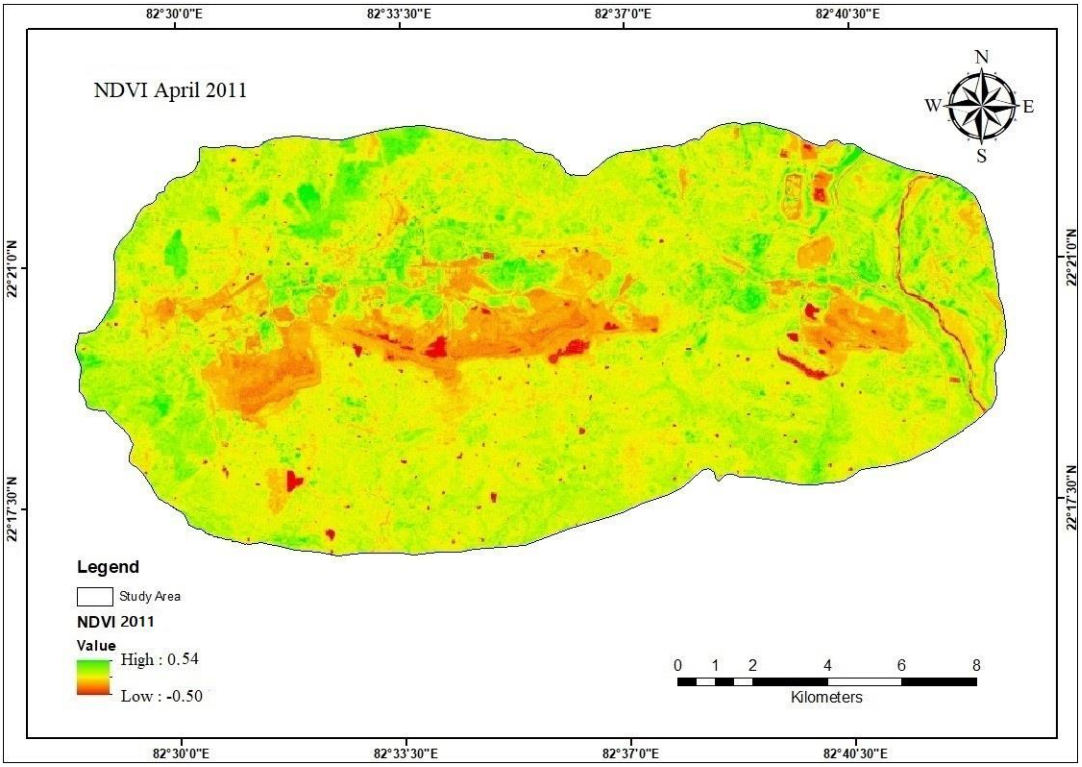

Fig.5.121 NDVI map for the year 2011

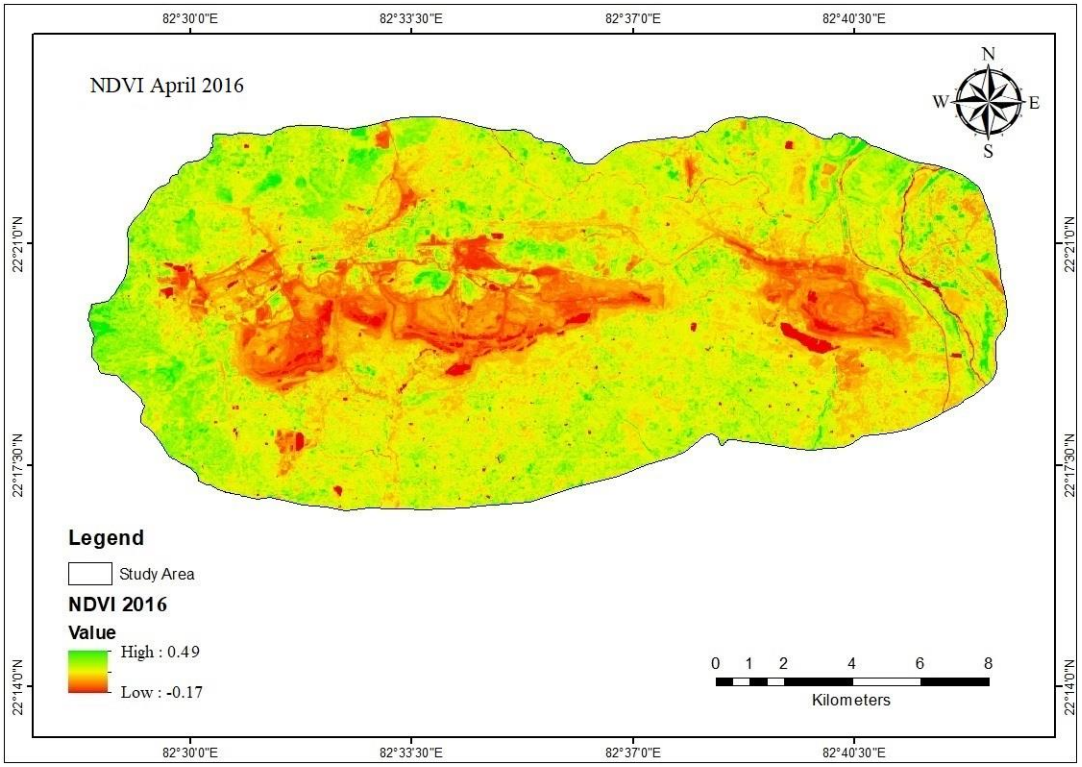

Fig.5.122 NDVI map for the year 2016

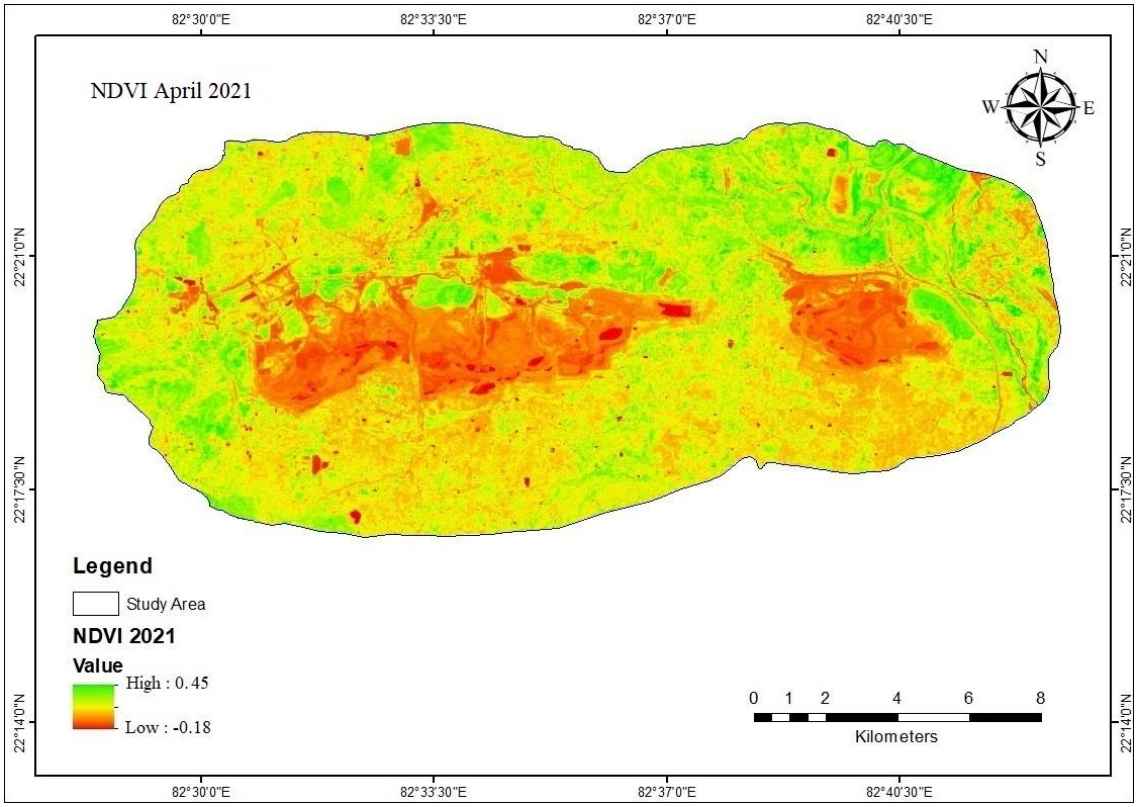

Fig.5.123 NDVI map for the year 2021

5.4.4 Correlation analysis of LST and NDVI

The LST and NDVI have the opposite tendency. The changes in NDVI have the potential to induce modifications in LST because of the high sensitivity of NDVI to changes. Although not clearly consistent, the relationship between NDVI and LST changed from season to season (Malik et al. 2019). The literature also suggests that NDVI and LST are negatively correlated, with low NDVI values being associated with high LST values and high NDVI values being associated with low LST values (Barbieri et al. 2018; Weng 2001). A correlation analysis was performed to examine the correlation between LST and NDVI, demonstrating a predominantly negative correlation. Based on our findings, it was observed that mining sites and urbanised regions had elevated surface temperatures, while locations characterised by abundant vegetation and water bodies displayed comparatively lower surface temperatures. All correlation map for selected year of 2001, 2006, 2011, 2016 & 2021 have been given in Fig.5.124 to Fig.5.128 respectively. The LST and NDVI

values were extracted for each year in order to conduct Pearson correlation analysis. The calculated Pearson linear correlation coefficient between LST and NDVI were low to very low negative across the whole period. The negative correlation of LST with NDVI in a region can be attributed to the cooling effects of vegetation. The high vegetation cover (high NDVI) increases evapotranspiration, shading, and soil moisture, which help in reducing surface temperatures. The respective linear regression coefficients with respect to LST and NDVI were reported in Table.5.52. The LST and NDVI values were found to be statistically inversely correlated, however the intensity of the correlation varies. In addition, the mean LST and NDVI values for each year were used to plot a scatter plot as given in Fig.5.129.

Two significant observations have been made from Fig.5.129. The first observation comprises a persistent rise in LST values, accompanied by a reduction in NDVI values from 2001 to 2021. Furthermore, it can be observed that years with higher NDVI values, specifically 2001, 2006, and 2011, corresponded to lower LST values. Conversely, years with lower NDVI values, namely 2016 and 2021, had higher LST values. This provides more evidence that there is a negative correlation between vegetation density and surface temperature which shows an increase in vegetation cover may help to lower a surface temperature of the area. The correlation between NDVI and LST changes seasonally without obvious regularity.

Table.5.52 Pearson's linear correlation (R^2) values between LST and NDVI

Date of acquisition	LST (mean)	NDVI (mean)	Correlation coefficient (R^2 value)
22 April 2001	28.40	0.09	0.061
28 April 2006	29.62	0.07	0.054
26 April 2011	29.98	0.06	0.119
23 April 2016	37.06	0.04	0.011
05 April 2021	38.27	0.03	0.230

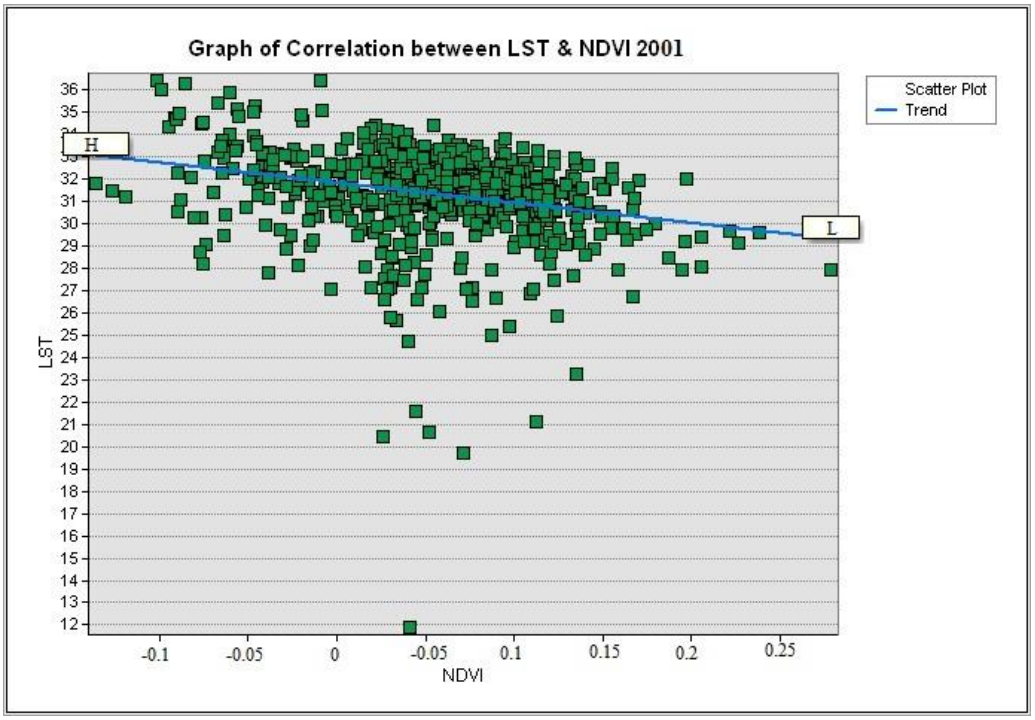

Fig.5.124 Correlation map between LST and NDVI in the year 2001

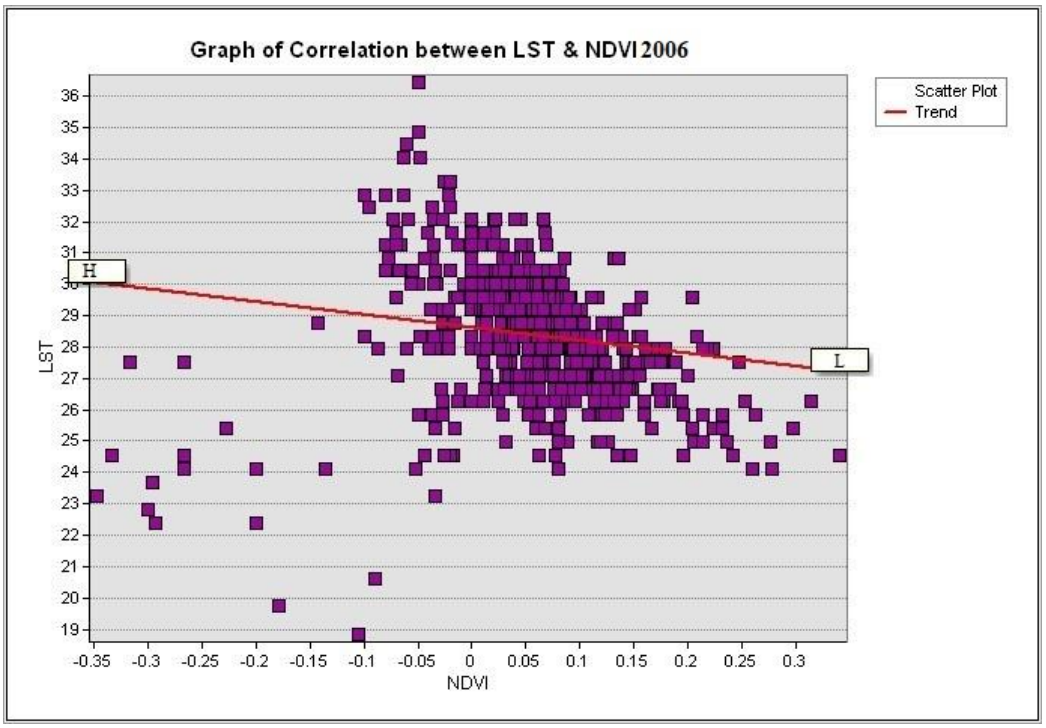

Fig.5.125 Correlation map between LST and NDVI in the year 2006

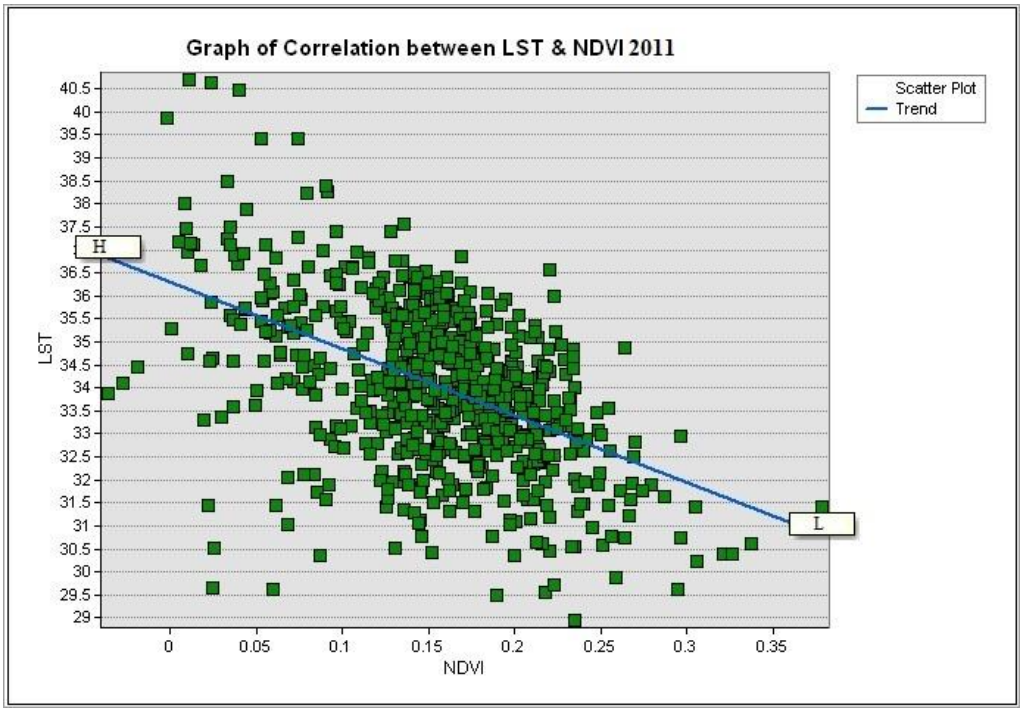

Fig.5.126 Correlation map between LST and NDVI in the year 2011

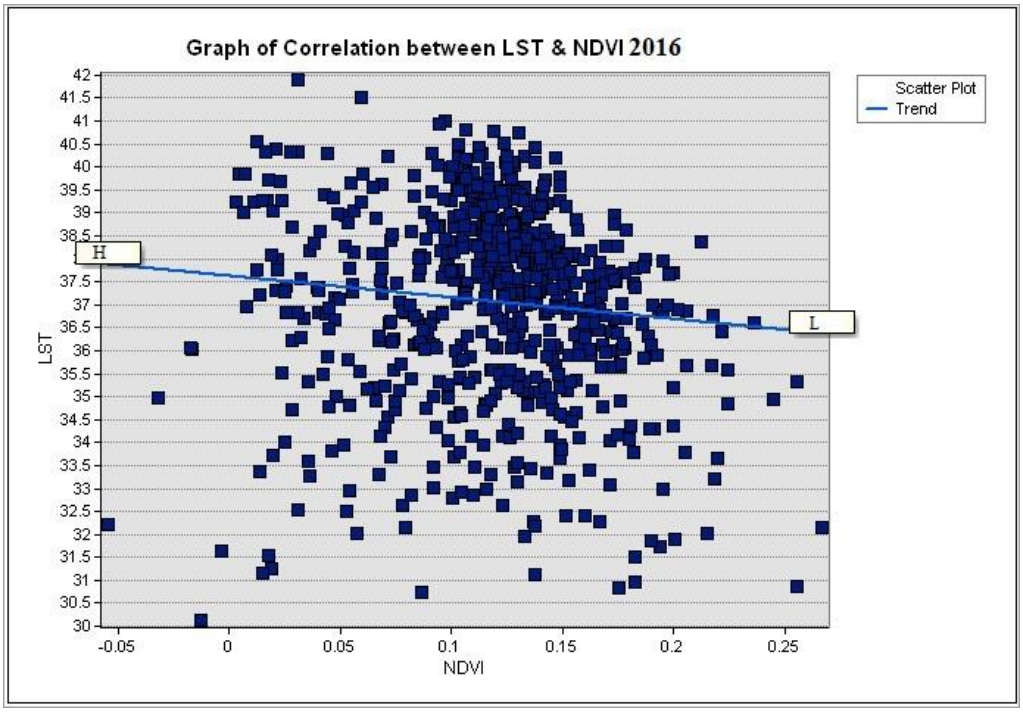

Fig.5.127 Correlation map between LST and NDVI in the year 2016

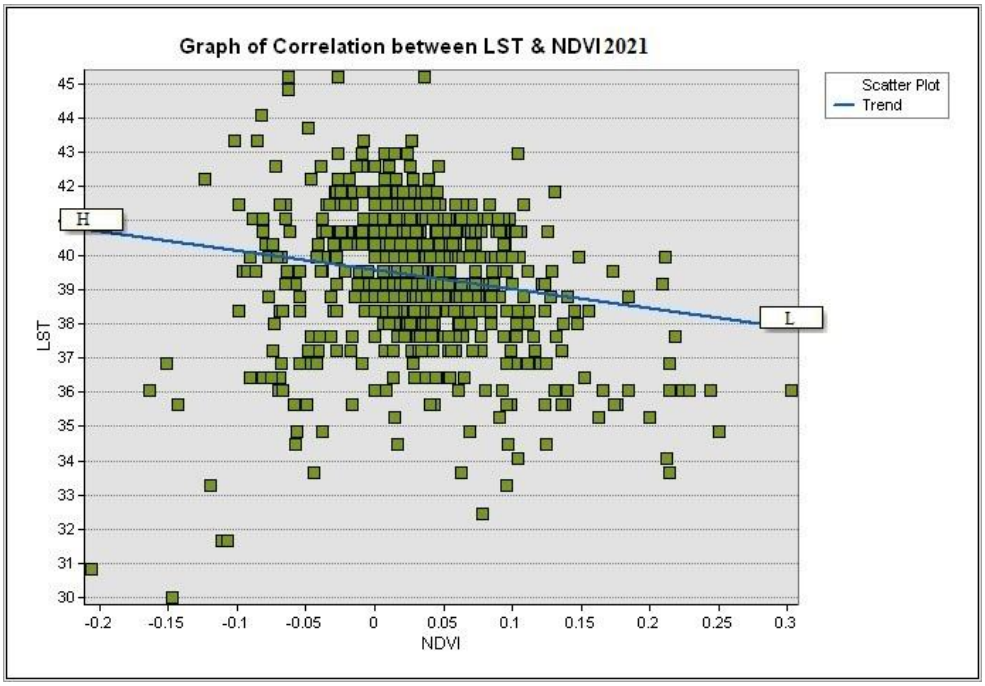

Fig.5.128 Correlation map between LST and NDVI in the year 2021

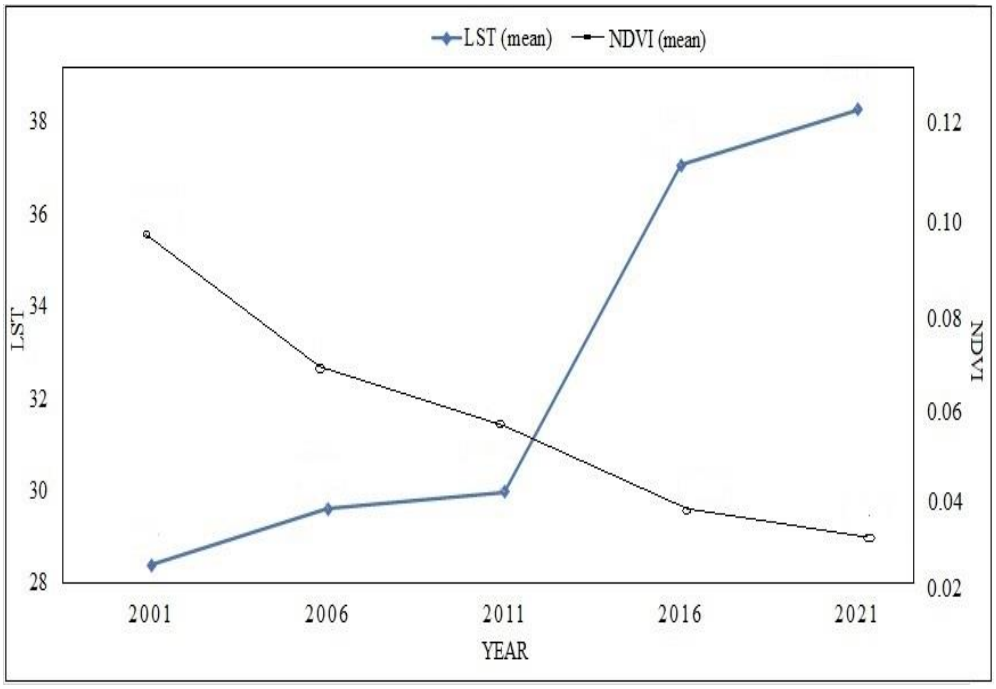

Fig.5.129 Scatter plot between mean LST and mean NDVI values

5.4.5 Normalized Difference Water Index (NDWI) Estimation

The NDWI was utilised to examine the reflectance proportion of water content in both soil and plant surfaces. Rather than simply focusing on a spectral band whose reflection intensity is strongly influenced by the phase of chlorophyll in leaf, in the addition of short wave near-infrared (SWIR) emphasized light absorption by water (Zygielbaum et al. 2009). The NDWI is widely used to determine the degree of wetness or dryness at this stage. The non-dimensional normalized difference water index (NDWI) is a metric that quantifies the presence of surface water, with values ranging from -1 to +1. The higher NDWI values indicate that the plant contains more water, whereas lower NDWI values show that the vegetation contains less water. Consequently, the rate of NDWI decreases during periods of water stress (Zhang et al. 2017). As precipitation increases, there is a corresponding rise in the NDWI value (Yaa et al. 2020). The formula for NDWI in Landsat 5 TM and ETM+ data is presented in equation (4.32), whereas for Landsat 8 OLI/TIRS data, it is presented in equation (4.33) in the preceding chapter.

The findings derived from the NDWI indicate that the upper portion of the tailings holds back the water, as indicated by the values obtained from this particular index. The presence of water in this context could potentially be attributed to either the rainy season or the period of tailing deposition. The findings indicate that variations in water bodies over several time periods (2001, 2006, 2011, 2016, and 2021) can be attributed to the presence of artificially constructed ponds, sumps, and canals in the region. These water storage facilities are designed to meet the water requirements of mining operations and other related activities.

The prepared map of NDWI in selected years has been shown in Fig.5.130 to Fig.5.134 respectively. The spatiotemporal variation of NDWI values with its mean value for the selected time period is given in Table.5.53. The data collected in the years 2001, 2006,

2011, 2016, and 2021 consistently indicate a decline in the presence of water bodies within the specified area.

The highest observed Normalized Difference Water Index (NDWI) values were 0.61, 0.54, and 0.47 in the years 2001, 2006, and 2011, respectively. Conversely, there has been a notable decline in NDWI intensity between 2016 and 2021, with minimum NDWI values of 0.18 and 0.19, respectively.

The water bodies in the KCF region have experienced a decline during the past two decades as also stated previously by analysis of LULC. The Normalized Difference Water Index may have experienced a decrease over a period of time due to changes in land use and land cover (LULC) within the designated region. According to the analysis of all five Normalized Difference Water Index maps, it can be shown that the east, central, and south-western regions of the study area exhibited higher NDWI values. However, the north, south, and western portions of the area had lower NDWI values, indicating the presence of a low NDWI zone. These areas were characterised by a significant proportion of bare land and built-up areas.

Table.5.53 Spatiotemporal variation of NDWI distribution in area from 2001 to 2021

Date of acquisition	NDWI (minimum)	NDWI (maximum)	NDWI (mean)	NDWI (standard deviation)
22 April 2001	-0.22	0.61	0.14	0.07
28 April 2006	-0.49	0.54	-0.12	0.10
26 April 2011	-0.52	0.46	-0.17	0.10
23 April 2016	-0.143	0.19	-0.18	0.06
05 April 2021	-0.48	0.18	-0.20	0.08

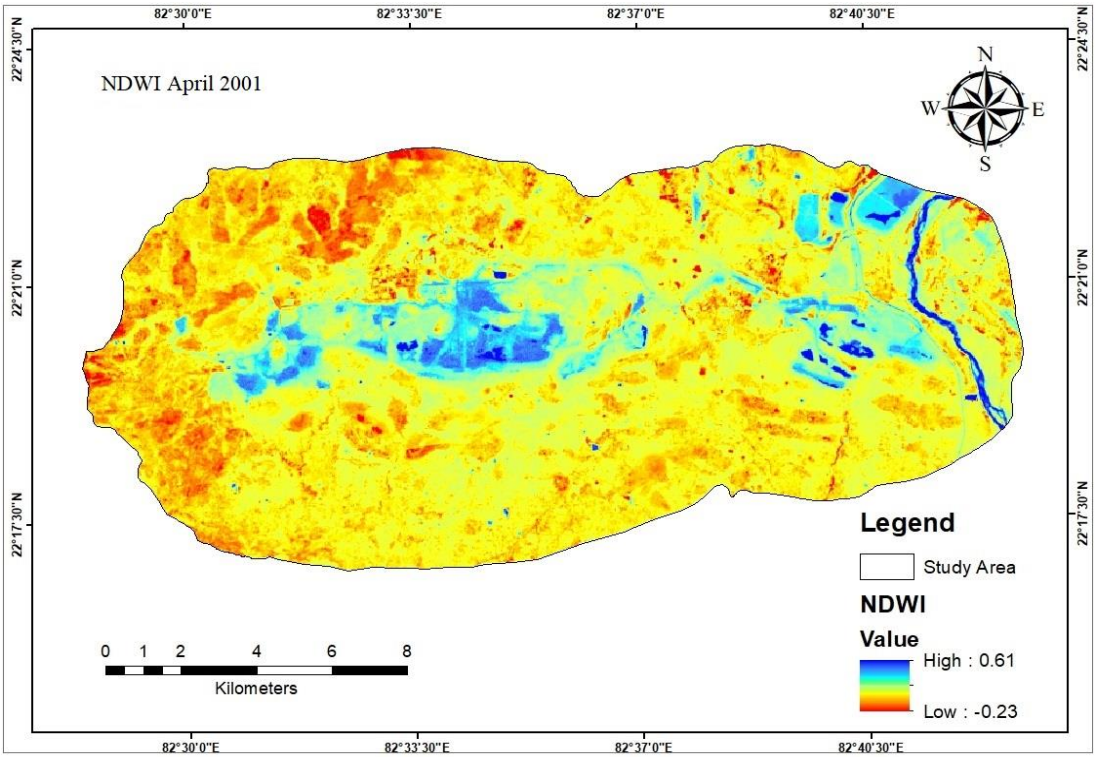

Fig.5.130 NDWI map for the year 2001

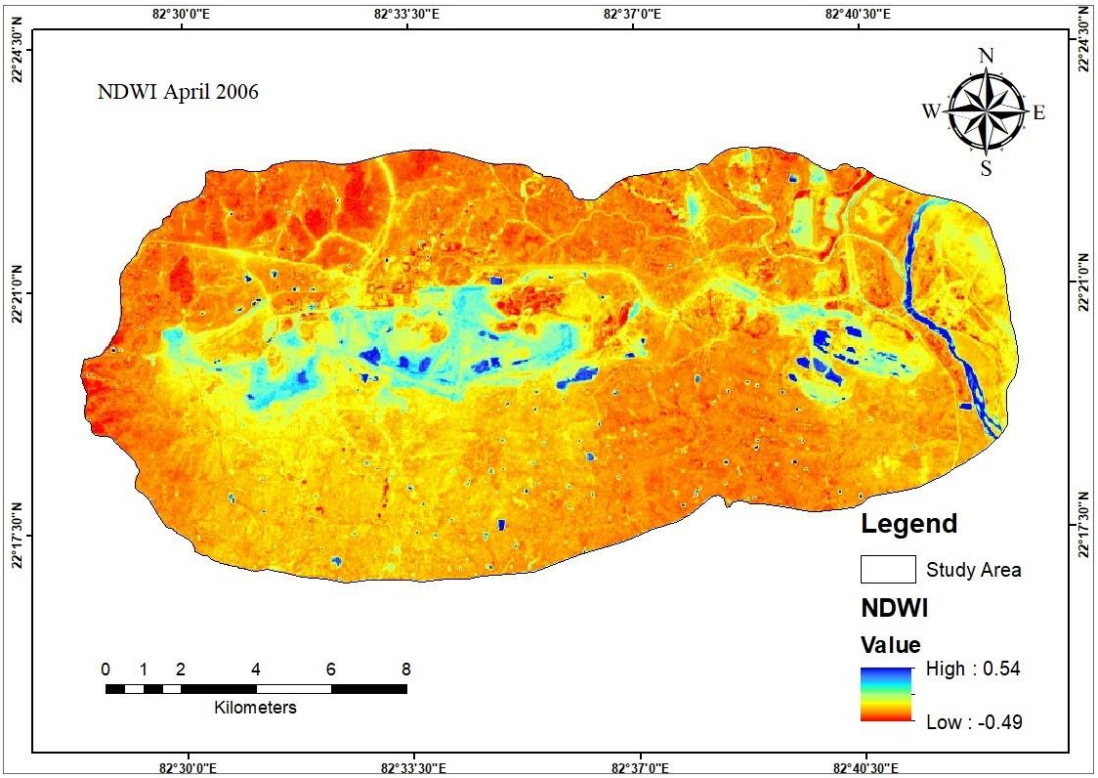

Fig.5.131 NDWI map for the year 2006

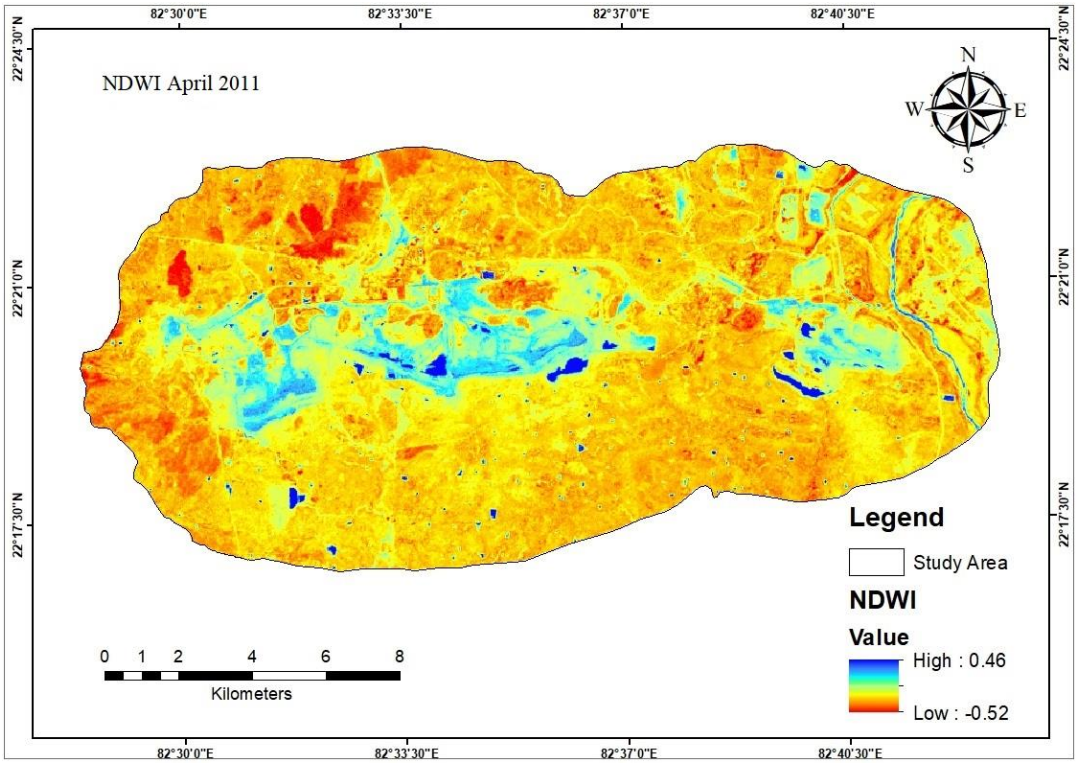

Fig.5.132 NDWI map for the year 2011

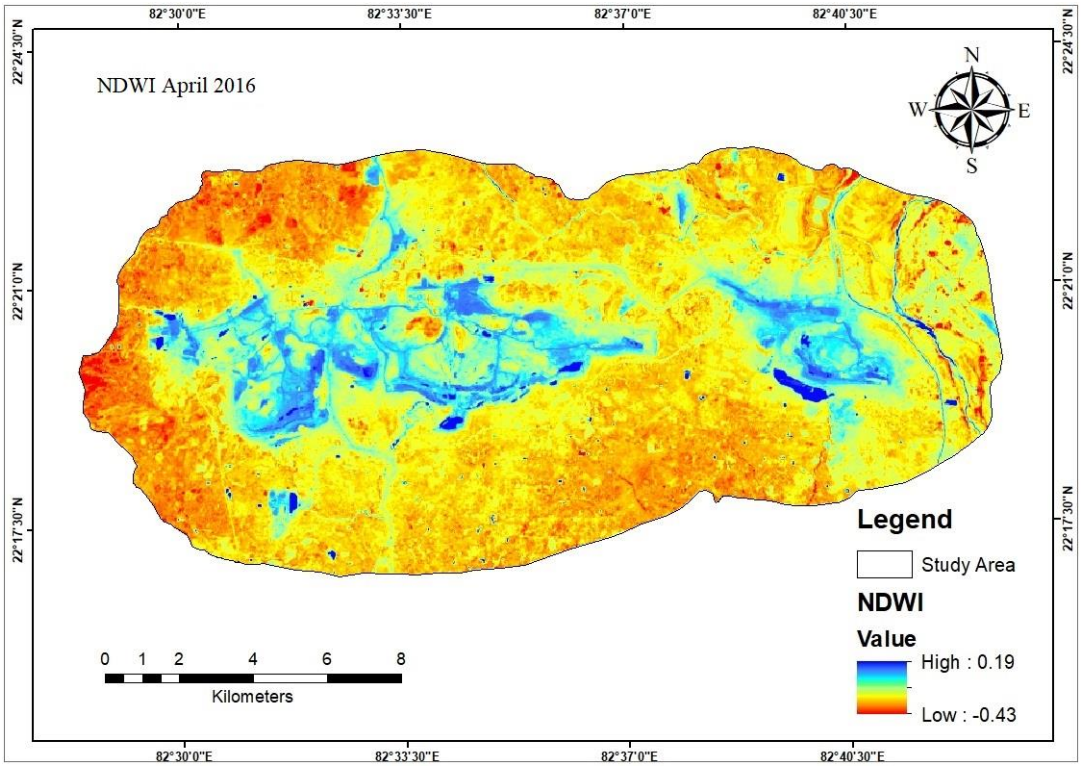

Fig.5.133 NDWI map for the year 2016

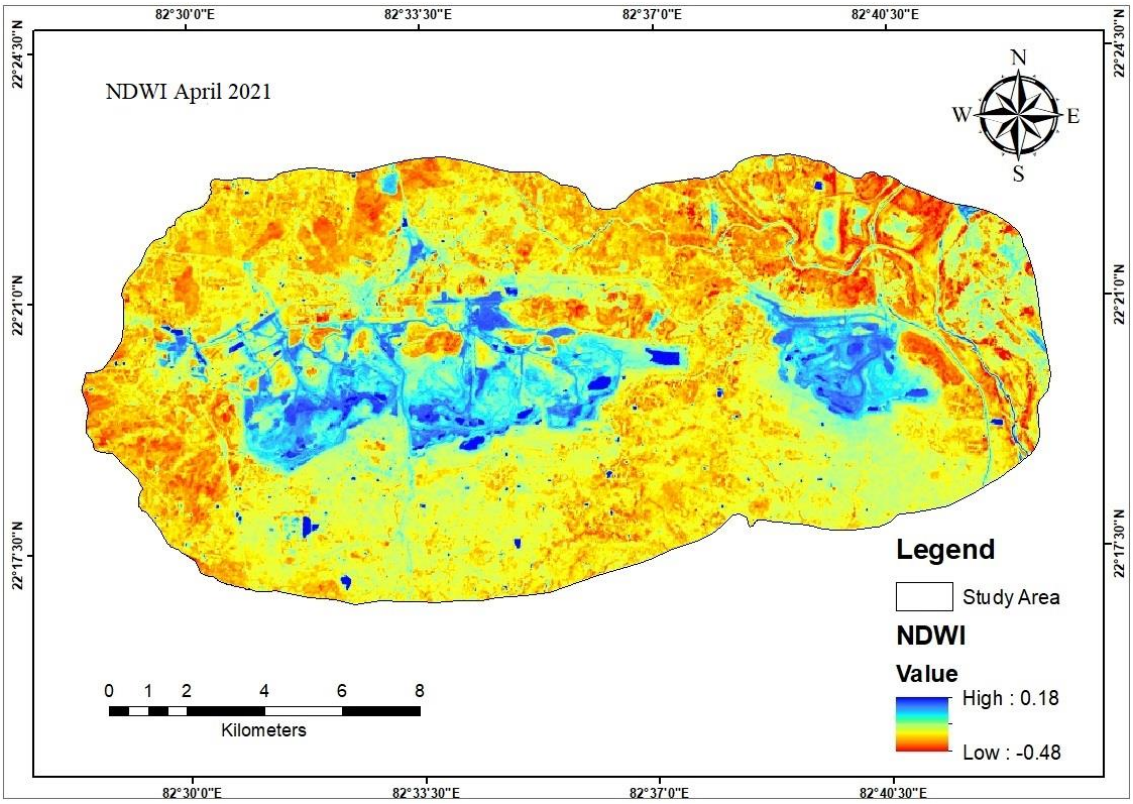

Fig.5.134 NDWI map for the year 2021

5.4.6 Correlation analysis of LST and NDWI

The NDWI is a metric used to assess the presence of water bodies on the Earth's surface. In contrast, surface temperature is a comprehensive concept that encompasses the total temperature of all components of the current surface. The LST and NDWI exhibit inverse trends over the selected area in this study. The negative correlation of LST with NDWI in a region can be attributed to the cooling effects of water content. The high-water content (high NDWI) increases the thermal mass and heat dissipation capacity of the surface, leading to lower LST. A statistical correlation between LST and NDWI was reported using a linear regression model in this analysis. The LST was considered to be a dependent variable, whereas the NDWI parameter was considered to be an independent variable. The measurement of the correlation between the LST and NDWI parameters was conducted by calculating correlation coefficients (R^2) obtained from Pearson's linear regression analysis.

This objective includes the presentation of the LST map in Fig.5.113 to Fig.5.117, and the NDWI map in Fig.5.130 to Fig.5.134. The prepared correlation maps between LST and NDWI for selected year 2001, 2006, 2011, 2016, and 2021 have been shown from Fig.5.135 to Fig.5.139, respectively. The study involved the calculation of average LST and NDWI values for each satellite data source. The resulting correlation coefficient value (R^2) indicated a weak to very weak negative association, as presented in Table.5.54. The map representations illustrate a consistent inverse spatial correlation between LST and NDWI across selected years in this study. The mean values of LST and NDWI for each map were calculated and presented as a scatter plot in Fig.5.140.

Two significant observations have been made based on the scatter plot depicted in Fig.5.140. The initial observation includes a steady rise in LST and a corresponding decline in NDWI between the years 2001 and 2021. Additionally, the graph illustrates a negative correlation between higher NDWI values and lower LST values in the year 2001. Conversely, lower NDWI values corresponded to higher LST values in the years 2006, 2011, 2016, and 2021 as shown in Fig.5.140. This finding supports current research indicating a negative correlation between the water index and surface temperature, implying that an increase in water bodies could potentially lead to a reduction in the surface temperature of the respective region. This specific pattern of the correlation between LST and NDWI was seen, which varies seasonally without any obvious regularity.

Generally, LST values presents weak negative correlation with NDWI value in this study. This particular pattern of the correlation between LST and NDWI were noticed in complete KCF region. The correlation between LST and NDWI have also shown low to very low negative correlation for the selected time period. KCF can be representative of other coal mines with similar geological, hydrological, and socio-economic contexts,

particularly in central and eastern India where similar sedimentary basins and coal mining practices are found but coalfields with different geological formations, mining practices, or socio-economic conditions, KCF's data might only partially apply.

Table.5.54 Pearson's linear correlation (R^2) values between LST and NDWI

Date of acquisition	LST (mean)	NDWI (mean)	Correlation coefficient (R^2 value)
22 April 2001	28.40	0.14	0.039
28 April 2006	29.62	-0.12	0.113
26 April 2011	29.98	-0.17	0.047
23 April 2016	37.06	-0.18	0.037
05 April 2021	38.27	-0.20	0.268

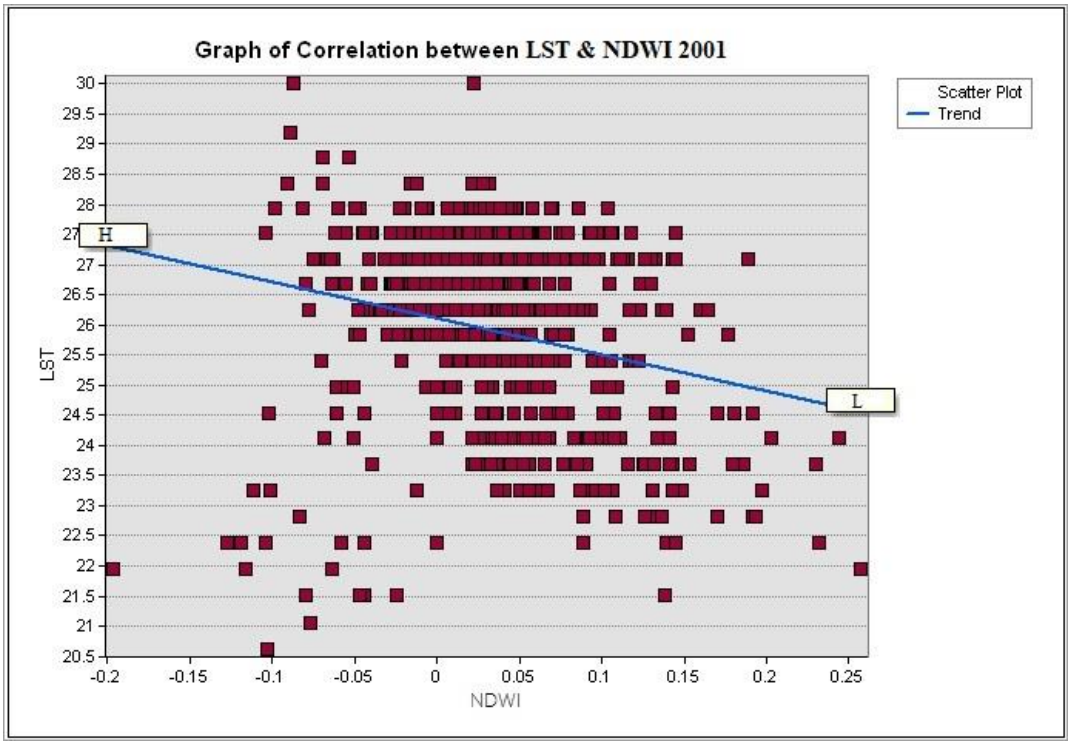

Fig.5.135 Correlation map between LST and NDWI in the year 2001

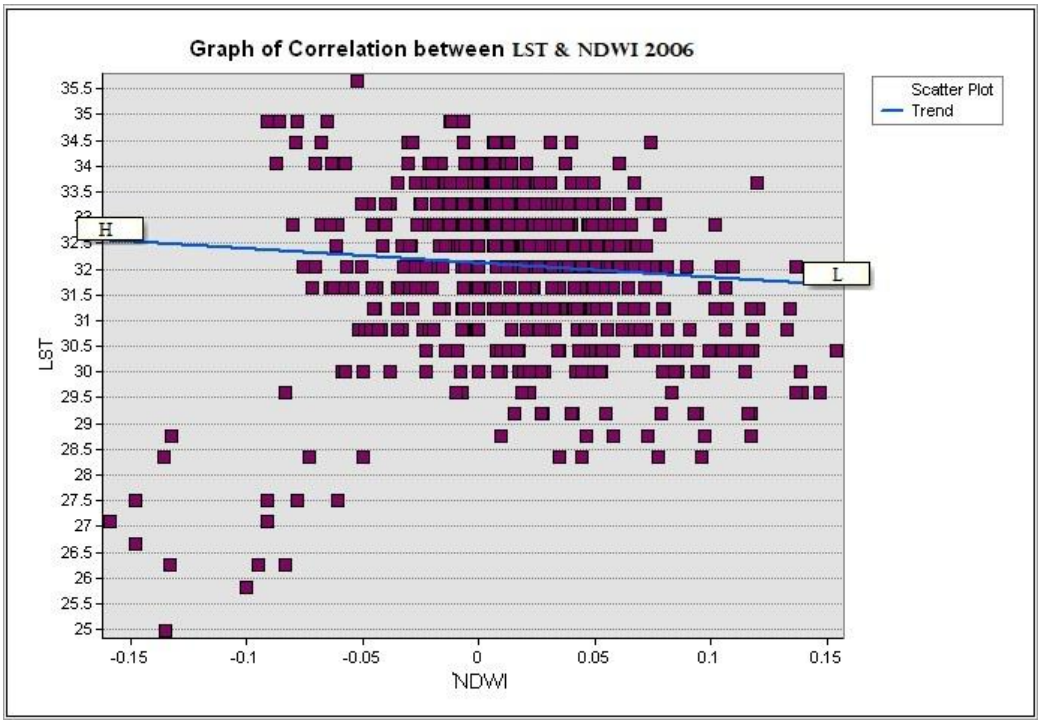

Fig.5.136 Correlation map between LST and NDWI in the year 2006

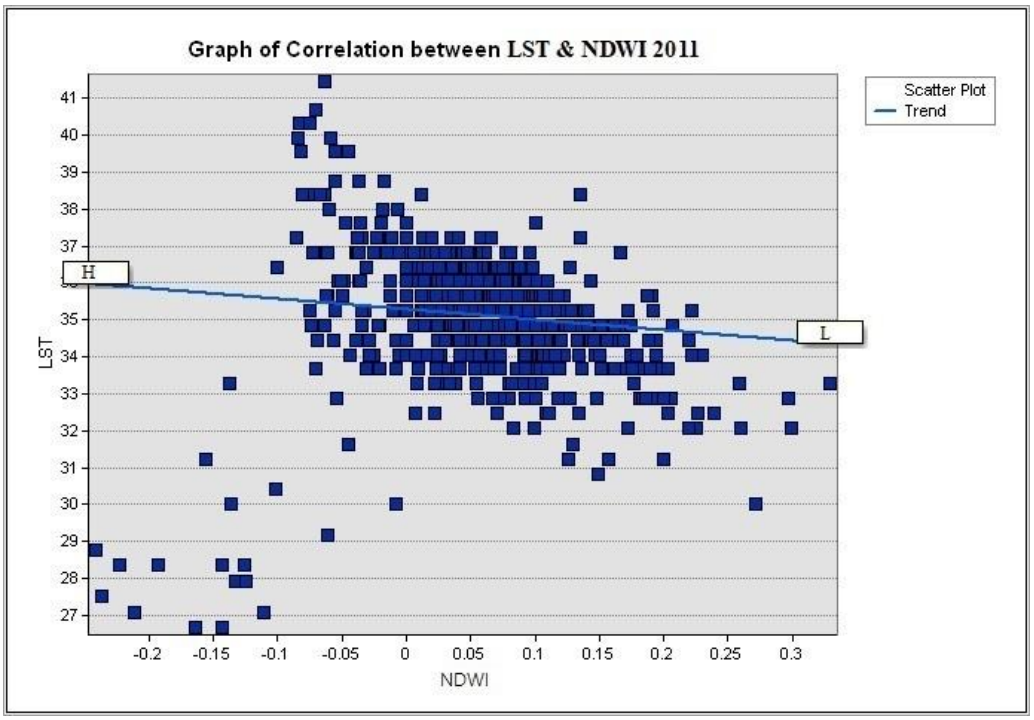

Fig.5.137 Correlation map between LST and NDWI in the year 2011

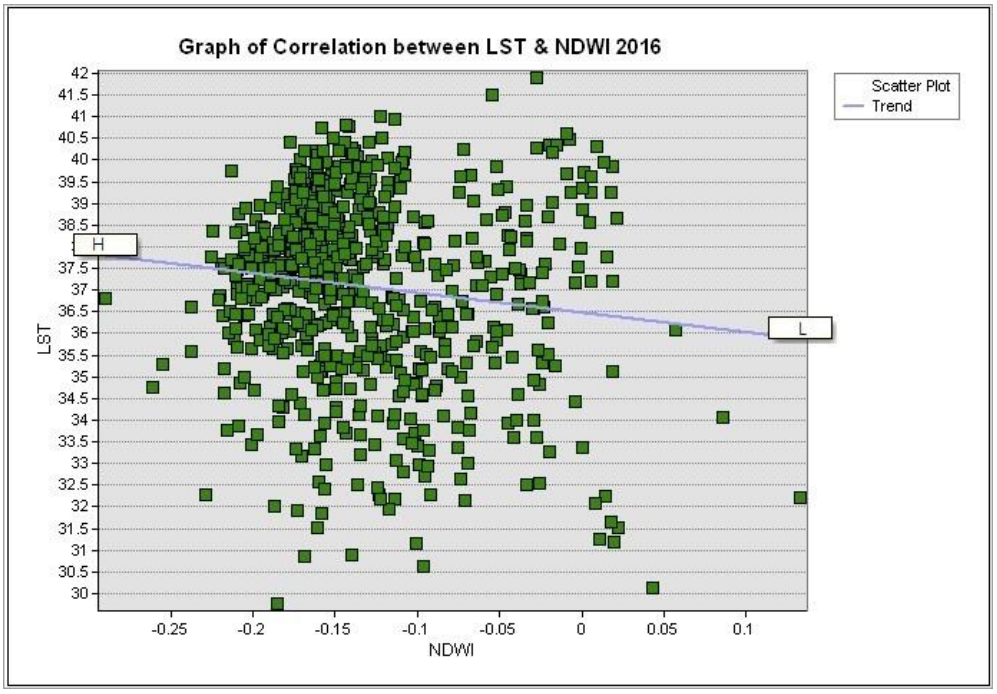

Fig.5.138 Correlation map between LST and NDWI in the year 2016

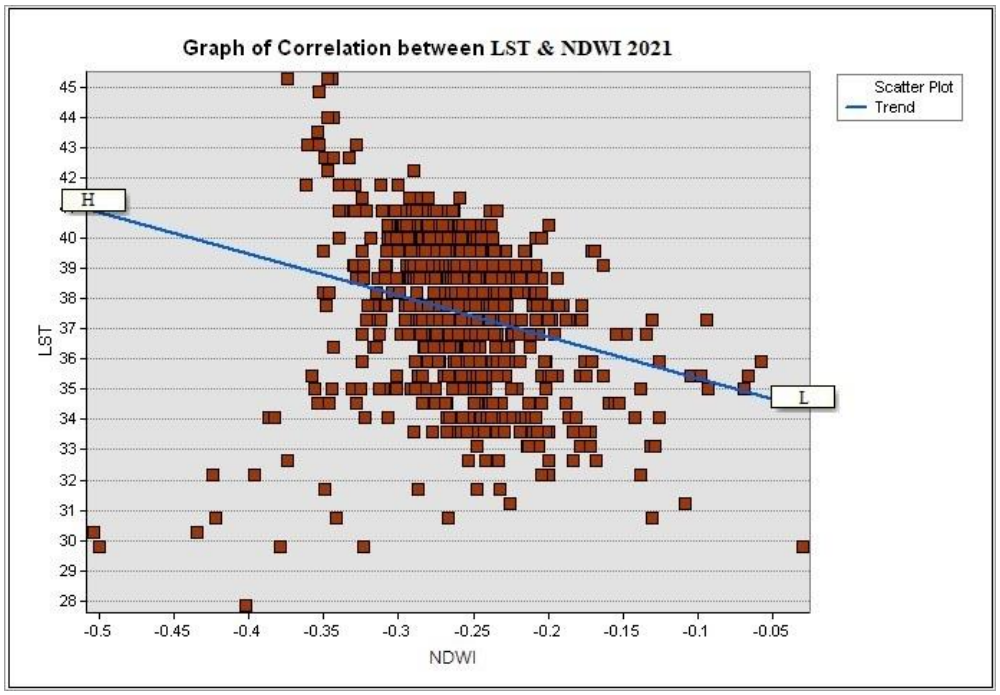

Fig.5.139 Correlation map between LST and NDWI in the year 2021

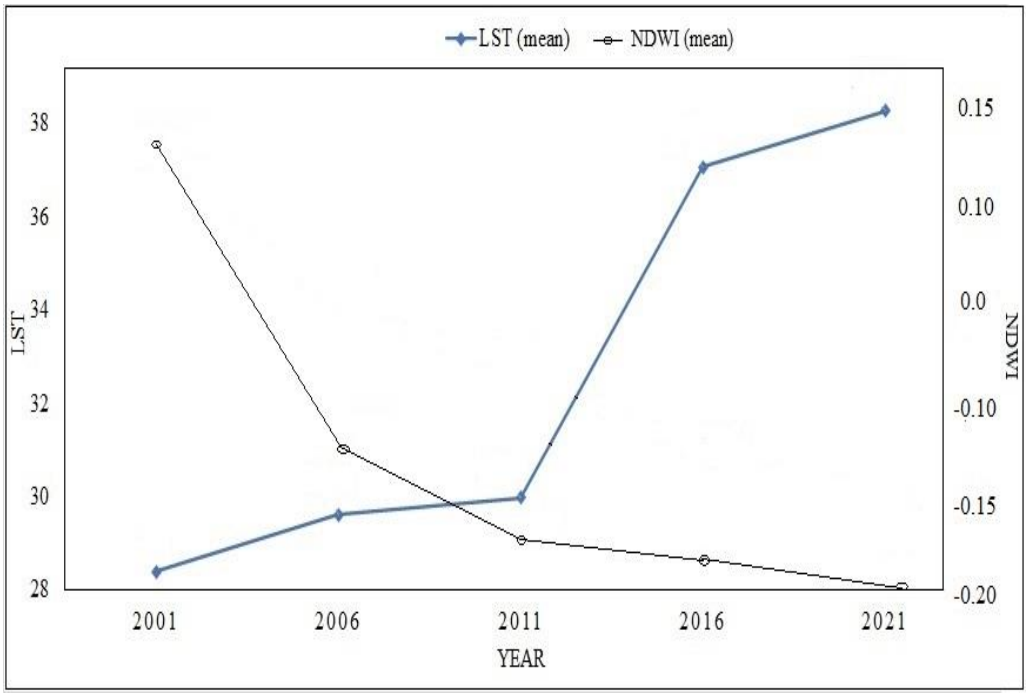

Fig.5.140 Scatter plot between mean LST and mean NDWI values